

# **Intraoperative HDR Brachytherapy: Present and Future**

ISBN: 90-8559-259-3

Printed by: Optima Grafische Communicatie, Rotterdam

Cover design: Thomas Kolkman

© Copyright:

2001 Arnold (Chapter 2)

1994 Elsevier Science Ireland Ltd. (Chapter 3)

2004 Elsevier Ireland Ltd. (Chapter 4)

1997 Elsevier Science Ireland Ltd. (Chapter 5)

2006 Elsevier Ireland Ltd. (Chapter 6)

2004 Elsevier Ireland Ltd. (Chapter 7)

2004 Elsevier Inc. (Chapter 8)

2001 Elsevier Science Ireland Ltd. (Chapter 9)

2002 Elsevier Science Ireland Ltd. (Chapter 10)

2004 American Association of Physicists in Medicine (Chapter 11)

Financial support for the publication of this thesis was given by Isodose Control B.V.

# **Intraoperative HDR Brachytherapy: Present and Future**

Intraoperatieve HDR brachytherapie: heden en toekomst

## **PROEFSCHRIFT**

ter verkrijging van de graad van doctor aan de  
Erasmus Universiteit Rotterdam  
op gezag van de  
rector magnificus

Prof.dr. S.W.J. Lamberts

en volgens het besluit van het College voor Promoties.

De openbare verdediging zal plaatsvinden op  
vrijdag 19 januari 2007 om 13.30 uur  
door

**Inger Karine Kirsten Kolkman-Deurloo**

geboren te Lørenskog, Noorwegen

Promotiecommissie

Promotor: Prof.dr. P.C. Levendag

Overige leden: Prof.dr. R.J. Baatenburg de Jong  
Prof.dr. B.J.M. Heijmen  
Prof.dr.ir. J.J.W. Lagendijk

This thesis has been prepared at the Department of Radiation Oncology, Erasmus MC - Daniel den Hoed Cancer Center, Rotterdam, The Netherlands.

Address for correspondence:

I.K.K. Kolkman-Deurloo, Department of Radiation Oncology, Division of Medical Physics, Erasmus MC - Daniel den Hoed Cancer Center, Groene Hilledijk 301, 3075 EA Rotterdam, The Netherlands.

E-mail: [i.kolkman-deurloo@erasmusmc.nl](mailto:i.kolkman-deurloo@erasmusmc.nl)



## CONTENTS

<b>Chapter 1</b>	<b>1</b>
<i>Introduction</i>	
<b>Chapter 2</b>	<b>5</b>
<i>High dose-rate interstitial and endocavitary brachytherapy in cancer of the head and neck</i>	
<b>Chapter 3</b>	<b>41</b>
<i>Optimization of interstitial volume implants</i>	
<b>Chapter 4</b>	<b>61</b>
<i>Anatomy based inverse planning in HDR prostate brachytherapy</i>	
<b>Chapter 5</b>	<b>73</b>
<i>Reconstruction accuracy of a dedicated localiser for filmless planning in intra-operative brachytherapy</i>	
<b>Chapter 6</b>	<b>93</b>
<i>On-line implant reconstruction in HDR brachytherapy</i>	
<b>Chapter 7</b>	<b>109</b>
<i>Intraoperative HDR brachytherapy for rectal cancer using a flexible intraoperative template: standard plans versus individual planning</i>	
<b>Chapter 8</b>	<b>119</b>
<i>High dose rate intraoperative radiotherapy for close or positive margins in patients with locally advanced or recurrent rectal cancer</i>	
<b>Chapter 9</b>	<b>135</b>
<i>Determination of the accuracy of implant reconstruction and dose delivery in brachytherapy in The Netherlands and Belgium</i>	

<b>Chapter 10</b>	<b>159</b>
<i>Quality control of brachytherapy equipment in The Netherlands and Belgium: current practice and minimum requirements</i>	
<b>Chapter 11</b>	<b>177</b>
<i>Determination of the reference air kerma rate for <math>^{192}\text{Ir}</math> brachytherapy sources and the related uncertainty</i>	
<b>Chapter 12</b>	<b>197</b>
<i>Summary, general conclusions and future perspectives</i>	
<b>Samenvatting</b>	<b>205</b>
<b>Dankwoord</b>	<b>209</b>
<b>List of publications</b>	<b>211</b>
<b>Curriculum vitae</b>	<b>215</b>

## CHAPTER 1. INTRODUCTION

Radiotherapy is one of the most effective modalities in cancer treatment, together with surgery and chemotherapy. Radiotherapy can be applied either by external beam radiotherapy, i.e. using high energy photon or electron beams directed from several directions outside the patient to the tumor, or by brachytherapy. Brachytherapy is a treatment modality in which tumors are irradiated by positioning radioactive sources very close to or in the tumor volume either by permanent implants or by temporarily inserted applicators or afterloading catheters.

The history of brachytherapy started at the beginning of the 20<sup>th</sup> century when the first treatments were performed with Radium-226 needles. Since then, several developments took place that greatly improved the therapy in terms of dosimetry, effectiveness and radiation exposure to personnel. Radium-226 was replaced by artificial radionuclides such as Cesium-137, Cobalt-60 and Iridium-192 [3]. Manual afterloading of sources into applicators or implanted needles replaced direct loading of the sources into the patient. Nowadays, manual afterloading is fully replaced by computer controlled remote afterloading allowing complete radiation protection. The introduction of computer controlled remote afterloading devices and the development of radiobiological models, predicting the response of tumors and normal tissues to irradiation, enabled replacing the low dose rate techniques, using Radium-226, Cesium-137 or Iridium-192, by (fractionated) high dose rate techniques [4], first using Cobalt-60 and nowadays using almost exclusively Iridium-192.

In general, temporary brachytherapy can be divided in several categories based on the dose rate applied [2]:

- Low dose rate (LDR) brachytherapy is delivered at dose rates between 0,4 and 2 Gy/h;
- Medium dose rate (MDR) brachytherapy is delivered at dose rates between 2 and 12 Gy/h;
- High dose rate (HDR) brachytherapy is delivered at dose rates higher than 12 Gy/h.

In pulsed dose rate (PDR) brachytherapy, an LDR treatment is simulated by a large number of fractions of short duration with time intervals between fractions of (less than) one to a few hours [1,6].

The use of (fractionated) HDR and PDR brachytherapy, usually performed with single stepping source afterloaders, has increased dramatically. The introduction of these afterloaders enabled new developments in order to optimize the treatment, e.g. optimization of the dose distribution through dwell time optimization and integration of the entire brachytherapy procedure in one session, and the introduction of intra-operative irradiation. In *chapter 2* the techniques and results of fractionated HDR and PDR brachytherapy for head and neck cancer are presented.

HDR/PDR single stepping source afterloaders contain a small Iridium-192 source, enabling optimization of the dose distribution by optimization of the dwell times over all dwell positions in the implant. In *chapter 3* the effects of one of the optimization algorithms, i.e. geometric optimization, on the dose distribution of interstitial volume implants have been studied in terms of the irradiated volume, the dose uniformity, and the choice of the reference dose. Based on the classical dwell time optimization techniques, i.e. dose point optimization and geometric optimization, an algorithm for anatomy based inverse planning was developed. The results of anatomy based inverse planning in HDR prostate implants are evaluated in *chapter 4*.

An Integrated Brachytherapy Unit (IBU) was established at the Erasmus MC – Daniel Den Hoed Cancer Center by equipping a shielded operating room with an HDR afterloader and a dedicated brachytherapy localiser, connected to a treatment planning computer (figure 1). This set-up enables integration of the entire brachytherapy procedure, i.e. implantation, implant reconstruction, dose planning and delivery in a single session. In *chapter 5* the reconstruction accuracy of this dedicated IBU localiser has been evaluated by simulations and by measurements using a QA phantom. Besides, the effect of the reconstruction accuracy on the treatment plan has been evaluated using phantoms representing clinical relevant implant geometries. When converting to on-line planning by importing the fluoroscopy images directly in the planning computer the image distortions present in fluoroscopy images should be eliminated. In *chapter 6*, the accuracy of on-line planning in the IBU using dedicated image distortion correction algorithms has been evaluated.

The availability of an HDR afterloader in the IBU enables the use of intraoperative brachytherapy (IOBT). HDR IOBT is applied using a 5 mm thick flexible intraoperative template (FIT). To reduce the procedure time, treatment planning is performed

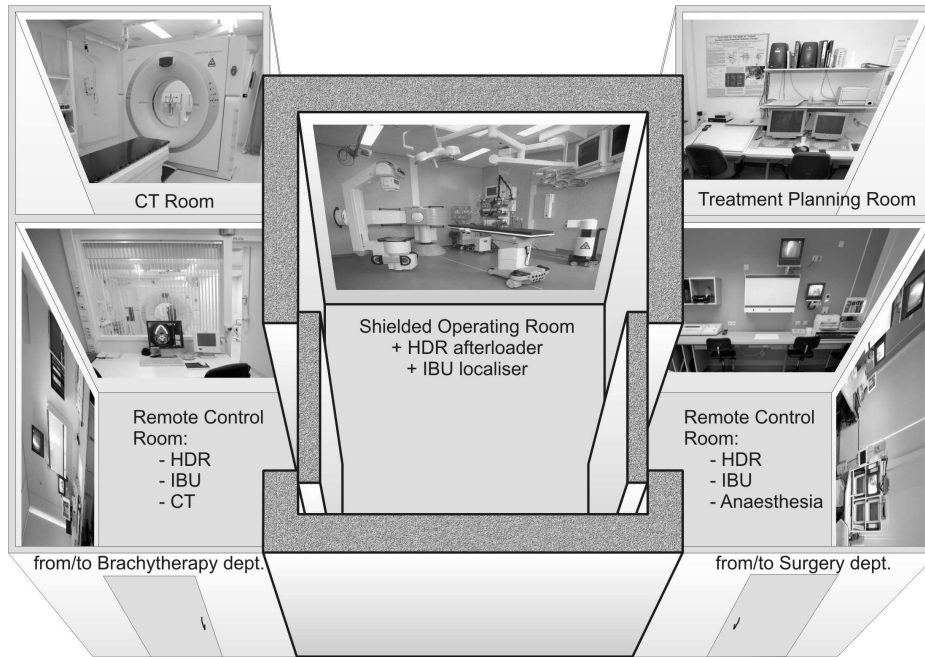


**Figure 1:** Schematic view of the Integrated Brachytherapy Unit at the Erasmus MC – Daniel Den Hoed Cancer Center

using standard plans, that neglect the curvature of the FIT. In *chapter 7* we have calculated the individual treatment plan, based on the real geometry of the FIT, and the dose at clips placed during surgery, of 32 patients with locally advanced rectal tumors treated this way. In *chapter 8* the technique and results, in terms of local failure and survival, of HDR IOBT for patients with locally advanced or recurrent rectal cancer are discussed.

With these developments in brachytherapy tools, there is an increasing need for quality assurance (QA), preferably through nation wide accepted guidelines. A taskgroup on QA of brachytherapy systems of the Netherlands Commission on Radiation Dosimetry (NCS) was established to develop guidelines for QA in brachytherapy [5]. The taskgroup investigated the accuracy of brachytherapy treatments in 33 radiotherapy institutions in The Netherlands and Belgium, by determining the accuracy of implant reconstruction and dose delivery (*chapter 9*). In *chapter 10* the practice of brachytherapy QA in The Netherlands and Belgium was evaluated and compared with international recommendations in order to establish minimum QA requirements. It was observed that two methods to obtain the air

kerma calibration factor of an ionization chamber for the spectrum of Iridium-192 were used, causing systematic differences in the determination of the reference air kerma rate of the sources. The determination of the reference air kerma rate for Iridium-192 sources and the related uncertainty are discussed in *chapter 11*.

In *chapter 12* the presented set-up for HDR (intraoperative) brachytherapy is discussed in some more detail and future perspectives are presented.

## 1.1 References

1. Brenner DJ, Hall EJ. Conditions for the equivalence of continuous to pulsed low dose rate brachytherapy. *Int J Radiat Oncol Biol Phys* 1991; 20: 181-190.
2. Gerbaulet A, Pötter R, Mazeron JJ, Meertens H, Limbergen van E. The GEC ESTRO handbook of brachytherapy. ESTRO, Brussels, Belgium, 2002.
3. Joslin CAF, Flynn A, Hall E. Principles and practice of brachytherapy (using afterloading systems). Arnold, London, Great Britain, 2001.
4. Nag S. High dose rate brachytherapy: a textbook. Futura, Armonk, NY, USA, 1994.
5. NCS (Netherlands Commission on Radiation Dosimetry). Quality control in brachytherapy. Report 13, 2000.
6. Visser AG, Aardweg van den GJM, Levendag PC. Pulsed dose rate and fractionated high dose rate brachytherapy: choice of brachytherapy schedules to replace low dose rate treatments. *Int J Radiat Oncol Biol Phys* 1996; 34: 497-505.

## **CHAPTER 2. HIGH DOSE-RATE INTERSTITIAL AND ENDOCAVITARY BRACHYTHERAPY IN CANCER OF THE HEAD AND NECK**

PC Levendag, C de Pan, D Sipkema, AG Visser, IKK Kolkman-Deurloo, PP Jansen

Modified after: Principles and practice of brachytherapy (using afterloading systems); Chapter 21; 296-316. Eds. CAF Joslin, A Flynn, EJ Hall; Arnold Publishing, London, 2001.

### **2.1 Introduction**

The development of manual afterloading techniques for radioactive sources and the introduction of artificial radionuclides have received considerable attention over the last few years and have contributed significantly to the renaissance of brachytherapy. The total elimination of radiation exposure to the nursing, medical and physics staff as well as to patients' relatives by remote controlled afterloading devices was a logical extension of the manual afterloading concept. In 1961, the first high dose-rate (HDR) remote-controlled afterloader was introduced in the Memorial Sloan Kettering Cancer Center group, using high-activity cobalt-60 pellets. When the manufacture of small, cylindrical (<1 mm), high-activity (100-400 GBq) iridium-192 sources became feasible, the so-called 'stepping-source technique' was introduced. In this way, 'isodose-volumes' can be created very flexibly by combining careful placement of the afterloading catheters or applicators and adjustment of the dwell positions and dwell times of the iridium-192 sources (i.e., optimization).

In the ErasmusMC - Daniel den Hoed Cancer Center (ErasmusMC-DDHCC), the first HDR afterloader (microSelectron-HDR) using such a high-activity iridium-192 point source was introduced for interstitial and/or endocavitary brachytherapy in cancer of the head and neck in 1990. Early on, it was recognized, however, that there might be a radiobiological disadvantage in applying large HDR (1-3 Gy min<sup>-1</sup>) single fractions, even if the catheters or applicators are carefully positioned and good immobility is achieved. Realizing this, one can, of course, try to fractionate the HDR brachytherapy to some extent.

Ultimately, it was proposed to try to combine the radiobiological advantage of low dose rate (LDR), as opposed to HDR, with the practical advantages of computerized stepping-source HDR afterloading techniques in ‘pulsed dose-rate’ (PDR) brachytherapy, i.e. using multiple small fractions (pulses) per day with a fixed (small) interval in between the pulses. This necessitated the availability of a second afterloader; this microSelectron-PDR was obtained in 1992. In principle, the design of the PDR afterloading machine is quite similar to that of the microSelectron-HDR, except for the fact that the iridium-192 source for the PDR machine is about ten times weaker (37 GBq), enabling one to deliver multiple (e.g., every 0.5-3 h), small (e.g., 0.5-3 Gy) fractions to a composite implant. However, confusion emerged as to what fraction size at what interval should be considered optimal. We took the opportunity to design and test two types of fractionation schedules, one to be used in conjunction with the microSelectron-HDR (fractionated HDR schedule; i.e., a regimen with a relatively low degree of fractionation), and one with the microSelectron-PDR (PDR-schedule; i.e., a regimen with a relatively high degree of fractionation); for details see section 2.2.

These two fractionation schedules have been consistently clinically tested with regard to tumor control and side-effects. This chapter summarizes the rationale for using either the microSelectron-HDR or microSelectron-PDR in our department. Some aspects regarding the brachytherapy techniques per se and the clinical brachytherapy protocols of the Rotterdam Head and Neck Cooperative Group are illustrated, and the findings obtained with fractionated HDR and PDR brachytherapy in cancer of the base of tongue, nasal vestibule (mould and interstitial brachytherapy), tonsillar fossa and soft palate (interstitial brachytherapy), and cancer of the nasopharynx (endocavitary brachytherapy) are reported. Finally, possibilities regarding the implementation of brachytherapy in the head and neck using an integrated brachytherapy unit (IBU) are discussed.

## **2.2 Brachytherapy schedules in Rotterdam**

### *2.2.1 Rationale for choice of type of remote-controlled afterloaders*

As stated in the previous section, in the ErasmusMC-DDHCC we have consistently used for all brachytherapy cases in the head and neck either the microSelectron-HDR or the microSelectron-PDR, i.e., we have departed from LDR totally since August 1990.



**Table 1:** *Advantages of fractionated HDR or PDR brachytherapy schedules.*

- 
1. Afterloading – elimination of radiation hazard
  2. High-activity point source (37-400 GBq) – no source preparation
  3. Stepping source – dose optimization (PLATO-BPS)
  4. Disconnection of patients during interval between fractions:
    - Easy doctor/nursing/family/care
    - Increased flexibility for patients (e.g. outpatient brachytherapy)
    - Potential for application of other modalities during interval (e.g. interstitial hyperthermia, hypoxic cell cytotoxins)
  5. Continuation/automation brachytherapy over weekend (PDR)
- 

For both types of remote-controlled afterloaders, different fractionation schedules were designed: either using a fraction size of 3 Gy, twice daily, with an interval of 6 h (fractionated HDR; daytime regimen; HDR afterloader), or 1, (1.5) or 2 Gy per fraction, (four or) eight fractions per day, 3-h interval (PDR; daytime regimen in the case of four fractions (seldom) or 24-h per day schedule in the case of eight fractions; PDR afterloader). For the calculation of the fractionated HDR and PDR schedules to be equivalent to LDR in tumor effect, the linear-quadratic (LQ) model was used in an incomplete repair formulation (for details, see section 2.2.2). The advantages of fractionated HDR and/or PDR brachytherapy over LDR are summarized in table 1.

The reasons for the implementation of two afterloading machines in conjunction with the different types of fractionation schedules are summarized in table 2. The choice of when to use which afterloading machine is somewhat arbitrary; however, given the potentially significant differences in biological outcome, the choice was made at least in a structured (protocolized) fashion. In summary: when the microSelectron-PDR is available, our preference will be the PDR schedule ('small fraction size' and potential for continuation of the irradiation over the weekend); if the PDR afterloader is connected to another patient or if it is felt that clinically and/or technically the patient (i.e., implant) is more suitable for fractionated HDR, we opt for the microSelectron-HDR (for details, see section 2.3).

Of course, not every department can implement (afford) two types of afterloading machines, in particular if the brachytherapy caseload is relatively small (e.g.  $\leq 100$  cases/year). As, logistically and biologically speaking, the fractionated HDR and

**Table 2:** Considerations that might favor having two afterloaders (e.g. microSelectron HDR and PDR) in conjunction with two different types of fractionation schedules – two fractions per day (daytime regimen, fractionated HDR), or eight fractions per day (24-h regimen, PDR) – in a single radiation therapy department (for details, see text).

Choice of afterloader	Rationale
HDR	<p>Some tumor sites benefit typically from an HDR single-fraction treatment (e.g. palliation in carcinoma of bronchus, oesophagus).</p> <p>With integrated brachytherapy unit, HDR afterloader is essential.</p> <p>From clinical experience, some implants (i.e. patients) are not suitable for a 24-h PDR schedule (implant technical and/or medical reasons, e.g. implants of the brain or nasal vestibule).</p> <p>Medical/physics support off-hours regarding safety precautions favor daytime HDR (depending also on national regulations).</p> <p>Brachytherapy on outpatient basis favors daytime HDR.</p>
PDR	<p>If HDR is radiobiologically more permissive regarding late side-effects, strong fractionation can be of importance (in fact, the use of small fractions, e.g. 1-3 Gy, with short intervals, e.g. 1-3 h has been proposed (PDR)). In cancer of the head and neck, in the great majority of cases BT is given as a boost; this also means that the potential for arriving at late side-effects if strong fractionation is of importance is somewhat minimized (the dose by BT is approximately ‘one-third’ of the treatment).</p> <p>For some (volume) implants, when using small fractions, transit times of high-activity point source (e.g. 100-400 GBq) are short; therefore, in the case of PDR (small fraction size), weaker point source (e.g. 37 GBq) needed.</p> <p>Surgical demands might force brachytherapy procedure into end of week; because HDR afterloader can only be used at daytime during week days, fractionated HDR brachytherapy as opposed to PDR sometimes cannot start until after the weekend.</p>
HDR and PDR	Large and variable brachytherapy caseload.

PDR schedules are quite different types of brachytherapy treatments, we hope that at some point in the near future we will be able to arrive at some kind of conclusion

which can contribute to making the ‘right’ departmental choice as to which fractionation schedule (and type of afterloader) is to be preferred (see also section 2.2.2).

### *2.2.2 Radiobiological considerations and dose fractionation for fractionated HDR and PDR schedules*

The incentive to initiate fractionated HDR and/or PDR brachytherapy, and to test its feasibility as a replacement for ‘classical’ LDR BT, is the wish to combine the (mainly radiobiological) advantages of LDR BT with the (mainly physical and socio-economic) advantages of modern HDR afterloaders, as summarized in the previous section. The conditions under which PDR BT may simulate LDR BT are being investigated in experimental models, both in vitro and in vivo in different laboratories [1]. This section deals with the choice of treatment schedules for fractionated HDR (with two fractions per day) and for PDR BT (with more than two fractions per day) as alternatives to ‘classical’ LDR treatments.

#### *2.2.2.1 Radiobiological model*

The model which is used to calculate fractionated HDR and PDR schedules is the linear-quadratic model in an incomplete-repair formulation as given by Brenner and Hall [2]. As stressed by these authors, the model is essentially based on the formalism described by Lea and Catcheside, published more than 50 years ago [3]. For a full description of the model, the reader is referred to the paper of Brenner and Hall [2]; only the main features are summarized here. The expression used for the survival of clonogenic cells is the familiar linear-quadratic one [4,5]. In order to take into account incomplete repair of sublethal damage, either during LDR irradiation or in the (limited) time between HDR/PDR fractions and during the (finite) duration of each radiation fraction, the quadratic term in the expression for the surviving fraction  $S(D)$  after a dose  $D$  is assumed to be reduced by a factor  $G$ :

$$S(D) = \exp(-\alpha D - G\beta D^2) \quad (1)$$

Brenner and Hall [2] have given the expressions for two specific cases of interest, that is, LDR BT with a continuous irradiation and PDR BT with a series of equal fractions at equal intervals. The expression for LDR irradiation is identical to the one given by Dale [6] and Thames et al. [7]. Treatment schedules with varying pulse

intervals or combinations of different treatment schedules can also be evaluated. In order to compare treatment schedules for clinical practice, the results of model calculations are usually expressed in the quantity:

$$BED = \frac{\ln S}{\alpha} \quad (2)$$

This quantity (with the unit dose) was designated by Barendsen [4] as the ETD (Extrapolated Target (or Tolerance) Dose) and by Fowler [8] as the BED (Biologically Effective Dose). We follow the latter nomenclature here. Apart from comparing treatment schedules in terms of survival level, the effect of a treatment can also be expressed in terms of Tumor Control Probability (TCP) or, if normal tissue effects are concerned, in Normal Tissue Complication Probability (NTCP). These quantities have the advantage of being directly related to data obtained from clinical studies, i.e. local control probability and complication probability. The TCP/NTCP model is based on the assumption that the probability of local control follows Poisson statistics, i.e. is an exponential function of the mean number of surviving clonogenic cells ( $N_s$ ) after treatment:

$$TCP = \exp(-N_s) = \exp(-N_0 S) = \exp(-N_0 \exp(-\alpha BED)) \quad (3)$$

where  $N_0$  is the average initial number of clonogenic cells. Regarding the probability of normal tissue complications the analogous quantity could be the number of ‘functional subunits’ without which the organ would lose its function.

In order to derive clinical HDR or PDR BT schedules we have applied the following procedure. Because more clinical data are available for external radiotherapy (ERT) it seems adequate to choose an ERT schedule as a reference schedule, giving one fraction of 2 Gy per day and five fractions per week. As a practical example, we will study a case in which a BT boost has to be given which should be equivalent in tumor effect to an ERT schedule of 11 fractions of 2 Gy, i.e 22 Gy physical dose. As we are dealing with the replacement of LDR BT schedules, subsequently LDR schedules equivalent to this reference ERT schedule were calculated. It should be stressed that we consider two treatment schedules ‘equivalent’ if both have the same BED value for a specific end-point (tumor effect or normal-tissue effect). That means that we have not applied the additional condition that the total physical dose and/or the overall time of a PDR treatment must be identical to the values for the corresponding LDR treatment regime. This additional condition was applied in proposals for PDR schedules by Brenner and Hall [2] and by Fowler [8]; however, we see no

**Table 3:** Values used for the model parameters.

Parameter	Type of effect	Value
LDR dose rate		50 cGy h <sup>-1</sup>
$\alpha/\beta$	Early effect / tumor	10 Gy
	Late effects	3 Gy
$\alpha$		0.3 Gy <sup>-1</sup>
Half-time of repair of sublethal damage	Early effect / tumor	1.0 h
	Late effects	3.0 h

significant reason why (slight) variations in physical dose and overall time between PDR and LDR BT schedules should not be allowed for. A longer overall treatment time might lead to an increased risk of tumor cell repopulation, but for the rather short treatment schedules in BT (mostly not longer than 1 week), the probability of increased tumor repopulation seems limited.

The BED of an LDR schedule is determined using:

$$BED = D \left[ 1 + \frac{2D}{\mu T \alpha / \beta} \left( 1 - \frac{1}{\mu T} [1 - \exp(-\mu T)] \right) \right] \quad (4)$$

The model parameters used are given in table 3. For the LDR schedules a constant dose rate of 50 cGy/h was taken. In our case, an LDR schedule of 46.3 h application time (physical dose 23.2 Gy) should have a tumor effect equal to that of the reference ERT schedule of 22 Gy. To determine an equivalent HDR or PDR schedule, first a fraction size and a fixed interfraction interval are chosen and the number of fractions can then be calculated, yielding a BED closest to the BED of the reference LDR schedule. The results are also shown in table 4.

It can be observed that this approach results in different physical doses, i.e. with the LDR schedule a physical dose of 23.2 Gy is given, and with the fractionated HDR schedule a lower dose of 21 Gy, while for the PDR schedule a somewhat higher dose of 24 Gy is applied.

#### 2.2.2.2 Effects of different repair half-times and of different $\alpha/\beta$ values

The values of the LQ parameters and the repair time constant used in the calculations are given in table 3. Unfortunately, limited data are available for human tumors and

**Table 4:** Fractionation schedules for fractionated HDR treatments (i.e. two HDR fractions per day with a minimum interval of 6 h) and PDR treatments (continuous treatment with a constant time interval of 3 h between pulses). (The schedules are intended to be equivalent in terms of tumor effect, applying the parameters as listed in table 3).

ERT dose (reference)	11 x 2 = 22 Gy
BED	26.4 Gy
Equivalent LDR (50 cGy h <sup>-1</sup> )	46.3 h = 23.2 Gy
Fractionated HDR (2 fractions/day) N x d = D	7 x 3.0 = 21.0 Gy
BED	27.1 Gy
PDR (3-h interval) N x d = D	24 x 1.0 Gy = 24.0 Gy
BED	27.0 Gy

normal tissues and, furthermore, a large variation can be expected for different tumors. Brenner and Hall [2] presented the following values (arithmetic mean  $\pm$  SD) for a set of 36 human cell lines in vitro:  $\alpha = 0.36 \pm 0.21 \text{ Gy}^{-1}$ ,  $\alpha/\beta = 7.3 \pm 5.4 \text{ Gy}$ , repair half-time ( $T_{1/2}$ ) =  $0.54 \pm 0.91 \text{ h}$ . The human data regarding recovery capacity ( $\alpha/\beta$ ) and repair kinetics ( $T_{1/2}$ ) have been reviewed by Thames et al. [7]. The results show that the differences observed for  $\alpha/\beta$  between early and late effects in animals also hold for humans; for early reactions  $\alpha/\beta$  is in the range 7 to 11 Gy and for late reactions  $\alpha/\beta$  is in the range 2 to 4 Gy. Data on repair kinetics are scarce, but the available data indicate that repair in human normal tissues might be slower than in rodents. For early skin reactions the repair half-time is about 1 h, whereas for late teleangiectasia it may be as long as 3 h. Pop et al. [9] have pointed out that, from the available clinical experience with head and neck cancer treatments with LDR brachytherapy on the one hand and with ERT on the other hand, constraints can be derived for the possible values of the repair half-times. The assumption of a long repair half-time (i.e.  $\geq 3 \text{ h}$ ) in combination with a high dose of LDR brachytherapy would lead to extremely high BED values which are rather improbable. Due to the uncertainties, the choice of a single set of parameters is necessarily rather arbitrary. Therefore we have chosen not only to calculate equivalent schedules for a chosen ‘plausible’ set of parameter values but also to evaluate the effects of varying the parameter values over a wide range.

For this purpose an approach proposed by de Boer [10] has been followed. By calculating equivalent HDR or PDR schedules for a large range of values, graphical ‘maps’ of the PDR/LDR dose ratio can be constructed as a function of the  $\alpha/\beta$  ratio

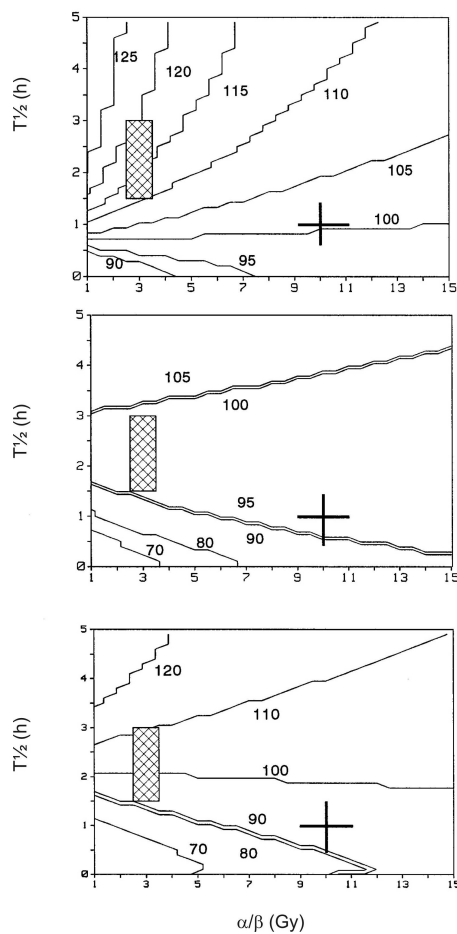


**Figure 1:** Ratio of total PDR (or fractionated HDR) dose to LDR dose as a function of  $\alpha/\beta$  (Gy) and the half-time for repair of sublethal damage ( $T_{1/2}$  in h) for different HDR/PDR schedules. The reference LDR schedule is the same for all three panels: 23.2 Gy in 46.3 h (i.e. a dose rate of 50 cGy  $h^{-1}$ ); this reference LDR schedule is a boost schedule, intended to have tumor effect equal to an ERT schedule of 22 Gy in 11 fractions of 2 Gy. Over the area of the 'map' the PDR or fractionated HDR dose has been calculated which would give an effect equal to that of the reference LDR schedule. Upper panel: PDR schedule with a time interval of 3 h between fractions and a fraction dose of 1.0 Gy. Central panel: 'daytime PDR' schedule applying 4 fractions of 2 Gy per day, with a time interval of 3 h between fractions. Lower panel: fractionated HDR schedule with 2 fractions of 3.0 Gy per day, with a time interval of 6 h between the two fractions on the same day. The hatched regions indicate parameter ranges considered plausible for early effects ( $\alpha/\beta$  of about 10 Gy) and late effects ( $\alpha/\beta$  of about 3 Gy), with repair half times varying, respectively, from 1 to 3 h and from 1.5 to 3 h.

(figure 1, horizontal axis, ranging from 1 to 15 Gy) and the repair half-time (figure 1, vertical axis, ranging from 0.1 to 5 h). For each 'map' a specific LDR reference schedule is used, e.g 23.2 Gy given in 46.3 h, with a dose rate of 50 cGy/h. Next, a specific equivalent schedule (fractionated HDR or PDR) is chosen by specifying the fraction dose and the interval between fractions. For each combination of  $\alpha/\beta$  and  $T_{1/2}$  values, the number of fractions is calculated, giving an effect equal to that of the LDR schedule (i.e. equal BED values). The curves in figure 1 represent the ratio of the PDR and LDR doses, expressed in percentages.

These ‘maps’ of the PDR/LDR dose ratio can be utilized to estimate the effect of different values for  $\alpha/\beta$  and  $T_{1/2}$  : if the PDR/LDR dose ratio is increasing going from tumor effects ( $\alpha/\beta = 10$ ) to late effects ( $\alpha/\beta = 3$ ), this means that the chosen schedule can be considered ‘safe’, because the late effects in normal tissues appear not to be dose limiting. If, however, the PDR/LDR dose ratio is decreasing going from tumor effects to late effects, one should be cautious because late responding normal tissues may be overdosed, i.e the probability of late effects in normal tissues may increase compared to the reference LDR treatment schedule.

In figure 1 PDR/LDR dose ratio maps are shown (see legend to figure 1). Plausible ranges for the values of  $\alpha/\beta$  and  $T_{1/2}$  are indicated by a cross mark and hatched rectangular areas, respectively: for early effects (including tumor effects)  $\alpha/\beta$  is taken to be 10 Gy and  $T_{1/2}$  is taken to be 1 h, as indicated by the cross mark. For late effects we assume that  $\alpha/\beta$  will be about 3 Gy and  $T_{1/2}$  slightly longer or equal to the value for early effects, i.e. a range of 1.5 to 3 h. From figure 1 one can conclude that when choosing a PDR schedule with equal tumor effect, the PDR/LDR dose ratio is somewhat higher than 100 %, depending on the value of  $T_{1/2}$  chosen. In other words, depending on the assumptions for the values for  $\alpha/\beta$  and  $T_{1/2}$ , the total dose of the PDR schedule is somewhat larger than that of the reference LDR schedule for an equal tumor effect. With regard to late effects in normal tissues, the PDR/LDR dose ratio for these PDR schedules varies from 110% to 120%. This seems satisfactory: the PDR/LDR dose ratio for late effects is higher than for tumor effects and therefore with this type of PDR schedules late effects in normal tissues appear not to be dose limiting. In the central and lower panels of figure 1 similar dose ratio maps are shown for schedules with fewer fractions, i.e. ‘daytime PDR’ schedules (four fractions of 2 Gy during daytime) and fractionated HDR schedules (two fractions of 3 Gy per day), respectively. It can be concluded that with less fractionation the dose ratio for late effects becomes closer to the dose ratios for early (tumor) effects, but even for the HDR schedule, there are no indications for overdosing late-responding normal tissues.

A general trend in these maps is that, provided that the repair half time for late effects is equal to or longer than that for tumor effects, the dose ratio for late effects is equal or greater than the dose ratio for early effects. The (PDR/LDR) dose ratios for late effects will decrease if the repair half-time for late effects is smaller than for tumor effects. However, current radiobiological data for repair kinetics point to longer repair times for late normal tissue effects [11-13].



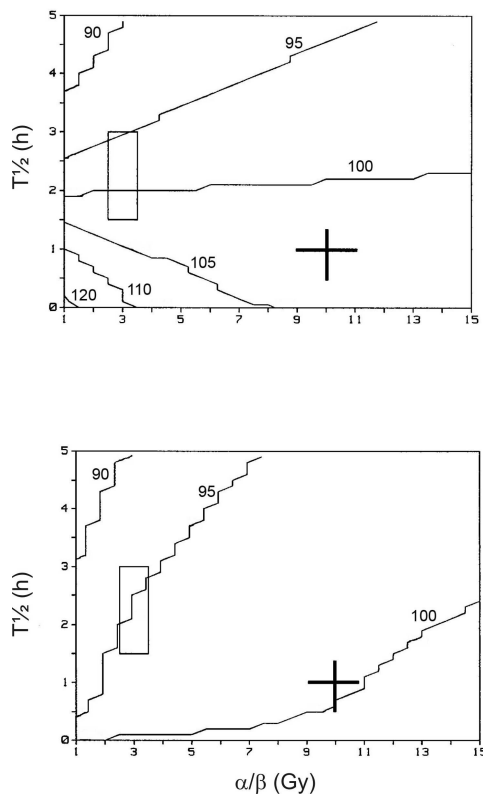


**Figure 2:** Ratio of total dose for a combined ERT + BT schedule and a treatment schedule using ERT alone, as a function of  $\alpha/\beta$  (Gy) and the half-time for repair of sublethal damage ( $T_{1/2}$ , in h) for two different BT schedules, i.e. fractionated HDR and PDR. The reference ERT schedule is 35 fractions of 2 Gy in 7 weeks. The ERT series in the combined treatment is 23 fractions of 2 Gy. For each combination of  $\alpha/\beta$  and  $T_{1/2}$  the number of fractions of the BT schedule (fractionated HDR or PDR) is calculated which would have a BED equal to that of the reference ERT schedule. Upper panel: a PDR schedule with a time interval of 3 h between fractions and a fraction dose of 1.0 Gy. Lower panel: a fractionated HDR treatment schedule applying 2 fractions of 3 Gy per day, with a time interval of 6 h between fractions.

### 2.2.2.3 Overall effect of external radiotherapy (ERT) and a brachytherapy (BT) boost

It should also be kept in mind that in clinical practice the majority of patients receiving some form of BT are treated with a combination of ERT and BT. This will dilute the potential differences between fractionated HDR, PDR and LDR, in particular in terms of risks of normal-tissue complications. This effect has been investigated in figure 2, where again dose ratio maps have been calculated, this time for the ratio (ERT+BT)/ERT, i.e. a combined treatment schedule in comparison to external-beam treatment alone.

The reference ERT schedule is 35 fractions of 2 Gy given in 7 weeks. In the combined schedule an ERT series of 23 fractions of 2 Gy is followed by a brachytherapy boost (see also the legend to figure 2). It can indeed be observed that the differences between the two brachytherapy regimes tend to be smaller in the combined treatment, i.e., the dose ratio for late effects for both HDR and PDR schedules is less than 5 % lower than the dose ratio for early effects (at the cross mark).

**Table 5:** Table of reference (in Gy) for fractionated HDR (fr.HDR) and PDR brachytherapy from 1991 to 2000.

Tumor site	EBRT	BED	LDR	BED	fr.HDR	BED	PDR	BED
equivalent								
<i>BT as full course:</i>								
Nasal vestibule T1	50	60	52.5	60	16 x 3	61.9		
Nasal vestibule T2,3	54	64.8	56.7	64.8	17 x 3	65.7		
Any other site T1,2	66	79.2	69.3	79.2	20 x 3	77.3	44 x 1.5	78.3
Any other site T3,4	68	81.6	71.4	81.6	21 x 3	81.2	46 x 1.5	81.9
Re-irradiation	58	69.6	60.9	69.6	18 x 3	69.6	39 x 1.5	69.4
<i>BT as boost:</i>								
Nasopharynx								
After 60Gy EBRT	20	24	21.1	24	6 x 3	23.2		
After 70Gy EBRT	14	16.8	14.8	16.8	4 x 3	15.5		
Any other site								
T1,2 after 46Gy EBRT	22	26.4	23.2	26.4	7 x 3	27.1	24 x 1	27
T3,4 after 46Gy EBRT	26	31.2	27.4	31.2	8 x 3	30.9	26 x 1	29.2

Total number of fractions for cancer of the nasal vestibule and other tumor sites relative to T stage. Full course: radiation is only given by means of brachytherapy. In the case of booster doses, generally 46/2 Gy are given by means of external beam radiation therapy (EBRT). The booster dose for cancer in the nasopharynx is given after either 60/2 Gy ERT (endocavitary brachytherapy 6x3 Gy) or 70/2 Gy ERT (endocavitary brachytherapy 4x3 Gy).

## 2.2.3 Dose fractionation: table of reference, fractionated HDR and PDR

As already mentioned, for each fractionation schedule (fractionated HDR or PDR) the fraction size, interfraction interval, and total number of fractions are fixed. We had chosen at the time first to tailor the total dose of brachytherapy according to T-stage (T1/2 versus T3/4). In case of re-irradiation, we have deliberately coned down the dose up-front, because it was felt from previous experience that we are only

**Table 6:** Table of reference (in Gy) for fractionated HDR (fr.HDR) and PDR brachytherapy as of 2001.

Tumor site	fr.HDR	PDR	SRT*
<i>BT as full course:</i>			
Nasal vestibule, Skin, Lip	4+12x3+4		
One-plane implant: microscopic disease	4+12x3+4	2.5+29x1.5+2.5	
Any other site T1-4	4+16x3+4	2.5+38x1.5+2.5	6x6
Re-irradiation nasopharynx	15x3		
Re-irradiation other tumors	4+15x3+4	2.5+35x1.5+2.5 (preference)	
<i>BT as boost:</i>			
Nasopharynx			
After 60Gy EBRT	4+3x3+4		
After 70Gy EBRT	4+3+4		4x2.8
Re-irradiation after 46 Gy EBRT	6x3		
One-plane implant: microscopic disease			
After 46Gy EBRT	4+3+4	2+8x1+2	
Any other site T1-4			
After 46Gy EBRT	4+4x3+4	2+18x1+2	3x5.5

*Total number of brachytherapy fractions. Full course: radiation is only given by means of brachytherapy. In the case of booster doses, generally 46/2 Gy are given by means of external beam radiation therapy (EBRT). The booster dose for cancer in the nasopharynx is given after either 60/2 Gy EBRT or 70/2 Gy EBRT. \*SRT means a booster dose by stereotactic radiation therapy (using the Cyberknife as of 2005).*

alleviating symptoms, i.e., we are aiming for (temporary) local-regional control as only rarely can patients be cured [14,15]. For cancer of the nasal vestibule, due to the severe acute (skin) reactions caused by brachytherapy (with tumors located in the skin) with otherwise excellent local control rates, we also lowered the total dose somewhat. Table 5 summarizes the fractionation regimens in use as of January 1995 until 2000. As of 2001 we have again slightly modified our brachytherapy schedules (table 6). This was done after rigorous evaluation of the clinical results, including side effects. The main changes have been to fix the total dose irrespective of T stage. A second change was to add 1 Gy to the first and last fraction of the BT scheme used. This was based on a concept at the time proposed by Brenner et al. [16].

## **2.3 Brachytherapy techniques and clinical results**

### *2.3.1 Introduction: clinical brachytherapy*

For afterloading fractionated HDR or PDR brachytherapy, either commercially available standard afterloading catheters (outer diameter 2 mm), in the case of interstitial implants, or a mould technique, for example in the case of cancer in the nasal vestibule and nasopharynx, are used. In general, brachytherapy techniques are not (very) dissimilar to those used for LDR. The following paragraphs briefly summarize some relevant aspects of our techniques, dosimetry guidelines, and clinical results in different clinical sites in the head and neck.

### *2.3.2 Base of tongue: technique of interstitial volume implant*

Implants of the base of tongue (and mobile tongue) are interstitial volume implants. The dose specification of these implants can be considered as a variation of the well-known Paris System used for LDR treatments. That is, we specify the dose as being 85% of the average dose in the local minima of the central plane. When treating this type of implant with an HDR or PDR afterloader using a single stepping-source, a dwell position separation of 5 mm is chosen. A sagittal view of a base of tongue implant is shown in figure 3 (taken from reference 17).

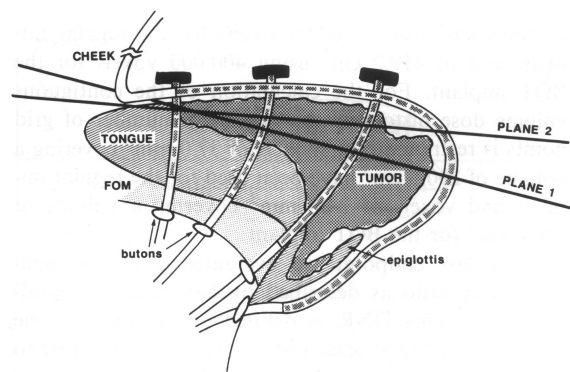


**Figure 3:** Schematic view of the sagittal plane of a base of tongue implant, showing a catheter running partly over the dorsum of the tongue as well as catheters sutured to this so-called looping catheter.

This type of implant usually consists of three sagittal planes, each containing a 'looping' catheter running over the dorsum of the base of tongue and two or three blind ending catheters with buttons sutured to the looping catheter. After reconstruction from orthogonal radiographs, a central plane is chosen more or less perpendicular to the main direction of the blind-ended catheters through the center of the active part of the implant, as indicated in figure 3. The minimal dose in the central plane will, in general, be located in the geometric centers of triangles which are constructed from the intersections with the catheters. These centers of the triangles are used as reference points and are designated as 'basal dose points.' The reference dose is specified as 85% of the average dose in the basal dose points. In order to increase the dose uniformity, the dose distribution is optimized using geometric optimization, i.e., the volume mode [17,18]. In this optimization method, the dwell time in a dwell position is inversely proportional to the dose contribution from all other dwell positions except the ones in the same catheter [19-21]. This optimization method is sensitive for deviations in spacing and/or divergence of catheters. An example of the result is presented in figure 4 (taken from reference 17), showing a sagittal view of an optimized and a non-optimized dose distribution of the base of tongue implant. After geometric optimization, the overdosed region receiving at least 200% of the reference dose is reduced, especially at the intersection of the blind-ended catheters and the looping catheter.

Base of tongue cancers are, in general, treated with a combination of a volume implant of the base of tongue and an external radiotherapy dose of 46 Gy (conventional fractionation) to the base of tongue and neck. In case of positive neck nodes,

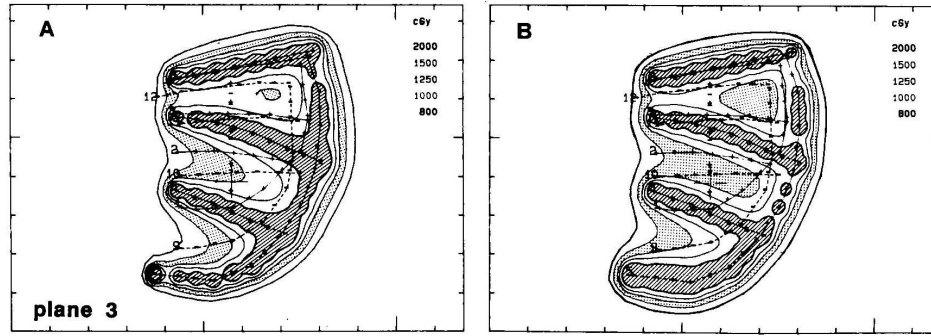


**Figure 4:** Sagittal plane through middle catheter running over dorsum of base of the tongue: (a) non-optimized and (b) optimized dose distribution.

the external radiotherapy of the neck is followed by a therapeutic (radical) neck dissection at the time of the implant. With regard to dose fractionation of base of tongue implants, the reader is referred to the guidelines given in table 6. For results, the reader is referred to references 22 and 23.

Current treatment schedule (as of January 2001) for all T-stages (T1-4): external radiotherapy 23 x 2 Gy. Brachytherapy in case of fractionated HDR 4Gy+4x3Gy+4Gy (total dose 20 Gy; 2 fractions per day) or PDR: 2Gy+18x1Gy+2Gy (total dose 22 Gy; 8 fractions per day).

### 2.3.3 Nasal vestibule: technique of interstitial single-plane implant

Although technically not obligatory, in the DDHCC, general anesthesia is preferred when implanting the nasal vestibule. After decongestion of the nose (R/xylometazoline), the points of entry for the trocar are demarcated on the skin. A hollow, stainless-steel guide needle and trocar are introduced interstitially. After removal of the trocar, afterloading catheters are inserted approximately 4 cm into the guide needle; subsequently, the guide needle is removed. Currently we have slightly modified the technique. That is, we introduce a solid stainless needle approximately 4 cm to create a 'channel'. After removal of the needle one then immediately introduces the afterloading catheter in the puncture 'guide channel'. Catheters are fixed and sutured to the skin by standard buttons. The number of catheters (generally four to five) is defined by the target volume. If the tumor is extending into the upper lip, an extra catheter is inserted 'horizontally' through the lip.

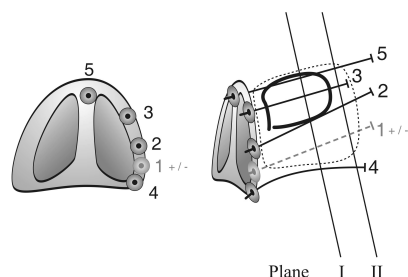


**Figure 5:** Schematic diagram of an interstitial implant in the nasal vestibule. (See also corresponding X-ray films in figure 6). The stippled zone represents the planning target.

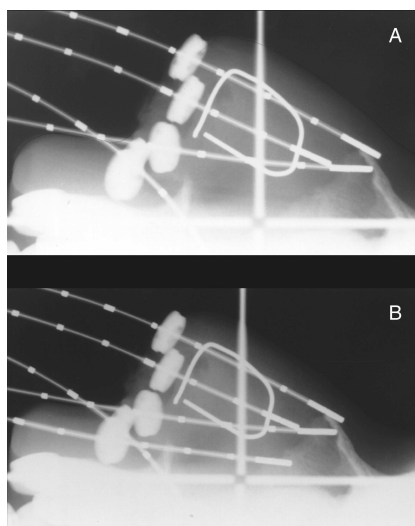


**Figure 6:** Lateral X-ray films of a patient with an interstitial implant in the nasal vestibule (left ala). During the operation, it was realized that the implant with four catheters (A) was suboptimal in terms of anticipated dose distribution. Subsequently, an extra catheter was implanted (B). Lead demarcation visualizes tumor core lateral surface nose (skin).

Due to the anatomy of the nose *per se* and the geometry of the target, the catheter separation frequently varies over the target volume after implantation (figure 5). The geometrical configuration of the implant is visualized on orthogonal X-rays postimplantation (or on the image intensifier in the Integrated Brachytherapy Unit (IBU), see section 2.4), with the patient still under general anesthesia. If the dose distribution of the implant is not satisfactory (i.e., anticipated coldspots and/or hotspots), additional catheters can be introduced (figure 6). The dose is usually prescribed in so-called dose points at a distance of 0.5 cm from the catheters. This clinical example demonstrates the advantage of optimization (compare B and C to A, and D to E in planes I and II of figure 7); however, it also demonstrates that, even with optimization, a 'poor' implant can never become a 'good' implant (compare A and C in planes I and II). After optimization of the implant (figure 7), fractionated HDR is applied.

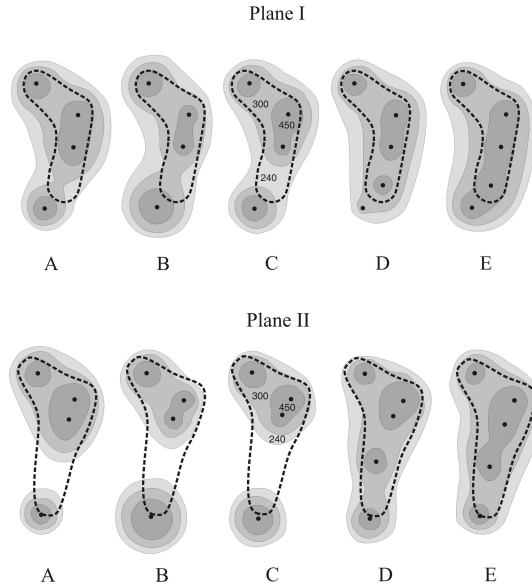


**Figure 7:** As an example, planes I and II were taken through the periphery of the target (See also the legend for figure 6). Five types of dose distributions (A, B, C, D, and E) are compared. A: dose distribution with four catheters - constant dwell times and dwell positions (= non-optimized, 'LDR equivalent'); B: dose distribution with four catheters, geometrically optimized; C: dose distribution of four-catheter implant, optimized on dose points 0.5 cm from catheters; D: dose distribution of five-catheter implant, optimized on dose points 0.5 cm from catheters; E: dose distribution with five catheters, constant dwell times and dwell positions (= non-optimized, 'LDR equivalent'). Fraction size was 300 cGy (fractionated HDR schedule).

Current treatment schedule for all T-stages as of January 2001 is: fractionated HDR 4Gy+12x3Gy+4Gy (total dose 44 Gy; 2 fractions per day), see table 6. Moreover, the mould technique (see section 2.3.5) has been abandoned and only an implant using standard afterloading catheters is being used.

In cancer of the nasal vestibule, only very rarely is the neck involved (less than 10%); we therefore do not treat the neck electively [24].

#### 2.3.4 Clinical results: nasal vestibule interstitial brachytherapy

The clinical results of interstitial radiation therapy to nasal vestibule are extremely rewarding in terms of local regional control as well as cosmesis. In short: from 1991 to 2005 64 patients were implanted; four local failures were seen with all failures



surgically salvaged. A recent objective evaluation by a panel regarding cosmesis demonstrated excellent results in 90% of the cases [25].

### 2.3.5 Nasal vestibule: mould technique

In selected cases (e.g., contraindication for general anesthesia, small and very superficial lesions of the mucosal lining of alae or septum, patient preference), a mould technique can be used. After topical anesthesia of the nasal vestibule, the hair in the nasal cavity (nostrils) is cut away and posteriorly the nasal airway is blocked by a cotton-wool plug. Subsequently, an impression is made with alginate material (R/CA 37 superiorpink). From this provisional model a 'negative impression' of plaster of Paris is constructed. Three flexible aluminium wires (outer diameter 2 mm)

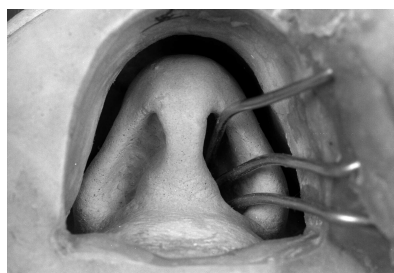


**Figure 8:** Plaster of Paris mould of carcinoma in the nasal vestibule ('negative' impression) with aluminium wires (outer diameter 2 mm) in situ. Subsequently, the definitive 'positive' silicone mould is manufactured with the aluminium wires replaced by afterloading catheters (see figure 9) The mould is placed in situ and held by a head strip (cord) during the irradiation. Dosimetry and dose prescription are similar to interstitial implant of the nasal vestibule.

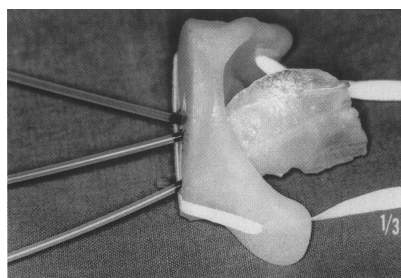


**Figure 9:** Final silicone mould for carcinoma of the nasal vestibule suitable for fractionated HDR brachytherapy on an outpatient basis. Three afterloading catheters are visible in the silicone mould.

are positioned and fixed into the plaster cast at the sites where afterloading catheters are to be positioned (see figure 8). Using this mould technique, about midway through the series of fractions, the insertion of the mould becomes painful and thus less accurate. In our center, therefore, the interstitial technique is definitely the technique of choice.

### *2.3.6 Tonsil and soft palate: technique of single-plane interstitial implant*

The implant of the tonsillar fossa and/or the soft palate can be performed as a single-plane or volume implant. Before embarking on such an implant, it is of paramount importance to investigate whether the target volume can be covered adequately by the implant. This means that computerized tomography (CT) and/or magnetic resonance imaging (MRI) of the tumor mass and neighboring structures (e.g., parapharyngeal space, nasopharyngeal side of the soft palate, retropharyngeal nodes etc. ) are mandatory. If the target is considered suitable for implantation, the primary visible lesion is tattooed under general anesthesia and/or marker seeds are implanted. The next question regards the neck. In case of bilateral N0 neck, for small tumors of the TF and/or SP the ipsilateral neck is treated electively by irradiation (46 Gy). In case of N+ neck, after 46 Gy an ipsilateral radical neck dissection is performed. The contralateral neck is treated only in case of primary tumor of the tonsil invading the tonsillar lingual sulcus or base of tongue, or in case of soft palate tumor surpassing the midline or when dealing with N2c, N3 disease.



**Figure 10:** Anteroposterior X-ray film of an interstitial implant in the tonsillar fossa and soft palate.

The implant *per se* is very straightforward. Basically, by means of hollow guide needles, catheters are introduced into the tonsillar fossa (anterior and posterior tonsillar pillars) and soft palate. In general, two to three parallel running catheters are needed (figure 10). The target is demarcated by permanent implantation of surgical clips or metallic seeds.

For dose prescription, dose points are positioned at a distance of 0.5-0.75 cm from the catheters and the implant is subsequently optimized. On rare occasions (e.g., retropharyngeal nodes) extra dose points can be positioned at specified locations. Tumors are treated by either fractionated HDR or PDR. (For the total number of fractions, see table 6).

### *2.3.7 Tonsil and soft palate: clinical results*

Results on tumor control, adverse late normal tissue sequelae, and functional performance in patients with tonsillar fossa and/or soft palate (SP) tumors have been recently published by Levendag et al. [26,27]. In short: Between 1986 and 2001, T1-T3 tonsillar fossa/SP tumors were treated using ERT to 46 Gy in 2-Gy fractions to the primary tumor and neck, followed by BT to the primary. Neck dissection was performed for node-positive disease (BT group; 104 patients). If BT was not feasible, patients underwent surgery and postoperative RT (PORT) to a dose of 50–70 Gy in 2-Gy fractions (surgery group; 86 patients). Local control, regional control, disease-free survival, and overall survival were determined. Late side effects were scored using the Radiation Therapy Oncology Group criteria. Univariate and multivariate Cox regression analyses were performed for regional failure (RF), with the parameters gender, age, site, TN stage, modality, dose, and overall treatment time. Recurrences in the contralateral neck were also related to significant ipsilateral involvement of the base of tongue and/or involvement of the SP crossing the midline. To determine the performance status scale scores and degree of xerostomia, a survey was conducted among patients living with no evidence of disease and a minimum of 2 years of follow-up. For that purpose, a research nurse interviewed patients regarding eating in public, normalcy of diet, normalcy of speech, and xerostomia. The tumor control rates after BT vs. surgery at 5 years were 88% vs. 88% for local control; 93% vs. 85% for regional control; 57% vs. 52% for disease-free survival; 67% vs. 57% for overall survival; and 5% vs. 6% for RF. No patient had RF in the contralateral untreated N0 neck (0 of 14 vs. 0 of 15). Multivariate Cox regression analysis for RF was statistically significant for Stage T2 vs. T3 (hazard ratio 0.09)

and for the dose to the neck >46 Gy (hazard ratio, 8.7; 95% confidence interval, 1.3–57.1). The significant late side effects in the BT group vs. surgery group were ulcer in 39% vs. 7% ( $p = 0.001$ ) and trismus in 1% vs. 21% ( $p = 0.005$ ). The performance status scale scores and response to questions regarding xerostomia for BT vs. surgery revealed no statistically significant differences for eating in public, normalcy of diet, normalcy of speech, and xerostomia. The mean visual analog score for xerostomia was 5.5 in the BT group vs. 6 in the surgery group. Excellent locoregional control was obtained in T1-T3 tonsillar fossa and/or SP tumors. The rate at 10 years was 84% (BT group) vs. 78% (surgery group). However, adverse late side effects were not negligible. In addition to modality-specific side effects (ulcer/trismus), both treatment groups were significantly affected by xerostomia. Only 6 recurrences (4%) were observed in the 149 electively treated contralateral necks, and no relapses were seen in the 29 untreated contralateral necks. We, therefore, suggest that it is not necessary to treat the contralateral neck, unless the tumor extends beyond the midline of the soft palate (uvula) or beyond the lateral one-third of the ipsilateral base of the tongue. Moreover, with the currently available CT-based neck level definitions, more conformal contours (i.e., tighter boundaries) around the clinical target volume can be designed. In this way, critical structures such as the temporomandibular joint and part of the pterygoid muscles can be avoided more easily. Also, when using highly conformal treatment techniques (e.g., intensity-modulated RT), one can further reduce the dose to the major salivary glands and oral mucosa. We believe these measures will lead to less trismus and less xerostomia.

As of January 2001, the treatment schedule has been slightly modified. For all T-stages (T1-4), a dose of 46 Gy by external radiotherapy is used. However, instead of five fractions we consistently used six fractions per week. Moreover, the ERT is given using IMRT techniques. Also the surdosage by brachytherapy for the primary consists of fractionated HDR 4Gy+4x3Gy+4Gy (total dose 20 Gy; 2 fractions per day). Or, in the case of PDR, 2Gy+18x1Gy+2Gy (total dose 22 Gy; 8 fractions per day).

### *2.3.8 Nasopharynx: technique of endocavitary brachytherapy*

As reported previously, in the case of cancer of the nasopharynx we treat the primary cancer by external radiotherapy, 6 fractions per week using IMRT techniques, to a dose of 70 Gy. Neck nodes are generally boosted to a dose of 70 Gy [28-32].

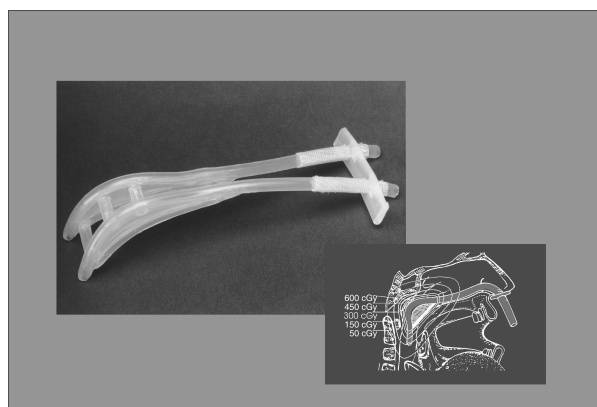


**Figure 11:** The silicone Rotterdam Nasopharynx Applicator: outer diameter 5.5 mm and inner diameter 3.5 mm.

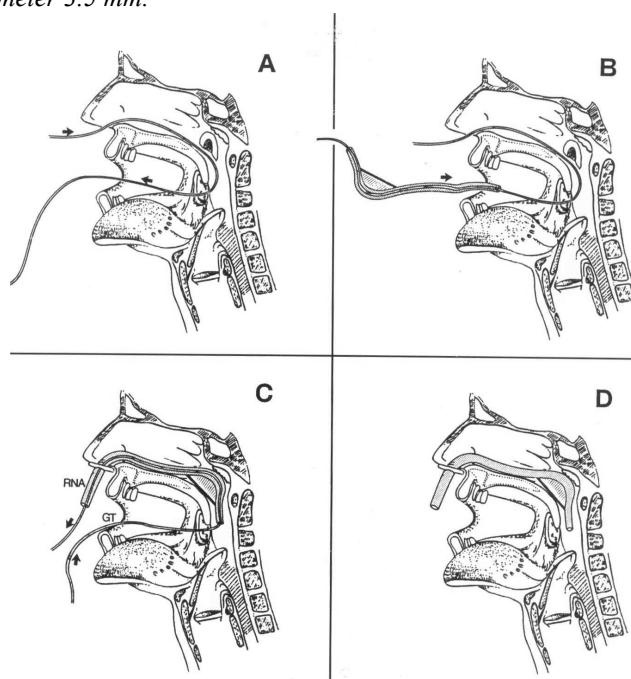


**Figure 12:** After decongestion (R/xylometazoline HCl 1%) and topical anesthesia (R/Concaine hydrochloride 7%) of the nasal mucosa and nasopharynx, guide tubes (outer diameter 2 mm) are introduced through the nose and exit through the mouth. The Rotterdam Nasopharynx Applicator (RNA) is guided intraorally over the guide tubes (GT) by pulling on the nasal part of the guide tubes. The applicator is finally placed in situ into the nasopharynx and nose. To facilitate positioning of the applicator into the nasopharynx, gently pushing the oral parts of the guide tubes intraorally using some standard type of forceps can sometimes be of additional help, as in C. By using a silicone flange, the Rotterdam Nasopharynx is secured in the correct position for the duration of the treatment, for example 3-4 days.

After completion of the external radiotherapy part of the treatment, a booster dose is applied by brachytherapy. With regard to the endocavitary brachytherapy, a silicone mould, the Rotterdam Nasopharyngeal Applicator (figure 11), is used for the treatment of the nasopharynx. Figure 12 shows schematically how this applicator is positioned. Planning of the brachytherapy treatment of the nasopharynx using the intracavitary mould is based on orthogonal radiographs. Patient points, representing tumor points and normal-tissue points, which will be used for dose optimization, are indicated on the lateral radiograph as indicated in figure 13. Following our protocol, the points are transferred to the anteroposterior (AP) radiograph at a prescribed distance from the midline.

Points are selected which should receive the reference dose. Usually, these are the nasopharynx points (Na) and the Rouviere node (R). The dose distribution is optimized such that these points receive the prescribed dose, i.e. an optimization on patient points [19]. If, during evaluation, the dose in specific points seems unsatisfactory, these points can be included in the optimization procedure as well. In that case,

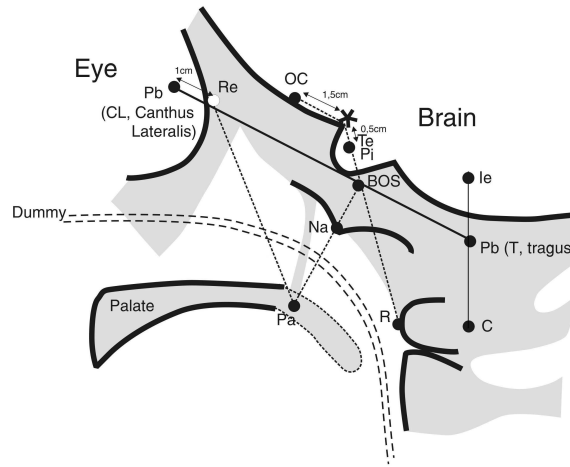


**Figure 13:** Schematic diagram of a lateral X-ray film of a patient with cancer of the nasopharynx and of the Rotterdam Nasopharyngeal Applicator in situ. Patient points - that is, normal tissue points (C: cord, Pi: pituitary gland, OC: optic chiasm, Re: retina, BOS: base of skull, Pa: palate, Te: temporal lobe, ie: inner ear) as well as tumor tissue points (Na: nasopharynx, R: node of Rouviere) - are indicated. For explanation see also table 7. The Pi, OC, R and C points are single midline patient points. Pa, BOS, Na, Te, Re and ie are bilateral points at 1, 1.5, 1.5, 2, 2.5 and 4 cm from the midline, respectively.

**Table 7:** Example of the planning of an endocavitary treatment of the nasopharynx.

Patient point	Percentage dose		
	Not optimized	Optimized on Na/R equal weighting	Optimized on Na/R/Pa variable weighting
Na-r	95.9	104.1	99.4
Na-l	104.1	95.9	100.6
C	51.2	36.0	31.7
R	207.8	120.6	103.8
Pi	25.6	26.4	21.9
Te-r	20.9	21.8	17.7
Te-l	21.9	21.9	18.5
OC	16.8	17.9	13.8
Re-r	24.7	27.7	17.4
Re-l	24.3	25.4	18.5
BOS-r	63.8	66.5	62.0
BOS-l	66.5	61.4	60.5
Ie-r	13.0	12.6	11.1
Ie-l	14.5	12.7	11.4
Pa-r	189.8	227.6	137.6
Pa-l	155.2	158.2	129.2

each patient point can be assigned a weighting factor for dose requirements. The planning procedure is illustrated by the example mentioned in table 7 [29].

Brachytherapy can be given on an outpatient basis in fractions of 3 Gy each, twice a day, with an interval of at least 6 h, using the HDR afterloader (see also table 5). Currently, as of 2001, using the UICC/AJCC 2002 classification system, the protocol for the brachytherapy boost has been slightly modified. For T1,2N0 tumors after external radiotherapy of 70 Gy a booster dose of 4Gy+3Gy+4Gy is given (total brachytherapy dose 11 Gy; 2 fractions per day). For good responding (that is response evaluated by means of MRI after a dose 40-46 Gy) T2b tumors, also a dose of 4Gy+3Gy+4Gy (total dose 11 Gy; 2 fractions per day) is given. Poorly responding T2b tumors and T3,4 cancers are preferentially treated by stereotactic radiation (using the Cyberknife as of 2005), i.e., by 4 fractions of 2.8 Gy.

### 2.3.9 Nasopharynx: clinical results

The clinical results have been published by Levendag et al. [33]. In short: Ninety-one patients with primary nasopharyngeal cancer, staged according to the 1997 UICC/AJCC classification system, were treated between 1991 and 2000 with 60–70 Gy external beam radiotherapy and 11–18 Gy ECBT. Of the 91 patients, 21 were treated in conjunction with CHT and 70 without CHT. Tumors were subdivided into undifferentiated (UD) and well, moderately, and poorly differentiated (WMP-D) subtypes. Treatment results were analyzed for local control (LC), disease-free survival (DFS), freedom from distant metastasis, and overall survival (OS). A univariate and multivariate Cox regression analysis found stage, treatment period, age, and grade significant for LC, DFS, and OS. At 2 years, for Stage I–IIB (1st period, 1991–1996), the LC, DFS, and OS were 96%, 88%, and 80%, respectively, vs. 65%, 46%, and 52% for Stage III–IVB. For the 2nd treatment period (1996–2000; CHT for Stage III–IVB), the LC, DFS, and OS at 2 years was 100%, 90%, and 61% (Stage I–IIB), respectively, vs. 86%, 74%, and 66% (Stage III–IVB). Three prognostic groups (PGs) were constructed. For the 1991–1996 period, at 2 years, patients in the good PG (UD Stage I–IIB disease) had 100% LC and 92% OS; those in the intermediate PG (UD Stage III–IVB or WMP-D Stage I–IIB), had 94% LC and 71% OS; and those in the poor PG (WMP-D Stage III–IVB) had 47% LC and 40% OS. For the 1996–2000 period, at 2 years, the good PG had 100% LC and 88% OS; the intermediate PG had 100% LC and 64% OS; and the poor PG had 71% LC and 60% OS. For Stage I–IIB disease treated between 1991 and 2000, at 3 years, the LC and OS was 97% and 67%, respectively. The results with 77–81 Gy without CHT warrant EBRT combined with ECBT to remain our standard of care for Stage I–IIB disease. For N2-3 and/or T3-4 tumors, in addition to high doses of RT, neoadjuvant CHT was administered as of 1996. For the 1991–2000 period, at 3 years, the LC was 86% and the OS was 72% with CHT, with little extra morbidity; they were 68% and 35% without CHT. Because of better target coverage and sparing, T3-4 tumors are currently boosted by stereotactic RT to 81.2 Gy.

### 2.4 Brachytherapy of the neck in an Integrated Brachytherapy Unit (IBU)

In October 1994, an IBU was installed in the DDHCC. At that time, the IBU was mainly used in attempts to improve on the quality of standard brachytherapy procedures; that is, the implant geometry was visualized (and/or changed) intraoperatively



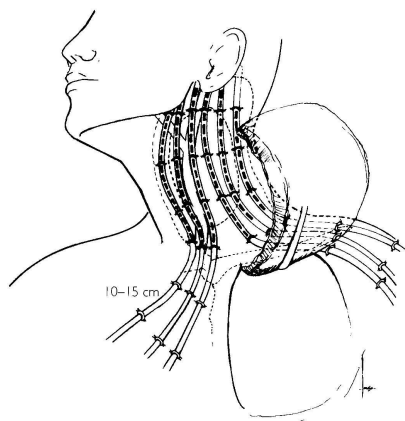


**Figure 14:** Schematic diagram of a single-plane implant in the neck using standard afterloading catheters (outer diameter 2 mm) sutured onto the soft tissues in the neck (tumor bed). The defect in the neck is reconstructed as a one-step procedure at the time of implantation. Catheters remain in situ for a number of days (3-10), depending on factors such as the condition of the patient, fractionation schedule, and total dose.

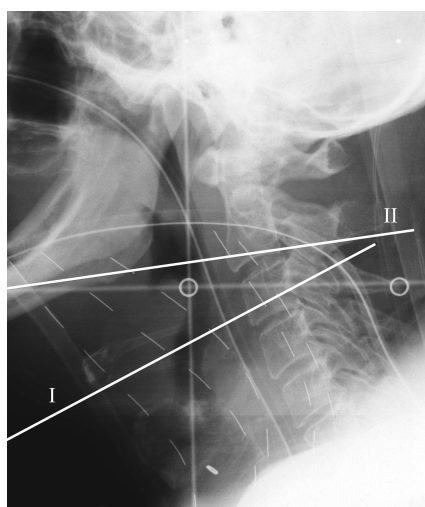


**Figure 15:** X-ray film of a single-plane implant tumor bed in the neck for re-irradiation by LDR brachytherapy in a patient with recurrent tumor after previous surgery and/or ERT. (See also the legend to figure 14.).

using fluoroscopy (see, for example nasal vestibule), and X-ray films for planning purposes were taken with the patient still under general anesthesia, thus reducing the 'time to start' of the actual irradiation. The next step was research and development of routine filmless planning, as discussed in chapters 5 and 6. The intraoperative brachytherapy procedure is illustrated by the following case report.

#### *2.4.1 Case report: re-irradiation of the neck*

Our experience with re-irradiation in cancer of the head and neck has been previously reported [34]. A variety of tumor sites, including the neck, appeared to have been re-irradiated by means of brachytherapy  $\pm$  external radiotherapy  $\pm$  surgery; 55%

of the patients obtained tumor control of the re-irradiated site. It was concluded that re-irradiation can be of benefit when pursuing long-lasting local-regional control and, in particular, the use of brachytherapy (albeit LDR at the time) was advocated. Regarding specifically the technique of implantation of the neck, after dissection the tumor bed was implanted using a variable number of catheters (usually six to nine) sutured onto the soft tissues in the neck (figures 14 and 15). As of 1990, similar techniques have been used for recurrent (after previous external radiotherapy and/or surgery) tumors in the neck in combination with fractionated HDR brachytherapy (total dose of fractionated HDR 54-60 Gy). In a preliminary analysis only four out of 13 (31%) had failed at the site of the fractionated HDR implant (data not published). Although these control rates seem satisfactory given the poor population subset, the procedure is laborious and, for the reconstructive surgeon, not particularly gratifying. This is partly due to the impediment of the implant *per se* at the time of the reconstructive procedure, to the catheters having to remain *in situ* for quite a number of days, with the potential risk for infections in the area of the newly reconstructed defect in the neck, as well as the risk of wound breakdown if, for technical reasons, the catheters have to be positioned (too) close to the covering skin (high skin dose; this, by the way, might also have implications regarding the type of reconstructive procedure chosen).

#### 2.4.2 Technical aspects of brachytherapy of the neck using a flexible intraoperative template

To eliminate the disadvantages of conventional implants of the neck by individual catheters (see figure 14), a novel technique was developed in our institution. In principle, it consists of a flexible silicone template to be used as a temporary single-plane

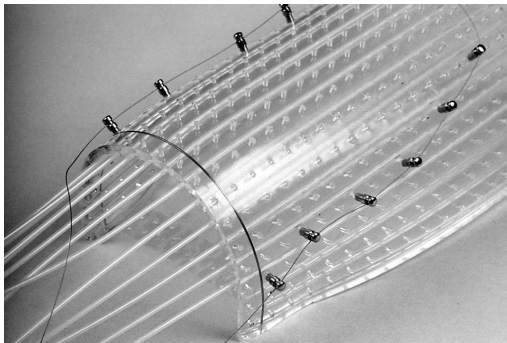


**Figure 16:** Photograph of a flexible intraoperative template with catheters and metallic buttons *in situ*, illustrating to some extent the flexibility in curvature and shape (silicone - easy to cut and bend) of the template.

implant intraoperatively. This silicone flexible intraoperative template has a thickness of only 0.5 cm (flexible), and can be easily cut into different shapes and sizes (custom made). In the center of the template, catheters are positioned 1 cm apart in prefixed channels (allowing for fixed spacing). In predetermined pinpoint holes (1 cm apart), metallic buttons can be introduced during the brachytherapy procedure to delineate to target when using fluoroscopy (figure 16).

If one combines the use of a flexible intraoperative template technique with an IBU, some extra advantages can be envisaged. First, the custom-made flexible intraoperative template is, in most cases, easily positioned (figure 17) and, after on-line computer planning, a single dose can be delivered intraoperatively using the HDR afterloader in the IBU with the patient still under general anesthesia. Second, after irradiation, the flexible intraoperative template is removed and reconstructive surgery can be performed without limitations due to the brachytherapy procedure *per se* (i.e., no remaining *insitu* catheters). Also, the covering skin is not at risk for too high doses of irradiation, i.e., there is less risk of wound breakdown. Finally, optimization of the dose distribution can be performed (see below).

#### 2.4.3 Case report: brachytherapy of the neck in an IBU using on-line planning and a flexible intraoperative template

Two patients presenting with a recurrent sarcoma in the neck serve as an example; the head and neck tumor board decided to re-resect the remaining tumor mass and irradiate the tumor bed intraoperatively by means of a flexible intraoperative template (delivering a single fraction of 10 Gy at 1 cm; see also figures 18 and 19),

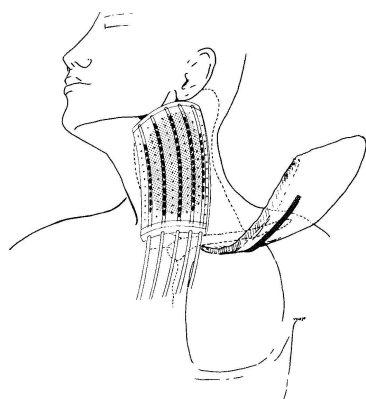


**Figure 17:** Schematic diagram showing a flexible intraoperative template for intraoperative re-irradiation of the neck (For explanation, see text. Compare also to figure 14.)



**Figure 18:** Photograph of neck dissection and a flexible intraoperative template *in situ* (including metallic buttons to demarcate target) in a patient with recurrent sarcoma in the right neck. (For explanation, see text).

followed by postoperative external radiotherapy (conventional fractionation of 2 Gy/day, total dose 46 Gy).

The technique of the brachytherapy procedure has been explained in section 2.4.2. The tailoring of the flexible intraoperative template itself, positioning of the template, the computer planning, and the actual irradiation took approximately 3 h. To demonstrate the advantage of optimized dose distributions using a flexible intraoperative template over a classical non-optimized LDR implant (in which catheters are sutured onto the tumor bed; see also figures 14 and 15), selected isodose patterns are compared in figure 20 (panels A-E) for different single-plane brachytherapy techniques. That is, typical examples are shown (in a central plane, I, as well as in a plane taken more in the periphery of the implant, II) for a non-optimized LDR implant (see also figure 20, panel A), for an implant optimized on dose points positioned at 1 cm from catheters (see also figure 20, panel B), for a dose calculation of ('standard') flexible intraoperative template (thus disregarding the possibly severe curvatures of a template in a real anatomical situation) optimized on dose points at 1 cm from the catheters with the dwell times transferred to the actual flexible intraoperative template (figure 20, panel C), for an optimized flexible intraoperative template used in the actual patient with dose points at 1 cm from catheters (figure 20, panel D), and, finally, for an optimized flexible intraoperative template as used for a typical situation with dose points at 1 cm in region 1 (e.g., at 'shallow depth') and dose points at 2 cm in region 2 (e.g., dose prescription to 'deeply located' dose points, for example due to anatomical constraints) (figure 20, panel E).

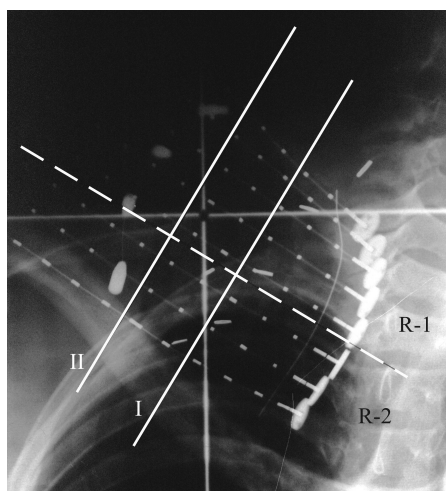


**Figure 19:** X-ray film of an implant in the neck using a flexible intraoperative template in an IBU (See also text and the legend to figure 29.).

In conclusion, in general, better dose distributions can be obtained with flexible intraoperative template as opposed to classical LDR catheter implants (compare panels A and B to C in figure 20). Also, a dose calculation using a standard flexible intraoperative template generates sufficiently adequate dose distributions as long as the curvature of the actual template is not too strong (compare also panel C to D in figure 20). In some instances, with a flexible intraoperative template one can even divert to dose points at different levels, thereby arbitrarily dividing the implant into different 'dose point regions' (panel E). As with data concerning other applications of intraoperative irradiation such as those generated by linear accelerators, we have to await and see whether, with the use of large, single fractions of brachytherapy, we will run into severe late side-effects.

## 2.5 Summary

Single stepping-source, computer-controlled afterloading devices have changed classical low dose-rate radiobiological thinking as well as the application techniques *per se* in brachytherapy considerably. In the Head & Neck Cancer Cooperative Group of the ErasmusMC / Daniel den Hoed Cancer Center, fractionated HDR or PDR brachytherapy schedules have been initiated and clinically tested since August, 1990. This chapter reviews our brachytherapy rationale, techniques, and dose specification methods as well as the clinical (brachytherapy) protocols in use for cancer of the head and neck. Clinical results in terms of local tumor control and complications (acute and late side-effects) are reported for cancer of the nasopharynx

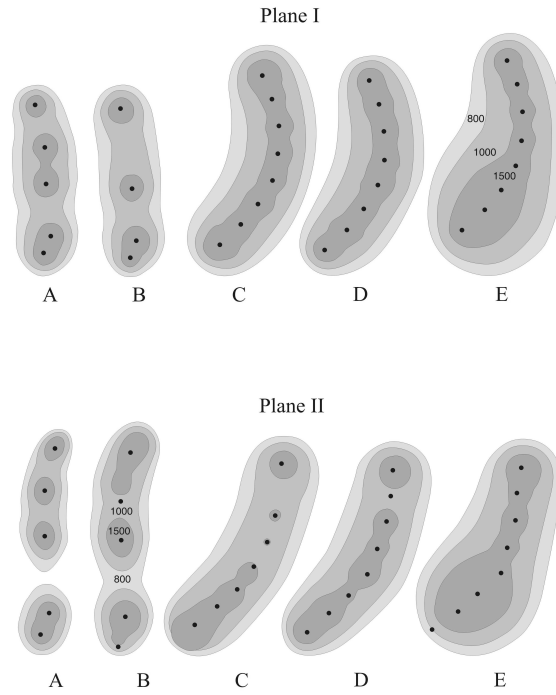


**Figure 20:** Comparison of different dose distributions for implant of the neck. Examples of isodose patterns are shown for a central plane (plane I) as well as for a plane taken more in the periphery of the implant (plane II). These dose distributions were calculated for a typical case of an LDR non-optimized implant (panel A); optimized catheter implant with dose points at 1 cm from catheters (panel B); optimized standard flexible intraoperative template with dose points at 1 cm from the center of the implant (panel C); optimized flexible intraoperative template used in the patient in figure 19, with dose points at 1 cm from catheters (panel D); and optimized flexible intraoperative implant to be used for situations with dose points at different depths, that is, with dose points at 1 cm (region 1; R-1) and 2 cm (region 2; R-2) (panel E). (For detailed explanation, see text.).

(endocavitary brachytherapy), nasal vestibule (mould and interstitial brachytherapy), tonsil and soft palate and base of tongue with fractionated HDR or PDR interstitial brachytherapy. Finally, some aspects regarding the way we are implementing (fractionated) HDR brachytherapy using an integrated brachytherapy unit are discussed.

## 2.6 References

1. Armour, E., Wang, Z., Corry, P. and Martinez, A. (1990) Equivalence of continuous and pulse simulated low dose rate irradiation in 9L gliosarcoma cells at 37° and 41° C. *Int. J. Radiat. Oncol. Biol. Phys.*, 22,109-14.
2. Brenner, D.J. and Hall, E.J. (1991) Conditions for the equivalence of continuous to pulsed low dose rate brachytherapy. *Int. J. Radiat. Oncol. Biol. Phys.*, 20,181-90.
3. Lea, D.E. and Catchside, D.G. (1942) The mechanism of the induction by radiation of chromosome aberrations in tradescantia. *J. Genet.*, 44,216-45.
4. Barendsen, G.W. (1982) Dose fractionation, dose rate and iso-effect relationships for normal tissue responses. *Int. J. Radiat. Oncol. Biol. Phys.*, 8,1981-97.
5. Thames, H.D. (1985) An 'incomplete-repair' model for survival after fractionated and continuous irradiations. *Int. J. Radiat. Oncol. Biol. Phys.*, 47,319-39.
6. Dale, R.G. (1985) The application of the linear-quadratic dose-effect equation to fractionated and protracted radiotherapy. *Br. J. Radiol.*, 58,515-28.
7. Thames, H.D., Bentzen, S.M., Turesson, I., Overgaard, M. and Van den Bogaert, W. (1990) Time-dose factors in radiotherapy: a review of the human data. *Radiother. Oncol.*, 19,219-35.
8. Fowler, J.F. (1989) The linear-quadratic formula and progress in fractionated radiotherapy. *Br. J. Radiol.*, 62, 679-94.
9. Pop, L.A.M., van den Broek, J.F.C.M., Visser, A.G. and van der Kogel A.J. (1996) Constraints in the use of repair half times and mathematical modeling for the clinical application of HDR and PDR treatment schedules as an alternative for LDR brachytherapy. *Radiother. Oncol.*, 38(2),153-162.
10. de Boer, R.W. and Lebesque, J.V. (1991) Equivalent doses of low-dose-rate brachytherapy and pulsed-dose-rate brachytherapy. First ESTRO Biennial Meeting on Physics in Clinical Radiotherapy, (Budapest, October 1991, abstract 14).
11. Ang, K.K., Guttenberger, R., Thames, H.D., Stephens, L.C., Smith, C.D. and Feng, Y. (1992) Impact of spinal cord repair kinetics on the practice of altered fractionation schedules. *Radiother. Oncol.*, 25,287-94.
12. Turesson, I., and Thames, H.D. (1989) Repair capacity and kinetics of human skin during fractionated radiotherapy: erythema, desquamation and telangiectasia after 3 and 5 years' follow-up. *Radiother. Oncol.*, 15,169-88.
13. van Rongen, E., Thames, H.D. and Travis, E.L. (1993) Recovery from radiation damage in mouse lung: interpretations in terms of two rates of repair. *Radiat. Res.*, 133,225-33.
14. Levendag, P.C., Meeuwis, C.A., Wijkthoff, S.J.M. and Visser, A.G. (1992) Reirradiation of recurrent head and neck cancers: external versus interstitial radiation therapy. *Activity*, 3,32-9.

15. Senan, S. and Levendag, P.C. (1999) Brachytherapy for recurrent head and neck cancer. *Hematol. Oncol. Clin. North. Am.*, 13(3),531-542.
16. Brenner, D.J., Hall, E.J., Huang, Y. and Sachs, R.K. (1994) Optimizing the time course of brachytherapy and other accelerated radiotherapeutic protocols. *Int. J. Radiat. Oncol. Biol. Phys.*, 29(4),893-901.
17. Kolkman-Deurloo, I.K.K., Visser, A.G., Niël, C.G.J.H., Driver, N. and Levendag, P.C. (1994) Optimization of interstitial volume implants. *Radiother. Oncol.*, 31,229-39.
18. Thomadsen, B.R., Houdek, P. V., van der Laarse, R., Edmundson, G.K., Kolkman-Deurloo, I.K.K. and Visser, A.G. (1994) Treatment planning and optimization. In *HDR Brachytherapy: A textbook*, ed. S. Nag. Amonk, NY, Futura Publishing Company, 79-145.
19. van der Laarse, R., Edmundson, G.K., Luthmann, R.W. and Prins, T.P.E. (1991) Optimization of HDR brachytherapy dose distributions. *Activity, Selectron Brachyther. J.*, 5(2),94-101.
20. Edmundson, G.K. (1991) Geometry based optimization for stepping source implants. *Activity, Selectron Brachyther. J.*, 5(4),22-6.
21. Edmundson, G.K. (1994) Volume optimization: an American viewpoint. In *Brachytherapy from Radium to Optimization*, ed. R.F. Mould, J.J. Battermann, A.A. Martinez and B.L. Speiser. Veenendaal, The Netherlands, Nucletron International BV, 314-18.
22. Levendag, P.C., Vikram, B., Flores, A.D. and Yin, W.B. (1994) High dose rate brachytherapy for cancer of the head and neck. In *High Dose Rate Brachytherapy: a Textbook*, ed. S. Nag. Amonk, NY, Futura Publishing Company, 237-73.
23. van de Pol, M., Levendag, P.C., de Bree, R.R., Franssen, J.H., Smeele, L.E., Nijdam, W.M., Jansen, P.P., Meeuwis, C.A. and Leemans, C.R. (2004) Radical radiotherapy compared with surgery for advanced squamous cell carcinoma of the base of tongue. *Brachytherapy*, 3(2),78-86.
24. Levendag, P.C. and Pomp, J. (1990) Radiation therapy of squamous cell carcinoma of the nasal vestibule. *Int. J. Radiat. Oncol. Biol. Phys.*, 19(6),1363-1367.
25. Levendag, P.C., Nijdam, W.M., van Moolenburgh, S.E., Tan, L., Noever, I., van Rooy, P., Mureau, M.A.M., Jansen, P.P., Munte, K. and Hofer, S.O.P. (2006) Interstitial radiation therapy for early stage nasal vestibule cancer: a continuing quest for optimal tumor control and cosmesis. *Int. J. Radiat. Oncol. Biol. Phys.*, 66(1),160-169.
26. Levendag, P.C., Schmitz, P.I.M., Jansen, P.P., Senan, S., Eijkenboom, W.M.H., Sipkema, D., Meeuwis, C.A., Kolkman-Deurloo, I.K.K., and Visser, A.G. (1997) Fractionated high-dose-rate brachytherapy: first clinical experience in squamous cell carcinoma of the tonsillar fossa and soft palate. *Int. J. Radiat. Oncol. Biol. Phys.*, 38(3),497-506.



27. Levendag, P.C., Nijdam, W.M., Noever, I., Schmitz, P.I.M., van de Pol, M., Sipkema, D., Braat, C., de Boer, M. and Jansen, P.P. (2004) Brachytherapy versus surgery in carcinoma of tonsillar fossa and/or soft palate: late adverse sequelae and performance status: can we be more selective and obtain better tissue sparing ? *Int. J. Radiat. Oncol. Biol. Phys.*, 59(3),713-724.
28. Levendag, P.C., Visser, A.G., Kolkman-Deurloo, I.K.K., Eijkenboom, W.M.H. and Meeuwis, C.A. (1994) HDR brachytherapy with special reference to cancer of the nasopharynx. In *Brachytherapy from Radium to Optimization*, ed. R.F. Mould, J.J. Battermann, A.A. Martinez and B.L. Speiser. Veenendaal, The Netherlands, Nucletron International BV, 121-31.
29. Levendag, P.C., Peter, R., Meeuwis, C.A., Visch, L.L., Sipkema, D., de Pan, C. and Schmitz, P.I.M. (1997) A new applicator design for endocavitary brachytherapy of cancer in the nasopharynx. *Radiother. Oncol.*, 45,95-8.
30. Levendag, P.C., Lagerwaard, F.J., de Pan, C., Noever, I., van Nimwegen, A., Wijers, O. and Nowak, P.J.C.M. (2002) High-dose, high-precision treatment options for boosting cancer of the nasopharynx. *Radiother. Oncol.*, 63(1),67-74.
31. Levendag, P.C., Nijdam, W.M., van Agthoven, M. and Uyl-de Groot, C.A. (2002) Chemotherapy and high-dose-rate brachytherapy in the management of advanced cancers of the nasopharynx: clinical impact of high technology – is it worth the cost ? *Brachytherapy*, 1(1),11-20.
32. Levendag, P.C., Schmitz, P.I.M., Jansen, P.P., Eijkenboom, W.M., Visser, A.G., Kolkman-Deurloo, I.K.K., Sipkema, D., Visch, L.L. and Senan, S. (1998) Fractionated high-dose-rate brachytherapy in primary carcinoma of the nasopharynx. *J. Clin. Oncol.*, 16(6), 2213-20.
33. Levendag, P.C., Lagerwaard, F.J., Noever, I., de Pan, C., van Nimwegen, A., Wijers, O., Schmitz, P.I.M., van Dieren, E. and Nowak, P.J.C.M. (2002) Role of endocavitary brachytherapy with or without chemotherapy in cancer of the nasopharynx. *Int. J. Radiat. Oncol. Biol. Phys.*, 52(3),755-768.
34. Levendag, P.C., Meeuwis, C.A. and Visser, A.G. (1992) Reirradiation of recurrent head and neck cancers: external and/or interstitial radiation therapy. *Radiother. Oncol.*, 23,6-15.



## CHAPTER 3. OPTIMIZATION OF INTERSTITIAL VOLUME IMPLANTS

IKK Kolkman-Deurloo, AG Visser, CGJH Niël, N Driver, PC Levendag  
Radiother Oncol 1994; 31; 229-239.

### 3.1 Abstract

For interstitial applications of high dose rate (HDR) afterloading brachytherapy, generally a single stepping Iridium-192 source is used, enabling optimization of the dose distribution by optimization of the relative time (dwell time) that the source remains at a certain position (dwell position). We analysed the effects of geometric optimization in a regular volume implant, with strictly parallel catheters, and in an irregular volume implant, such as an implant for tumours of the base of the tongue characterized by a non-parallel geometry and varying catheter separations. In both examples the reference dose is specified at 85% of the mean central dose (as is done in the Paris system for dose specification) in the non-optimized as well as the optimized plan. The irradiated volume, the dose uniformity, and the choice of the reference dose of optimized and non-optimized dose distributions were compared. This was done by isodose plots for representative planes, volume dose histograms (distributed, contiguous, and natural), and dose nonuniformity ratios (DNRs). For the regular implant, optimization results in a 28% increase in the treated volume with a similar increase in the overdosed volumes. In order to keep the treated volume comparable with the non-optimized dose distribution, 90-95% of the mean central dose should be chosen as a reference dose or the range of active dwell positions should be shortened in case of optimization. In case of the irregular volume implant at the base of the tongue, the method for dose specification should be kept unchanged after geometric optimization as the volume enclosed by the reference isodose does not increase. It is clear from the volume dose histograms that there is a reduction of the overdosed volume due to optimization. This is accompanied by an increase in the uniformity index and a decrease of the DNR. In conclusion, geometric optimization appears to be an effective tool to improve the dose distribution of interstitial volume implants. Contiguous and natural volume dose histograms appear, apart from planar dose plots, valuable methods for evaluating the dose distribution of an implant.

### 3.2 Introduction

High dose rate (HDR) brachytherapy is usually performed with single stepping source afterloaders. These afterloaders contain a small Iridium-192 source mounted at the end of a steel wire, which is transported under computer control in previously implanted applicators. The machine is programmed to position the source at predefined positions (dwell positions) in the applicators. The time the source spends at each dwell position (dwell time) can be freely chosen. This enables optimization of the dose distribution by optimization of the dwell times over all dwell positions in the implant [10]. If the target volume is characterized by a sufficient number of reference points (dose points), the dose distribution can be optimized such that a certain reference dose is obtained in these points (optimization on dose points). This procedure can be followed by adding normal tissue points and requiring that the dose in these normal tissue points should be below a chosen tolerance level. In the third optimization method, geometric optimization, the relative dwell times are determined by the geometry of the implant by assigning an individual weight factor for the dwell time at each dwell position, which is inversely proportional to the dose contribution from neighbouring source locations. It is expected that geometric optimization can produce better and more homogeneous dose distributions in interstitial volume implants. This study focusses on the effects of geometric optimization on the dose distribution for both 'regular' interstitial volume implants (consisting of parallel catheters with a constant spacing) and 'irregular' interstitial volume implants (which consist of non-parallel catheters with varying catheter separations).

A comparison has been made between the optimized and the non-optimized dose distributions for an example of a 'regular' implant (a two-plane implant of seven parallel catheters) and a representative example of an 'irregular' implant (a twelve-catheter implant of the base of the tongue). We evaluated the effect of optimization on the irradiated volume, the dose uniformity, and the choice of the reference dose for both implants.

### 3.3 Material and methods

The *regular volume implant* consists of seven parallel catheters located in two planes according to the Paris system [2] as shown in figure 1. This type of implant is often used in conservative treatment of breast cancer. One plane consists of three catheters with a length of 80 mm and one catheter with a length of 75 mm. The second plane

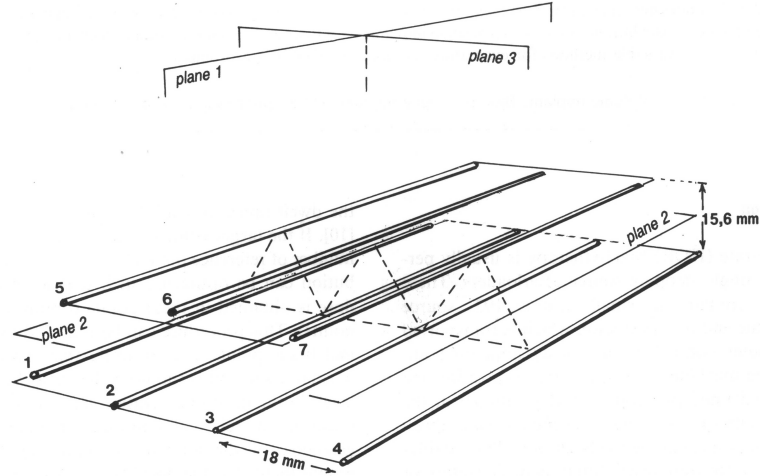


**Figure 1:** The geometry of the regular implant. The lengths of the catheters are: 1: 75 mm; 2,3,4: 80 mm; 5: 60 mm; 6,7: 55 mm. Indicated are the three orthogonal planes through the center of the implant, either parallel (plane 1,2) or perpendicular (plane 3) to the catheters.

consists of two catheters of 55 mm and one catheter of 60 mm. The spacing between the catheters is 18 mm, the distance between the two planes is 15.6 mm.

Base of tongue (BOT) implants, which in our study serve as an example of an *irregular volume implant*, consist of catheters implanted in three parallel sagittal planes. Each plane consists of one posterior catheter running through the BOT, caudal to the posterior tumour margin and subsequently over the surface of the tongue. Two or three (depending on the tumour size) blind-ended catheters are implanted through the tumour tissue with the anterior catheters ventral to the anterior tumour margin. The blind end of each of these catheters is sutured with a button to the posterior catheter (figure 2).

For the regular implant basal dose points are defined according to the Paris system [2]. The reference dose is specified at 85% of the mean central dose, i.e. the average dose over the basal dose points. For the BOT implant, a method similar to the Paris system is used. A central plane passing through the geometric center of the implant is defined, approximately perpendicular to the main direction of the blind-ended catheters (figure 2). In this central plane triangles are constructed from the intersections with the catheters. Only non-obtuse triangles should be constructed, because the geometric center of an obtuse triangle is located outside the triangle. The geometric

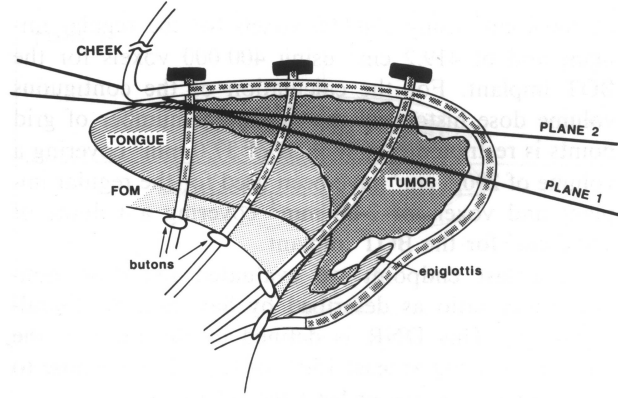


**Figure 2:** Schematic view of a BOT implant showing the posterior catheter running partly over the surface of the tongue and the blind-ended catheters sutured to it. Indicated are the position of plane 1, the central plane, and plane 2, at the surface of the tongue.

centers of these triangles are used as reference points as the minimal dose in the central plane will, in general, be located in the geometric centers of these triangles. These reference points can be regarded as ‘basal dose points’. The mean central dose is defined as the average dose over these basal dose points. The reference dose for this type of implant is again specified at 85% of the mean central dose. A reference dose of 1000 cGy was chosen for both implants.

The non-optimized situation assumes equal dwell times of the point source in all dwell positions. The optimized dose distribution is calculated using geometric optimization [3,4] as implemented in the Nucletron Planning System (Nucletron B.V., The Netherlands; module UPS). The relative dwell time of each dwell position depends on its distance to other dwell positions and their corresponding relative dwell times:

$$t_i \sim \left( \sum \frac{t_j}{r_{ij}^2} \right)^{-1} \quad (1)$$

where:

$t_i$  = relative dwell time at the dwell position  $i$ ,

$t_j$  = relative dwell time at another dwell position  $j$ ,

$r_{ij}$  = distance between dwell position  $i$  and  $j$ .

In this way the relative dwell time is inversely proportional to the dose contribution from all other dwell positions. For these volume implants a mode of geometric optimization is applied where the only active dwell positions considered are those in catheters other than the one containing the dwell position for which its dwell time is calculated. The source is considered to be isotropic. Subsequent calculations in which anisotropy was taken into account have shown that for volume implants of this type, the effect of source anisotropy on the dose distribution is quite marginal and can indeed be neglected. The spacing between neighbouring dwell positions inside a catheter is set at 5 mm.

In order to evaluate the resulting dose distributions, isodose plots have been made in different planes passing through the implant. In case of the regular implant three orthogonal planes through the center of the implant (figure 1) were used, either parallel (planes 1 and 2) or perpendicular (plane 3) to the catheters.

For the BOT implant a set of orthogonal planes through the center of the implant has been defined (figure 3), with plane 1 being the central plane and plane 3 the central sagittal plane, together with a plane (plane 2) approximately parallel to the central

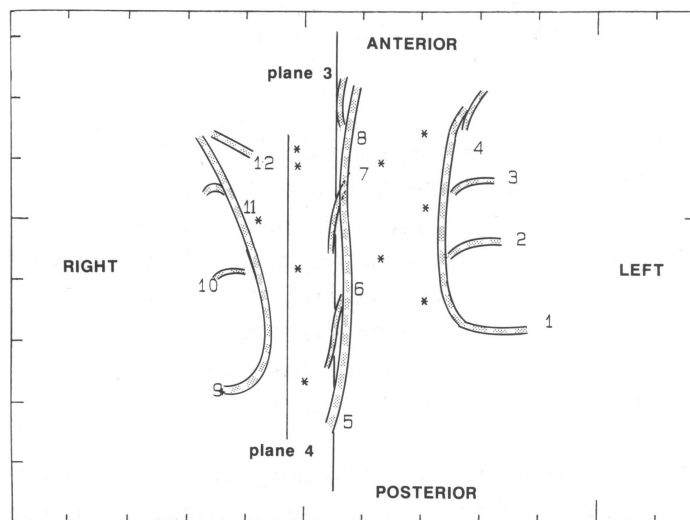


**Figure 3:** The central plane of the BOT implant with the projections of the catheters indicated. The asterisks denote the position of the basal dose points. The position of plane 3, the sagittal plane, and plane 4, a sagittal plane in between the central and right sagittal source plane, are indicated.

transversal plane (figure 2). The latter plane is used to evaluate the dose distribution at the surface of the tongue. In order to be able to compare the dose distributions in regions in between the sagittal source planes, an additional sagittal isodose plane (plane 4) has been defined between the central sagittal source plane and the right parasagittal source plane (figure 3).

The second evaluation method consists of volume dose histograms of a box encompassing the implant. Generally, the overdosed volume will be distributed over multiple small volumes throughout the implanted volume or it can consist of a large single volume. 'Distributed' volume dose histograms, representing the total volume receiving at least a specific dose, have been calculated, using arbitrary grid points [9]. As a large single overdosed volume is expected to be associated with an increased risk of complications, an evaluation using a 'contiguous' volume analysis [6,11] has been applied to the dose distributions mentioned above. The largest single (contiguous) volume is calculated receiving at least a specific dose level. It was suggested by Visser et al. [11] that this method may be more sensitive to irregularities in implant configurations than a distributed volume analysis. As this is not incorporated in the NPS it has been calculated using a brachytherapy planning system developed in the DDHCC (using the dwell weights calculated with NPS).

Both distributed and contiguous volume dose histograms are difficult to interpret due to the effect of the inverse square law dose gradient on the dose distribution. We therefore analyzed also 'natural' volume dose histograms as introduced by Anderson [1], in which  $dV/du$  is plotted as a function of  $u$ , with  $u = D^{-3/2}$ . The main intention of this analysis method is to suppress the effects of the inverse square law dose gradient, a characteristic of the dose distribution around a point source. A point source will give a horizontal line at  $(4/3)\pi S^{3/2}$  with  $S$  being the source strength. The volume receiving at least a given dose is still kept proportional to the area under the curve. A peak in the histogram represents a large volume with a low dose-gradient. For volume implants it follows that a better dose uniformity is characterised by a high and narrow peak. The position of the peak (indicated by the parameters LD and HD, being the doses at half maximum of the peak at, respectively, the low dose side and the high dose side) relative to the actual treatment dose, TD, is a measure of the choice of the reference isodose in relation to the relatively homogeneous irradiated volume. Ideally, TD should coincide with LD. Choice of a treatment dose, TD, with  $TD < LD$  produces a relative low uniformity index. On the other hand, a treatment dose, TD, with  $TD > LD$  indicates a large volume with a low dose gradient, receiving



lower doses than the reference dose. A uniformity index UI can be extracted from the natural volume dose histogram [1], defined as:

$$UI = \frac{V(TD - HD)}{V(TD)} * \frac{u(TD)}{u(TD) - u(HD)} \quad (2)$$

with:

TD = treatment dose,

HD = the dose at half maximum of the peak at the high dose side,

V(TD-HD) = volume receiving a dose between TD and HD,

V(TD) = volume receiving at least the treatment dose TD,

$u(D) = D^{-3/2}$ .

It can be seen that the uniformity index depends not only on the uniformity of the dose distribution but also on the choice of the reference isodose. It expresses the amount of the treatment volume which is concentrated between the treatment dose, TD, and the high dose side of the peak, HD.

In this analysis the distributed and natural volume dose histograms have been calculated for a box volume of 266.4 cm<sup>3</sup> using 250000 voxels for the regular implant and of 419.2 cm<sup>3</sup> using 400000 voxels for the BOT implant. For the calculation of the contiguous volume dose histogram the maximum number of grid points is restricted [11]. Voxels of 37.0 mm<sup>3</sup> covering a volume of 290.5 cm<sup>3</sup> have been used for the regular implant and voxels of 24.6 mm<sup>3</sup> covering a volume of 440.6 cm<sup>3</sup> for the BOT implant.

As a last endpoint we evaluated the Dose Nonuniformity Ratio as described by Saw and Suntharalingam [8]. This DNR is defined as the ratio of the volume receiving at least 150% of the reference dose to the volume receiving at least the reference dose, i.e.

$$DNR = \frac{Volume(D \geq 1.5 * D_{ref})}{Volume(D \geq D_{ref})} \quad (3)$$

As stated by Saw and Suntharalingam [8] the DNR as function of the reference dose will show a minimum. In order to obtain the best uniformity in a dose distribution the reference dose should be chosen close to the minimum of this function.

### 3.4 Results

Five basal dose points were defined in the regular implant. Geometric optimization induces a significant decrease of the standard deviation of the dose (presented as percentage of the reference dose) in these basal dose points (table 1).

In figure 4 the isodose distributions in three orthogonal planes are shown for both the non-optimized case (left side) and the geometric optimized case (right side). It can be seen that after geometric optimization the reference isodose of 1000 cGy covers a larger volume. Moreover, as shown in plane 3, it becomes clear that without optimization the 1250 cGy isodose surrounds the three central catheters which is not the case after geometric optimization.

The total volume enclosed by the reference isodose increases 28% due to the optimization (table 1). The distributed volume dose histogram (figure 5A) indicates a similar increase for the volumes enclosed by other isodoses.

From the contiguous volume dose histogram (table 1) approximately the same increase (26%) is seen in the largest single volume enclosed by the reference isodose due to optimization. After geometric optimization the largest contiguous volume enclosed by the 125% isodose is 40% of that from the non-optimized plan (figure 5B). This is reflected in the fact that after optimization the 125% isodose does not

**Table 1:** Data for the regular implant for both the non-optimized and optimized case: relative dose in the basal dose points expressed as a percentage of the actual reference dose, distributed and largest contiguous volume enclosed by the reference dose and DNR and UI for the actual reference dose.

	Not optimized	Optimized
Dose in basal dose points (%):		
Range	112-123	117-118
85% mean dose	100	100
SD ( $\sigma_n$ )	4.5	0.5
Distributed volume (cm <sup>3</sup> )	80.2	102.3
Contiguous volume (cm <sup>3</sup> )	79.7	100.5
DNR	0.23	0.23
UI	1.84	1.93

surround the three central catheters anymore (figure 4, plane 3).

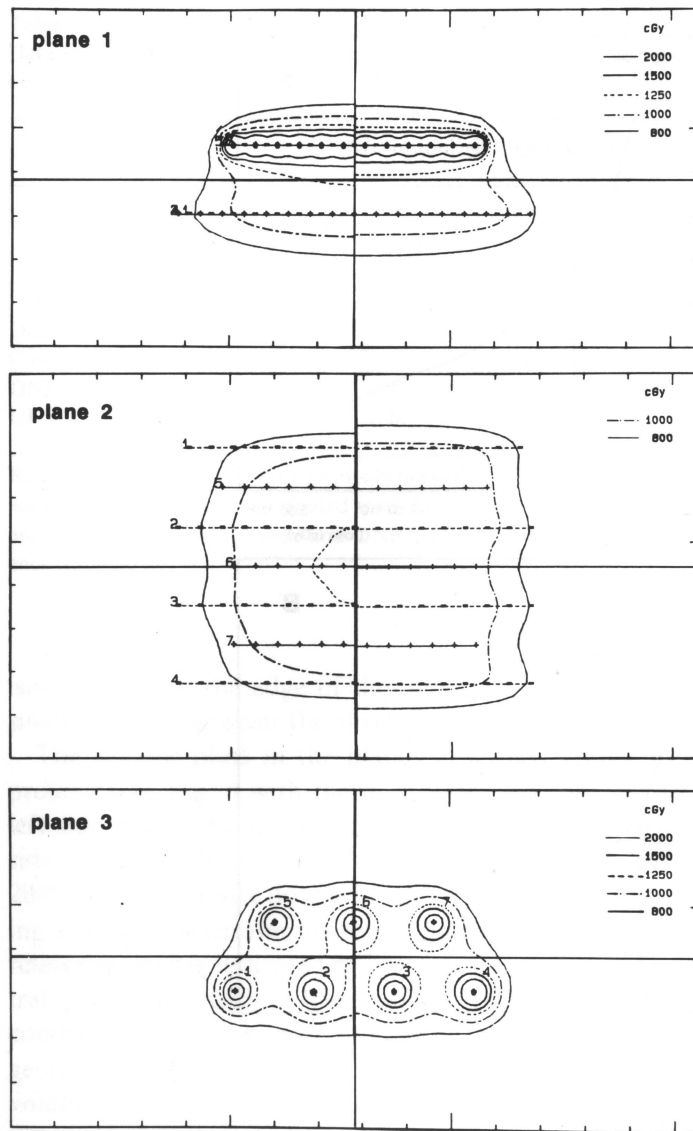


**Figure 4:** The dose distribution of the regular implant in three orthogonal planes through the center of the implant. The left panels present the non-optimized dose distribution, the right panels the dose distribution due to geometric optimization.

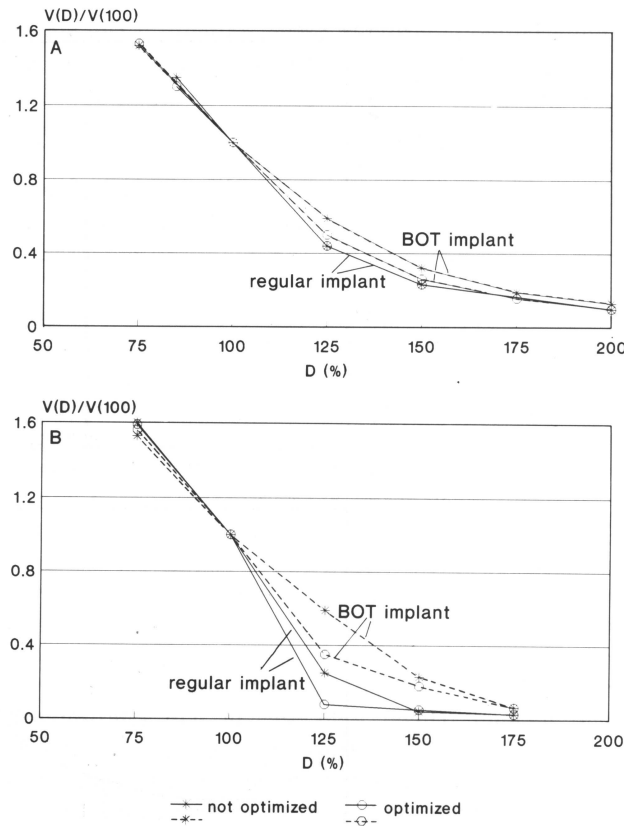


**Figure 5:** The distributed (panel A) and contiguous (panel B) volumes as a function of dose for the regular and the BOT implant. The actual reference dose is 100%. The curves are normalized to the volume corresponding to the reference dose,  $V(100)$ , (tables 1 and 2).

The natural volume dose histogram (figure 6) consists of a broad peak with TD very close to LD without optimization. After geometric optimization the peak becomes significantly narrower and higher with  $TD < LD$ . In spite of the significant change in the shape of the natural volume dose histogram, the change in the Uniformity Index UI, from 1.84 in the non-optimized case to 1.93 after geometric optimization (table 1), is relatively small, because LD is much larger than TD in the latter case.

The Dose Nonuniformity Ratio DNR (figure 7) shows a minimum at 105% and at 110% in the non-optimized and optimized situation, respectively. For both situations the DNR at the actual reference dose is 0.23 (table 1).

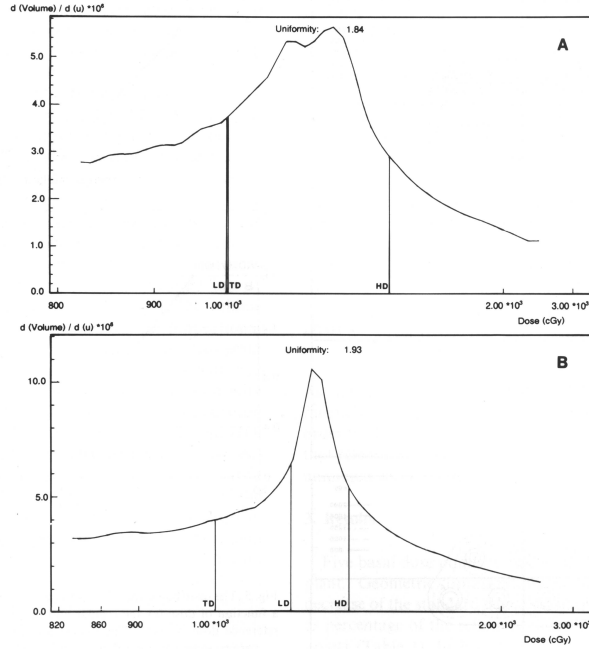


**Figure 6:** The natural volume dose histograms for the regular implant. Panel A presents the non-optimized case, panel B the optimized case. The scaling of the plots is not identical. Both cases:  $TD = 1000$  cGy; non-optimized:  $LD = 998.9$  cGy,  $HD = 1371.8$  cGy; optimized:  $LD = 1133.9$  cGy,  $HD = 1273.1$  cGy.

As to our example of an irregular implant, a base of tongue implant, 11 basal dose points were defined as shown in figure 3 (indicated by the asterisks). In contrast to the regular implant the standard deviation in the dose in the basal dose points increases due to optimization (table 2). This is mainly caused by one basal dose point located at the posterior side of the implant in between the central and the right sagittal source plane, which is an isolated area at the edge of the implant with a relative small spacing between the three catheters.

The isodose plots in the planes described above are presented in figure 8 with the non-optimized case at the left side (panel A) and the optimized case at the right side (panel B). For clarity the region receiving at least 200% of the reference dose is hatched. The region receiving a dose between the reference dose and 125% of the reference dose is indicated by dots. In plane 1, the central plane, no major differences are recognized when comparing the non-optimized and optimized case. After geometric optimization a reduction of the overdosed volume receiving at least 200% of the reference dose at the surface of the tongue is seen in plane 2. A similar effect,

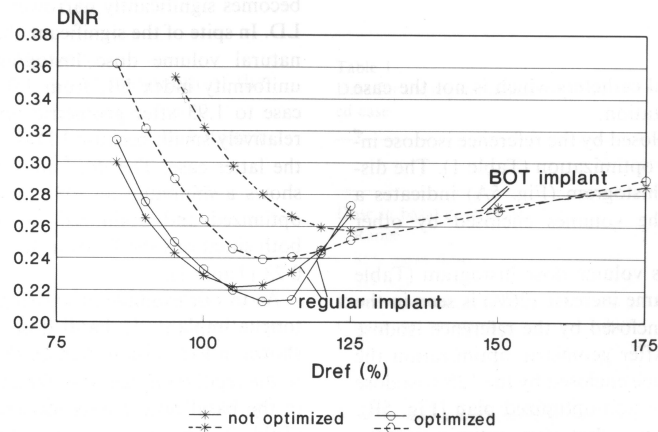


**Figure 7:** The Dose Nonuniformity Ratio DNR for the regular and the BOT implant, resulting from the data of the distributed volume dose table, as a function of the reference dose,  $D_{ref}$ , which is represented as a percentage of the actual reference dose.

especially at the intersection of the blind-ended catheters and the posterior catheter, occurs in plane 3, the central sagittal source plane. Plane 4 shows only a slight reduction of the volume covered by the 150% isodose at the surface of the tongue, but accompanied with a better coverage of the posterior part of the implant by the reference dose after optimization.

Geometric optimization of this implant results in a reduction of approximately 15% of the total overdosed volume as shown by the distributed volume dose histogram (figure 5A) with an equal volume encompassed by the reference isodose (table 2). Figure 5B and table 2 indicate a reduction of the largest contiguous overdosed volume in combination with an equal contiguous volume receiving at least the reference dose, due to optimization.

The natural volume dose histogram (figure 9) shows a broad peak with the treatment dose TD almost on top of LD for the non-optimized case (panel A). Geometric optimization results in a much narrower and higher peak indicating an increase in the uniformity of the dose distribution (panel B). The uniformity index is, respectively, 1.40 for the non-optimized situation and 1.58 for the optimized situation (table 2). Without optimization the DNR reaches a minimum at 125% of the actual chosen reference isodose (figure 7). In case of the optimized situation the minimum is shifted to 110%. At 100% the DNR is 0.32 for the non-optimized and 0.26 for the optimized case (table 2).

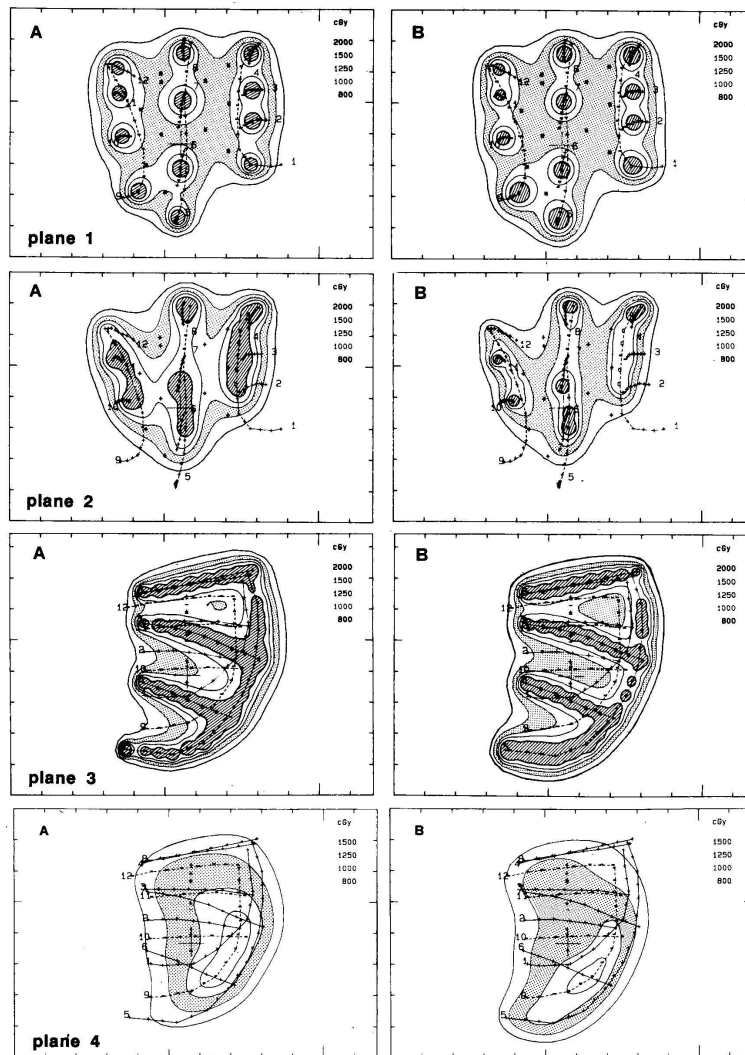


**Figure 8:** The dose distribution for the BOT implant for the non-optimized case (panel A) and the optimized case (panel B): plane 1, the central plane; plane 2, the surface of the tongue; plane 3, the central sagittal source plane; plane 4, an extra sagittal plane in between the right and central sagittal source plane.

**Table 2:** Data for the BOT implant for both the non-optimized and optimized case: relative dose in the basal dose points expressed as a percentage of the actual reference dose, distributed and largest contiguous volume enclosed by the reference dose and DNR and UI for the actual reference dose.

	Not optimized	Optimized
Dose in basal dose points (%):		
Range	111-126	106-140
85% mean dose	100.4	99.6
SD ( $\sigma_n$ )	5.5	9.2
Distributed volume (cm <sup>3</sup> )	89.8	90.9
Contiguous volume (cm <sup>3</sup> )	87.4	88.6
DNR	0.32	0.26
UI	1.40	1.58

### 3.5 Discussion

Since the introduction of single stepping source brachytherapy, dose distributions can, in contrast to linear sources, be optimized. Different methods for optimization exist. We evaluated the possibilities of geometric optimization, as it is expected that geometric optimization can produce better and more homogeneous dose distributions in interstitial volume implants.

The isodose plots in figure 4 indicate that due to optimization of the regular implant, the volume enclosed by the reference dose significantly increases, especially in a direction along the catheters. This increase is similar for the volumes enclosed by other isodoses, as shown by the distributed volume dose histogram. This example demonstrates that in case of a regular implant one should exercise caution in applying the geometry rules of the Paris system when using a single stepping source in combination with geometric optimization. In order to irradiate a volume comparable with the one treated with uniform line sources (with the reference dose specified at 85% of the mean central dose) one should in case of geometric optimization choose a higher isodose for dose specification. However, this would slightly affect the position of the reference isodose in the cross-sectional view. A different approach would be to continue specifying the dose at 85% of the mean central dose but with a reduction of



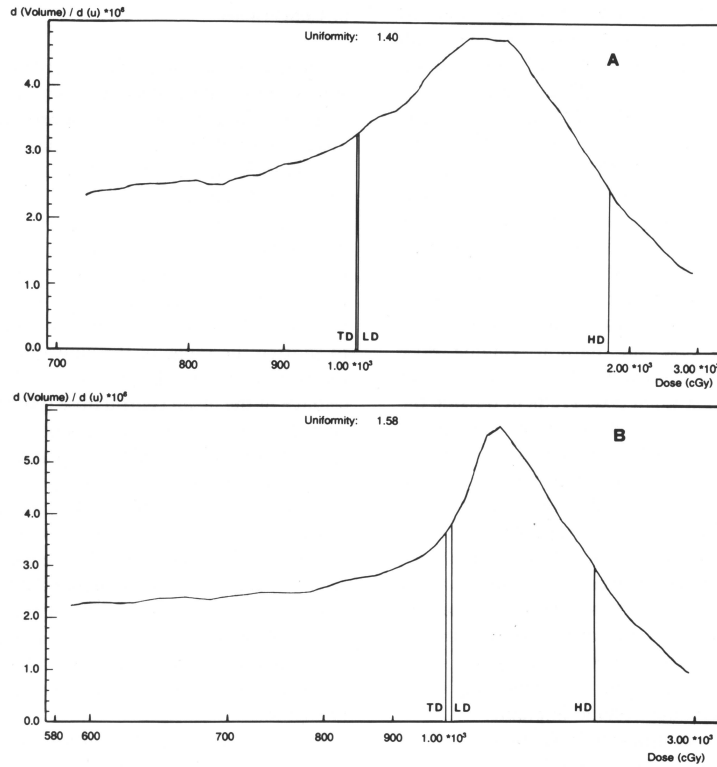


**Figure 9:** The natural volume dose histograms for the BOT implant. The non-optimized case is presented in panel A, the optimized case in panel B. The scaling of both plots is not identical. Both cases: TD = 1000 cGy; non-optimized: LD = 1003.2 cGy, HD = 1828.3 cGy; optimized: LD = 1012.3 cGy, HD = 1562.3 cGy.

the range of active dwell positions (i.e. to reduce the active source lines) in order to obtain a comparable treated volume.

Another significant difference between the optimized and non-optimized situation is observed from the shape of the 125% isodose. This is expressed in the isodose plots and in the contiguous volume dose histogram in which the separation of the volume, receiving at least 125% of the reference dose, around the three central catheters in three individual smaller volumes expresses the advantage of optimization. This reduction may be of clinical relevance.

It is not surprising that the DNR (for the actual chosen reference dose) does not change when going from a non-optimized to an optimized situation (table 1), as the volumes enclosed by the reference dose and the 150% isodose both increase equally.

From the DNR analysis it can be concluded that, ideally, a slightly higher isodose should have been chosen as reference dose, i.e. 105% for the non-optimized, respectively 110% for the optimized case.

After geometric optimization the shape of the natural volume dose histogram shows a significant increase in uniformity. This is not reflected in the uniformity index UI because TD is much lower than LD in the optimized case. Ideally, TD should be on top of LD, i.e. in this case 1133.9 cGy. In that case UI would have been higher (and the DNR lower) as the position of TD relative to the peak position is included in the expression for UI.

As to the example of the irregular volume implant of the base of tongue the volume enclosed by the reference isodose does not increase after geometric optimization. We therefore recommend that the method for dose specification, i.e. at 85% of the mean central dose, remains unchanged for optimized volume implants of the base of tongue. The advantage of geometric optimization is a more homogeneous dose distribution and a reduction of the overdosed volume. This benefit is shown in the volume dose histograms and the Dose Nonuniformity Ratios.

In the distributed and the contiguous volume dose histogram this is expressed in a reduction of the overdosed volume (figure 5). From this example it seems that the contiguous volume dose histogram is a slightly more sensitive method to evaluate possible benefits from optimization than the distributed volume dose histogram, as the reduction of the largest single overdosed volume seems to be more pronounced than the reduction of the total overdosed volume due to optimization.

The increase in dose uniformity is also shown by an increase of UI and a decrease of the DNR (table 2). When evaluating the natural volume dose histogram (figure 9) geometric optimization results in a narrower and higher peak, accompanied by an increase in the UI. There is, however, a difference in analysing the dose distribution of an implant using either the natural volume dose histogram or the DNR, since both methods use different arguments for the choice of an optimal reference isodose. This choice is based on the best obtainable dose uniformity solely when using the DNR. In case of the natural volume dose histogram the choice of the reference isodose is based on a reduction of the irradiated volume outside the reference isodose together with achieving an optimal uniformity. This is best seen when evaluating TD and LD.  $TD \leq LD$  indicates a steep dose fall-off for doses smaller than TD while  $TD > LD$  indicates a smaller gradient in this region.  $TD < LD$ , however, results in a lower UI. This indicates that ideally TD should coincide with LD. In this example the natural

volume dose histogram indicates an optimal choice of the reference dose, i.e. on top of LD, for the non-optimized case. However, the DNR suggests that, ideally, a higher isodose should have been chosen for dose specification, i.e. 125%, in order to achieve a better dose uniformity. In that case the natural volume dose histogram would have resulted in a higher UI, but with  $TD > LD$ , suggesting a small dose gradient outside the volume surrounded by the reference dose. This means that the DNR is a good tool to compare the dose uniformity of different treatment plans. On the other hand, analysis of the natural volume dose histogram seems more suitable for choosing the optimal reference isodose, since it gives more information on both the dose homogeneity and the steepness of the dose gradient outside the chosen reference dose. This information, together with evaluation of the overdosed volume by means of the contiguous volume dose histogram seems a valuable method for evaluating and comparing treatment plans from interstitial volume implants.

With regard to our example, the BOT implant, it was shown that geometric optimization results in a reduction of the overdosed volume and an increase of the dose homogeneity. Optimization resulted in a reduction of the overdosage at the surface of the tongue, especially at the intersection of the blind-ended catheters with the posterior catheters (see figure 8 plane 3 and plane 4). Since an overdosage at this site can cause ulcers and pain at the surface of the tongue and due to the possibility of optimization of the dose distribution it has been attempted to restrict the active dwell positions in the posterior catheters to the part running through the base of tongue [9]. This so called 'interrupted loading pattern' possibly reduces side effects, because the part of the posterior catheter running over the surface of the tongue is not loaded. It was demonstrated that for the latter configuration, optimization resulted in a slightly better and more homogeneous dose distribution than for the non-optimized case. However, it was not clearly shown that with optimization an underdosage at the surface of the tongue in between catheters could be avoided. Therefore it seems hazardous to generalize the interrupted loading pattern to all BOT implants. One should very carefully evaluate the relation between the actual implant and the clinical demand in each patient individually and decide, based on the dose distribution at the surface of the tongue, which type of loading in the posterior catheters should be used.

### 3.6 Conclusions

These examples show the benefits of using a stepping source afterloading machine from the dose distribution point of view as it offers the opportunity to optimize the

dose distribution for interstitial volume implants, especially for rather difficult irregular implants, e.g. of the base of tongue.

When converting from uniform line sources to a single stepping source different consequences arise from the choice of the reference dose when comparing the regular and the irregular volume implant. For the regular implant it is concluded that one should either choose to shorten the range of the active dwell positions or (if the same active lengths are used) to choose a higher percentage of the mean central dose (90-95%) for the reference dose. The latter choice results in an increase of the dose uniformity inside the implant, but with a slight shrinking of the reference isodose in the cross sectional direction (figure 4 plane 3). In case of a less regular volume implant, e.g. for the base of tongue, it appears that 85% of the mean central dose can still be chosen as reference dose without changing the treated volume. In that case an increase is seen in the dose uniformity. These effects on the uniformity and the choice of the reference dose for the regular as well as the irregular implant are best illustrated by the natural volume dose histograms.

Besides evaluating dose plots, it appears useful to evaluate contiguous and natural volume dose histograms when analyzing the dose distribution of a volume implant after optimization. However, these evaluation methods do not yet consider the dose distribution in relation to the clinical target volume. It would be useful to expand computer planning for brachytherapy, similar to current developments in teletherapy planning, by evaluating the effects of dose distribution manipulation separately for the clinical target volume and for normal tissue volume outside the target volume. In order to achieve the latter, an analysis including a coverage index (CI), a relative dose homogeneity index (HI) and an external volume index (EI) should be carried out [5,7,8]. This would necessitate a different way of visualizing an implant in relation to the target volume and the anatomy of the patient, e.g. using multiple CT slices for an accurate indication of the target volume.

### 3.7 References

1. Anderson, L.L. A "natural" volume-dose histogram for brachytherapy. *Med. Phys.* 13 (6): 898-903, 1986.
2. Dutreix, A., Marinello, G., Wambersie, A. *Dosimétrie en Curiethérapie*. Masson, Paris, France, 1982.
3. Edmundson, G.K. Geometry based optimization for stepping source implants, *Activity, Selectron Brachytherapy Journal*, 5(4): 22-26, 1991.

4. Edmundson, G.K. Geometric optimisation: an american view. In: International brachytherapy, p 256-257. Editor: R.F. Mould, Nucletron International B.V., Veenendaal, The Netherlands, 1992.
5. Meertens, H., Borger, J., Steggerda, J., Blom, A. Evaluation & optimisation of interstitial brachytherapy dose distributions. In: International brachytherapy, p 112-116. Editor: R.F. Mould, Nucletron International B.V., Veenendaal, The Netherlands, 1992.
6. Neblett, D.L., Syed, A.M.N., Puthawala, A.A., Harrop, R., Frey, H.S., Hogan, S.E. An interstitial implant technique evaluated by contiguous volume analysis. *Endocurie. Hypertherm. Oncol.* 1: 213-221, 1985.
7. Saw, C.B., Suntharalingam, N. Reference dose rates for single- and double plane <sup>192</sup>Ir implants. *Med. Phys.* 15(3): 391-396, 1988.
8. Saw, C.B., Suntharalingam, N. Quantitative assessment of interstitial implants. *Int. J. Radiat. Oncol. Biol. Phys.* 20: 135-139, 1991.
9. Thomadsen, B., Houdek, P., van der Laarse, R., Edmundson, G.K., Kolkman-Deurloo, I.K.K., Visser, A.G. Treatment planning and optimization. In: HDR Brachytherapy: A Textbook. Editor: S. Nag. Armonk, NY: Futura; 1994. pp. 79-145.
10. Van der Laarse, R., Edmundson, G.K., Luthmann, R.W., Prins, T.P.E. Optimisation of HDR brachytherapy dose distributions. *Activity, Selectron Brachytherapy Journal* 5(2): 94-101, 1991.
11. Visser, A.G., Levendag, P.C., Driver, N., van Putten, W.L.J. Application of volume-dose calculations in brachytherapy: experience from "irregular" head and neck implantations. In: Brachytherapy 2, p 397-403. Editor: R.F. Mould, Nucletron International B.V., Veenendaal, The Netherlands, 1989.



## **CHAPTER 4. ANATOMY BASED INVERSE PLANNING IN HDR PROSTATE BRACHYTHERAPY**

IKK Kolkman-Deurloo, XGJ Deleye, PP Jansen, PCM Koper

Radiother Oncol 2004; 73; 73-77.

### **4.1 Abstract**

The purpose of this study is to evaluate anatomy based inverse planning as implemented in PLATO BPS 14.2 for planning of HDR prostate implants. Six patients were analysed. The dose distributions were optimized using Geometric Optimization followed by Graphical Optimization (GO), anatomy based inverse planning or Standard Inverse Optimization (SIO), Tuned Inverse Optimization (TIO) and Tuned Inverse Optimization followed by Graphical Optimization (GOTIO). The mean target coverage was  $93\% \pm 4\%$ ,  $53\% \pm 11\%$ ,  $74\% \pm 8\%$ ,  $90\% \pm 3\%$ , respectively, for GO, SIO, TIO and GOTIO. The Conformal Index COIN was  $0.74 \pm 0.02$ ,  $0.43 \pm 0.15$  and  $0.77 \pm 0.07$ , respectively, for GO, SIO and GOTIO. Improved dose homogeneity was found when comparing GOTIO with GO.

## 4.2 Introduction

In our institute, patients with localised prostate cancer, i.e. T1c - T2a, PSA < 10, Gleason score < 7, and a prostate volume on transrectal ultrasound imaging < 60 cm<sup>3</sup>, are treated with HDR brachytherapy followed by external beam radiotherapy. The brachytherapy consists of three fractions of 6 Gy each. The external beam treatment is started within 2 weeks after finishing the brachytherapy and consists of 25 fractions of 1.8 Gy using a three field technique. The template based brachytherapy technique strongly resembles the one described by Mate et al. [11]. Plastic needles (6F ProGuide needles, Nucletron, The Netherlands) are inserted under transrectal ultrasound guidance. After implantation the needles are proceeded with the aid of flexible cystoscopy such that the needle tips are positioned submucosally in the bladder wall to ensure adequate target coverage at the base of the prostate. Treatment planning is based on postimplant CT imaging and is performed using PLATO BPS (Nucletron, The Netherlands). Implant reconstruction is facilitated by automatic catheter reconstruction [12] and autoactivation of source dwell positions [2]. However, treatment planning is still challenging and time consuming due to the location of the organs at risk, with the rectum located very close to the target and the urethra running through the target.

One of the frequently mentioned advantages of HDR irradiation instead of permanent implantation of <sup>125</sup>Iodine or <sup>103</sup>Palladium seeds is the ability of dose optimization using dwell time optimization [16]. This optimization enables improvement of the dose homogeneity inside the implanted volume [3] and better conformation of the dose to the target volume delineated on CT, MRI or ultrasound. However, in case of brachytherapy of the prostate, not only dose conformation to the target is important but also sparing of the urethra and rectum. Therefore, the dose limits for these organs at risk should also be taken into account in the optimization procedure.

In contrast to the classical dwell time optimization methods, i.e. geometric optimization and dose point optimization [16], the input in anatomy based inverse planning consists of both the contoured target and organs at risk, each with their individual dose constraints. Anatomy based inverse planning based on simulated annealing was proposed by Lessard and Pouliot [9]. This method was succesfully applied in gynaecology and prostate HDR brachytherapy [5,10]. Lahanas et al. [6] introduced multiobjective genetic algorithms for anatomy based dose optimization in brachytherapy and applied them to different clinical implant geometries. Deterministic



gradient based dose optimization algorithms are discussed in [8,13]. Lahanas et al. [7] combined deterministic algorithms with genetic algorithms in a hybrid approach.

Recently a novel algorithm for interactive anatomy based inverse planning was introduced in PLATO BPS version 14.2 (Nucletron, The Netherlands) [4]. The purpose of this study is to evaluate this algorithm for planning of HDR prostate implants, in terms of target coverage, dose homogeneity, sparing of organs at risk and planning time.

### **4.3 Materials and methods**

The implementation of interactive anatomy based inverse planning (or Inverse Optimization) in PLATO BPS differs from the inverse planning algorithms described in literature [5-10,13] as it is based on the well known geometric and dose point optimization and adapted to account for sparing of critical organs. Both methods are used in the first phase of the planning process in which the potential for optimization of the implant is determined, i.e. the possibility to modify the dose distribution while maintaining the prescribed dose in the prescription points. Both the implant geometry and the anatomy of the patient determine to what extent optimization is achievable, which is then quantified by the range of maximum dose values achievable in each organ at risk. This range gives an indication to the user whether his clinical goals can be achieved. In the second phase the user enters the dose limit for each organ at risk, which should of course be in the dose range, and the system delivers a dose distribution.

Six implant configurations were selected from the patients treated at our institute to evaluate inverse optimization. These configurations were chosen as they formed a wide range of situations varying strongly in target volume, coverage of the target by the implant and location of the organs at risk. The target volumes of these six patients, as delineated on the postimplant CT scan, ranged from 54 cm<sup>3</sup> to 113 cm<sup>3</sup>. The number of catheters implanted ranged between 17 and 25. For the clinical treatments the dose distributions were optimized using Geometric Optimization followed by Graphical Optimization (GO). Therefore, a geometric optimization (volume mode) [3,16] was performed, followed by manual adjustments of the isodose lines on the screen using the mouse. The reference isodose was the isodose that conformed optimally to the prostate's peripheral margin as delineated on the

postimplant CT scan. The dose at the urethra and the rectum should remain below 120% and 85% of the reference dose, respectively.

The dose distributions were also optimized using different modes of Inverse Optimization, i.e. Standard Inverse Optimization (SIO), Tuned Inverse Optimization (TIO) and Tuned Inverse Optimization followed by Graphical Optimization (GOTIO). In Standard Inverse Optimization an inverse optimization was performed as implemented in PLATO BPS 14.2 with the dose limit of the rectum equal to 85% and of the urethra equal to 120%. In Tuned Inverse Optimization the dose limit of the urethra was altered such that the urethra DVH reached 120% of the reference dose at 2% of the volume. Fine tuning of the latter method using graphical optimization was performed in Tuned Inverse Optimization followed by Graphical Optimization. In Standard and Tuned Inverse Optimization the reference dose was defined as the average dose in dose points placed on the target contour. The location of the reference isodose was manipulated when adding graphical optimization in GOTIO, such that the reference isodose conformed optimally to the prostate's peripheral margin as delineated on the postimplant CT scan.

The dose distributions were evaluated using Dose Volume Histograms (DVH) of the target, rectum and urethra, the target coverage and the maximum urethral dose. The maximum urethral dose was defined in a volume of 2% of the urethra,  $D_{2,urethra}$ . Besides target coverage irradiation of the surroundings should also be taken into account. In order to compare normal tissue irradiation, the Conformal Index (COIN) [1,14], describing the conformity of the dose distribution to the target, was evaluated. In case of a PTV with surrounding normal tissue COIN is defined as:

$$COIN = c_1 * c_2 \quad (1)$$

with:

$$c_1 = \frac{PTV_{ref}}{PTV} \quad (2)$$

$$c_2 = \frac{PTV_{ref}}{V_{ref}} \quad (3)$$

$PTV_{ref}$  = the part of the PTV covered by the reference dose,

$V_{ref}$  = total volume covered by the reference dose.

The fraction of the PTV which is enclosed by the reference isodose is described by  $c_1$  and the fraction of the total volume covered by the reference dose that belongs to the PTV by  $c_2$ . COIN can take values between 0 and 1 with 1 associated with full conformity.

The dose homogeneity was analysed using the Dose Nonuniformity Ratio [15], which is defined as the ratio of the volume receiving at least 150% of the reference dose to the volume receiving at least the reference dose, i.e.

$$DNR = \frac{Volume(D \geq 1.5 * D_{ref})}{Volume(D \geq D_{ref})} \quad (4)$$

#### 4.4 Results and discussion

Figure 1 shows the dose volume histograms of the target, urethra and rectum of patient A to illustrate the results of the different optimization methods.

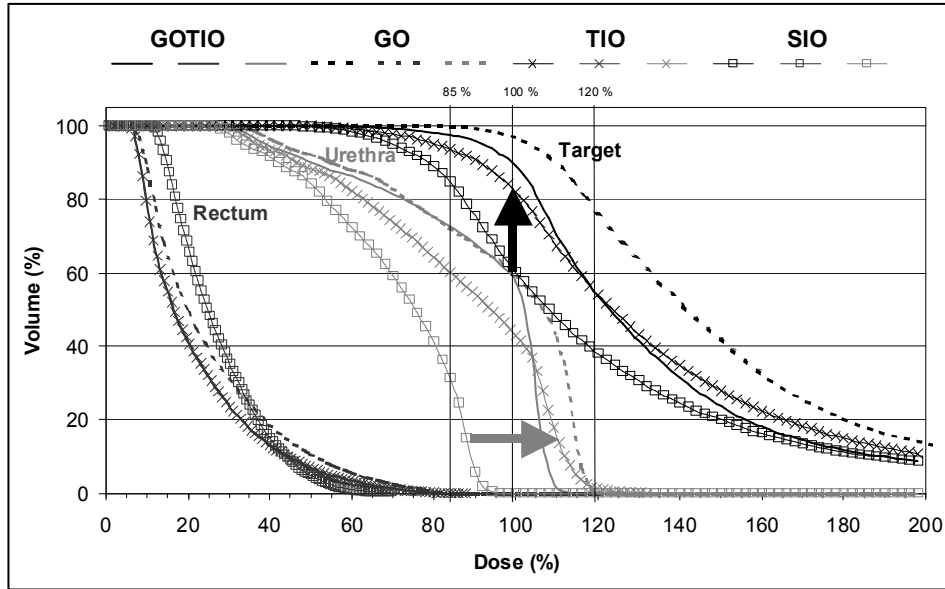


**Figure 1:** Dose volume histograms of patient A for the target, urethra and rectum. The dose distribution was optimized using Geometric Optimization followed by Graphical Optimization (GO), Standard Inverse Optimization (SIO), Tuned Inverse Optimization (TIO) and Tuned Inverse Optimization followed by Graphical Optimization (GOTIO). The arrows indicate the changes induced by replacing SIO by TIO.

For the method clinically used, i.e graphical optimization after geometric optimization (GO), the target coverage was 97% and the maximum urethral dose 120%. When applying standard inverse optimization (SIO) the target coverage was only 60%. The maximum urethral dose  $D_{2,\text{urethra}}$  was only 92%, still enabling a further dose increase. By increasing the dose constraint of the urethra up to 220% in tuned inverse optimization (TIO) the target coverage was increased to 82% as indicated by the arrow (figure 1). In that case the full dose range in the urethra was used, with  $D_{2,\text{urethra}}$  equal to 120%. When applying graphical optimization after tuned inverse optimization (GOTIO), the target coverage was increased to 89%.

The target coverage for each patient as a function of the optimization technique is shown in figure 2. The average target coverage for our clinical method, graphical optimization after geometric optimization (GO), was  $93\% \pm 4\%$ . When applying inverse optimization as implemented in PLATO BPS 14.2 (SIO) the target coverage was as low as  $53\% \pm 11\%$ . The maximum urethral dose  $D_{2,\text{urethra}}$  for all patients using standard inverse optimization (SIO) was on average  $92\% \pm 4\%$ . When increasing the urethra constraint up to  $185\% \pm 46\%$  on average, using tuned inverse optimization

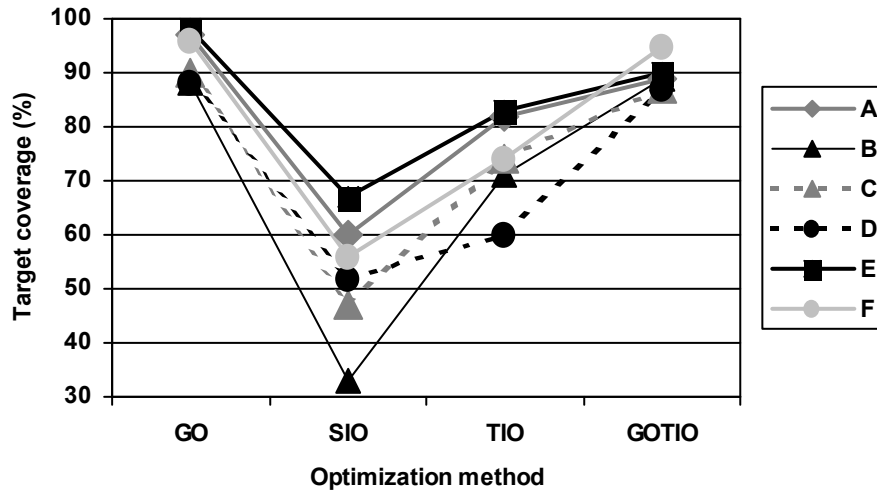


**Figure 2:** The target coverage for patients A to F as a function of the optimization method used, i.e. Geometric Optimization followed by Graphical Optimization (GO), Standard Inverse Optimization (SIO), Tuned Inverse Optimization (TIO) and Tuned Inverse Optimization followed by Graphical Optimization (GOTIO).

(TIO), the target coverage increased to  $74\% \pm 8\%$ , with the  $D_{2,urethra}$  equal to 120% for each patient. The target coverage was further increased to  $90\% \pm 3\%$  by adding graphical optimization (GOTIO) without compromising the urethra dose. For all patients a significantly lower target coverage for SIO than for the other three methods was seen. For four out of six patients the target coverage of GO and GOTIO were almost equal; however for patients A and E an 8% lower target coverage was seen in GOTIO. When looking in detail to the DVH's for these latter two patients it was noticed that not the full range of the urethra dose was used, suggesting the possibility for further dose optimization. Both methods including graphical optimization, i.e. GO and GOTIO, not only had the largest target coverage but also the smallest variation in coverage.

As the target coverage showed no significant difference between GO and GOTIO the COIN values were determined in order to compare normal tissue irradiation (figure 3). The average COIN values were  $0.73 \pm 0.02$  and  $0.77 \pm 0.07$ , respectively, for GO and GOTIO. Only a slightly better sparing of the surrounding normal tissues was seen for GOTIO. Therefore, the average COIN values for GO and GOTIO were not significantly different. However, for five out of 6 patients the COIN of GOTIO was better than for GO. Patient C, i.e. the patient with the smallest target volume, was the

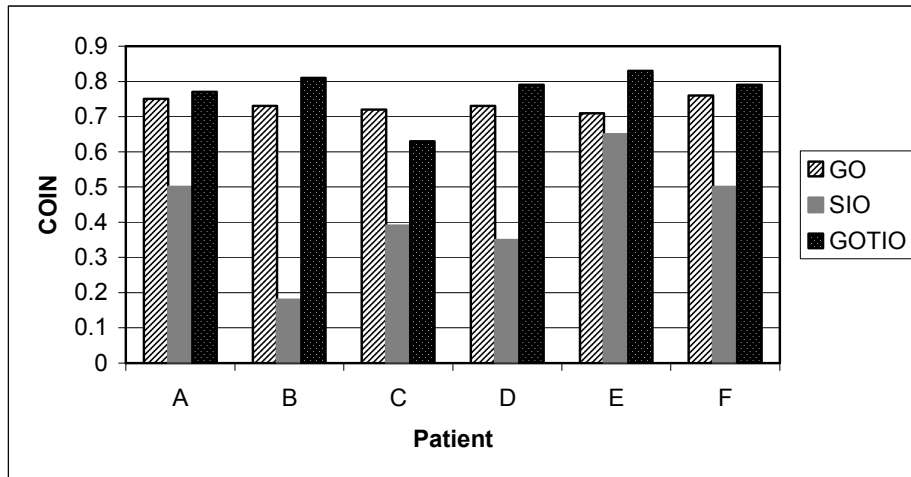


**Figure 3:** The coverage index COIN for patients A to F as a function of the optimization method used, i.e. Geometric Optimization followed by Graphical Optimization (GO), Standard Inverse Optimization (SIO) and Tuned Inverse Optimization followed by Graphical Optimization (GOTIO).

only patient with a smaller COIN for GOTIO, due to an increase in normal tissue irradiation. The significantly smaller average target coverage for SIO compared to GO translated into a significantly smaller COIN for SIO, i.e.  $0.43 \pm 0.15$ , as a similar normal tissue irradiation was found.

The Dose Nonuniformity Ratio DNR for each patient is shown in figure 4 for different optimization techniques. The average DNR values were  $0.38 \pm 0.04$  for GO,  $0.31 \pm 0.05$  for SIO,  $0.30 \pm 0.04$  for TIO and  $0.29 \pm 0.03$  for GOTIO. An increase in dose homogeneity can be seen when replacing the currently used method GO by GOTIO. For all patients, except patient B, i.e. the patient with the largest target volume in combination with a low catheter density, the introduction of inverse optimization in SIO, TIO and GOTIO resulted in a better DNR. It can be noticed that for those patients with a relatively low DNR for GO, e.g. patients B,C and D, the improvement due to GOTIO was limited. However, for those patients with a high DNR for GO, e.g. patients A and E, larger improvements were seen.

The maximum urethral dose was evaluated using  $D_{2,urethra}$ , i.e. the dose in a predefined volume of 2% of the urethra. This 2% volume was rather arbitrarily chosen. A similar evaluation could have been performed using other volumes, e.g.  $D_{10,urethra}$  which is the dose in 10% of the urethra. The absolute values would have been different, however the general behaviour would have been similar, also indicating

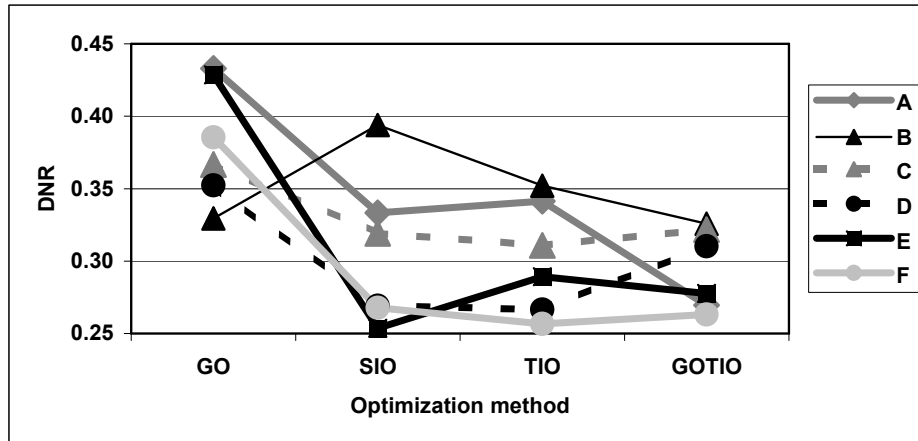


**Figure 4:** The Dose Nonuniformity Ratio DNR for patients A to F as a function of the optimization method used, i.e. Geometric Optimization followed by Graphical Optimization (GO), Standard Inverse Optimization (SIO), Tuned Inverse Optimization (TIO) and Tuned Inverse Optimization followed by Graphical Optimization (GOTIO).

that graphical optimization is needed for fine tuning of the dose distribution.

It can be concluded that the current implementation of anatomy based inverse planning or standard inverse optimization (SIO) in PLATO BPS resulted in an unacceptable low target coverage. The algorithm could be improved by implementing a dose volume constraint for the organs at risk. The latter method was simulated by applying tuned inverse optimization (TIO). As this method still resulted in a too low target coverage graphical optimization was needed for fine tuning of the dose distribution. Graphical optimization was shown to be a powerful tool with significantly higher COIN values for GO and GOTIO compared to SIO.

When comparing the current implementation of anatomy based inverse planning in PLATO BPS to other methods described in literature [5-10,13] one should keep in mind the fundamental differences in the algorithms used. The PLATO BPS method is inverse planning in the way that it is anatomy based planning, i.e. the target and organs at risk are used as input. This input is used in the first phase of the planning process in which a set of treatment plans is generated using classical dwell time optimization methods to determine the potential for optimization of the implant. In the second phase a treatment plan is chosen from this set fulfilling the dose constraints of the target and organs at risk. The methods described in literature [5-10,13] use multiobjective optimization algorithms in order to optimize a set of objective functions. Comparisons between these inverse optimization algorithms and the classical dwell time optimization methods when used by experienced planners have been published [5-7,13]. In general these inverse optimization algorithms show a better target coverage and dose conformity with more homogeneous dose distributions, more consistent results from one patient to another patient and better protection of the organs at risk. In this paper we investigated whether our currently used planning method, consisting of geometric optimization in combination with graphical optimization (GO), could be replaced by a method incorporating anatomy based inverse planning as implemented in PLATO BPS. It was shown that by using a modified version of anatomy based inverse planning, i.e. tuned inverse optimization followed by graphical optimization (GOTIO), the target coverage and dose conformity were at least as good. Despite the differences in the algorithms, both the results presented in literature [5-7,13] and our results showed an improved dose homogeneity when using anatomy based inverse planning. With graphical optimization being a time consuming process the reduction of the planning time remains limited when replacing GO by GOTIO. This process can take up to an hour, which is significantly more than the few minutes as described by Lahanas et al. [7] when using multiobjec-

tive optimization algorithms. The multiobjective anatomy based dose optimization algorithms described in [6-8,13] are implemented in a new real-time HDR ultrasound based prostate treatment planning system (SWIFT, Nucletron, The Netherlands). The introduction of these algorithms in combination with the real time planning procedure during catheter implementation is promising. It is expected that this system will shorten the time from catheter implantation to the delivery of the first HDR fraction. Besides, the real time planning procedure enables modification of the implant geometry based on dosimetric considerations. As the treatment plan is predominantly determined by the implant quality this will probably result in larger improvements than relying on dwell time optimization only.

#### 4.5 References

1. Baltas D, Kolotas C, Geramani K, et al. A conformal index (COIN) to evaluate implant quality and dose specification in brachytherapy. *Int J Radiat Oncol Biol Phys* 1998; 40:515-524.
2. Giannouli S, Baltas D, Milickovic N, et al. Autoactivation of source dwell positions for HDR brachytherapy treatment planning. *Med Phys* 2000; 27:11:2517-2520.
3. Kolkman-Deurloo IKK, Visser AG, Niël CGJH, Driver N, Levendag PC. Optimization of interstitial volume implants. *Radiother Oncol* 1994; 31:3:229-239.
4. Kouwenhoven HJ, van der Laarse R. Interactive inverse planning in HDR brachytherapy. In: *Proceedings 10<sup>th</sup> International Brachytherapy Conference*, Nucletron BV, The Netherlands, 2000; pp.96.
5. Lachance B, Béliveau-Nadeau D, Lessard E, et al. Early clinical experience with anatomy based inverse planning dose optimization for high dose rate boost of the prostate. *Int J Radiat Oncol Biol Phys* 2002; 54:1:86-100.
6. Lahanas M, Baltas D, Zamboglou N. Anatomy-based three-dimensional dose optimization in brachytherapy using multiobjective genetic algorithms. *Med Phys* 1999; 26:9:1904-1918.
7. Lahanas M, Baltas D, Zamboglou N. A hybrid evolutionary algorithm for multi-objective anatomy-based dose optimization in high-dose-rate brachytherapy. *Phys Med Biol* 2003; 48:399-415.
8. Lahanas M, Baltas D, Giannouli S. Global convergence analysis of fast multi-objective gradient-based dose optimization algorithms for high-dose-rate brachytherapy. *Phys Med Biol* 2003; 48:599-617.
9. Lessard E, Pouliot J. Inverse planning anatomy based dose optimization for HDR brachytherapy of the prostate using fast simulated annealing algorithm and dedicated objective function. *Med Phys* 2001; 28:5:773-779.



10. Lessard E, Hsu IC, Pouliot J. Inverse planning for interstitial gynaecologic template brachytherapy: truly anatomy based planning. *Int J Radiat Oncol Biol Phys* 2002; 54:4:1243-1251.
11. Mate TP, Gottesman JE, Hatton J, Gribble M, van Hollebeke L. High dose-rate afterloading 192-Iridium prostate brachytherapy: feasibility report. *Int J Radiat Oncol Biol Phys* 1998; 41:3:525-533.
12. Milickovic N, Giannouli S, Baltas D, et al. Catheter autoreconstruction in computed tomography based brachytherapy treatment planning. *Med Phys* 2000; 27:5:1047-1057.
13. Milickovic N, Lahanas M, Papagiannopoulou M, Zamboglou N, Baltas D. Multi-objective anatomy-based dose optimization for HDR-brachytherapy with constraint free deterministic algorithms. *Phys Med Biol* 2002; 47:2263-2280.
14. van 't Riet A, Mak ACA, Moerland MA, Elders LH, van der Zee W. A conformation number to quantify the degree of conformality in brachytherapy and external beam irradiation: application to the prostate. *Int J Radiat Oncol Biol Phys* 1997; 37:3:731-736.
15. Saw CB, Suntharalingam N. Quantitative assessment of interstitial implants. *Int J Radiat Oncol Biol Phys* 1991; 20:135-139.
16. Thomadsen BR, Houdek PV, van der Laarse R, Edmunson G, Kolkman-Deurloo IKK, Visser AG. Treatment planning and optimization. In: Nag S, editor. *HDR Brachytherapy: A Textbook*. Armonk, NY: Futura; 1994. pp. 79-145.



## CHAPTER 5. RECONSTRUCTION ACCURACY OF A DEDICATED LOCALISER FOR FILMLESS PLANNING IN INTRA-OPERATIVE BRACHYTHERAPY

IKK Kolkman-Deurloo, AG Visser, MHM Idzes, PC Levendag

Radiother Oncol 1997; 44; 73-81.

### 5.1 Abstract

*Background and purpose:* With the use of HDR and PDR afterloaders containing a single stepping source, brachytherapy dose distributions can be optimized by varying the source dwell time. With the goal of implementing 'conformal brachytherapy', i.e. ensuring that the dose distribution conforms as accurately as possible to the target volume, we evaluated a set-up which enabled on-line implant localisation and dose planning during implantation.

*Material and methods:* The set-up, designated as an Integrated Brachytherapy Unit (IBU), consists of a shielded operating room equipped with an HDR afterloader and a dedicated brachytherapy localiser connected to a treatment planning computer. The localiser is isocentric and has an extra degree of freedom in comparison to conventional simulators (i.e. an L-arm in combination with a C-arm) and enables viewing of the implant from any direction. A reconstruction algorithm which takes into account both rotation axes, i.e. the L- and C-arm angle, was developed for the localiser. The reconstruction procedure was tested by using the IBU localiser to measure the reconstruction accuracy with a phantom (containing 25 markers at well defined positions) and using reconstruction from radiographs. These results were compared to simulations where the accuracy of reconstruction was determined as a function of the reconstruction angle and the accuracy of read-outs of the localiser settings. On-line localisation and dose planning during implantation is based on filmless planning, i.e. fluoroscopy images and the corresponding localiser settings are imported into the treatment planning computer during implantation. The accuracy of filmless planning was determined using fluoroscopy images in the same set-up as for the experiments with the radiographs. The effect of reconstruction inaccuracies on the total irradiation

time and the dose in target or normal tissue points was elucidated for clinically relevant implant geometries. The treatment plans of two phantoms based on reconstruction from films as well as fluoroscopy images were compared with plans for implants defined by exact coordinates.

*Results:* The average reconstruction error due to the accuracy of the read-out of the localiser settings varied between -0.18 mm and 0.24 mm, with a standard deviation (arising from digitization errors) ranging from 0.11 mm to 0.22 mm. Using filmless reconstruction and the 10 inch field of view of the image intensifier (without applying correction for the geometric distortions) the average reconstruction error ranged from 0.01 mm to 0.65 mm, and the standard deviation ranged from 0.40 mm to 0.73 mm. These errors arose as a consequence of the finite pixel size and geometric distortions. These limited errors did not influence the treatment time for clinical implant geometries and had only a minor effect ( $< 1\%$ ) on the dose in markers during filmless planning.

*Conclusion:* This IBU set-up, with a dedicated brachytherapy localiser, allows for a rapid and accurate filmless planning procedure based on implant localisation from fluoroscopy images.

## 5.2 Introduction

High-dose-rate (HDR) and pulsed-dose-rate (PDR) afterloaders are increasingly used in brachytherapy. These afterloaders contain a single stepping source which enables optimization of the dose distribution through variation of the time the source dwells at each location inside the applicators [5,15]. Such optimization allows for a better adaptation of the dose distribution to the target volume and is a step towards 'conformal brachytherapy'.

Brachytherapy treatment planning is traditionally based upon implant reconstruction using localisation radiographs. For more 'conformal' brachytherapy, a better delineation of the target volume and of critical normal tissues (e.g. based on CT or MRI data) is necessary as is the case for treatment planning for external beam radiotherapy. Conformal brachytherapy can also be hampered by limitations imposed by the geometry of the implant and the latter can be prevented by an on-line planning procedure during implantation of the afterloading catheters. Such a method will allow for deficiencies in the dose distribution to be identified whilst the patient is in the operating room, and the implant modified accordingly.

An Integrated Brachytherapy Unit (IBU) (Nucletron, The Netherlands) comprises a shielded operating room equipped with an HDR afterloader and a dedicated brachytherapy localiser, which is connected to a treatment planning computer. This set-up enables integration of the entire brachytherapy procedure, i.e. implantation, implant reconstruction and dose planning in a single session. The availability of an HDR afterloader in the operating room also enables the use of intra-operative radiotherapy.

Recently an IBU has been established at the Daniel Den Hoed Cancer Center. A microSelectron HDR (Nucletron, The Netherlands) and an IBU localiser (Nucletron, The Netherlands) with a carbon fiber operating table have been installed in a shielded operating room. The localiser is connected to the PLATO planning system (Nucletron, The Netherlands) and the video images of the image intensifier are imported into the workstation (Indigo R3000 workstation, Silicon Graphics) by means of a frame grabber (Silicon Graphics IndigoVideo board, 8 bit, 752 \* 582 pixels), thereby allowing 'filmless planning'.

The dedicated IBU localiser consists of an L-arm in combination with a C-arm (figure 1). It is an isocentric localiser but has an extra degree of freedom compared to conventional simulators, thereby enabling viewing of the implant from any freely chosen direction.

The reconstruction of brachytherapy implants is performed with either a non-isocentric imaging system or an isocentric simulator intended for simulation of external beam radiotherapy. In case of a non-isocentric localisation procedure, one could either use a 'reconstruction box' placed over the patient or rely on a set of fiducial markers to determine the relative geometry of the two localisation images [3,10]. The reconstruction algorithm to be used in conjunction with an isocentric localiser has been described by Siddon [14].

A dedicated reconstruction algorithm had to be developed for the IBU localiser, taking into account both rotation axes, i.e. the L- and C-arm angle. We tested this algorithm by measuring the reconstruction accuracy of the localiser using a phantom containing 25 markers at well defined positions. The measured results were compared to simulations which determined the reconstruction accuracy as a function of the L-arm and C-arm angle, and as a function of the accuracy of the read-out of the localiser settings.

In order to evaluate filmless planning, fluoroscopy images were used for implant reconstruction. As extra inaccuracy can be introduced due to geometric distortions

present in fluoroscopy images [1,11,12], the effect of such distortions on reconstruction accuracy had to be quantified and the accuracy was studied using fluoroscopy images in the same set-up as for the experiments with radiographs.

In addition, treatment plans of two phantoms representing clinical implant geometries based on reconstruction from films as well as fluoroscopy images were compared with plans based on implant definition by coordinates. The effect of reconstruction inaccuracies on the total irradiation time and the dose in points representing the target or normal tissue points was elucidated.

### 5.3 Materials and methods

The IBU localiser (Nucletron, The Netherlands) consists of an L-arm in combination with a C-arm (figure 1). The L-arm can rotate over an angle  $\alpha$  of plus and minus  $195^\circ$  with  $\alpha = 0^\circ$  for the L-arm in the vertical plane. The C-arm can rotate over an angle  $\beta$  of plus and minus  $135^\circ$  with  $\beta = 0^\circ$  when the C-arm is aligned along the L-arm. In

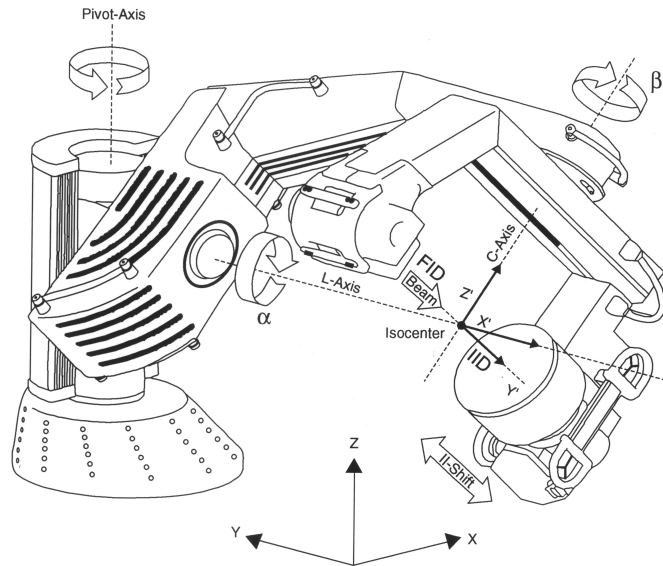


**Figure 1:** The IBU localiser (Nucletron, The Netherlands). Indicated are the rotation angles  $\alpha$  and  $\beta$  around the L- and C-arm axes, respectively.

addition, the localiser can be rotated over  $40^\circ$  around the vertical pivot-axis (figure 1) into a parking position which allows for maximum access to the operating table during implantation. It is equipped with an image intensifier with 'zoom modes' of 7, 10 or 15 inches. The nominal focus isocenter distance (FID) of this localiser is 800 mm, the isocenter image intensifier distance (IID) is variable with a maximum of 440 mm.

The geometry of an implant can be reconstructed from two images made with this IBU localiser. As it is isocentric, the reconstruction algorithm for the localiser takes into account the L-arm angle  $\alpha$ , the C-arm angle  $\beta$ , the focus isocenter distance (FID) and the isocenter image intensifier distance (IID). It could be considered as a modification of the algorithm proposed by Siddon [14].

An orthogonal coordinate system is defined with its origin in the isocenter of the localiser, like the F-system in Siddon [13], being a coordinate system fixed in the treatment room. According to Siddon [13] the Y-axis is oriented along the L-arm axis and the Z-axis points upwards (figure 1). A second coordinate system is defined, again with its origin in the isocenter, like the G-system in Siddon [13], being a gantry coordinate system. In this system the X'-axis and Z'-axis are oriented along the projection of the crosshairs in the image plane and the Y'-axis points towards the image intensifier. The transformation matrix  $T$  of the X-, Y- and Z-axes into the X'-, Y'- and Z'-axes can be written as:

$$T = R_y(\alpha).R_z(\beta) \quad (1)$$

where  $R_y(\alpha)$  is the rotation matrix around the Y-axis over angle  $\alpha$  and  $R_z(\beta)$  is the rotation matrix around the Z-axis over angle  $\beta$ .

Let  $\mathbf{q}$  be a point with coordinates  $(x_q, y_q, z_q)$  in the first coordinate system and coordinates  $(x'_q, y'_q, z'_q)$  in the second coordinate system. These are then related by:

$$\begin{pmatrix} x_q \\ y_q \\ z_q \end{pmatrix} = R_y(\alpha).R_z(\beta) \cdot \begin{pmatrix} x'_q \\ y'_q \\ z'_q \end{pmatrix} \quad (2)$$

This could be considered as an extension of the coordinate transformation proposed by Siddon [13] transforming the coordinates of point  $\mathbf{q}$  expressed in the G-system (the gantry coordinate system) into coordinates expressed in the F-system (coordinate system fixed in the room).

An object point  $\mathbf{P}$  is reconstructed from two images made with the localiser using two different set-ups. These set-ups are characterised by two focal positions  $\mathbf{f}_1$  and  $\mathbf{f}_2$  and two transformation matrices, i.e.  $(R_y(\alpha).R_z(\beta))_1$  and  $(R_y(\alpha).R_z(\beta))_2$ . Let  $\mathbf{p}_1$  and  $\mathbf{p}_2$  be the projections of the object point  $\mathbf{P}$  on these two images, with the coordinates of  $\mathbf{p}_1$  and  $\mathbf{p}_2$  expressed in both G-systems as  $(a_1, \text{IID}_1, b_1)$  and  $(a_2, \text{IID}_2, b_2)$  respectively. The coordinates of  $\mathbf{f}_1$  and  $\mathbf{f}_2$ , expressed in both G-systems, are  $(0, -\text{FID}, 0)$  as FID is fixed. These parameters can be expressed in the F-system by applying equation (2).

Two rays  $\mathbf{r}_1(\lambda)$  and  $\mathbf{r}_2(\mu)$  are constructed connecting the image points  $\mathbf{p}_1$  and  $\mathbf{p}_2$  with the focal positions  $\mathbf{f}_1$  and  $\mathbf{f}_2$  respectively:

$$\mathbf{r}_1(\lambda) = \mathbf{f}_1 + \lambda(\mathbf{p}_1 - \mathbf{f}_1) \quad (3)$$

$$\mathbf{r}_2(\mu) = \mathbf{f}_2 + \mu(\mathbf{p}_2 - \mathbf{f}_2) \quad (4)$$

Ideally, these rays  $\mathbf{r}_1(\lambda)$  and  $\mathbf{r}_2(\mu)$  intersect at the position of the object point  $\mathbf{P}$ , which in general is not the case due to digitization inaccuracies and patient movement. According to Siddon [14] the object point  $\mathbf{P}$  is found by minimizing the distance from this point to both rays. Therefore, a line between both rays is constructed which in general is described by:

$$(\mathbf{r}_2(\mu) - \mathbf{r}_1(\lambda)) \quad (5)$$

The following equations have to be solved in order to find the line that is perpendicular to both rays with directions  $(\mathbf{p}_1 - \mathbf{f}_1)$  and  $(\mathbf{p}_2 - \mathbf{f}_2)$ :

$$(\mathbf{r}_2(\mu) - \mathbf{r}_1(\lambda)) \cdot (\mathbf{p}_1 - \mathbf{f}_1) = 0 \quad (6)$$

$$(\mathbf{r}_2(\mu) - \mathbf{r}_1(\lambda)) \cdot (\mathbf{p}_2 - \mathbf{f}_2) = 0 \quad (7)$$

yielding the solution  $(\lambda_0, \mu_0)$ .

The object point  $\mathbf{P}$  is then given by:

$$\mathbf{P} = \frac{1}{2}(\mathbf{r}_1(\lambda_0) + \mathbf{r}_2(\mu_0)) \quad (8)$$

The reconstruction accuracy of the IBU localiser has been simulated as a function of the accuracy of the parameters  $\alpha$ ,  $\beta$ , FID and IID. A point  $\mathbf{P}$  in the target volume and two settings  $(\alpha, \beta, \text{FID and IID})$  of the localiser were chosen. For both settings the two-dimensional projection of point  $\mathbf{P}$  on the image plane was calculated. Perturbations  $(\delta\alpha, \delta\beta, \delta\text{FID and } \delta\text{IID})$  on the settings of the localiser were introduced and a



point  $P'$  was reconstructed from the projection of  $P$  on both images using the perturbed settings ( $\alpha + \delta\alpha$ ,  $\beta + \delta\beta$ ,  $FID + \delta FID$  and  $IID + \delta IID$ ). Finally, the distance between  $P$  and  $P'$  was calculated, representing the reconstruction deviation. This has been repeated for different combinations of perturbations, in order to find the maximum deviation when assuming maximum read-out errors  $\delta\alpha_{\max}$ ,  $\delta\beta_{\max}$ ,  $\delta FID_{\max}$  and  $\delta IID_{\max}$ . The perturbations consisted of varying  $\delta\alpha$  between  $-\delta\alpha_{\max}$  and  $\delta\alpha_{\max}$ ,  $\delta\beta$  between  $-\delta\beta_{\max}$  and  $\delta\beta_{\max}$ ,  $\delta FID$  between  $-\delta FID_{\max}$  and  $\delta FID_{\max}$  and  $\delta IID$  between  $-\delta IID_{\max}$  and  $\delta IID_{\max}$ . In case of orthogonal reconstruction the maximum deviation has been determined as a function of the accuracy of the read-outs of the localiser settings. Assuming a known accuracy of these read-outs the deviation was also simulated as a function of the reconstruction angle.

For these simulations a focus isocenter distance (FID) of 765 mm had been chosen. The isocenter image intensifier distance (IID) is variable. However, all simulations have been performed with the smallest IID, i.e. 130 mm. For the location of point  $P$  three different cases have been studied. The  $x$ ,  $y$  and  $z$  coordinates of  $P$  were either in the range of -30 mm to 30 mm, -60 mm to 60 mm or -120 to 120 mm relative to the isocenter.

The reconstruction accuracy in case of orthogonal reconstruction was measured using a QA phantom. A QA phantom is a lucite phantom consisting of six identical

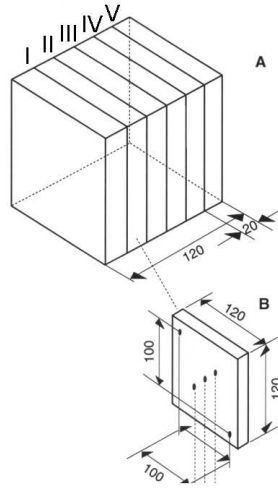


**Figure 2:** The geometry of the QA phantom (a). It consists of six identical slabs (b) of 20 mm thickness containing five markers at each boundary I,II,III,IV,V.

slabs of 20 mm thickness containing five markers (spheres with a diameter of 1 mm) as indicated in figure 2b at each boundary (indicated as I,II,III,IV,V in figure 2a). The phantom was positioned on the treatment table with the central marker close to the isocenter of the localiser. Eight orthogonal X-ray films were made with the localiser settings as mentioned in table 1. Subsequently eight fluoroscopy images were captured with a 10 inch field of view of the image intensifier with equal localiser settings. The position of the markers was reconstructed from film and fluoroscopy images using the eight combinations shown in table 1. For each reconstruction the error in the spacing between reconstructed markers (taking into account three markers in each row, i.e. in planes I, III and V) has been determined (105 combinations).

In addition to the accuracy in the distance between reconstructed marker positions, the *absolute* reconstruction accuracy was of importance, i.e. the absolute coordinates of the implant relative to the isocenter. For this purpose, variations in the reconstructed absolute coordinates of the central marker of the phantom were determined by comparing the results from all reconstruction combinations mentioned in table 1.

**Table 1:** Localiser set-up for the films and images used for reconstruction of the QA phantom (FID = 795 mm, IID = 358 mm).

Combination	C-arm angle (°)	L-arm angle (°) film/image 1	L-arm angle (°) film/image 2	Orientation
A	90	0	90	RL + AP
B	90	90	180	LR + AP
C	90	0	270	RL + PA
D	90	180	270	LR + PA
E	270	0	90	LR + PA
F	270	90	180	RL + PA
G	270	0	270	LR + AP
H	270	180	270	RL + AP

In order to determine the effect of the reconstruction accuracy on the treatment plan, phantoms representing clinical implant geometries (figure 3) were used. The first phantom consisted of a two-plane implant (representative of a breast implant) with seven needles of 80 mm length each and eight markers (figure 3a). The second phantom was a gynaecological applicator (an intrauterine tube with two ovoid applicators) (figure 3b). In this phantom two markers were placed at points A according to the Manchester system [16], i.e. 2 cm cranial and 2 cm lateral of the

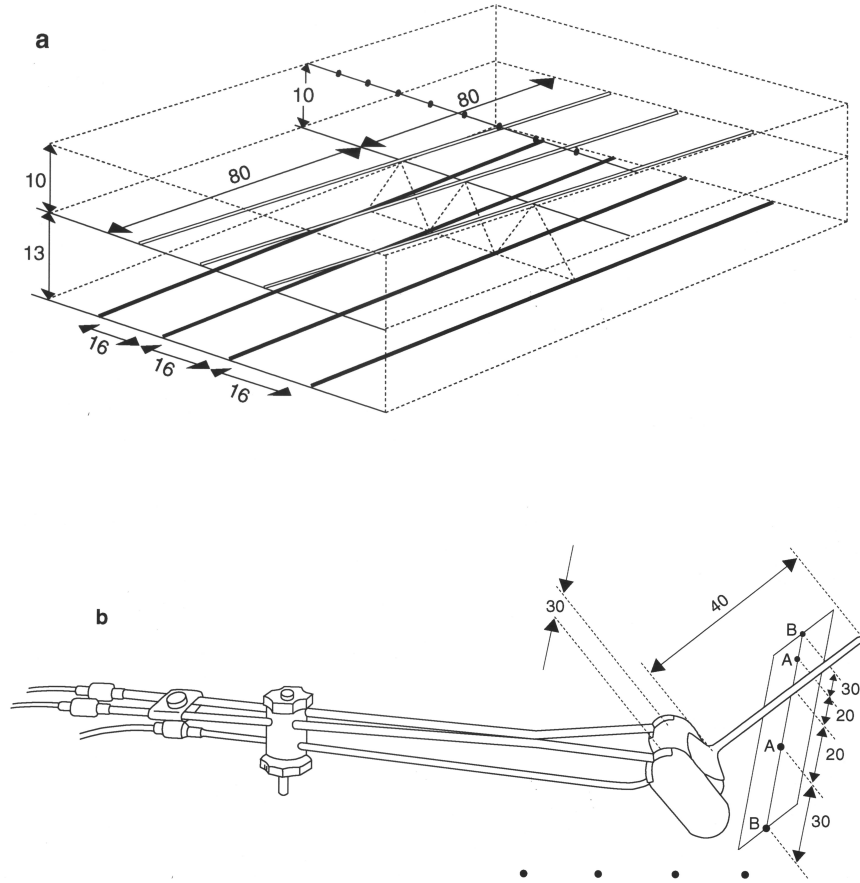


**Figure 3:** The geometry of the two phantoms representing clinical implants: (a) a two plane implant with seven needles and eight markers at the surface of the phantom, (b) a gynaecology applicator with eight markers representing rectal markers and points A and B.

**Table 2:** *Set-up of the reconstruction films/images used for the clinical phantoms.*

	C-arm angle (°)	L-arm angles (°)
Breast phantom	90	45; 315
Gynaecological phantom	90	0; 90

flange of the intrauterine tube, and two markers 30 mm lateral of these reference markers (points B). Extra markers, representative for rectal markers, were added.

Treatment plans for an HDR stepping source afterloader were calculated using uniform source dwell times (i.e. no optimization). The set-up for the reconstruction images is summarized in table 2.

For the breast phantom, coordinates of the dwell positions and the markers were accurately known. Three treatment plans were calculated and a plan based on implant definition using the known coordinates served as reference plan. This plan was compared to plans based on reconstruction from orthogonal X-ray films as well as fluoroscopy images.

For calculation of the dose distribution of the breast phantom, a central plane passing through the center of the implant was defined perpendicular to the main direction of the needles. In this plane, the intersections of the needles formed five equilateral triangles. The geometric centers of these triangles were used as reference points, so called basal dose points [2]. The mean central dose was defined as the average dose over these basal dose points. The reference dose was defined at 85% of the mean central dose, according to the Paris system [2].

For the gynaecological phantom, only a plan based on reconstruction from orthogonal X-ray films has been compared to the plan based on reconstruction from fluoroscopy images, as the coordinates of the markers were not accurately known. The reference dose has been specified as the average dose in the markers at both points A, respectively right and left from the applicator.

## 5.4 Results

### 5.4.1 Results of error simulation

The simulations were intended to determine the maximum deviation between the reconstructed point and the original point from a combination of  $\delta\alpha$ ,  $\delta\beta$ ,  $\delta FID$  and  $\delta IID$  within the range of the chosen maximum read-out errors  $\delta\alpha_{\max}$ ,  $\delta\beta_{\max}$ ,  $\delta FID_{\max}$  and  $\delta IID_{\max}$ .

In figure 4 the absolute deviation of the reconstructed point was determined as a function of the maximum read-out error  $\delta\alpha_{\max}$  and  $\delta\beta_{\max}$  (with  $\delta\alpha_{\max} = \delta\beta_{\max}$ ) in case of orthogonal reconstruction, i.e.  $\beta$  was  $90^\circ$  in both images and  $\alpha$  was  $0^\circ$  and  $90^\circ$ , respectively.  $\delta FID_{\max}$  and  $\delta IID_{\max}$  were assumed to be 1 mm. The latter were introduced by the accuracy of the indicator measuring the actual IID, which is better than 0.5 mm, and the calibration procedure of FID and IID. Two rulers were imaged

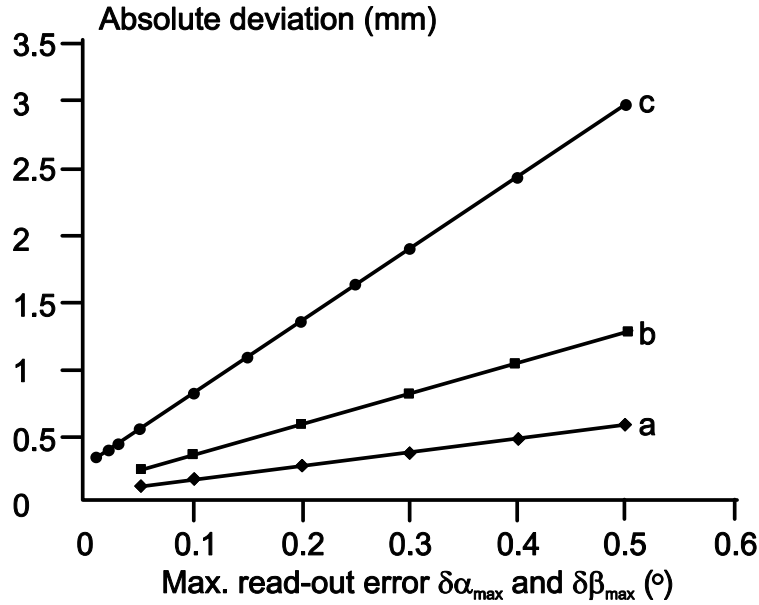


**Figure 4:** The simulated absolute maximum deviation of a reconstructed point as a function of the maximum read-out error in the L- and C-arm angles, i.e.  $\delta\alpha_{\max}$  and  $\delta\beta_{\max}$ , in case of orthogonal reconstruction.  $FID = 765$  mm,  $IID = 130$  mm,  $\delta FID_{\max} = \delta IID_{\max} = 1$  mm. The x, y and z coordinates of P are in the range of -30 mm to 30 mm (a), -60 mm to 60 mm (b) and -120 to 120 mm (c) relative to the isocenter.

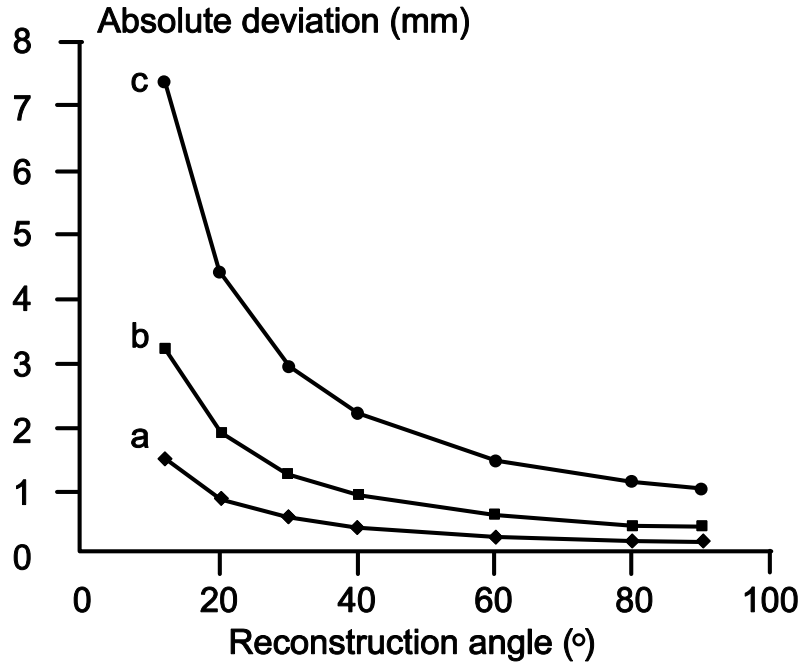


**Figure 5:** The simulated absolute maximum deviation of a reconstructed point as a function of the reconstruction angle.  $FID = 765$  mm,  $IID = 130$  mm,  $\delta FID_{max} = \delta IID_{max} = 1$  mm,  $\delta\alpha_{max} = \delta\beta_{max} = 0.2^\circ$ ,  $\beta = 90^\circ$ ;  $\alpha = (90^\circ - 1/2 \text{ reconstruction angle})$  in the first image and  $\alpha = (90^\circ + 1/2 \text{ reconstruction angle})$  in the second image. The  $x$ ,  $y$  and  $z$  coordinates of  $P$  are in the range of  $-30$  mm to  $30$  mm (a),  $-60$  mm to  $60$  mm (b) and  $-120$  to  $120$  mm (c) relative to the isocenter.

for the calibration procedure, with one ruler positioned along the L-arm axis and the other one parallel to it at a known distance.

The deviation was dependent on the position of the original point in the implant, as points further away from the isocenter showed a larger deviation when introducing perturbations in the localiser settings during reconstruction. This introduced a reconstruction error, i.e. an error in spacing between different points in an implant. As the lines in figure 4 are diverging as a function of  $\delta\alpha_{max}$  and  $\delta\beta_{max}$ , the error in spacing between different points increases as a function of  $\delta\alpha_{max}$  and  $\delta\beta_{max}$ .

Assuming a read-out accuracy of  $\alpha$  and  $\beta$  of  $0.2^\circ$  ( $\delta\alpha_{max} = \delta\beta_{max} = 0.2^\circ$ ), i.e. the accuracy of the angle indicators ( $0.1^\circ$ ) and of the calibration procedure of these indicators (using a spiritlevel at horizontal and vertical positions of the localiser), the deviation as a function of the reconstruction angle is plotted in figure 5.

In this simulation  $\beta$  was kept at  $90^\circ$  and  $\alpha = (90^\circ - 1/2 \text{ reconstruction angle})$  in one image and  $\alpha = (90^\circ + 1/2 \text{ reconstruction angle})$  in the other image which was similar to variable angle reconstruction. As would be expected, the smallest deviation occurred for a reconstruction angle of  $90^\circ$ , i.e.  $\alpha_1 = -45^\circ$  and  $\alpha_2 = 45^\circ$ .

#### 5.4.2 Reconstruction results with the QA phantom

While the simulations determined the distribution of absolute displacements due to reconstruction, the experiments with the QA phantom were intended to measure the

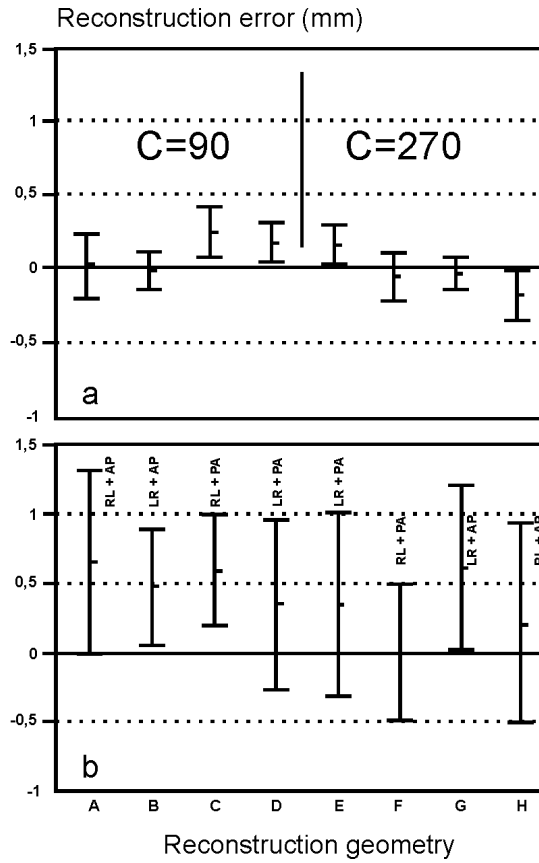


**Figure 6:** The relative reconstruction accuracy of the IBU localiser for reconstruction from orthogonal films (a) and fluoroscopy images (b) for the eight reconstruction combinations mentioned in table 1.

**Table 3:** Deviation of the total treatment time for the reconstructed clinical phantoms (see table 2) compared to the reference plan. (\*For the gynaecological phantom the image based plan is compared to the film based plan.)

	Film (%)	Images (%)
Breast phantom	0.0	0.0
Gynaecological phantom	-	0.1*

error in the spacing between markers due to reconstruction. In order to perform these measurements the localiser was positioned at the values mentioned in table 1. The focus isocenter distance of our localiser is 795 mm. The isocenter image intensifier distance was kept constant at 358 mm during these measurements. The mean reconstruction error for the 105 marker combinations (with error bars representing the standard deviation) is shown in figure 6a in case of reconstruction from orthogonal films for the eight reconstruction combinations mentioned in table 1. The average reconstruction error for all combinations was 0.04 mm. This value increased to 0.4 mm when performing the same measurements using reconstruction from fluoroscopy images (10 inch field of view of the image intensifier) instead of reconstruction from film (figure 6b). The positive sign of the results indicates that the reconstructed spacing is systematically slightly smaller than the actual spacing.

The deviation in the coordinates of the central marker of the phantom as a function of the localiser settings in case of orthogonal reconstruction showed a variation in the x-coordinate between -1.2 mm and 1.3 mm, in the y-coordinate between -1.0 mm and 1.4 mm and in the z-coordinate between -0.6 mm and 0.6 mm.

#### 5.4.3 Reconstruction results with the clinical phantoms

The deviation of the total treatment time of the reconstruction-based plans compared to the reference plan for experiments with the clinical phantoms (see table 2) is shown in table 3. A positive sign in these results indicates that the treatment time of the planning based on a reconstructed implant is greater than that of the reference plan.

The dose in the reconstructed markers was compared to the marker dose in the reference plan. These results are summarized in table 4.



**Table 4:** Deviation of the marker dose for the reconstructed clinical phantoms (see table 2) compared to the reference plan. The number of markers is denoted in parentheses. (\*For the gynaecological phantom the image based plan is compared to the film based plan.)

	Film (%)	Images (%)
Breast phantom (8)	$0.4 \pm 0.4$	$-0.7 \pm 0.5$
Gynaecological phantom (8)	-	$0.9 \pm 2.3^*$

## 5.5 Discussion

A reconstruction algorithm for the dedicated brachytherapy localiser has been developed. Simulations were performed to determine the reconstruction accuracy of this localiser as a function of the reconstruction angle and the accuracy of the read-outs of the L-arm and C-arm angle and the isocenter image intensifier distance. In figures 4 and 5 the absolute deviation between the position of the original point and the position of a point reconstructed from two images using perturbed localiser settings is shown. In both figures, each point indicates a worst case situation as the combination of perturbations resulting in the largest error was chosen for each point.

These simulations have been limited to the determination of the reconstruction errors due to inaccuracies in  $\alpha$ ,  $\beta$ , FID and IID read-outs. For example, we have not taken mechanical deformations of the localiser into account and this can have a major effect on the absolute position of the origin of the coordinate system relative to the object. Furthermore, errors due to digitization or patient motion, as described by Löffler-Rombold [8], Lam and Ten Haken [6], Li et al [7], were neglected.

The experiments with the QA phantom were intended to determine the reconstruction accuracy as the accuracy in the spacing between markers, which is the most relevant parameter for brachytherapy planning. An error in spacing between a dose point and an applicator, for example, will lead to an error in dose calculation. The average accuracy was determined for 105 combinations with spacings ranging from 20 to 162.5 mm. Reconstructing from orthogonal films (fixed on the image intensifier) resulted in an average reconstruction error of 0.04 mm, indicating the absence of a systematic inaccuracy, e.g. an incorrect calibration of the combination of FID and IID which would show up as a systematic error in the magnification factor throughout all reconstructions. The average reconstruction error for each reconstruction combination ranged from -0.18 mm to 0.24 mm. For each combination this average

error indicates the overall set-up accuracy for both films used for the reconstruction, arising as a result of the actual localiser settings (L-arm and C-arm angle and IID) and mechanical deformations of the localiser. The standard deviation for each combination, ranging from 0.11 mm to 0.22 mm, can arise due to digitization errors.

After digitizing 75 markers from a simulator film, Lam and Ten Haken [6] found a manual digitization error of 0.09 mm. However, when this study was repeated using a film made on a linear accelerator, a slightly larger error of 0.23 mm was found which was attributed to an inferior image quality. Their results are comparable to the standard deviation of our measurements. Lam and Ten Haken [6] have also determined the reconstruction error in case of orthogonal films which arise due to the accuracy of the equipment. They defined the reconstruction error as the root-mean-square of the minimum separation between the rays connecting an image point and the focus. The theoretical error which arose solely due to inaccuracies in the manual digitization process was calculated to be 0.07 mm using reconstruction from simulator films. The observed error derived from reconstruction from two orthogonal films was 0.79 mm, with the increase from 0.07 mm to 0.79 mm due to inaccuracies in the simulator settings. When applying a minimization procedure based on Metz and Fencil [10] the authors were able to reduce this error to the value solely caused by the digitization inaccuracy.

In case of reconstruction from fluoroscopy images, without applying any correction for the geometric distortions, the average reconstruction error increased to 0.4 mm. This could be caused by geometric distortions present in fluoroscopy images. Such distortions usually consist of a pincushion effect due to the geometry of the image intensifier, i.e. a curved photocathode in combination with a flat output screen [1,12], and an S-distortion which is caused by the earth's magnetic field. The pincushion effect is a constant distortion whereas the S-distortion depends on the orientation of the image intensifier. The latter is maximal when the magnetic vector is perpendicular to the image plane [12]. In our case, measurements with a phantom, consisting of a copper plate with holes at a regular grid, fixed to the image intensifier, have demonstrated that the pincushion effect can be neglected when using a 10 inch field of view. The average reconstruction error for each combination varied between 0.01 mm and 0.65 mm (with a standard deviation ranging from 0.40 mm to 0.73 mm). As a result of this standard deviation, no significant difference was seen between the different combinations.

The pixel size in our configuration was 0.43 mm. The effect of pixel size on the reconstruction accuracy has been studied by Fencil and Metz who used a reconstruction algorithm based on a set of fiducial markers [3,10]. Assuming perfect conditions, i.e. with the image coordinates exactly computed, the reconstruction accuracy was in the order of  $10^{-7}$  mm. However, in a situation where the image coordinates were only known to the nearest pixel, the reconstruction accuracy decreased to 5 mm for a pixel size of 0.35 mm (using eight fiducial markers). This algorithm was relatively sensitive to experimental errors and the accuracy was improved to 0.3 mm by the use of 30 fiducial markers. After taking into account the number of fiducial markers and inaccuracies both in the imaging geometry, e.g. angle between two imaging views, and in the measured quantities, e.g. origin of the image coordinate system, Fencil and Metz [3] concluded that with their reconstruction algorithm object points can be reconstructed with an overall accuracy on the order of 1 to 2 mm. To a lesser extent, a similar effect could explain the increase in the standard deviation which we observed when converting from film to fluoroscopy images having a pixel size of 0.43 mm.

The overall accuracy for filmless planning with the IBU localiser, ranging from 0.01 mm to 0.65 mm for each reconstruction combination, is due to a combination of the accuracy of the read-out of the actual localiser settings, and the geometric distortions. The effect of the read-outs of the settings was similar to the case where reconstruction was based on radiographs and appeared to be of limited magnitude (figure 6a). We conclude, therefore, that the increase in the reconstruction error as compared to reconstruction from film was mainly due to the S-distortion.

When matching the implant geometry with other imaging modalities using matching of coordinate systems (e.g. CT/MRI and localisation coordinate systems), the absolute coordinates of the implant relative to the isocenter are important. No systematic reconstruction inaccuracy was seen when reconstructing from film (figure 6a), indicating that the absolute deviation of the coordinates of the central marker is a good indicator for the deviation of the position of the phantom. This indicates that choosing different reconstruction combinations, e.g. D or E (both consisting of a left-to-right and a PA radiograph, table 1), would result in a different projection of the implant geometry (reconstructed from the radiographs) and dose distribution in the anatomy (e.g. derived from CT). The maximum variation was 2.5, 2.4 and 1.2 mm in the x-, y- and z-directions, respectively. This was caused by the position of the isocenter itself which is within a sphere with a diameter of 2 mm and by uncertainties in the positioning of the X-ray tube and the crosswires.

The accurate results when reconstructing the markers in the QA phantom from film (figure 6a) were also reflected in the results for the breast phantom. From table 3 it can be seen that the calculated treatment time was equal to the treatment time of the reference plan and that the dose in eight extra markers was accurately calculated.

When converting to reconstruction from fluoroscopy images, the calculated treatment time remained unchanged for both phantoms (table 3). The small difference for the gynaecological phantom (0.1%) is in the order of the error in treatment planning due to rounding off (typically 0.1 s per dwell position). In this case, the dwell time per dwell position was 25.2 s, resulting in a rounding error of 0.3%.

With regard to the dose in additional markers (table 4), the inaccuracy due to filmless reconstruction was comparable to reconstruction from film. However, a relatively large standard deviation was seen for the gynaecological phantom.

In a similar experiment, Li et al [7] determined the accuracy of reconstructing the source positions of a Fletcher-Suit applicator from simulator films. They showed that as a result of reconstruction errors in the source positions, a 5% variation was seen in the dose in a point in the cervix, a 1% variation was seen in the bladder and a 0.3% variation was seen in the rectum.

## 5.6 Conclusions

This study shows that accurate implant reconstruction from film is possible using the IBU localiser in combination with the IBU reconstruction algorithm. The average reconstruction error due to the accuracy of the read-out of the localiser settings varies between -0.18 mm and 0.24 mm. In addition, a standard deviation due to digitization errors of 0.11 mm to 0.22 mm was found. Using the 10 inch field of view of the image intensifier, without applying any correction for the geometric distortions, the S-distortion introduced an average reconstruction error ranging from 0.01 to 0.65 mm. Due to the finite pixel size, the standard deviation varied between 0.40 and 0.73 mm. These small errors did not influence the treatment time, when considering clinical implant geometries, and had a minor effect ( $< 1\%$ ) on the dose in markers obtained by filmless planning.

This data should be considered in the light of other inaccuracies in brachytherapy treatment planning such as inaccuracies in source calibration [17], source positioning and dose calculation algorithms [4,9,18]. Furthermore, the overall accuracy of the

implantation procedure and the determination of relevant separations in brachytherapy is limited to 1 to 2 mm.

It can be concluded that the set-up of this Integrated Brachytherapy Unit enables a fast and accurate filmless planning procedure based on implant localisation by on-line importing fluoroscopy images and localiser settings in the treatment planning computer.

## 5.7 References

1. Boone, J.M., Seibert, J.A., Barrett, W.A., Blood, E.A. Analysis and correction of imperfections in the image intensifier-TV-digitizer imaging chain. *Med. Phys.* 18: 236-242, 1991.
2. Dutreix, A., Marinello, G., Wambersie, A. *Dosimétrie en Curiethérapie*. Masson, Paris, France, 1982.
3. Fencil, L.E., Metz, C.E. Propagation and reduction of error in three-dimensional structure determined from biplane views of unknown orientation. *Med. Phys.* 17: 951-961, 1990.
4. Feroldi, P., Galelli, M., Belletti, S. A comparison of accuracy of computer treatment planning systems in brachytherapy. *Radiother. Oncol.* 24: 147-154, 1992.
5. Kolkman-Deurloo, I.K.K., Visser, A.G., Niël, C.G.J.H., Driver, N., Levendag, P.C. Optimization of interstitial volume implants. *Radiother. Oncol.* 31: 229-239, 1994.
6. Lam, K.L., Ten Haken, R.K. Improvement of precision in spatial localization of radio-opaque markers using the two-film technique. *Med. Phys.* 18: 1126-1131, 1991.
7. Li, S., Pelizzari, C.A., Chen, G.T.Y. Unfolding patient motion with biplane radiographs. *Med. Phys.* 21: 1427-1433, 1994.
8. Löffler-Rombold, E. Technik und rechnergestützte Dosimetrie der interstitiellen ferngesteuerten LDR-Afterloadingtherapie im Rahmen der brusterhaltenden Behandlung des Mammakarzinoms. Thesis, 1990.
9. Meertens, H. A comparison of dose calculations at points around an intracavitary cervix applicator. *Radiother. Oncol.* 15: 199-206, 1989.
10. Metz, C.E., Fencil, L.E. Determination of three-dimensional structure in biplane radiography without prior knowledge of the relationship between the two views: theory. *Med. Phys.* 16: 45-51, 1989.
11. Morton, E.J., Evans, P.M., Ferraro, M., Young, E.F., Swindell, W. Development of video frame store and distortion correction facilities for an external-beam radiotherapy simulator. *Br. J. Rad.* 64: 747-750, 1991.
12. Rudin, S., Bednarek, D.R., Wong, R. Accurate characterization of image intensifier distortion. *Med. Phys.* 18: 1145-1151, 1991.

13. Siddon, R.L. Solution to treatment planning problems using coordinate transformations. *Med. Phys.* 8: 766-774, 1981.
14. Siddon, R.L., Chin, L.M. Two-film brachytherapy reconstruction algorithm. *Med. Phys.* 12: 77-83, 1985.
15. Thomadsen, B.R., Houdek, P.V., Laarse van der, R., Edmundson, G.K., Kolkman-Deurloo, I.K.K., Visser, A.G. Treatment planning and optimization. In: HDR brachytherapy: a textbook, pp.79-145. Editor: Nag, S. Futura Publishing Company, Amonk, NY, USA, 1994.
16. Tod, M.C., Meredith, W.J. A dosage system for use in the treatment of cancer of the uterine cervix. *Br. J. Radiol.* 11: 809-824, 1938.
17. Venselaar, J.L.M., Brouwer, W.F.M., Straaten van, B.H.M., Aalbers, A.H.L. Intercomparison of calibration procedures for Ir-192 HDR sources in The Netherlands and Belgium. *Radiother. Oncol.* 30: 155-161, 1994.
18. Visser, A.G. An intercomparison of the accuracy of computer planning systems for brachytherapy. *Radiother. Oncol.* 15: 245-258, 1989.

## CHAPTER 6. ON-LINE IMPLANT RECONSTRUCTION IN HDR BRACHYTHERAPY

IKK Kolkman-Deurloo, WJM de Kruijf, PC Levendag

Radiother Oncol 2006; 78; 53-59.

### 6.1 Abstract

*Purpose:* To evaluate the accuracy of on-line planning in an Integrated Brachytherapy Unit (IBU) using dedicated image distortion correction algorithms, correcting the geometric distortion and magnetic distortion separately, and to determine the effect of the reconstruction accuracy on clinical treatment plans in terms of deviations in treatment time and dose.

*Material and methods:* The reconstruction accuracy has been measured using 20 markers, positioned at well known locations in a QA phantom. Treatment plans of two phantoms representing clinical implant geometries, have been compared with reference plans to determine the effect of the reconstruction accuracy on the treatment plan. Before clinical introduction, treatment plans of three representative patients, based on on-line reconstruction, have been compared with reference plans.

*Results:* The average reconstruction error for 10 inch images reduces from  $-0.6$  mm (range  $-2.6$  ;  $+1.0$  mm) to  $-0.2$  mm (range  $-1.2$  ;  $+0.6$  mm) after image distortion correction and for 15 inch images from  $0.8$  mm (range  $-0.5$  ;  $+3.0$  mm) to  $0.0$  mm (range  $-0.8$  ;  $+0.8$  mm). The error in case of eccentric positioning of the phantom, i.e.  $0.8$  mm (range  $-1.0$  ;  $+3.3$  mm), reduces to  $0.1$  mm (range  $-0.5$  ;  $+0.9$  mm). Correction of the image distortions reduces the deviation in the calculated treatment time of maximally 2.7% to less than 0.8% in case of eccentrically positioned clinical phantoms. The deviation in the treatment time or reference dose in the plans based on on-line reconstruction with image distortion correction of the three patient examples is smaller than 0.3%.

*Conclusion:* Accurate on-line implant reconstruction using the IBU localiser and dedicated correction algorithms separating the geometric distortion and the magnetic

distortion is possible. The results fulfill the minimum requirements as imposed by the Netherlands Commission on Radiation Dosimetry (NCS) without limitations regarding the usable range of the field of view of the image intensifier. However, the C-arm angle is limited to those angles for which magnetic distortion corrections have been obtained.

## **6.2 Introduction**

Single stepping source afterloaders as used in high dose rate (HDR) and pulsed dose rate (PDR) brachytherapy enable optimization of the dose distribution through dwell time optimization [1-6]. However, the success of adapting the dose distribution to the target volume is mainly determined by the geometry of the implant. Therefore, on-line planning during implantation is required, allowing for deficiencies in the dose distribution to be identified whilst the patient is in the operating room, and the implant modified accordingly. Moreover, HDR brachytherapy, with its significantly shorter treatment time than PDR or LDR brachytherapy, is preferably performed in a single room. By avoiding transport between the brachytherapy treatment room and the simulator room, the risk of applicator displacement is eliminated. Such a set-up has been realized based on on-line planning with a non-isocentric C-arm present in the brachytherapy treatment room [7-9]. A more sophisticated approach is the development of an Integrated Brachytherapy Unit (IBU) (Nucletron BV, The Netherlands), a shielded operating room equipped with a carbon fiber operating table, a microSelectron HDR and a dedicated isocentric brachytherapy localiser connected to the PLATO treatment planning system [10]. The entire brachytherapy procedure, i.e. implantation, implant reconstruction, dose planning and, if requested, intra-operative irradiation can be performed in a single session in this IBU.

The IBU in the Erasmus MC – Daniel Den Hoed Cancer Center has proven to be an ideal and economic environment both for (fractionated) HDR brachytherapy [11-13] and for intraoperative brachytherapy [14,15]. An on-line planning procedure, which will be referred to as 'filmless planning', was realised by importing the video images of the image intensifier of this localiser into the PLATO workstation by means of a frame grabber.

It is well known that fluoroscopy images contain distortions [16-21]. In order to enable accurate applicator reconstruction using filmless planning, algorithms should be implemented correcting these distortions [8].



In a previous paper [10], the reconstruction algorithm and the reconstruction accuracy of the IBU localiser were presented. The reconstruction error, due to the finite pixel size and image distortions had only a minor effect when limiting the use of filmless planning to implants located near the isocenter.

Recently, our IBU was upgraded with dedicated image distortion correction algorithms. This paper discusses the distortions present in fluoroscopy images and the proposed corrections. In order to quantify the results of these corrections for brachytherapy planning, experiments with the QA phantom and clinical phantoms similar to the previous paper [10] have been performed. Also, clinical treatment plans based on reconstruction from film are compared with filmless planning.

### 6.3 Materials and methods

#### 6.3.1 Introduction

The IBU localiser consists of an L-arm in combination with a C-arm [10]. The L-arm can rotate over an angle  $\alpha$  with  $\alpha = 0^\circ$  for the L-arm in the vertical plane, the C-arm over an angle  $\beta$  with  $\beta = 0^\circ$  when the C-arm is aligned along the L-arm. It is equipped with an image intensifier with 'zoom modes' of 7, 10 or 15 inches. The nominal focus-isocenter-distance (FID) is 800 mm, the isocenter-image-intensifier-distance (IID) is variable with a maximum of 440 mm. The reconstruction algorithm, which needs two images as input, takes into account  $\alpha$ ,  $\beta$ , FID and IID [10]. The FID of our localiser is 795 mm; the IID was kept constant at the maximum value of 438 mm during all experiments.

#### 6.3.2 Image distortion correction

Images from the IBU image intensifier suffer from a *geometric distortion* and a *magnetic distortion*.

The geometric distortion consists of the pincushion distortion, due to the projection of the object onto the curved image-intensifier entrance plane, and the electro-optical distortion, resulting from the electro-optical focussing inside the image intensifier, mapping the electrons from the curved input surface to the flat output screen [16-21]. Rudin et al. [20] introduced a generalized equation for describing the geometric distortion. In this equation the radial distance  $h$  of a feature from the center of the

image without distortion is determined from the radial distance  $h'$  from the center of the image with distortion:

$$h' = h + D_t h^3 + E_t h^5 \quad (1)$$

where  $D_t$  and  $E_t$  are parameters including both pincushion and electro-optical focussing effects. These parameters have been derived for the IBU localiser and the resulting correction algorithm has been implemented in the PLATO treatment planning system. In the 10 inch mode of the IBU image intensifier the geometric distortion can be neglected as the pincushion distortion and the electro-optical distortion compensate each other.

The magnetic distortion is due to interaction of the electrons in the image intensifier with the earth magnetic field [20,21]. The shape and the magnitude of this distortion depend on the electromagnetic fields in the image intensifier and the position of the image intensifier relative to the earth magnetic field. These are therefore strongly dependent on  $\alpha$  and  $\beta$ . The magnetic distortions are quantified by means of distortion matrices derived from calibrations for  $\beta = 90^\circ$  and  $270^\circ$  and various  $\alpha$ 's. So, magnetic distortion correction is limited to image set-ups with  $\beta$  equal to  $90^\circ$  or  $270^\circ$ .

The distortion correction as implemented in the PLATO treatment planning system consists of three steps: First, the image is resized with the image diameter and number of pixels for the corrected image in mind, such that the image intensifier plane is located at the film plane. Then, the geometric distortions are corrected using expression (1). Finally, the magnetic distortion is corrected using the distortion matrices. In this way, the geometric distortions are independently solved from the magnetic distortions.

### 6.3.3 QA-phantom measurements

We measured the reconstruction accuracy using a QA phantom containing 25 markers at well known positions [10]. Twenty markers were used, eliminating the five markers in the central row. The spacing between these markers varied between 20 mm and 162.5 mm. Eight images ( $\beta = 90^\circ$  or  $270^\circ$ ,  $\alpha = 0^\circ$ ,  $90^\circ$ ,  $180^\circ$  or  $270^\circ$ ) were captured with the center of the phantom aligned to the isocenter of the localiser both using the 10 inch and 15 inch mode. The position of the markers was reconstructed using eight orthogonal image combinations indicated as A to H (see table 1 in [10]). For each reconstruction the error in the marker spacing was determined (190

**Table 1:** Set-up of the reconstruction images used for the clinical phantoms.

	C-arm angle (°)	L-arm angles (°)
Breast phantom	270	200, 290
Gynaecological phantom	270	190, 280

combinations). Both raw images without distortion correction and images with distortion correction were used. In the 15 inch mode two extra images were captured ( $\beta = 90^\circ$ ,  $\alpha = 90^\circ$  and  $180^\circ$ ) with the phantom positioned such that it appeared at the edge of both images.

#### 6.3.4 Clinical phantom measurements

Phantoms representing a two-plane breast implant and a gynaecological application were used to determine the effect of the reconstruction accuracy on the treatment plan. The breast implant consisted of seven needles and eight markers. The gynaecological phantom consisted of an intrauterine tube with two ovoids, and eight markers, i.e. points A and B left and right of the applicator and four rectum markers [10]. Treatment plans with uniform source dwell times were calculated for an HDR afterloader. The localiser settings of the images used for both phantoms are shown in table 1.

For the breast phantom, a treatment plan based on implant definition using the known coordinates of the dwell positions and the markers served as a reference plan. Treatment plans based on reconstruction from fluoroscopy images with and without distortion correction were compared with the reference plan. The reference dose was defined at 85% of the mean central dose [10]. The phantom was positioned near the isocenter of the localiser as well as eccentrically such that it appeared at the edges of both images occupying one quadrant of the images only.

For the gynaecological phantom, a treatment plan based on reconstruction from orthogonal films served as reference plan as the coordinates of the markers were not accurately known. It has been compared to plans based on images with and without distortion correction. The phantom was positioned eccentrically such that it appeared in one half of each image. The reference dose has been specified as the average dose in the markers at both points A, leaving six markers for evaluation [10].

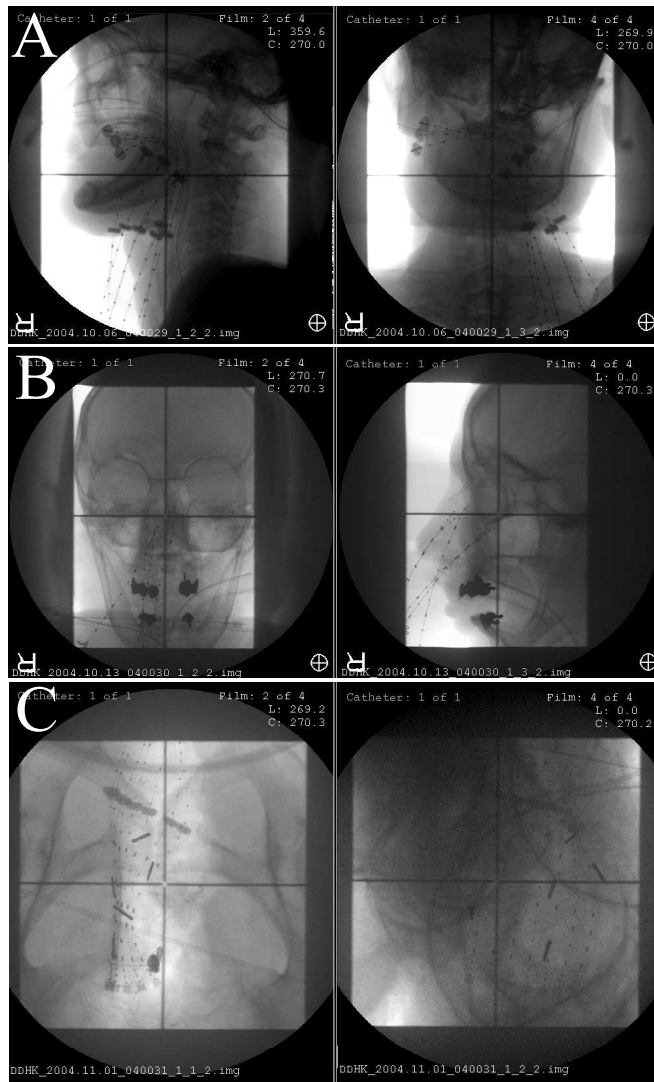


**Figure 1:** Reconstruction images (corrected for image distortion) of the clinical applications: (A) a six-catheter implant of the left tonsil and base-of-tongue, (B) a five-catheter implant of the right nasal vestibule, (C) a pelvic IOBT application with a flexible intraoperative template containing seven catheters.

### 6.3.5 Clinical applications

Before clinical introduction, treatment plans of three representative patients, based on reconstruction from radiographs, were compared with plans based on reconstruction from 15 inch images (figure 1). Implant A consists of a six-catheter implant of the

left tonsil and base-of-tongue. Dose points between the catheters along the whole active lengths have been defined according to the stepping source dosimetry system (SSDS) [2]. The dose distribution was optimized using geometric optimization and the reference dose was defined at 85% of the mean dose in all dose points. Implant B consists of a five-catheter implant of the right nasal vestibule. Dose points ‘at-lowest-dose’ were defined relative to all active dwell positions at a distance of 5 mm. The dose distribution was optimized using dose point optimization. The mean dose in the dose points served as reference dose. Implant C consists of the reconstruction of a pelvic intraoperative brachytherapy (IOBT) application using a flexible intraoperative template (FIT) containing seven catheters. The dwell times as calculated from the standard treatment plan have been imported into the reconstructed geometry and the actually delivered dose was calculated as the average dose in dose points at 10 mm depth from the FIT surface [14]. For implants A and B the deviation in the calculated treatment time was evaluated, for implant C the deviation in the calculated delivered dose.

### 6.3.6 Evaluation parameters

In the comparison between the image based plans and the reference plan the errors in treatment time,  $\Delta T$ , and marker dose,  $\Delta D$ , have been evaluated as:

$$\Delta T = \frac{T_{predicted} - T_{ref.plan}}{T_{ref.plan}} \quad (2)$$

and,

$$\Delta D = \frac{D_{predicted} - D_{ref.plan}}{D_{ref.plan}} \quad (3)$$

with  $T_{predicted}$  the predicted treatment time,  $T_{ref.plan}$  the reference treatment time,  $D_{predicted}$  the predicted marker dose and  $D_{ref.plan}$  the reference marker dose.

The marker dose error is composed of the treatment time error in combination with an error in the marker location. In clinical practice,  $\Delta D_{clinical}$ , the difference between the predicted marker dose ( $D_{predicted}$ ), as determined by the image based plan, and the actually delivered dose ( $D_{delivered}$ ), determined by importing the image based treatment time into the reference plan, should be considered:

$$\Delta D_{clinical} = \frac{D_{predicted} - D_{delivered}}{D_{delivered}} \quad (4)$$

Using equations (2) and (3):

$$\Delta D_{clinical} = \frac{(1 + \Delta D).D_{ref.plan} - (1 + \Delta T).D_{ref.plan}}{(1 + \Delta T).D_{ref.plan}} \quad (5)$$

So:

$$\Delta D_{clinical} = \frac{\Delta D - \Delta T}{1 + \Delta T} \quad (6)$$

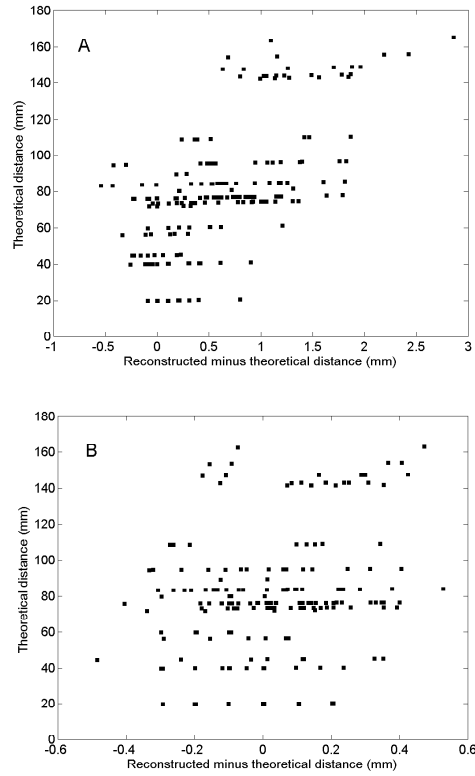


**Figure 2:** Scatterplot showing the reconstruction error, i.e. the reconstructed minus the theoretical distance of the markers in the QA phantom, versus the theoretical distance using 15 inch images for combination A both without image distortion correction (A) and with image distortion correction (B).

## 6.4 Results

### 6.4.1 QA phantom

Figure 2 shows the reconstruction error as a function of the marker spacing for combination A using 15 inch images, without distortion correction (figure 2A) and with distortion correction (figure 2B). The reconstruction error for the 8 combinations A to H is shown in figure 3. A positive sign indicates that the reconstructed distances are larger than the real distances. The average error for 10 inch images without distortion correction is  $-0.6$  mm (range  $-2.6$  ;  $+1.0$  mm). With distortion correction the error reduces to  $-0.2$  mm (range  $-1.2$  ;  $+0.6$  mm). For 15 inch images the average error without distortion correction is  $0.8$  mm (range  $-0.5$  ;  $+3.0$  mm), which reduces to  $0.0$  mm (range  $-0.8$  ;  $+0.8$  mm) after distortion correction. Reconstruction of the phantom positioned such that it appears at the edge of the images (combination B) results in an average error of  $0.8$  mm (range  $-1.0$  ;  $+3.3$  mm) when using images without distortion correction and of  $0.1$  mm (range  $-0.5$  ;  $+0.9$  mm) when using images with distortion correction.

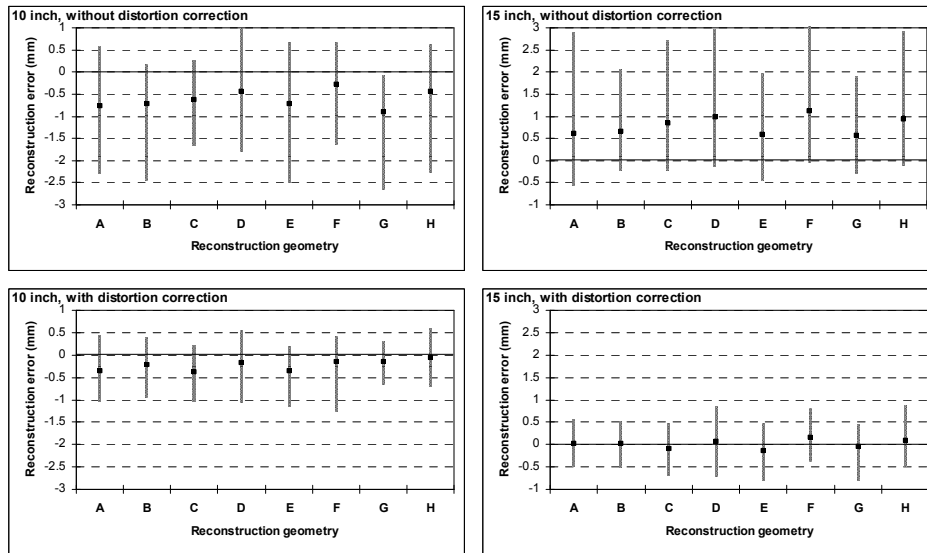


**Figure 3:** The reconstruction error measured with the QA phantom for reconstruction from orthogonal images in the 10 inch and 15 inch mode of the image intensifier both using images without distortion correction and images with distortion correction. Indicated are the average errors and the range of errors.

### 6.4.2 Clinical phantoms

The deviation of the total irradiation time and the average marker dose of the treatment plans based on image reconstruction compared to the reference plan is shown in table 2.

**Table 2:** Deviation of the total irradiation time ( $\Delta T$ ), average marker dose ( $\Delta D$ ) and average clinical marker dose ( $\Delta D_{\text{clinical}}$ ) of a treatment plan based on image reconstruction compared to a reference plan for the breast (8 markers) and the gynaecological phantom (6 markers). In the '15 inch-edge' plan the phantom was positioned such that it appeared at the edge of both reconstruction images.

	Film	10 inch	15 inch	15 inch (edge)
<b>BREAST PHANTOM</b>				
Without distortion correction				
$\Delta T$ (%)	0.0	-0.2	0.6	2.7
$\Delta D$ (%)*	$0.1 \pm 0.5$	$0.8 \pm 1.4$	$0.7 \pm 1.7$	$3.2 \pm 1.4$
$\Delta D_{\text{clinical}}$ (%)*	$0.1 \pm 0.5$	$1.0 \pm 1.4$	$0.0 \pm 1.7$	$0.5 \pm 1.4$
With distortion correction				
$\Delta T$ (%)	--	0.2	0.2	-0.6
$\Delta D$ (%)*	--	$0.4 \pm 0.5$	$-0.5 \pm 0.8$	$0.7 \pm 0.9$
$\Delta D_{\text{clinical}}$ (%)*	--	$0.2 \pm 0.5$	$-0.7 \pm 0.8$	$1.3 \pm 0.9$
<b>GYNAECOLOGICAL PHANTOM</b>				
Without distortion correction				
$\Delta T$ (%)	--	-2.0	0.9	--
$\Delta D$ (%)*	--	$0.1 \pm 0.5$	$0.7 \pm 1.4$	--
$\Delta D_{\text{clinical}}$ (%)*	--	$2.1 \pm 0.5$	$-0.3 \pm 1.4$	--
With distortion correction				
$\Delta T$ (%)	--	-0.8	0.5	--
$\Delta D$ (%)*	--	$-0.7 \pm 1.0$	$0.2 \pm 0.7$	--
$\Delta D_{\text{clinical}}$ (%)*	--	$0.2 \pm 1.0$	$-0.3 \pm 0.7$	--

\*: average  $\pm$  standard deviation



**Table 3:** Deviation of the total irradiation time ( $\Delta T$ ) or reference dose ( $\Delta D$ ) of the filmless treatment plans for the three clinical applications A to C.

	Without distortion correction	With distortion correction
A: $\Delta T$ (%)	1.1	-0.3
B: $\Delta T$ (%)	0.5	0.0
C: $\Delta D$ (%)	-1.3	-0.3

#### 6.4.3 Clinical applications

The deviation of the calculated treatment time (implants A and B) and of the reference dose (implant C) of the treatment plans based on image reconstruction compared to the reference plan is shown in table 3 for the three clinical applications.

### 6.5 Discussion

The experiments with the QA phantom have been performed to quantify the reconstruction error in filmless planning. This method was also applied when determining the accuracy of implant reconstruction in all radiotherapy institutions in The Netherlands and Belgium [22], as part of a project to study the current practice of quality control of brachytherapy equipment and to develop minimum requirements [23]. It is recommended to test the accuracy of the reconstruction procedure at least once a year and after each change in the equipment or software used for reconstruction. The reconstruction error should be smaller than 2 mm for 95% of the measured distances. The results fulfill these requirements when applying image distortion correction, with an average reconstruction error of  $-0.2$  mm (range  $-1.2$  ;  $+0.6$  mm) for 10 inch images and  $0.0$  mm (range  $-0.8$  ;  $+0.8$  mm) for 15 inch images (figure 3). The error in case of eccentric positioning of the phantom, i.e.  $0.1$  mm (range  $-0.5$  ;  $+0.9$  mm), is also within the requirements. The error is larger for images without distortion correction, i.e.  $-0.6$  mm (range  $-2.6$  ;  $+1.0$  mm) for 10 inch images and  $0.8$  mm (range  $-0.5$  ;  $+3.0$  mm) for 15 inch images (figure 3). According to the requirements [23], 10 inch images can be used without image distortion correction as 98.5% of the measured distances have an error less than 2 mm. In case of 15 inch images a reconstruction error less than 2 mm was measured in 94.4% of the reconstructed distances, indicating that image distortion correction is needed to fulfill the requirements [23]. This is also demonstrated by the eccentrically positioned phantom with an average error of  $0.8$  mm (range  $-1.0$  ;  $+3.3$  mm) and only 91% of the recon-

structed distances having an error less than 2 mm when using images without correction. As for this combination 99% of the errors was within 2 mm, when positioning the phantom near the isocenter of the localiser, this also demonstrates the increasing error towards the edge of the images. The increase is not due to an incorrect magnification factor of the localiser as the reconstruction error reduces significantly to 0.1 mm (range  $-0.5$  ;  $+0.9$  mm) after distortion correction. Figure 2 also shows that the correlation between reconstruction error and distance is due to image distortion as it disappears after distortion correction. The correlation in figure 2A is most likely caused by geometric distortion as geometric distortion is a function of the distance from the center of the image and magnetic distortion is not.

Similar experiments have been performed by other authors [7-9] to measure the reconstruction accuracy of filmless planning using non-isocentric C-arms. Pálvölgyi [9] has not implemented image distortion correction algorithms but limits the use of the C-arm to the central region of the image intensifier where the error in measured distances in an image is less than 1.0 mm, limiting the freedom in image set-ups. Liu et al. [8] implemented a distortion correction algorithm using a seven-parameter polynomial filter. Using this correction the average residual error in an image is 0.3 mm while the maximum error over the entire image intensifier plane is 1.0 mm. Cuijpers [7] reports a reconstruction accuracy of  $1.2 \text{ mm} \pm 0.6 \text{ mm}$  (1 SD) with a maximum error of 3.6 mm without distortion correction.

Dose calculation errors due to reconstruction errors have been evaluated with two clinical phantoms and verified with the patient examples. The error in the total irradiation time for the breast phantom positioned near the isocenter is very limited in all situations as it remains below 0.6% (table 2). The increasing image distortion towards the edge of the images is illustrated by the eccentrically positioned breast phantom. The error is 2.7% using images without distortion correction, with the total implant geometry affected by the distortions. The projections of the markers in each image are relatively close to the projections of the nearest dwell positions. Therefore, the error in the marker dose is mainly determined by the irradiation time error. The remaining part of the error due to the error in the location of the markers,  $\Delta D_{\text{clinical}}$ , is limited to  $0.5\% \pm 1.4\%$ . The distortions are successfully eliminated by the image distortion correction algorithms as the irradiation time error decreases to  $-0.6\%$ .

Eccentric positioning of the gynaecological phantom results in an error of  $-2\%$  in the irradiation time when using 10 inch images without distortion correction. This error decreases to  $-0.8\%$  after correcting the distortions. As geometric distortion is

neglected in the 10 inch mode this must be due to correcting the magnetic distortion. The error in the location of the six markers is compensated by the error in the irradiation time resulting in a negligible error in the marker dose and an error in  $D_{\text{clinical}}$  of the same order as the irradiation time error. These errors disappear after correcting the distortions. Similar effects are seen in the 15 inch mode, but then the improvement is a combination of correcting the geometric and magnetic distortions.

Regarding the clinical applications it is seen that for both head and neck examples (patients A and B) a small deviation in the calculated irradiation time is found when reconstructing from fluoroscopy images without distortion correction (table 3). This deviation becomes negligible after correction. The planning technique in these examples was chosen such that the location of prescription points could be easily reproduced without introducing deviations due to human errors. The error in the calculated actually delivered dose in the IOBT application (patient C) is of the same order, i.e.  $-1.3\%$  without distortion correction and  $-0.3\%$  after distortion correction (table 3).

The reconstruction accuracy should be considered in the light of other inaccuracies in brachytherapy treatment planning and delivery such as inaccuracies in the source calibration, source positioning and dose calculation algorithms [22,24-26]. The accuracy of the overall dose delivery in 33 institutions in The Netherlands and Belgium was investigated by asking to deliver a prescribed dose in a dedicated phantom [22]. As the treatment time had to be calculated by manually entering the source position coordinates in the treatment planning system the accuracy of source calibration, source positioning and dose calculation algorithms was measured independently from the reconstruction accuracy. The results indicated that the dose delivery accuracy was  $0.9\% \pm 1.3\%$  and  $1.0\% \pm 2.3\%$  for the HDR and PDR afterloaders respectively. Furthermore, the overall treatment accuracy is limited by the accuracy of the implantation procedure and the delineation of target volume and surrounding normal tissues, in combination with very steep dose-gradients, e.g. up to 10% per mm near the prescription isodose.

## 6.6 Conclusions

Accurate implant reconstruction is possible with filmless planning using the IBU localiser and dedicated correction algorithms separating the geometric distortion and the magnetic distortion. The final results fulfill the minimum requirements as

imposed by the NCS [23] without limitations regarding the usable range of the field of view of the image intensifier. However, the C-arm angle is limited to angles for which the magnetic distortion has been calibrated.

## 6.7 References

1. Kolkman-Deurloo IKK, Visser AG, Niël CGJH, Driver N, Levendag PC. Optimization of interstitial volume implants. *Radiother Oncol* 1994; 31:229-239.
2. Thomadsen BR, Houdek PV, van der Laarse R, Edmunson G, Kolkman-Deurloo IKK, Visser AG. Treatment planning and optimization. In: Nag S, editor. *HDR Brachytherapy: A Textbook*. Armonk, NY: Futura; 1994. pp. 79-145.
3. Nickers P, Lenaerts E, Thissen B, Deneufbourg JM. Does inverse planning applied to Iridium192 high dose rate brachytherapy improve the optimization of the dose afforded by the Paris system. *Radiother Oncol* 2005; 74:131-136.
4. Mahmoudieh A, Tremblay C, Beaulieu L, et al. Anatomy-based inverse planning dose optimization in HDR prostate implant: a toxicity study. *Radiother Oncol* 2005; 75:318-324.
5. Yoshioka Y, Nishimura T, Kamata M, et al. Evaluation of anatomy-based dwell position and inverse optimization in high-dose-rate brachytherapy of prostate cancer: a dosimetric comparison to a conventional cylindrical dwell position, geometric optimization, and dose-point optimization. *Radiother Oncol* 2005; 75:311-317.
6. Kolkman-Deurloo IKK, Deleye XGJ, Jansen PP, Koper PCM. Anatomy based inverse planning in HDR prostate brachytherapy. *Radiother Oncol* 2004; 73:73-77.
7. Cuijpers JP. Clinical use of a non-isocentric C-arm unit for on-line filmless reconstruction of brachytherapy applicators. *Radiother Oncol* 2001; 61:203-209.
8. Liu L, Bassano DA, Prasad SC, Keshler BL, Hahn SS. On the use of C-arm fluoroscopy for treatment planning in high dose rate brachytherapy. *Med Phys* 2003; 30:2297-2302.
9. Pálvölgyi J. To what extent can digital images obtained with a non-isocentric C-arm be used for brachytherapy treatment planning in gynaecology. *Radiother Oncol* 2003; 67:107-112.
10. Kolkman-Deurloo IKK, Visser AG, Idzes MHM, Levendag PC. Reconstruction accuracy of a dedicated localiser for filmless planning in intra-operative brachytherapy. *Radiother Oncol* 1997; 44:73-81.
11. Levendag PC, Schmitz PIM, Jansen PP, et al. Fractionated high-dose-rate and pulsed-dose-rate brachytherapy: first clinical experience in squamous cell carcinoma of the tonsillar fossa and soft palate. *Int J Radiat Oncol Biol Phys* 1997; 38:497-506.
12. Levendag PC, Schmitz PIM, Jansen PP, et al. Fractionated high-dose-rate brachytherapy in primary carcinoma of the nasopharynx. *J Clin Oncol* 1998; 16:2213-2220.

13. Levendag PC, Nijdam W, Noever I, et al. Brachytherapy versus surgery in carcinoma of tonsillar fossa and/or soft palate: late adverse sequelae and performance status: can we be more selective and obtain better tissue sparing? *Int J Radiat Oncol Biol Phys* 2004; 59:713-724.
14. Kolkman-Deurloo IKK, Nuyttens JJ, Hanssens PEH, Levendag PC. Intraoperative HDR brachytherapy for rectal cancer using a flexible intraoperative template: standard plans versus individual planning. *Radiother Oncol* 2004; 70:75-79.
15. Nuyttens JJ, Kolkman-Deurloo IKK, Vermaas M, et al. High dose rate intraoperative radiotherapy for close or positive margins in patients with locally advanced or recurrent rectal cancer. *Int J Radiat Oncol Biol Phys* 2004; 58:106-112.
16. Boone JM, Seibert JA, Barrett WA, Blood EA. Analysis and correction of imperfections in the image intensifier-TV-digitizer imaging chain. *Med Phys* 1991; 18:236-242.
17. Chakraborty DP. Image intensifier distortion correction. *Med Phys* 1987; 14:249-252.
18. Cosby NS, Leszczynski KW. Computer-aided radiation therapy simulation: image intensifier spatial distortion correction for large field of view digital fluoroscopy. *Phys Med Biol* 1998; 43:2265-2278.
19. Pietka E, Huang HK. Correction of aberration in image intensifier systems. *Computerized Medical Imaging and Graphics* 1992; 16:253-258.
20. Rudin S, Bednarek DR, Wong R. Accurate characterization of image intensifier distortion. *Med Phys* 1991; 18:1145-1151.
21. Schueler B, Hu X. Correction of image intensifier distortion for three-dimensional x-ray angiography. *Proc. SPIE* 1995, 2432:272-279.
22. Elfrink RJM, Kolkman-Deurloo IKK, van Kleffens HJ, et al. Determination of the accuracy of implant reconstruction and dose delivery in brachytherapy in The Netherlands and Belgium. *Radiother Oncol* 2001; 59:297-306.
23. Elfrink RJM, Kolkman-Deurloo IKK, van Kleffens HJ, et al. Quality control of brachytherapy equipment in The Netherlands and Belgium: current practice and minimum requirements. *Radiother Oncol* 2002; 62:95-102.
24. Dijk van E, Kolkman-Deurloo IKK, Damen PMG. Determination of the reference air kerma rate for  $^{192}\text{Ir}$  brachytherapy sources and the related uncertainty. *Med Phys* 2004; 31:2826-2833.
25. Heeney C, McClean B, Kelly C. A dosimetric intercomparison of brachytherapy facilities in Ireland, Scotland and the North of England. *Radiother Oncol* 2005; 74:149-156.
26. Granero D, Pérez-Calatayud J, Ballester F. Monte Carlo calculation of the TG-43 dosimetric parameters of a new Bebig Ir-192 HDR source. *Radiother Oncol* 2005; 76:79-85.



## **CHAPTER 7. INTRAOPERATIVE HDR BRACHYTHERAPY FOR RECTAL CANCER USING A FLEXIBLE INTRAOPERATIVE TEMPLATE: STANDARD PLANS VERSUS INDIVIDUAL PLANNING**

IKK Kolkman-Deurloo, JJ Nuyttens, PEJ Hanssens, PC Levendag  
Radiother Oncol 2004; 70; 75-79.

### **7.1 Abstract**

HDR intraoperative brachytherapy (IOBT) is applied to locally advanced rectal tumors using a 5 mm thick Flexible Intraoperative Template (FIT). To reduce the procedure time, treatment planning is performed using standard plans, that neglect the curvature of the FIT. We have calculated the individual treatment plan, based on the real geometry of the FIT, and the dose at clips placed during surgery. A mean treatment dose of  $9.55 \pm 0.21$  Gy was found for the individual plan, compared to the prescribed 10 Gy ( $p < 0.0001$ ). The mean central dose was  $10.03 \pm 0.10$  Gy in the standard plan and  $9.20 \pm 0.32$  Gy in the individual plan ( $p < 0.0001$ ). The mean dose at the corners of the FIT was 10.3 Gy in the standard plan and ranged between 10.3 and 10.5 Gy in the individual plan. In 63% of the clips, the dose was larger than 15.0 Gy, which is equivalent to a gap between the FIT and the target smaller than 5 mm. In 18% of the clips, the dose was smaller than 13.0 Gy indicating that locally the gap was larger than 5 mm. Clinical practice will have to prove if these small dose deviations influence the clinical outcome.

## 7.2 Introduction

High dose rate (HDR) intraoperative brachytherapy (IOBT) is a treatment modality in radiation therapy used as an adjuvant to surgery for locally advanced cancers [5]. It involves the delivery of a single large radiation dose to residual (microscopic) tumor at the time of surgery with a remotely controlled HDR afterloader. For IOBT, the source is transported into catheters embedded in a surface applicator. After tumor resection an appropriately sized and shaped (custom made) applicator is placed on the residual (microscopic) tumor and secured into place. Adjacent organs can be either shielded or retracted away from the treatment area. The irradiation time is determined either through individual planning after simulation of the IOBT geometry [15] or using preplanned atlases [3,13].

In 1994 an Integrated Brachytherapy Unit (IBU) (Nucletron, The Netherlands), i.e. a shielded operating room equipped with an HDR afterloader (microSelectron HDR, Nucletron, The Netherlands) and a dedicated brachytherapy localiser (Nucletron, The Netherlands) was established at the Erasmus MC – Daniel den Hoed Cancer Center [8]. This set-up enables integration of the entire brachytherapy procedure, i.e. implantation, implant reconstruction, dose planning and irradiation in a single session. The IBU is an ideal and economic environment both for (fractionated) HDR brachytherapy [9,10] as well as for IOBT.

In our institution, IOBT is used as part of a multimodality treatment for locally advanced primary or recurrent rectal tumors since 1997 using a Flexible Intraoperative Template (FIT). To reduce the total procedure time, treatment planning during IOBT is performed using standard geometries, i.e. flat templates neglecting the curvature of the FIT, present in the treatment planning system. For each patient an individual treatment plan is calculated after finishing the procedure. The individual treatment plan is based on reconstruction of the FIT geometry and clip locations from isocentric films and importing the actual dwell times. The purpose of this paper is to discuss the feasibility of our technique for IOBT of rectal tumors. The question is raised whether the dose reduction towards the treated area, caused by the curvature of the FIT, can be neglected. For this reason, the individual treatment plans and the standard plans were compared in terms of dose at the prescribed depth from the surface of the FIT. IOBT applicators are always presented as blankets enclosing every irregularity. However, with catheters in place, the flexibility of the applicator is reduced and small irregularities are not covered. Even after pressing gauze dressings into the pelvis, the applicator could reshape and a gap between the applicator and the



target surface can occur. The only way to define the dose at the surface retrospectively was to determine the dose at the clips, enabling calculation of the gap between the FIT and the target surface at the clip areas.

### 7.3 Materials and methods

IOBT is applied to locally advanced primary or recurrent rectal tumors using a FIT. The FIT is a 5 mm thick flexible silicon template containing parallel catheters spaced 1 cm apart (figure 1). The shape of the FIT can be rectangular or corners can be cut off to conform to the target area. During surgery the size and shape of the FIT are determined by the surgeon and radiation oncologist. The shape, in combination with the catheter positions, is overlaid on a paper template which is used as input for the treatment planning system (Plato BPS, Nucletron, The Netherlands). Treatment planning is performed using standard geometries, i.e. flat templates neglecting the curvature of the FIT, present in the treatment planning system. Active dwell positions are chosen according to the size and shape of the actual FIT as present on the paper template. The dose is specified at the reference depth (usually 10 mm from the surface of the FIT, which is equal to 12.5 mm from the center of the catheters). For

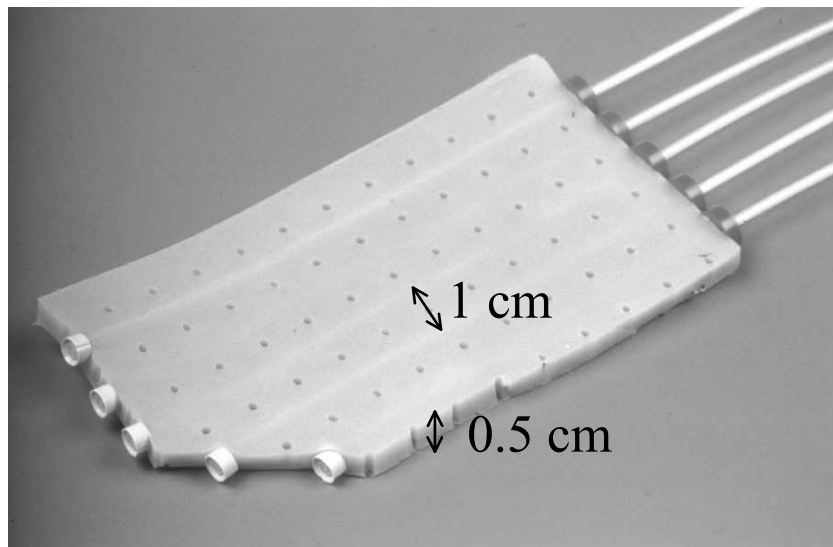


**Figure 1:** The Flexible Intraoperative Template (FIT); indicated are the catheter spacing of 1 cm and the FIT thickness of 0.5 cm.

each active dwell position, a dose point is placed on a line perpendicular to the FIT at the reference depth. The dwell times are optimized such that the dose in the dose points is as homogeneous as possible using the ‘optimization on dose points on distance’ algorithm as implemented in Plato BPS (Nucletron, The Netherlands) [16]. The reference dose is defined as the average dose in the dose points and is in the case of rectal cancer 10.0 Gy. The procedure with standard plans is chosen to eliminate the time-consuming catheter reconstruction. Before the irradiation is started, the irradiation time is checked by an independent manual calculation [14]. During treatment planning, isocentric reconstruction films are made using the dedicated brachytherapy localiser [8]. Reconstruction of the actual FIT geometry, using these films, is performed after the IOBT procedure is finished. The individual treatment plan is calculated by importing the dwell times from the standard treatment plan in the reconstructed FIT geometry. The actually delivered dose, i.e. the treatment dose, is defined as the average dose in dose points, placed on a line perpendicular to the reconstructed FIT at the prescribed depth. This dose is expected to be less than 10.0

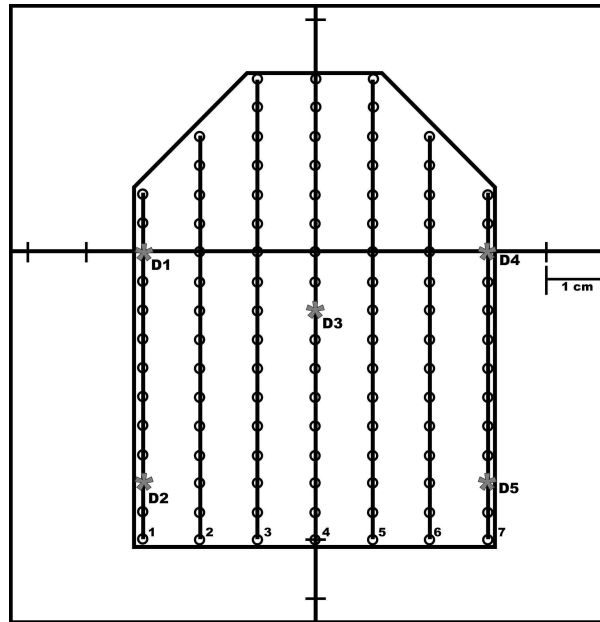


**Figure 2:** Example of a (flat) FIT geometry (a rectangle with two corners cut off), consisting of seven catheters spaced 1 cm apart with active dwell positions spaced 5 mm apart. (\*: the position of the five dose points (D1, D2, D3, D4, D5) used for evaluation).

Gy due to the anatomy of the pelvis.

For evaluation of the procedure, the treatment dose, as calculated in the individual plan, was compared to the prescribed dose of 10.0 Gy. Also, a comparison of the dose in a selection of five dosepoints, located at the prescribed depth in both the standard plan and the individual plan, was made. One dose point was chosen centrally in the target area and four on each corner, i.e. located at the outermost catheters at the third dwell position (10 mm from the edge) (figure 2).

During surgery, clips were placed at the tissue surface to delineate the target area.

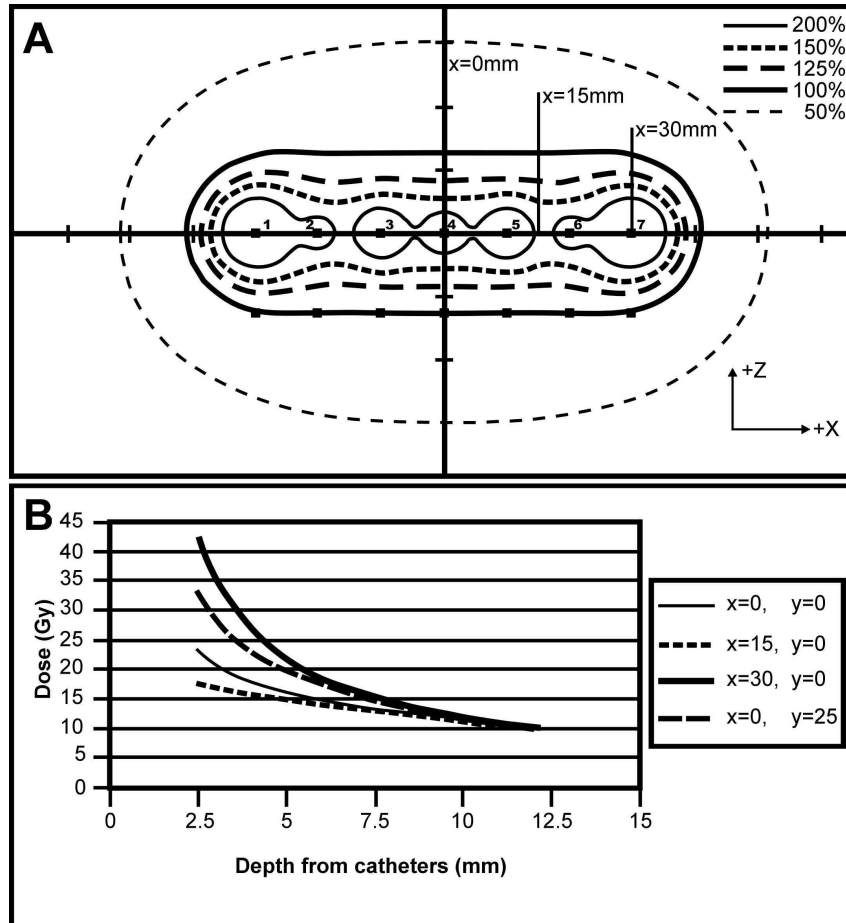


**Figure 3:** (A) A plane through the center ( $y = 0$  mm) of a FIT containing seven catheters of 6 cm each, with the 200%, 150%, 125%, 100% and 50% isodose lines shown. (B) The depth dose curves along the z-axis for the FIT geometry shown in (A).

The position of the clips was reconstructed from the reconstruction films. The calculated dose in the clip locations in the individual treatment plan is representative for the local dose at the target surface and was used as a measure of the gap between the FIT surface and the target. This way the depth in tissue covered by the reference dose can be determined. A FIT containing seven catheters of 6 cm each was considered. The central plane of this FIT, i.e. the plane perpendicular to the catheters and located at the center of the catheters ( $y = 0$  mm) is drawn in figure 3A. Three trajectories are indicated, i.e. at the center of the FIT ( $x = 0$  mm), in between catheters 5 and 6 ( $x = 15$  mm) and at the edge of the FIT ( $x = 30$  mm). For each of these trajectories a depth dose curve, i.e. the dose along the  $z$ -axis, is printed in figure 3B. A fourth trajectory is calculated at  $x = 0$  mm and  $y = 25$  mm (5 mm from the edge of the FIT, i.e. through the second dwell position in catheter 4). The dose is plotted as a function of the distance from the centers of the catheters which are located at  $z = 0$  mm. The distance between the clips (located at the tissue surface) and the center of the catheters would be 2.5 mm in case of a perfect fit between the FIT and the target. This corresponds with a dose ranging between 17.5 and 42.5 Gy, strongly depending on the location along the FIT (figure 3B). In case of a 5 mm gap between the FIT and the target, the clips would be at 7.5 mm from the center of the catheters. The dose at the clip locations will then vary between 13.0 and 15.0 Gy. In the latter case, the actually delivered dose will be located at 5 mm depth in tissue as the dose was prescribed at 10 mm from the FIT surface.

#### 7.4 Results and discussion

Thirty-nine patients were included in the analysis. The number of catheters used was on average 8.4 (range 5 – 14), corresponding to an average of 146.3 dwell positions (range 49 – 341). The number of clips placed in each patient varied between 0 and 7, mean 3.5. The reference depth was 10 mm from the FIT surface in 37 cases. In two cases a combination of two reference depths, i.e. 5 mm and 10 mm, was used. The average air kerma strength of the HDR source was 29300 cGy.h<sup>-1</sup>.cm<sup>2</sup> (range 16000 – 46300 cGy.h<sup>-1</sup>.cm<sup>2</sup>) resulting in an average irradiation time of 26 min 28 s (range 9 min 5 s – 66 min 2 s). When recalculating the irradiation time using a newly installed HDR source (with a source strength of approximately 40840 cGy.h<sup>-1</sup>.cm<sup>2</sup>) an average irradiation time of 17 min 8 s (range 8 min 42 s – 32 min 14 s) was found depending on the size of the FIT. When looking at the total procedure time, other factors have to be taken into account too, e.g. preparation of the radiation oncologist, adjustment and

positioning of the FIT, treatment planning, preparation for the irradiation, check cable run and removal of the FIT. In literature wide ranges are found for total irradiation times and procedure times in similar IOBT studies [4,13]. We estimate that the time needed for treatment planning could be reduced by about 45 minutes when using standard plans.

In four patients, the standard plan was only available because it was not possible to make (isocentric) reconstruction films. For two patients the standard plan was not available as the individual treatment plan was calculated during the application. One patient was excluded from the evaluation because he was treated at two separate sites using a single standard plan. Therefore, the standard plan could be compared to the individual plan in 32 patients. An average treatment dose of  $9.55 \pm 0.21$  Gy was found for the individual treatment plan while the reference dose in the corresponding standard plan was always 10.0 Gy ( $p < 0.0001$ ). The dose in the individual plan was lower than in the standard plan due to the curvature of the FIT and because the dose was prescribed at the convex side of the FIT. The average central dose, i.e. the dose in dose point D3, was  $10.03 \pm 0.10$  Gy in the standard plan and  $9.20 \pm 0.32$  Gy in the individual plan ( $p < 0.0001$ ). In the standard plan, the average dose in the dose points at the corners of the FIT, i.e. D1, D2, D4 and D5, was 10.3 Gy (figure 4). The variation of the dose in these points was small as a result of the dwell time optimiza-

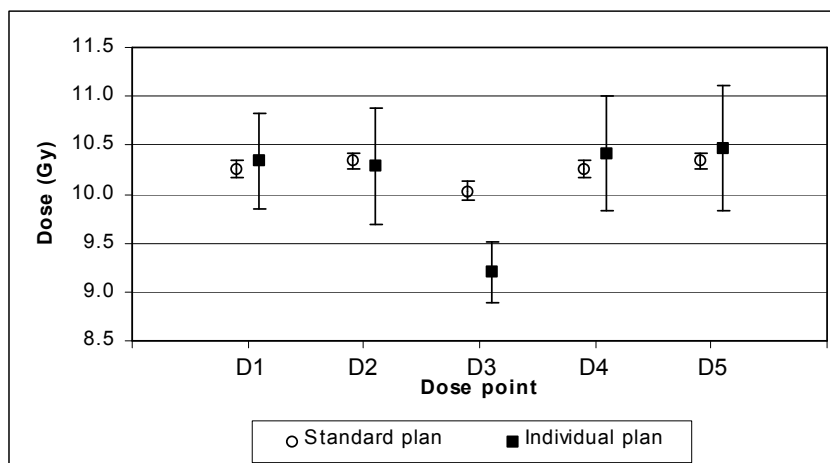


**Figure 4:** Dose in dose points D1 to D5 averaged over all patients for both the standard plan and the individual plan. For the location of dose points D1 to D5 see figure 2. Indicated is the average dose for each dose point and the standard deviation.

tion. In the individual plan the average dose in these points varied between 10.3 and 10.5 Gy (figure 4). In other studies using preplanned dosimetry atlases [1-4,6,11-13] no information is provided on the actual dose delivered at the reference depth. This dose will deviate from the prescribed dose due to the curvature of the applicator. Harrison et al. [3] have investigated the effect of applicator curvature in order to make an extensive atlas of both planar and moderately curved applicators. Kneschaurek et al. [7] also investigated this effect. However, they use equal dwell times and prescribe the dose in the center of the target at the applicator surface. Clinically they do not account for the applicator curvature as the effect is negligible when prescribing at the applicator surface.

On a total of 134 clips implanted, 113 clips were located perpendicular under the FIT. In 20 clips (18%) a dose lower than 13.0 Gy was found, indicating a gap of 5 mm or more between these clips and the FIT surface (figure 3). Therefore, the reference dose was located at less than 5 mm depth in tissue. For 71 out of 113 clips, the calculated dose was larger than 15.0 Gy which is equivalent to a gap smaller than 5 mm, meaning that locally a dose of 10.0 Gy was delivered to at least 5 mm depth in tissue (figure 3). In 22 clips (19%) a dose between 13.0 and 15.0 Gy was calculated. In this case the conclusion on gaps depends on the location of the clip along the FIT (figure 3). Unfortunately this evaluation does not give us the dose in the center of the target, i.e. the area most at risk, because the clips were positioned at the edge of the close or positive resection margins. Therefore, we recommend that extra clips should be placed in the center of the target. In that case the same evaluation method could give information on the gap between the target and the FIT surface and thus the depth of the treatment isodose in tissue right in the area most at risk. In general in IOBT literature, information is given on a prescribed dose and a reference depth as a distance from the surface of the applicator [1-4,6,11-13]. However, the gap between the applicator and the tissue surface determines the actual reference depth in tissue. Due to the curvature of the target area it is not realistic to assume that this gap will always be negligible. The actual dose in tissue should be presented, e.g. by analysing the dose in clips placed centrally at the target surface. Clinical practise will have to prove if the small dose deviations caused by neglecting the FIT curvature in the standard plans and by potential gaps between the FIT and the target influence the clinical outcome.

## 7.5 References

1. Alektiar KM, Zelefsky MJ, Paty PB, et al. High-dose-rate intraoperative brachytherapy for recurrent colorectal cancer. *Int J Radiat Oncol Biol Phys* 2000; 48:1:219-226.
2. Harrison LB, Enker WE, Anderson LL. High-dose-rate intraoperative radiation therapy for colorectal cancer – Part 1. *Oncology* 1995; 9:679-683.
3. Harrison LB, Enker WE, Anderson LL. High-dose-rate intraoperative radiation therapy for colorectal cancer – Part 2. *Oncology* 1995; 9:737-741.
4. Harrison LB, Minsky BD, Enker WE, et al. High dose rate intraoperative radiation therapy (HDR-IORT) as part of the management strategy for locally advanced primary and recurrent rectal cancer. *Int J Radiat Oncol Biol Phys* 1998; 42:2:325-330.
5. Hu KS, Enker WE, Harrison LB. High-dose-rate intraoperative irradiation: current status and future directions. *Semin Radiat Oncol* 2002; 12:1:62-80.
6. Huber FT, Stepan R, Zimmermann F, Fink U, Molls M, Siewert JR. Locally advanced rectal cancer: resection and intraoperative radiotherapy using the flab method combined with preoperative or postoperative radiochemotherapy. *Dis Colon Rectum* 1996; 39:7:774-779.
7. Kneschaurek P, Wehrmann R, Hugo C, Stepan R, Lukas P, Molls M. Die Flabmethode zur intraoperativen Bestrahlung. *Strahlenther Onkol* 1995; 171:2:61-69.
8. Kolkman-Deurloo IKK, Visser AG, Idzes MHM, Levendag PC. Reconstruction accuracy of a dedicated localiser for filmless planning in intra-operative brachytherapy. *Radiother Oncol* 1997; 44:73-81.
9. Levendag PC, Schmitz PIM, Jansen PP, et al. Fractionated high-dose-rate and pulsed-dose-rate brachytherapy: first clinical experience in squamous cell carcinoma of the tonsillar fossa and soft palate. *Int J Radiat Oncol Biol Phys* 1997; 38:3:497-506.
10. Levendag PC, Schmitz PIM, Jansen PP, et al. Fractionated high-dose-rate brachytherapy in primary carcinoma of the nasopharynx. *J Clin Oncol* 1998; 16:6:2213-2220.
11. Mannaerts GHH, Rutten HJT, Martijn H, Hanssens PEJ, Wiggers T. Comparison of intraoperative radiation therapy – containing multimodality treatment with historical treatment modalities for locally recurrent rectal cancer. *Dis Colon Rectum* 2001; 44:12:1749-1758.
12. Mannaerts GHH, Rutten HJT, Martijn H, Hanssens PEJ, Wiggers T. Effects on functional outcome after IORT-containing multimodality treatment for locally advanced primary and locally recurrent rectal cancer. *Int J Radiat Oncol Biol Phys* 2002; 54:4:1082-1088.
13. Martinez-Monge R, Nag S, Martin EW. Three different intraoperative radiation modalities (electron beam, high-dose-rate brachytherapy and iodine-125 brachytherapy) in the adjuvant treatment of patients with recurrent colorectal adenocarcinoma. *Cancer* 1999; 86:2:236-247.

14. Murrer LHP, Kolkman-Deurloo IKK. Manual calculation of treatment time for high dose rate brachytherapy with a flexible intraoperative template (FIT). *Phys Med Biol* 2001; 46:1075–1084.
15. Strassman G, Walter S, Kolotas C, et al. Reconstruction and navigation system for intraoperative brachytherapy using the flab technique for colorectal tumor bed irradiation. *Int J Radiat Oncol Biol Phys* 2000; 47:5:1323-1329.
16. Thomadsen BR, Houdek PV, van der Laarse R, Edmunson G, Kolkman-Deurloo IKK, Visser AG. Treatment planning and optimization. In: Nag S, editor. *HDR Brachytherapy: A Textbook*. Armonk, NY: Futura; 1994. pp. 79-145.



## **CHAPTER 8. HIGH DOSE RATE INTRAOPERATIVE RADIOTHERAPY FOR CLOSE OR POSITIVE MARGINS IN PATIENTS WITH LOCALLY ADVANCED OR RECURRENT RECTAL CANCER**

JJ Nuyttens, IKK Kolkman-Deurloo, M Vermaas, FT Ferenschild, WJ Graveland, JH De Wilt, PEJ Hanssens, PC Levendag

Int J Radiat Oncol Biol Phys; 2004; 106-112.

### **8.1 Abstract**

*Purpose:* A high dose rate intraoperative radiotherapy (HDR-IORT) technique for rectum cancer was developed and the technique, local failure, and survival were analyzed.

*Methods and materials:* After the exclusion of metastatic patients, 37 patients were treated with external beam RT, surgery and HDR-IORT between 1997 and 2000. Primary locally advanced rectum cancer was found in 18 patients and recurrent disease in 19. HDR-IORT was only administered if the resection margins were  $\leq 2$  mm. The flexible intraoperative template is a 5-mm-thick pad with 1-cm spaced parallel catheters. Clips were placed during surgery to define the target area. A dose of 10 Gy was prescribed at 1 cm depth from the template surface and calculated using standard plans. After treatment, the dose at the clips was calculated using the reconstructed template geometry and the actual treatment dwell times. The median follow-up of surviving patients was 3 years. No patients were lost to follow-up.

*Results:* Overall, 12 patients (32%) had local recurrence, 5 (14%) of which were in the HDR-IORT field. The 3-year local failure rate for primary tumors and recurrent tumors was 19% and 52%, respectively ( $p=0.0042$ ). The 3-year local failure rate was 37% for negative margins and 26% for positive margins ( $p=0.51$ ). A high mean dose at the clip (17.3 Gy) was found. The overall survival was significantly different for primary vs. recurrent tumors, stage and grade.

*Conclusion:* Because of the HDR technique, a high dose at the clips was found, with good local control. More out-of-field than in-field failures were seen. The local failure rate was significantly different for primary vs. recurrent disease.

## 8.2 Introduction

Primary locally advanced and recurrent rectum tumors are a heterogeneous group of tumors, that include intrapelvic tethered rectum tumors, fixed tumors, enlarged nodes and metastatic disease.

The risk of developing local recurrence after treatment of a primary tumor increases with increased stage. Treatment of early-stage rectal cancer with preoperative radiotherapy (RT) and total mesorectal excision resulted in a recurrence-free rate of 94% for stage II and 85% for stage III tumors [1]. More advanced rectal tumors treated with postoperative RT and chemotherapy resulted in a recurrence-free rate of 73% for low-risk patients (T1-2N+/T3N0) and 48% for high-risk patients (T3N+/T4, any N) [2].

Survival after recurrence depends on stage and treatment and this results in a 3-year survival rate varying from 0% to 60% [3-5]. The cause of death in these patients is often systemic disease. However, a mortality rate of 16 to 44% owing to local failure has been reported [6,7]. Fixed or tethered rectum tumors often invade the adjacent organs or pelvic wall and result in an even worse local control and survival. To treat these latter tumors, intraoperative RT (IORT) was developed, because the conventional doses and techniques were insufficient or would lead to a greater incidence of radiation complications.

Two techniques have been in use: intraoperative electron beam radiotherapy (IOERT) and high dose rate brachytherapy (HDR-IORT). The advantages of IOERT are the treatment depth to >1 cm with a choice of electron energies and quick delivery of the radiation (<10 min). The flexible template in HDR brachytherapy can treat all surfaces; however, the treatment times and total procedure times are longer. The steep dose gradient between the target surface and the reference depth is another advantage, because the highest dose is at the area at risk. However, it also limits the use of intraoperative brachytherapy to target depths <0.5-1 cm. Because of these differences, the treatment indications can be different and the results of these two techniques are not completely comparable. IOERT is the most frequently used

technique. At least 14 cancer centers [5,7-19] have reported their results with IOERT, and only 3 have reported their results with HDR-IORT [4,20,21].

These three cancer centers used a 1-cm-thick pad as a template and often prescribed a dose of 15 Gy at the surface or at 0.5 cm depth from the pad. We changed this technique to create a high dose at the surface and a steep dose gradient. We developed a 0.5-cm-thick pad and prescribed a dose of 10 Gy at 1 cm depth from the pad surface. In 1997, the HDR-IORT program was started at the Erasmus MC-Daniel

**Table 1:** Patient characteristics.

		Total (%)	Primary (%)	Recurrent (%)
Number of patients		37	18 (49)	19 (51)
Median follow up of surviving patients (y)		3.0	2.8	3.3
Stage	T3 N0	20 (54)	12 (66)	8 (42)
	T4 N0	12 (32)	3 (16)	9 (47)
	T1-4 N1	5 (14)	3 (16)	2 (11)
Margin	Negative	19 (51)	11 (61)	8 (42)
	Positive	18 (49)	7 (39)	11 (58)
Gender	Male	25 (70)	12 (66)	13 (74)
	Female	12 (30)	6 (34)	6 (26)
Differentiation grade	1	3 (8)	3 (17)	0 (0)
	2	29 (78)	14 (78)	15 (79)
	3	4 (11)	0 (0)	4 (21)
	Unknown	1 (3)	1 (6)	0 (0)
Resection	LAR	1 (3)	0 (0)	1 (5)
	APR	21 (57)	15 (83)	6 (31)
	ASR	15 (40)	3 (17)	12 (63)
Age (y)	0-49	9 (24)	6 (33)	3 (16)
	50-69	18 (49)	8 (44)	10 (53)
	70-79	10 (27)	4 (22)	6 (31)

*LAR: lower anterior resection; APR: abdominoperineal resection; ASR: abdomino-sacral resection.*

Den Hoed Cancer Center. The HDR-IORT was only performed if the resection margins on frozen section analysis were  $\leq 2$  mm. Thirty-nine patients with locally advanced primary or locally recurrent rectum cancer had close or positive margins on frozen section analysis and were treated during surgery with HDR-IORT. All patients received preoperative external beam RT (EBRT) to the tumor and pelvis. To evaluate our alternative HDR-IORT technique, an analysis of the local failures was made with regard to the location of the local recurrence.

### 8.3 Methods and materials

#### 8.3.1 EBRT and surgery

Between 1997 and 2000, 97 patients with locally advanced primary or recurrent rectum tumors were treated with EBRT. After preoperative screening (CT scan of thorax, abdomen and pelvis), 23 patients were not eligible for surgery because of poor performance status, inoperable tumors or distant metastases. Of the 74 patients, 39 had close or positive resection margins and were treated with HDR-IORT. During resection, 2 patients were diagnosed with metastasis and were excluded from this analysis. Of the remaining 37 patients, 18 had primary locally advanced rectum cancer and 19 had a recurrence. All patients had adenocarcinoma. The patient characteristics are shown in table 1. Five patients received 25 Gy preoperative EBRT in five fractions and 31 patients received 50 Gy in 25 fractions. One patient with recurrent cancer was previously treated with 50.4 Gy and received for the second RT session an EBRT dose of 30.6 Gy in 1.8 Gy fractions. EBRT was delivered by either a three-field technique, using one posterior and two lateral portals or a four-field box technique. The pelvic field borders were defined as follows: the lateral borders extended 1.5 cm lateral of the bony pelvis, with the cranial border the promontory (L5-S1), and the caudal border was at least below the foramina obturatoria to 2 cm under the anus, depending on the tumor position. The dorsal border encompassed the sacrum, and the anterior border was chosen in such a way that the tumor region was widely covered. None of the patients received pre- or postoperative chemotherapy. Some patients were treated with chemotherapy, if metastases were diagnosed during follow-up. For each patient, the selected type of surgery was based on the fixation and location of the tumor. One low anterior resection, 21 abdominoperineal and 15 abdominosacral resections were performed.

**Table 2:** *Resection of organs.*

Resection	No (n)	Yes (n)	Partially (n)
Bladder	28	7	2
Prostate	13	7	5
Posterior vaginal wall	5	7	0
Uterus with adnex	8	4	0
Small bowel	33	0	4
Sacrum	22	0	15
Psoas	33	0	4

Forty organs or adjacent structures were completely or partially resected (table 2). The median follow-up of the surviving patients was 2.8 years for the patients with primary tumors and 3.3 years for those with recurrence. No patients were lost to follow-up.

### 8.3.2 Intraoperative RT

The Flexible Intraoperative Template (FIT) developed at our department is a 5-mm-thick pad made of flexible silicon with 1-cm-spaced parallel source guide tubes running through the center of the template. Before positioning the FIT, three to four surgical clips were placed generously around the target surface. The size and shape of the FIT were then adjusted to the target surface. The FIT, in combination with the catheter positions, was overlaid on a paper template. The paper template was used as input for the treatment planning system (Plato BPS, versions 13.3 and 13.7, Nucletron, The Netherlands). After positioning, the FIT was pressed against the area at risk by filling the pelvis with gauze pads. This was done to avoid the bolus effect from blood and/or surgical fluid during IORT and to push critical organs away from the FIT. Two orthogonal radiographs were taken to see whether the target surface (clips) was encompassed by the applicator. Treatment planning was performed using the standard geometries present in the treatment planning system. A dose of 10 Gy was delivered, usually at 1 cm depth from the applicator surface. The prescription depth was altered to a combination of 0.5 and 1 cm for one patient and for another patient to 1 and 2 cm. After treatment, the dose at the clips was calculated using the reconstructed template geometry and the actual treatment times. IORT was only administered if resection margins to the tumor were  $\leq 2$  mm, which was judged on frozen

**Table 3:** *Place of FIT in the pelvis.*

Place of FIT	number
Posterior pelvic wall	1
Posterior and left lateral pelvic wall	8
Posterior and right lateral pelvic wall	9
Posterior, left and right lateral pelvic wall	2
Posterior, left and right lateral, and anterior pelvic wall	0
Anterior pelvic wall	6
Anterior and left lateral pelvic wall	0
Anterior and right lateral pelvic wall	1
Anterior, left and right pelvic wall	4
Left lateral pelvic wall	2
Right lateral pelvic wall	4

section analysis. In the final pathology report, positive margins were found in 18 patients and negative margins in 19 patients. Of these 19 patients, 4 had a resection margin  $<1$  mm. Profuse bleeding or haemodynamic instability during surgery occurred in 7 patients. For these 7 patients, clips were not placed and/or orthogonal radiographs were not taken to reduce the operation time. In total, 129 clips were placed; 112 clips were apparently positioned directly under the FIT and 17 just at the edge of the FIT. The posterior and/or right pelvic walls were most frequently treated with the FIT (table 3). On average, 8 tubes with a FIT surface of  $69 \text{ cm}^2$  were used. The mean radiation time was 27 minutes (table 4).

### 8.3.3 Definitions and statistical method

A local recurrence was defined as tumor regrowth within the EBRT field and an IORT in-field recurrence was defined as a recurrence completely or partially within the IORT field, as seen on CT or MRI. Local recurrence and distant metastasis were scored until patient death and censored thereafter. Local control and survival curves were calculated using the actuarial Kaplan-Meier method. Comparisons for survival were made using the logrank test. For other comparisons, the Kruskal-Wallis test was used.

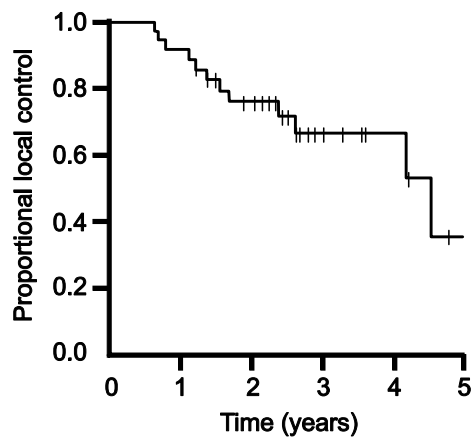
**Table 4:** IORT characteristics.

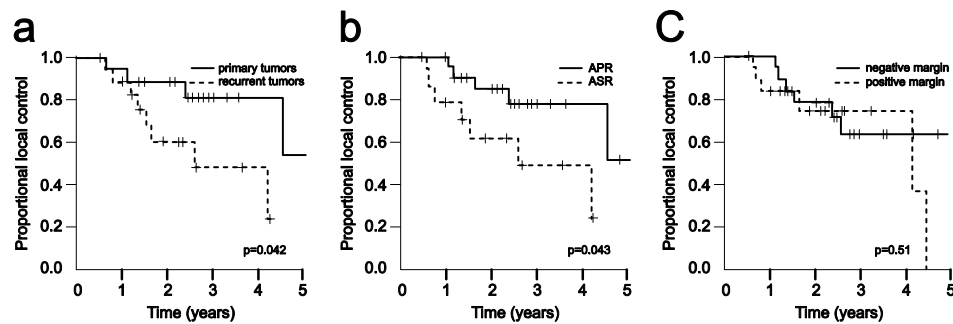
	Median (range)	Mean	SD
Number of catheters	7 (5–14)	8	2.7
FIT surface (cm <sup>2</sup> )	60 (24–161)	69	35
Radiation time (min)	21 (10–66)	27	14
Number of clips	4 (2–7)	4	1.1

## 8.4 Results

### 8.4.1 Local control

Twelve patients (33%) developed local recurrence, five recurrences were in the IORT field and seven were out-of-field. One IORT in-field failure (1/18; 6%) was seen in the primary locally advanced group and four (4/19; 21%) in the recurrence group. Three IORT in-field failures were diagnosed in patients with positive resection margins. The median time to local recurrence was 4.5 years (figure 1). The 3-year actuarial failure rate for primary tumors and recurrent tumors was 19% and 52%, respectively ( $p=0.042$ , fig. 2a). For patients with an abdominoperineal resection, the mean time to local failure was 4.2 years; for those with an abdominosacral resection, it was 2.8 years ( $p=0.043$ , fig. 2b). The 3-year local failure rate was 37% for those with negative margins and 26% for those with positive margins ( $p=0.51$ ,

**Figure 1:** Overall time to local recurrence.



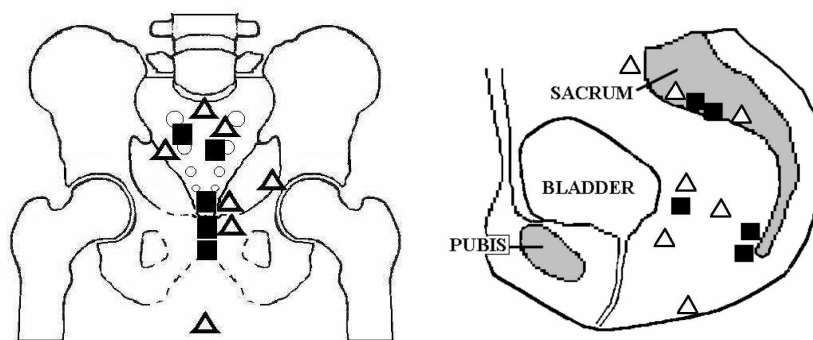
**Figure 2:** Time to local recurrence for primary/recurrent tumors (a), resection type (b), resection margin (c). APR: abdominoperineal resection; ASR: abdominosacral resection.

fig. 2c). Out-of-field failures were seen earlier than in-field failures (median time 16 vs. 31 months,  $p = 0.077$ ).

Eight of the 12 local failures were located in the posterior pelvis (figure 3). The median distance of the out-of-field recurrence to the area treated with the FIT was 2 cm (range 1–5 cm). Four recurrences were found growing in the sacrum or sacral foramina.

#### 8.4.2 IORT technique

The mean dose to all clips was 15.79 Gy. The mean dose to the 112 clips under the FIT and 17 clips at the edge was 17.27 and 6.05 Gy, respectively. Of the 112 clips,



**Figure 3:** Place (centrum) of recurrence after IORT. Triangles indicate out-of-field IORT recurrence; squares indicate in-field IORT recurrence.



20 received a dose <13 Gy. A dose <10 Gy was calculated in 4 of these 20. Patients with and without an in-field recurrence had a mean clip dose of 18.00 Gy (range 12.39-24.42 Gy) and 17.21 Gy (range 7.15-42.64 Gy). Patients with an in-field recurrence had a mean FIT of 82 cm<sup>2</sup> compared with 67 cm<sup>2</sup> for the rest of the patients ( $p=0.63$ ). No relationship between the size of the FIT, number of resected organs or topography of local recurrences was found.

#### 8.4.3 Complications

At the start of EBRT, 57% of the patients complained of pain, 32% of irregular stools, 27% of intrapelvic discomfort and 5% of urinary problems. Postoperatively, many complications were diagnosed, including a delay in wound healing in 46%, abscesses in 16%, leakage at the anastomosis site in 5% and fistulas in 8%. Plexopathy was found in 14% of the patients. Only 3 patients had late complications: one had chronic diarrhea (RTOG grade 1), another had chronic pain in the pelvis (RTOG grade 2), and the last had radiating pain to the lower extremities (RTOG grade 2). Sacral necrosis was not found.

#### 8.4.4 Overall survival

The actuarial 5-year survival rate was 38%, with a median survival of 2.8 years

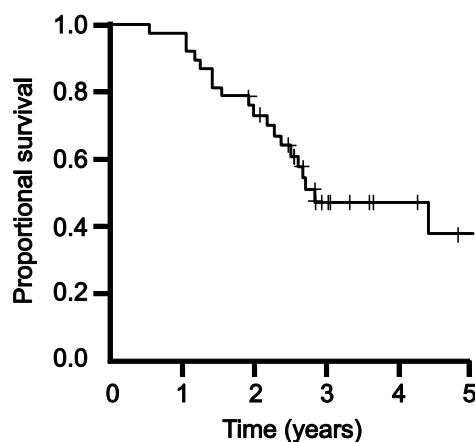


**Figure 4:** Overall survival.

(figure 4). The 3-year overall survival rate for patients with primary and recurrent tumors was 61% and 34%, respectively (figure 5a), and this difference was statistically significant ( $p = 0.016$ ). Two patients (5%) died of local disease and 17 (46%) of metastases. Of these 17 patients, 4 died of peritonitis carcinomatosa. Seventeen patients were still alive, 13 without disease, at last follow-up. The overall survival was significantly different according to stage ( $p=0.0016$ ) and grade ( $p=0.0012$ ) (figure 5b,c). Patients  $< 50$  years had a median survival of 2.2 years compared with 4.4 years for patients  $>50$  ( $p=0.31$ ).

Distant metastases were found in 18 patients. Several patients had metastasis in more than 1 organ: 5 patients had metastasis in the liver, 8 in the lung, 4 in the peritoneum and 7 in other locations. No patients with liver metastasis were rescued by surgery. Metastases were found in 44% and 53% of the patients with primary and recurrent tumors, respectively. The metastasis-free survival was not significantly different between primary and recurrent tumors ( $p=0.45$ ).

## 8.5 Discussion

The use of IORT for rectal cancer has been reported by at least 17 cancer centers, however, only 3 of these 17 used HDR-IORT. Two centers [4,22] used a 1-cm-thick pad (HAM applicator) and usually prescribed a dose of 15 Gy at 0.5 cm from the pad surface. The third center also developed a 1-cm-thick pad, but prescribed a dose of 15 Gy to the surface [23]. Our technique is different, with the use of a 0.5-cm-thick pad and a prescribed dose of 10 Gy to 1 cm from the pad surface. The advantages of

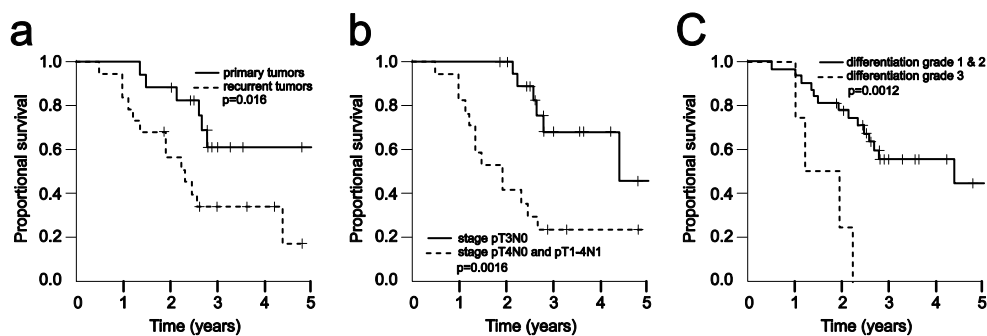


**Figure 5:** Survival according to primary/recurrent tumor (a), stage (b), and grade (c).

this thinner pad are the increased flexibility and a higher surface dose. In combination with dwell time optimization, doses up to 40 Gy to the clips were found at the corners of the template, as verified by the clip doses. According to the dosimetric characteristics of our technique, a clip dose of 13 Gy or higher indicated a gap between the FIT and the area of risk of  $<5$  mm or a well-positioned template at the clip. An adequate dose at the clip was found in 82%. Although the thinner template is more flexible, we still found a gap of  $\geq 5$  mm between the FIT surface and the clips in 18%. However, we only found a dose  $<10$  Gy in 3.5% of the clips, so we may assume that our technique was well carried out. The cause of the in-field failures was not found. No dose difference in patients with and without in-field failures was found.

Although high doses were applied to the surface, only 3 patients complained of late toxicity. Two patients reported chronic radiating pain and one chronic diarrhea. The postoperative toxicity of the integral treatment was high, as reported by many authors [4,7,10,20,24,25]. Many patients underwent extended resection combined with preoperative RT. It was often difficult to assign a particular complication as being a result of surgery or RT. Huber et al. [21] found a significant greater complication rate in patients treated with HDR-IORT, Hashiguchi et al. [7] described a trend and Noyes et al. [26] found no difference in their combined analysis of 220 patients.

Five of the 12 local recurrences were IORT in-field recurrences. Because more out-of-field failures were found than in-field failures, it can be assumed that IORT is an effective treatment. However, a randomized trial is needed to confirm this. Nine studies [7,8,10,11,19-21,24] also reported the site of recurrence. For primary tumors and recurrent tumors, 17% and 49% of the local failures were in-field, respectively (table 5). Because out-of-field failures were more frequent than in-field failures, the question is raised of how the occurrence of these out-of-field failures can be reduced. Our out-of-field failures were within 5 cm of the IORT area and could be included by extending the FIT. However, four local failures were located in the sacrum or sacral foramina. HDR-IORT probably could not have prevented these local failures, because they were situated close to the nerves. The question arises whether higher doses or larger FITs could have prevented the other recurrences, without increasing the toxicity.

As opposed to other reports, we did not find that close or positive margins resulted in differences in the local recurrence rate ( $p=0.51$ ). Many authors [4,8,11,14,22,27] have reported a statistically significant difference in the local failure rate according to

**Table 5:** Number of in-field failures according to author and technique.

Tumor	Author	In-field failure	Total failures	%	Technique
Primary	Huber <i>et al.</i> [21]	0	3	0	HDR-IORT
	Gunderson <i>et al.</i> [11]	1	8	13	IOERT
	Calvo <i>et al.</i> [18]	1	3	30	IOERT
	Present study	1	4	25	HDR-IORT
	Total	3	18	17	
Recurrent	Bussieres <i>et al.</i> [8]	9	21	43	IOERT
	Pezner <i>et al.</i> [19]	8	13	62	IOERT
	Haddock <i>et al.</i> [24]	12	18	67	IOERT
	Eble <i>et al.</i> [10]	4	9	44	IOERT
	Hashiguchi <i>et al.</i> [7]	1	9	11	IOERT
	Nag <i>et al.</i> [20]	7	14	50	HDR-IORT
	Present study	4	8	50	HDR-IORT
	Total	45	92	49	

*HDR-IORT: High Dose Rate IntraOperative Radiotherapy; IOERT: IntraOperative Electron Radiotherapy*

the resection margin. However, they usually compared negative margins with microscopically positive margins or gross total resection margins and not close margins (<2 mm) with positive margins. Extended resections, such as abdominosacral resections and total and partial organ resection, were often performed. Patients who underwent abdominosacral resection had a significantly different greater local failure rate than did patients with abdominoperineal resection ( $p=0.043$ ). This can be explained by the larger amount of disease or more aggressive character of the tumor when abdominosacral resections were necessary.

Of our patients, 33% had local failure. For primary locally advanced tumors, the 3-year local failure rate was 19%. Other authors found a comparable 3-year local failure rate of 16% and 23% [1,2]. Harrison *et al.* [27] reported a 2-year local failure rate of 19%. Recurrent tumors had a 3-year local failure rate of 52%. The reported 3-year local failure rate varies between 53% and 79% [4,6,8,19,22]. A statistically significant difference ( $p = 0.042$ ) in the time to local failure between the primary and recurrent tumors was found, but has not been previously reported.

Patients with primary tumors survived longer than patients with recurrence ( $p=0.016$ ). The 2-, 3-, and 5-year overall survival rate for patients with primary

tumors was 89%, 61%, and 61%, respectively. Harrison et al. [27] reported a 2-year survival rate of 69%, and other authors [11,14,21] reported a 3-, and 5-year survival rate of 55 and 45%, respectively. In this study, patients with recurrent tumors had a 3-year overall survival rate of 34%. Most authors [4,5,7,8,22] reported a 3-year survival rate of 30% to 50%; however, other authors [10,24] found a 3-year survival rate of 12% and 64%. Patients with pathologic proven positive nodes, T4 tumors or grade 3 differentiation had a statistically significant lower survival. Complete or partial resection [4-7,10,11,22,27], the use of IORT plus EBRT [4,22], concomitant chemoradiotherapy [11], and larger irradiated target areas [20] were found to be other significant prognostic factors by other authors.

## 8.6 Conclusion

The HDR-IORT technique for rectal cancer resulted in a high local control rate. Because of the calculation of the dose to the clips, we can conclude that our technique was well carried out. The local failure rate for those with positive margins compared with those with close margins did not differ. Because IORT out-of-field recurrences were common, a greater EBRT dose, a larger FIT area or the addition of concurrent chemotherapy may be of benefit for these patients. Patients with primary tumors had significantly greater local control and survival than did patients with recurrent tumors. Other prognostic factors for survival were stage and differentiation grade.

## 8.7 References

1. Kapiteijn E, Marijnen CA, Nagtegaal ID, *et al.* Preoperative radiotherapy combined with total mesorectal excision for resectable rectal cancer. *N Engl J Med* 2001;345:638-646.
2. Tepper JE, O'Connell M, Niedzwiecki D, *et al.* Adjuvant therapy in rectal cancer: analysis of stage, sex, and local control - final report of intergroup 0114. *J Clin Oncol* 2002;20:1744-1750.
3. Wong CS, Cummings BJ, Brierley JD, *et al.* Treatment of locally recurrent rectal carcinoma-results and prognostic factors. *Int J Radiat Oncol Biol Phys* 1998;40:427-435.
4. Alektiar KM, Zelefsky MJ, Paty PB, *et al.* High-dose-rate intraoperative brachytherapy for recurrent colorectal cancer. *Int J Radiat Oncol Biol Phys* 2000;48:219-226.

5. Wiig JN, Tveit KM, Poulsen JP, *et al.* Preoperative irradiation and surgery for recurrent rectal cancer. Will intraoperative radiotherapy (IORT) be of additional benefit? A prospective study. *Radiother Oncol* 2002;62:207-213.
6. Lindel K, Willett CG, Shellito PC, *et al.* Intraoperative radiation therapy for locally advanced recurrent rectal or rectosigmoid cancer. *Radiother Oncol* 2001;58:83-87.
7. Hashiguchi Y, Sekine T, Sakamoto H, *et al.* Intraoperative irradiation after surgery for locally recurrent rectal cancer. *Dis Colon Rectum* 1999;42:886-893; discussion 893-885.
8. Bussieres E, Gilly FN, Rouanet P, *et al.* Recurrences of rectal cancers: results of a multimodal approach with intraoperative radiation therapy. French Group of IORT. Intraoperative Radiation Therapy. *Int J Radiat Oncol Biol Phys* 1996;34:49-56.
9. Crucitti F, Ratto C, Sofo L, *et al.* Preoperative radiotherapy and IORT in resectable rectal cancer at high risk for local recurrence. *Rays* 1995;20:190-196.
10. Eble MJ, Lehnert T, Treiber M, *et al.* Moderate dose intraoperative and external beam radiotherapy for locally recurrent rectal carcinoma. *Radiother Oncol* 1998;49:169-174.
11. Gunderson LL, Nelson H, Martenson JA, *et al.* Locally advanced primary colorectal cancer: intraoperative electron and external beam irradiation +/- 5-FU. *Int J Radiat Oncol Biol Phys* 1997;37:601-614.
12. Kim HK, Jessup JM, Beard CJ, *et al.* Locally advanced rectal carcinoma: pelvic control and morbidity following preoperative radiation therapy, resection, and intraoperative radiation therapy. *Int J Radiat Oncol Biol Phys* 1997;38:777-783.
13. Lanciano RM, Calkins AR, Wolkov HB, *et al.* A phase I/II study of intraoperative radiotherapy in advanced unresectable or recurrent carcinoma of the rectum: a Radiation Therapy Oncology Group (RTOG) study. *J Surg Oncol* 1993;53:20-29.
14. Willett CG, Shellito PC, Tepper JE, *et al.* Intraoperative electron beam radiation therapy for primary locally advanced rectal and rectosigmoid carcinoma. *J Clin Oncol* 1991;9:843-849.
15. Mannaerts GH, Rutten HJ, Martijn H, *et al.* Comparison of intraoperative radiation therapy-containing multimodality treatment with historical treatment modalities for locally recurrent rectal cancer. *Dis Colon Rectum* 2001;44:1749-1758.
16. Weinstein GD, Rich TA, Shumate CR, *et al.* Preoperative infusional chemoradiation and surgery with or without an electron beam intraoperative boost for advanced primary rectal cancer. *Int J Radiat Oncol Biol Phys* 1995;32:197-204.
17. Sadahiro S, Suzuki T, Ishikawa K, *et al.* Intraoperative radiation therapy for curatively resected rectal cancer. *Dis Colon Rectum* 2001;44:1689-1695.
18. Calvo FA, Gomez-Espi M, Diaz-Gonzalez JA, *et al.* Intraoperative presacral electron boost following preoperative chemoradiation in T3-4Nx rectal cancer: initial local effects and clinical outcome analysis. *Radiother Oncol* 2002;62:201-206.

19. Pezner R, Chu D, Ellenhorn J. Intraoperative radiation therapy for patients with recurrent rectal and sigmoid colon cancer in previously irradiated fields. *Radiother Oncol* 2002;64:47.
20. Nag S, Martinez-Monge R, Mills J, *et al.* Intraoperative high dose rate brachytherapy in recurrent or metastatic colorectal carcinoma. *Ann Surg Oncol* 1998;5:16-22.
21. Huber FT, Stepan R, Zimmermann F, *et al.* Locally advanced rectal cancer: resection and intraoperative radiotherapy using the flab method combined with preoperative or postoperative radiochemotherapy. *Dis Colon Rectum* 1996;39:774-779.
22. Martinez-Monge R, Nag S, Martin EW. Three different intraoperative radiation modalities (electron beam, high-dose-rate brachytherapy, and iodine-125 brachytherapy) in the adjuvant treatment of patients with recurrent colorectal adenocarcinoma. *Cancer* 1999;86:236-247.
23. Kneschaurek P, Wehrmann R, Hugo C, *et al.* [The flab method of intraoperative radiotherapy]. *Strahlenther Onkol* 1995;171:61-69.
24. Haddock MG, Gunderson LL, Nelson H, *et al.* Intraoperative irradiation for locally recurrent colorectal cancer in previously irradiated patients. *Int J Radiat Oncol Biol Phys* 2001;49:1267-1274.
25. Gunderson LL, Nelson H, Martenson JA, *et al.* Intraoperative electron and external beam irradiation with or without 5-fluorouracil and maximum surgical resection for previously unirradiated, locally recurrent colorectal cancer. *Dis Colon Rectum* 1996;39:1379-1395.
26. Noyes RD, Weiss SM, Krall JM, *et al.* Surgical complications of intraoperative radiation therapy: the Radiation Therapy Oncology Group experience. *J Surg Oncol* 1992;50:209-215.
27. Harrison LB, Minsky BD, Enker WE, *et al.* High dose rate intraoperative radiation therapy (HDR-IORT) as part of the management strategy for locally advanced primary and recurrent rectal cancer. *Int J Radiat Oncol Biol Phys* 1998;42:325-330.





## **CHAPTER 9. DETERMINATION OF THE ACCURACY OF IMPLANT RECONSTRUCTION AND DOSE DELIVERY IN BRACHYTHERAPY IN THE NETHERLANDS AND BELGIUM**

RJM Elfrink, IKK Kolkman-Deurloo, HJ van Kleffens, A Rijnders, B Schaeken, AHL Aalbers, WJF Dries, JLM Venselaar

Radiother Oncol 2001; 59; 297-306.

### **9.1 Abstract**

*Purpose:* To gain insight into the accuracy of brachytherapy treatments, the accuracy of implant reconstruction and dose delivery was investigated in 33 radiotherapy institutions in The Netherlands and Belgium.

*Materials and Methods:* The accuracy of the implant reconstruction method was determined using a cubic phantom containing 25 spheres at well-known positions. Reconstruction measurements were obtained on 41 brachytherapy localizers, 33 of which were simulators. The reconstructed distances between the spheres were compared with the true distances. The accuracy of the dose delivery was determined for High Dose Rate (HDR), Pulsed Dose Rate (PDR) and Low Dose Rate (LDR) afterloading systems using a polymethyl methacrylate cylindrical phantom containing an NE 2571 ionization chamber in its centre. The institutions were asked to deliver a prescribed dose at the centre of the phantom. The measured dose was compared with the prescribed dose.

*Results:* The average reconstruction accuracy was  $-0.07$  mm ( $\pm 0.4$  mm, 1 SD) for 41 localizers. The average deviation of the measured dose from the prescribed dose was  $+0.9\%$  ( $\pm 1.3\%$ , 1 SD) for 21 HDR afterloading systems,  $+1.0\%$  ( $\pm 2.3\%$ , 1 SD) for 12 PDR afterloaders, and  $+1.8\%$  ( $\pm 2.5\%$ , 1 SD) for 15 LDR afterloaders.

*Conclusions:* This comparison showed a good accuracy of brachytherapy implant reconstruction and dose delivery in The Netherlands and Belgium.

## 9.2 Introduction

Brachytherapy is performed in 39 different institutions in The Netherlands and Belgium. The remote afterloading equipment that is currently installed in these institutions is shown in table 1. Each institution has its own quality assurance (QA) programme for checking the accuracy of relevant physical parameters, guided by the many directives published on this subject [3-5,7,8,11,12,14,21,25]. Because of this, the test frequency, test methodology and accuracy criterion of the QA tests differ significantly between the institutions.

A taskgroup on QA of brachytherapy systems of the Netherlands Commission on Radiation Dosimetry (NCS) has developed guidelines for QA in brachytherapy [17], in the same way as was done before for medical accelerators and simulators and computed tomography (CT) scanners [15,16]. To achieve this goal, four stages have been distinguished by the task group.

**Table 1:** Remote afterloading High Dose Rate (HDR), Pulsed Dose Rate (PDR) and Low Dose Rate (LDR) systems installed in The Netherlands and Belgium.

Brachytherapy	Afterloading system	Source(s)	No. of installed systems
HDR	Nucletron <sup>1</sup> microSelectron	<sup>192</sup> Ir	17
HDR	Sauerwein <sup>2</sup> Gammamed	<sup>192</sup> Ir	3
HDR	Varian <sup>3</sup> Varisource	<sup>192</sup> Ir	1
PDR	Nucletron microSelectron	<sup>192</sup> Ir	12
PDR	Sauerwein Gammamed	<sup>192</sup> Ir	3
LDR	Nucletron Selectron	<sup>137</sup> Cs	16
LDR	Nucletron microSelectron	<sup>192</sup> Ir / <sup>137</sup> Cs	13
LDR	Arplay <sup>4</sup> Telegyn	<sup>137</sup> Cs	1
LDR	CIS bio <sup>5</sup> Curietron	<sup>137</sup> Cs	2

<sup>1</sup> Nucletron B.V., The Netherlands; <sup>2</sup> Isotopen-Technik Dr. Sauerwein GmbH, Germany; <sup>3</sup> Varian Medical Systems, Inc., USA; <sup>4</sup> Arplay Medical, France; <sup>5</sup> Cis bio International, France.

1. Gain insight into the current practice of QA of brachytherapy.
2. Determine the accuracy of implant reconstruction and dose delivery in all institutions.
3. Compare the current QA-practice with existing recommendations on QA.
4. Formulate a set of minimum requirements on QA.

To gain insight in the current QA practice, an extensive questionnaire on the QA of brachytherapy systems was completed by the radiotherapy institutions in The Netherlands and Belgium in 1998. The accuracy of the implant reconstruction and dose delivery was determined by performing on-site measurements with two dedicated phantoms in the institutions. The current QA practice and the results of the on-site measurements were compared with international QA recommendations. From this, a set of minimum requirements on QA, suitable for the situation in The Netherlands and Belgium, was formulated and published as an NCS report [17].

The accuracy of a brachytherapy treatment depends on many parameters, such as source activity, source position, irradiation time, implant reconstruction and dose calculated by the treatment planning software. In practice, an accuracy of physical dose delivery of 5-10% is thought to be achievable [12].

Clearly, source calibration is the physical parameter in brachytherapy dose delivery that is most frequently studied [1,2,18,20,23]. However, the dose delivery accuracy depends on many physical parameters. Although a check of the individual parameters is part of most QA programmes, the delivered dose is generally not directly determined. It was decided to gain more insight into the accuracy of implant reconstruction and dose delivery in brachytherapy. Therefore, on-site measurements with two dedicated phantoms were performed in all institutions using brachytherapy in The Netherlands and Belgium. The methods and results are presented in this paper.

### **9.3 Materials and methods**

#### *9.3.1 Reconstruction measurements*

To check the reconstruction methods used with brachytherapy localizers, a cubic polymethyl methacrylate (PMMA) phantom (further referred to as reconstruction phantom) was used consisting of six identical 20 mm thick slabs [3]. At each

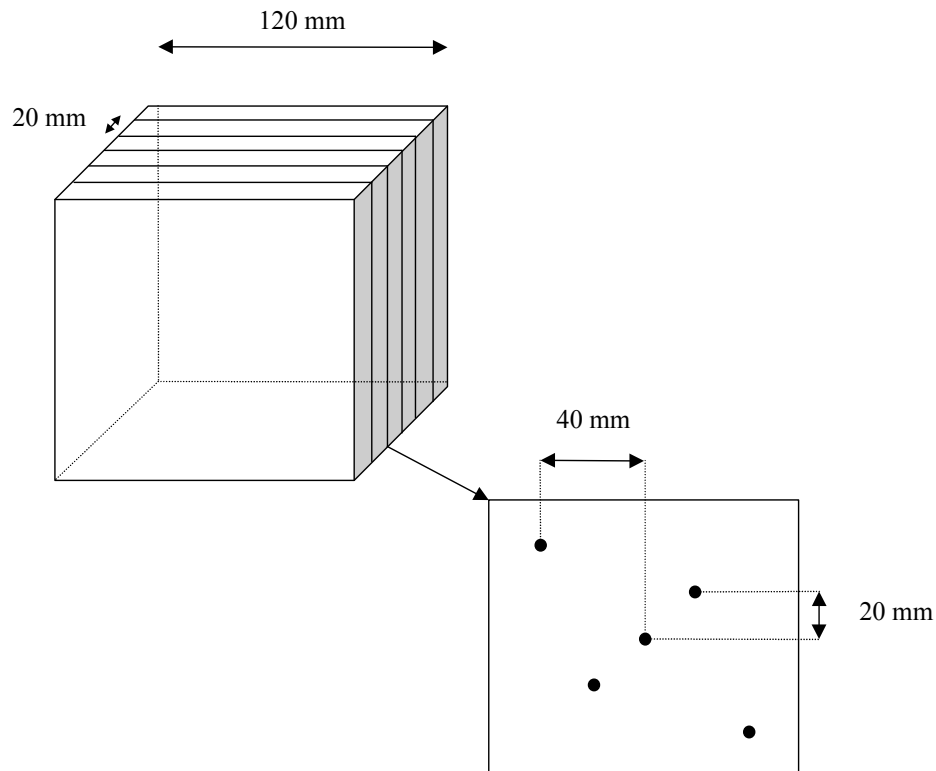


**Figure 1:** The geometry of the reconstruction phantom. The phantom contains 25 spheres at well-known positions, from which 300 inter-sphere distances can be calculated, varying between 20 and 140 mm.

interface between the slabs, five 2 mm spheres are inserted (see figure 1). The positions of the spheres are known with an accuracy of  $\pm 0.10$  mm (1 SD).

The institutions were asked to reconstruct the phantom using the equipment and procedures that are routinely used for reconstruction of brachytherapy implants. For this purpose, the phantom was positioned on the treatment table with the central marker close to the isocentre of the localizer, in the case of an isocentric localizer. For non-isocentric localizers, a reconstruction box was used. The coordinates of the spheres were determined by reconstruction from two X-ray films, except for a CT-based reconstruction. From these coordinates, 300 inter-sphere distances were calculated, ranging from 20 to 140 mm, with an average of 66 mm. The reconstructed distances were compared with the true distances leading to an average

deviation of the 300 inter-sphere distances. In this way, the final result reflects the geometrical accuracy of the localizer, the digitizer and the reconstruction algorithm.

Reconstruction of brachytherapy implants is commonly performed on a simulator (29 institutions). Some institutions have more than one localizer available for brachytherapy implant reconstruction. The reconstruction measurements were performed on 41 localizers (33 simulators, five C-arms, one mobile X-ray unit, one Integrated Brachytherapy Unit (IBU) localizer and one CT scanner) in 33 institutions. The magnification factor used as input in case of isocentric localization varied between 1.35 and 1.55. Orthogonal reconstruction was used on all simulators, except for one case, where a variable angle reconstruction was applied using gantry angles of  $-30^\circ$  and  $+30^\circ$ .

### 9.3.2 Dose measurements

To determine the accuracy of the dose delivery in the institutions, a solid phantom (further referred to as dose phantom) was used, as designed by Meertens [10]. The phantom is a PMMA cylinder with a diameter of 20.0 cm and a height of 15.0 cm. An NE 2571 (Nuclear Enterprises Ltd, UK) ionization chamber is positioned centrally in the phantom and three brachytherapy applicators are placed at 5.0 cm from the ionization chamber, equally spaced at  $120^\circ$  angles (see figure 2). The dose delivered during the treatment is measured by the ionization chamber surrounded by

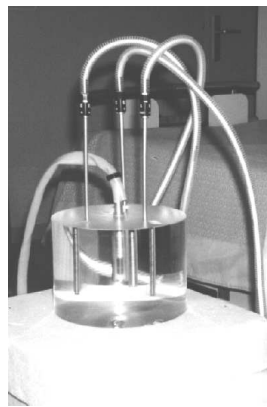


**Figure 2:** Cylindrical dose phantom. Three applicators are positioned at 5.0 cm from the centrally placed ionization chamber.

its build-up cap, in combination with a Precitron (Precitron AB, Sweden) Janus electrometer. The chamber was calibrated in combination with the electrometer in September 1998 at The Netherlands Measurements Institute (NMI), the National Standards Laboratory for Ionizing Radiation.

#### *9.3.2.1 Measurement procedure*

The institutions were asked to prepare a treatment plan to deliver a prescribed dose in the centre of the ionization chamber using fixed source positions. The source positions used during the measurements are based on the source calibration protocols for  $^{192}\text{Ir}$  HDR sources [14] and  $^{137}\text{Cs}$  pellets [13] for this phantom. For HDR and PDR afterloaders, one source position per catheter is used in the same plane as the effective point of measurement (the centre of the ionization chamber). For Selectron LDR afterloaders, six sources per catheter are used, three on both sides of the central plane of the phantom at distances of 17.5 mm, 20.0 mm and 22.5 mm from that plane (figure 3).

Because the reconstruction accuracy is measured separately, the source positions are entered in the treatment planning system (TPS) using coordinates and not by reconstruction of the phantom. In this way, the error in dose delivery caused by an error in reconstruction of the set-up is avoided. However, in some TPSs, source position coordinates cannot be entered directly. In the two institutions using such a TPS, the geometry was reconstructed from a drawing of the experimental set-up as accurately as possible.

The value for the prescribed dose was determined as a compromise between the accuracy of the electrometer and practical considerations, such as the required measuring time. A prescribed dose of 75 cGy for HDR, 40 cGy for PDR, and 20 cGy for LDR afterloaders was used. These doses resulted in treatment times (depending on the exact source strength) of approximately 5 minutes for a 2 cGy<sup>2</sup>/h HDR  $^{192}\text{Ir}$  source, 25 minutes for a 0.22 cGy<sup>2</sup>/h  $^{192}\text{Ir}$  PDR source, and 45 minutes for 18  $^{137}\text{Cs}$  LDR sources with a source strength of 0.004 cGy<sup>2</sup>/h.

After installation of the phantom, air temperature and pressure were recorded. The dose delivery measurement is performed three times, using the dwell times calculated by the TPS. The measurement is performed with plastic catheters or needles, corresponding to the normal use for treatments in the institution.

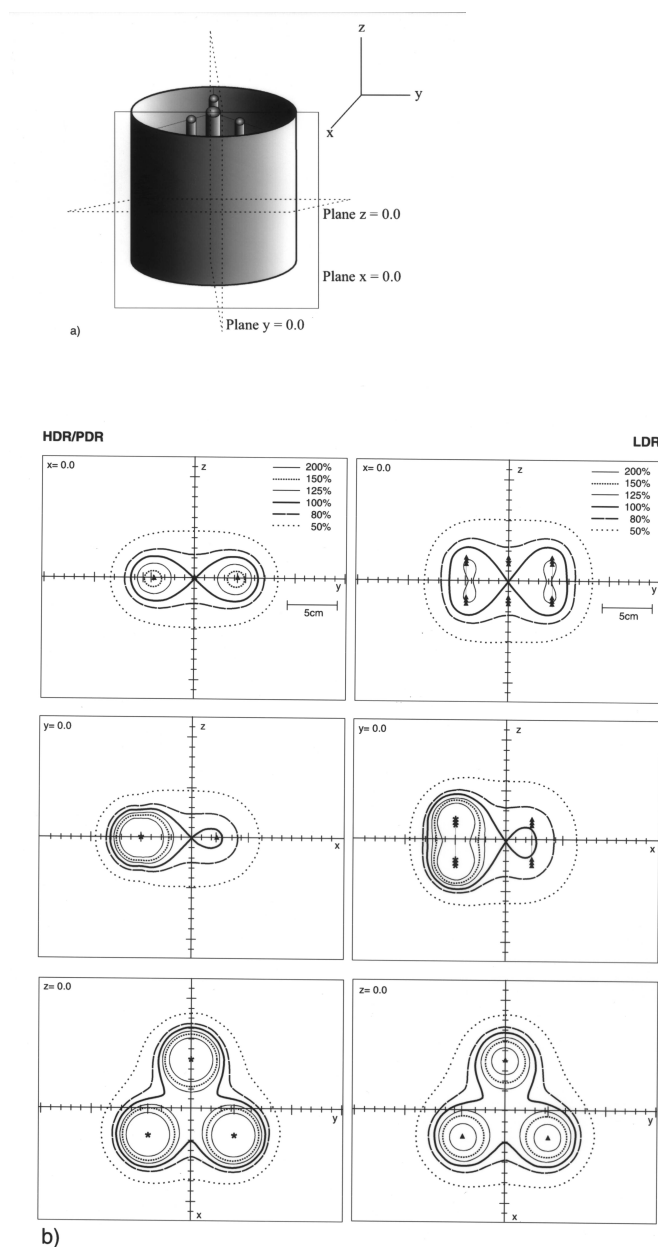


**Figure 3:** The dose distribution for the cylindrical dose phantom (a) for HDR/PDR and Selectron LDR afterloaders in three orthogonal planes passing through the effective measurement point of the ionization chamber (b).

**Table 2:** Factors for conversion of the electrometer reading to dose in water for  $^{192}\text{Ir}$  and  $^{137}\text{Cs}$  sources measured in the PMMA cylindrical phantom (see also references [10,13,14,22]).

Factor	Description	Value for $^{192}\text{Ir}$ in the phantom	Value for $^{137}\text{Cs}$ in the phantom
$M_{\text{uncor}}$	Uncorrected instrument reading		
$p_t$	Temperature correction factor	$(T_{\text{meas}} + 273.15 / T_{\text{calibration}})$	
$p_p$	Air pressure correction factor	$(p_{\text{calibration}} / p_{\text{meas}})$	
$p_{\text{hum}}$	Humidity correction factor	1.000	
$p_{\text{ion}}$	Ion recombination correction factor	1.000	
$p_{\text{pol}}$	Correction factor for polarity effects	1.000	
$N_K$	Air kerma calibration factor	From calibration	
$p_r$	Correction factor for replacement of PMMA by the ionization chamber	1.016	0.997
$p_{\text{ce}}$	Correction factor for the effect of the central electrode during the measurement	1.000	
$k_w$	Correction factor for attenuation and scatter in the chamber wall	0.984	0.9904
$k_{\text{st}}$	Correction for the stem effect during calibration	1.000	
$k_{\text{ce}}$	Correction for the effect of the central electrode during calibration	1.000	
$f_{\text{tr}}$	Correction factor for source transport time	Variable	1.000
$f_{\text{ph}}$	Conversion factor from the specified PMMA phantom to a full-scatter water phantom	1.033	1.041
$f_{\text{geo}}$	Correction factor for absorption and scatter in water	$1 / S(d)$	
$f_{\text{cath}}$	Correction factor for attenuation in plastic catheter / needles	1.000 / 1.009	Included in $f_{\text{ph}}$
$S(d)$	Correction factor for scattering and absorption in the phantom material	See Refs. [10,13,14,22]	
$(\mu / \rho)_{\text{air}}^{\text{water}}$	Mass-energy absorption coefficient	1.11	
$g$	Fraction of kinetic energy of secondary particles converted to bremsstrahlung	0.000	0.003



### 9.3.2.2 Conversion of electrometer readings to dose in water

The electrometer reading is converted to a dose to water value using the equation [14]:

$$D_w = MN_K \Pi k_i \Pi p_i \Pi f_i S(d) \left( \frac{\mu}{\rho} \right)_{air}^{water} (1 - g) \quad (1)$$

where:

$$M = M_{uncorr} P_i P_p P_{hum} P_{ion} P_{pol}$$

$$\Pi p_i = p_r p_{ce}$$

$$\Pi k_i = k_w k_{st} k_{ce}$$

$$\Pi f_i = f_{tr} f_{ph} f_{geo} f_{cath}$$

The meaning and value of these factors are described in table 2. Most of these factors were determined in previous studies [10,13,14,22]. The air kerma calibration factor for  $^{192}\text{Ir}$  and  $^{137}\text{Cs}$  of the ionization chamber with build-up cap in combination with the electrometer was derived from  $N_k$  factors obtained during calibration at the National Standards Laboratory. Values for the mass-energy absorption coefficient  $(\mu / \rho)_{air}^{water}$  for  $^{192}\text{Ir}$  and  $^{137}\text{Cs}$  were taken from the literature [4,19]. In TPSs, either the value 1.10 or 1.11 is used. Here, the value 1.11 was used in the calculations. The influence of the transit dose ( $f_{tr}$ ) and the applicator attenuation ( $f_{cath}$ ) had to be determined separately and will be discussed in the next paragraphs.

### 9.3.2.3 Determination of the transit dose correction factor

The clinical treatment planning generally neglects the transit dose, i.e. the dose delivered during transport of the source from the afterloader to the patient. The transit dose depends on the source strength, the velocity of the source transport and the geometry of the set-up. To compare the dose measured in the phantom with the dose calculated by the planning system, and to compare measurements in different institutions, the measured dose was corrected for the transit dose using the factor  $f_{tr}$  [14]. For a fixed geometry, such as the dose phantom, the value for this factor can be derived from:

$$f_{tr} = 1 - \frac{M_{t0}}{M_t} \quad (2)$$

where  $t$  is the dwell time,  $M_{t0}$  is the electrometer reading at  $t=0$  (zero dwell time, only dose contribution during source transport) and  $M_t$  is the electrometer reading for dwell time  $t$ . The value for  $t=0$ ,  $M_{t0}$ , is determined for the specific geometry by programming dwell times in the range of 5 to 120 seconds per channel and by linear extrapolation of the measured doses to  $t=0$ . Since the transit dose linearly depends on the source strength, and experience has shown that the source transport velocities on identical machines are comparable, its value for identical machines in different institutions can be calculated from the value measured on a single afterloader with reasonable accuracy.

#### 9.3.2.4 Attenuation in the applicator wall

To determine the difference in attenuation between plastic catheters and metal needles during HDR/PDR measurements, a correction factor  $f_{cath}$  was determined. The value for  $f_{cath}$  was determined as the ratio of the reading obtained when using plastic catheters and the reading obtained when using needles, and was found to be  $1.009 (\pm 0.003, 1 \text{ SD})$ . To compare the dose measured in the phantom with the dose calculated by the TPS, and to compare measurements in different institutions, the measured dose was corrected for the attenuation in institutions where needles were used during the measurements.

For the Selectron LDR afterloader, the factor  $f_{cath}$  for the replacement of water-equivalent catheters by the stainless steel standard catheters is included in the factor  $f_{ph}$  [10].

#### 9.3.3 Source positioning accuracy for HDR and PDR afterloaders

In the solid phantom dose delivery measurements, the combined accuracy of source calibration, source positioning, timer and dose calculation of the treatment planning software is determined. An error in source calibration, timer or dose calculation will influence the measured dose proportionally. For example, an error in source calibration of 2% will be measured as an error in the delivered dose of 2%. However, an error in source positioning along the catheter will hardly influence the measured dose. This is caused by the relatively uniform dose distribution around the ionization chamber, which is the result of the applied source configuration. To illustrate this, the electrometer reading is plotted as a function of the source position along a single

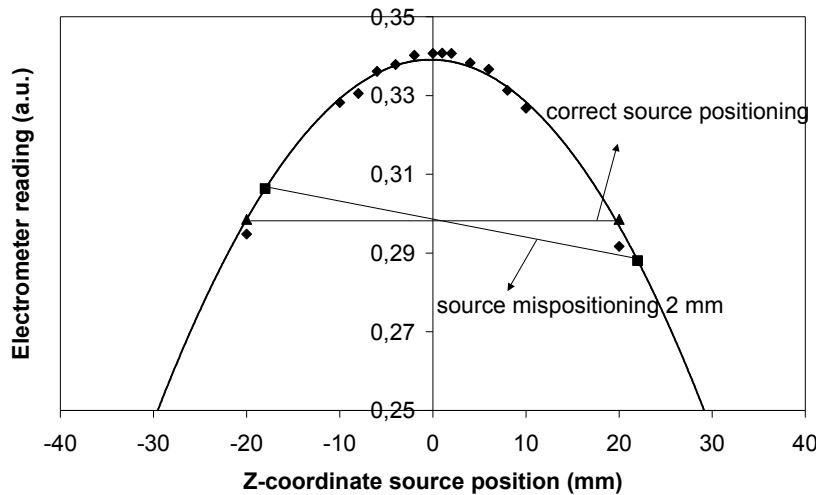


**Figure 4:** Electrometer reading as function of the source position along the catheter ( $z$ -direction) in the dose phantom (for the geometry see figure 3). The maximum reading is obtained at  $z=0$  mm, when the source is opposite to the ionization chamber. The difference in reading between  $z=-20$  mm and  $z=+20$  mm is used to estimate the error in source positioning.

catheter for a HDR-unit in figure 4. The maximum reading is obtained at  $z=0$  mm, when the source is opposite to the ionization chamber. An error of 2 mm in the source position around this optimum will result in a deviation in the measured dose of only 0.2% (figure 4).

In clinical treatments, however, a systematic error in source positioning of 2 mm for the entire implant can result in a significant error in dose delivery because of the possible geometrical miss of the target volume. It would therefore be useful to also obtain information on the source positioning accuracy. Because the effect of source positioning on the electrometer reading is much larger on the slopes of the curve, it was decided for HDR and PDR afterloaders to use two extra measurements at positions +20 mm and -20 mm from the optimum source position ( $z=0$  mm). The difference in electrometer reading between a source at +20 mm and a source at -20 mm is used to calculate the error in the source position. For example, if in an institution an error in source positioning of 2 mm exists, the source is positioned at  $z=+2$  mm for the measurements; the difference in electrometer reading between source position  $z=-18$  mm and  $z=+22$  mm is then approximately 6% (figure 4), which can easily be measured. For Cs LDR afterloaders, a systematic error in source

positioning is less probable because of the fixed source positions. This extra measurement was therefore not performed for the LDR afterloaders.

## 9.4 Results

### 9.4.1 Reconstruction measurements

The results of the measurements with the reconstruction phantom for the 41 localizers are shown in figure 5 as the average reconstruction error of 300 reconstructed distances. The deviation of the reconstructed distances was smaller than 0.5 mm for 36 localizers, and even smaller than 0.25 mm for 27 localizers. For one C-arm, the error was -2.1 mm, and for another C-arm (with reconstruction box) the deviation was +1.3 mm. For the 41 localizers, an average deviation of 0.1 mm ( $\pm 0.5$  mm, 1 SD) was found.

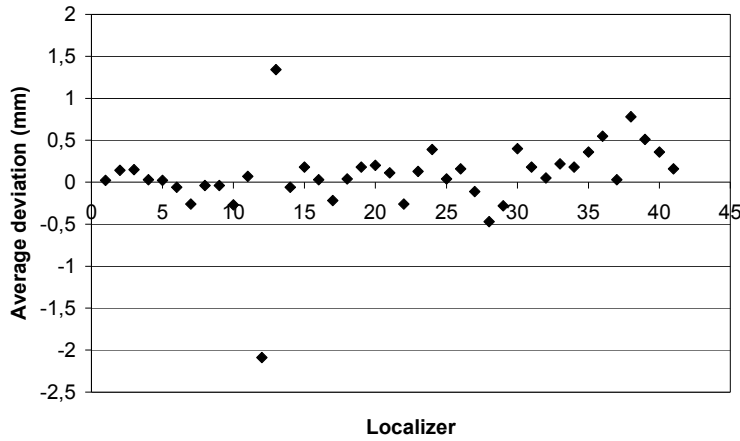


**Figure 5:** Results of the reconstruction accuracy measurements on 41 brachytherapy localizers: average deviation of 300 reconstructed distances (ranging from 20 mm to 140 mm) from the true distances between 25 spheres in the reconstruction phantom. A positive deviation indicates a reconstructed distance larger than the true distance.

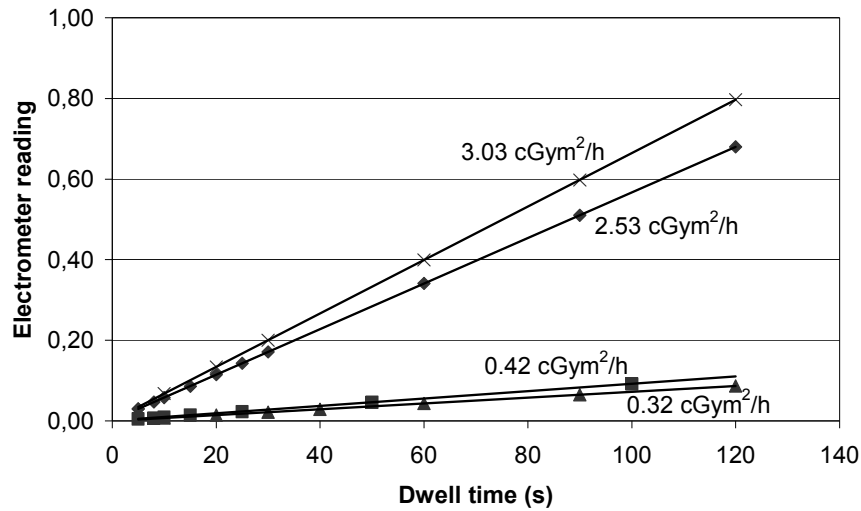


**Figure 6:** Determination of the transit dose for microSelectron HDR and PDR afterloaders in four different institutions. The electrometer reading is measured for dwell times varying from 5 to 120 seconds. The y-axis cut-off represents the transit dose for this specific experimental setup.

#### 9.4.2 Dose measurements

##### 9.4.2.1 Transit dose correction factor

The transit dose correction factor for the specific phantom has been determined for microSelectron HDR and PDR afterloaders (Nucletron, The Netherlands) by measuring the electrometer reading with the source position opposite to the ionization chamber at different dwell times (see figure 6). The measurements are repeated for four afterloaders.

The y-axis cut-off of these curves determines the transit dose delivered, which is expected to vary linearly with source strength. The axis cut-off is converted into dose units and is plotted as a function of the source strength in figure 7. The measurements were performed on two HDR and two PDR afterloaders. Since the transit dose linearly depends on the source strength, and because the source transport velocity on identical machines is comparable, its value for identical machines in different institutions was calculated from the value measured on the four afterloaders. For non-Nucletron machines, the transit dose was determined on each individual machine using the described method.

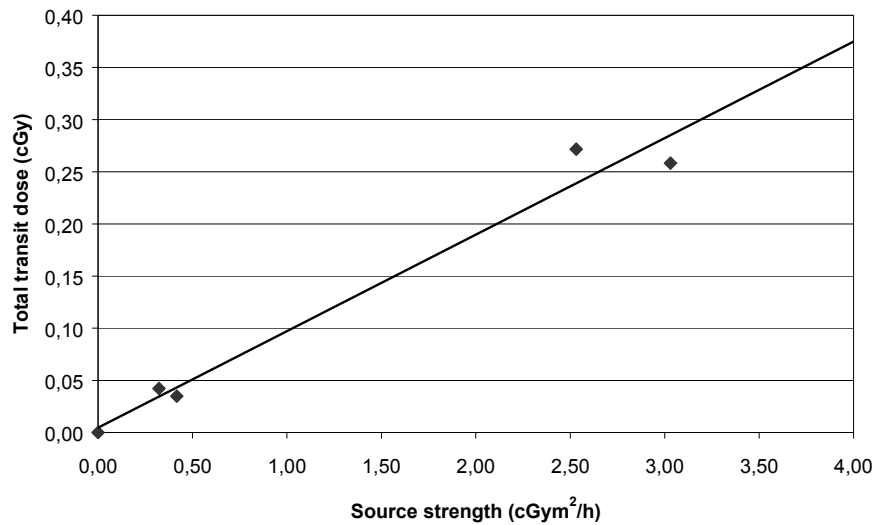


**Figure 7:** Results of measurements of the transit dose for the experimental setup in different institutions as a function of the source strength for microSelectron HDR and PDR afterloaders.

As can be seen from this figure, the transit dose amounts for this specific experimental set-up (i.e. measurements in the solid phantom with the source positioned at 5.0 cm from the applicators and a dwell time range of 0-120 s on Nucletron afterloaders) were approximately 0.4 cGy for a 4 cGym<sup>2</sup>/h HDR source and 0.04 cGy for a 0.4 cGym<sup>2</sup>/h PDR source. Relative to the prescribed dose of 75 cGy for HDR and 40 cGy for PDR afterloaders, the maximum contribution of the transit dose to the measured dose is 0.5% for HDR and 0.1% for PDR afterloaders. For LDR afterloaders the relative contribution of the transit dose to the prescribed dose has not been determined, but will be lower than for the PDR afterloaders because of the longer measuring times. The measured doses on HDR afterloaders were corrected according to figure 7. For PDR and LDR afterloaders, the effect of the transit dose was neglected.

#### 9.4.2.2 Dose measurements

Dose measurements were performed on 21 HDR afterloaders, 12 PDR afterloaders and 15 LDR afterloaders. The results of the dose measurements are summarized in figure 8. In the histogram, the percentage difference is shown between the measured

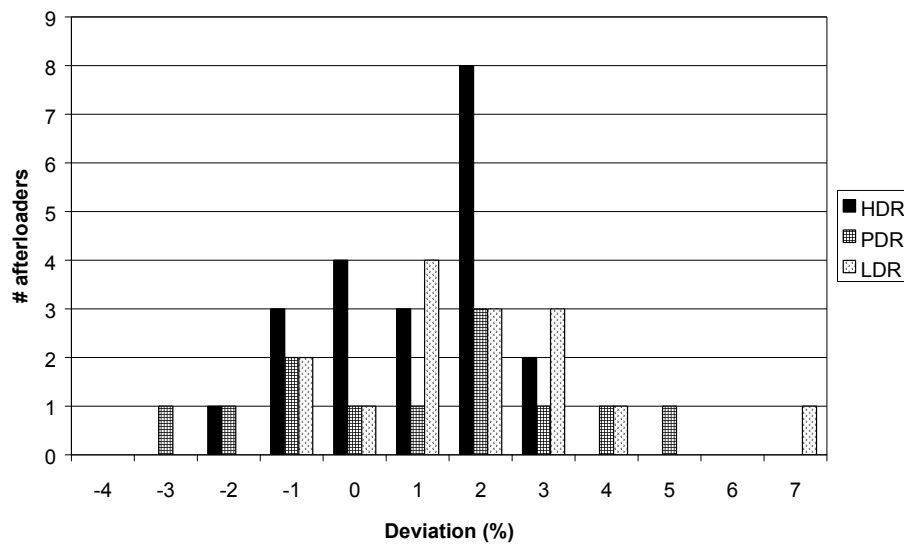


**Figure 8:** Results of dose delivery measurements on 21 HDR, 12 PDR and 15 LDR afterloaders in The Netherlands and Belgium: percentage difference between the measured dose in the phantom and the prescribed dose in the planning system. The average deviation is +0.9% for HDR, +1.0% for PDR and +1.8% for LDR afterloaders. All results were within a range of -3.3% to +6.8%.

dose and the prescribed dose. For the 21 HDR afterloaders, an average deviation of +0.9% ( $\pm 1.3\%$ , 1 SD) was measured, with two afterloaders having a deviation of more than 2%. For the 12 PDR afterloaders, the average deviation was +1.0% ( $\pm 2.3\%$ , 1 SD) with five afterloaders having a deviation of more than 2%. For measurements on 15 Selectron LDR afterloaders, an average deviation of +1.8% ( $\pm 2.5\%$ , 1 SD) was found, with five afterloaders having a deviation of more than 2% and a range of -3.3% to +6.8%.

#### 9.4.3 Source positioning accuracy

The accuracy of the source positioning was measured for HDR and PDR afterloaders by the method described. The average error on source positioning was measured on 16 HDR afterloaders and was found to be 0.2 mm ( $\pm 1.0$  mm, 1 SD). In three institutions, a deviation larger than 1 mm was observed, with a maximum deviation of 2.3 mm. For 11 PDR afterloaders, the average error in source positioning was 0.2

mm ( $\pm 1.1$  mm, 1 SD), with four institutions having deviations larger than 1 mm, and a maximum deviation of 2.0 mm.

## 9.5 Discussion

### 9.5.1 Reconstruction measurements

The results of the reconstruction measurements (figure 5) reflect the geometrical accuracy of the localizer, the digitizer and the reconstruction algorithm. For two C-arms, an average deviation of larger than 1 mm was observed. The reason for this deviation can be found when plotting the deviation of each reconstructed distance for this C-arm as a function of the reconstructed distance (figure 9). For comparison, a similar graph is shown for a simulator with a very small average deviation.

As can be seen from figure 9, the deviation of the reconstructed distance increases with the distance between the spheres for the C-arm, whereas for the simulator there is no correlation between deviation and distance. This shows that the deviation for the C-arm is most likely caused by an incorrect magnification factor of the localizer.

In a comparison of computer planning systems performed in 1987, Visser [24] found deviations of up to 5 mm when reconstructing gynaecological applicators from orthogonal radiographs, leading to discrepancies of 10% in the dose rate. Kolkman-Deurloo et al. [9] found an average reconstruction error of 0.04 mm for a dedicated brachytherapy localizer using a similar phantom and orthogonal reconstruction. This value increased to 0.4 mm when reconstructing from fluoroscopy images instead of using film. It was found that these deviations did not influence the treatment time when considering clinical implant geometries.

The results in the present work indicate that the reconstruction accuracy errors in The Netherlands and Belgium are comparable to those found by Kolkman-Deurloo et al. [9] and that these errors will have only a minor effect on the overall treatment time. The reconstruction accuracy has improved enormously since the 1987 investigation of Visser [24]. Based on the results of these measurements, the task group recommends an annual check of the reconstruction accuracy by reconstruction of a phantom with a well-known geometry. It is emphasized that the reconstruction error measured in this work represents the physical error in an ideal situation. In practice, the error can be larger due to, for example, patient movement.



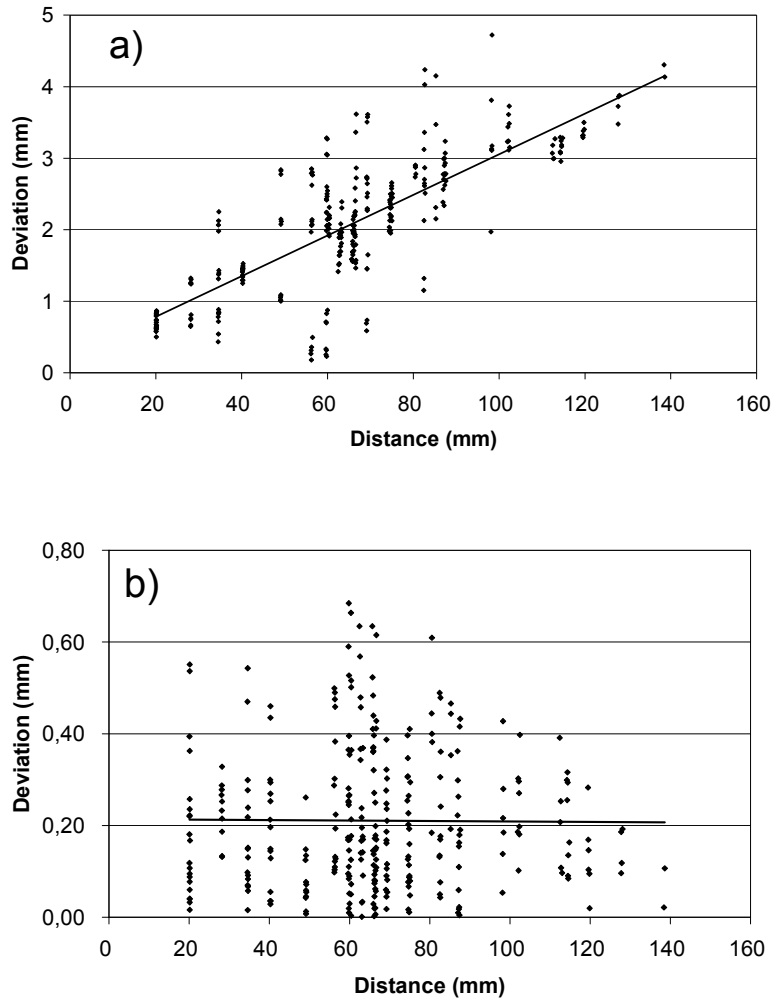


**Figure 9:** Absolute value of the reconstruction deviation as a function of the reconstructed distance for a C-arm with an average deviation of 2.09 mm (a) and a simulator with an average deviation of 0.03 mm (b). The line shows that the deviation increases with reconstructed distance for the C-arm, while this is not the case for the simulator.

#### 9.5.2 Dose measurements

The difference between the measured dose and the prescribed dose is the result of the sum of errors in source calibration, dose calculation of the TPS, source positioning and irradiation timer.

Clearly, source activity is one of the most important physical parameters in brachytherapy dose delivery. In a comparison of source calibration procedures for  $^{192}\text{Ir}$  HDR sources in The Netherlands and Belgium performed in 1992, Venselaar et al. [23] found deviations from the certificate's value of up to 6.8%. Baltas et al. [2] reported deviations from the certificate in the range of  $-13.0\%$  to  $+6.0\%$  for  $^{192}\text{Ir}$  HDR sources. In a recent comparison of calibration procedures for  $^{192}\text{Ir}$  HDR sources in Brazil, De Almeida et al. [1] found deviations in the range of  $-4.6\%$  to  $+2.4\%$ .

For  $^{137}\text{Cs}$  LDR sources, Meertens [10] found deviations from the source strength certificate in the range of  $-2.3\%$  to  $+3.9\%$  in nine institutions.

It is recommended by the NCS that the user of  $^{192}\text{Ir}$  afterloading equipment performs his own calibration for each new source [14]. In the current investigation, it was found that the strength of each  $^{192}\text{Ir}$  HDR-source is independently determined in 20 out of 21 institutions using HDR and in all institutions using PDR, mostly using the in-air method with a calibration jig. In one institution, the calibration of the source is not yet performed, but is planned for the near future. The current practice of in-house source calibration in The Netherlands and Belgium was investigated by means of a questionnaire on the QA of brachytherapy and is summarized in table 3.

Apart from source calibration, the dose calculation by the TPS is expected to be a significant cause of deviations in the measured dose. For example, Feroldi et al. [6] showed in a comparison of TPSs that dose rate errors larger than 5% may occur. To

**Table 3:** Source calibration practice of HDR, PDR and LDR brachytherapy in The Netherlands and Belgium. The number of institutions performing an in-house calibration method as well as the type of calibration method are listed. Furthermore, it is listed whether the in-house measured source activity value or the value from the certificate is used in the TPS. The different methods available for in-house calibration of brachytherapy sources are described in [10,13,14].

	In-house calibration method				Value in TPS	
	In-air	In-phantom	Well chamber	No calibration	In-house measured	Certificate
HDR	15	2	3	1	14	7
PDR	11	1	-	-	8	4
Cs-LDR	2	7	4	2	5	10

investigate the effect of the different TPSs on the total treatment time, the treatment time as calculated by the TPS in each institution for the specific experimental setup and prescribed dose was normalized to a fixed source strength. The treatment time calculated by the TPS of an institution is then compared with the average normalized treatment time of all institutions. For HDR and PDR brachytherapy the normalized treatment times for the different TPSs varied between  $-0.7\%$  and  $+1.3\%$  around the average calculated treatment time. For TPSs in use for Selectron LDR brachytherapy, the effect of the TPS on the measured dose was larger: the calculated treatment times ranged from  $-2.9\%$  to  $+3.7\%$  around the average time. The effect of applicator attenuation is ignored in most TPSs. The use of needles instead of plastic catheters results in an attenuation of approximately  $0.9\%$ . The effect of the TPS on the measured dose is thus found to be small ( $<2\%$ ) for TPSs in use for HDR and PDR brachytherapy and larger (up to  $4\%$ ) for TPSs in use for LDR brachytherapy.

In our study, for one PDR afterloader, a deviation in dose of  $+5.0\%$  was measured. The reason for this deviation was found to be an error in source positioning within the calibration jig. After repair of the jig, the deviation was reduced to  $+2.4\%$ . For one Cs LDR afterloader, a deviation in dose of  $+6.8\%$  was measured. Repeating the dose measurement several weeks later confirmed the initial measurement. The reason for the deviation is most probably an error in the source strength value as specified on the certificate of the manufacturer. This was never checked independently and was used in the TPS.

It should be emphasized that the measured values represent the physical accuracy of the treatment. In practice, one should keep in mind that these ideal conditions are not always fulfilled due to, for example, patient movement and the lack of full scatter conditions. Therefore, the accuracy of the dose delivered to a patient will be lower.

### *9.5.3 Source positioning accuracy*

Because of the high dose gradient near brachytherapy sources, accurate source positioning is required to obtain accurate dose delivery. In international reports, tolerance levels of  $1\text{ mm}$  [12,25] or  $2\text{ mm}$  [7,17] are recommended. The results of source positioning measurements on 16 HDR and 11 PDR afterloaders showed that seven institutions had a deviation in source positioning larger than  $1\text{ mm}$ . Three of these exceeded the recommended tolerance level of  $2\text{ mm}$ .

#### 9.5.4 Uncertainties

Uncertainties are distinguished as random (type A) and systematic (type B) uncertainties. Type A uncertainties are caused by small deviations in the readings of the electrometer, in the reading of the air pressure and temperature and statistical deviations in the distance between the source and ionization chamber. Since the inner diameter of the (Nucletron) catheters is 1.8 mm and the outer diameter of the  $^{192}\text{Ir}$  source is 1.1 mm, there is always an uncertainty in the position of the source within the applicator in the radial direction, with a maximum margin of 0.35 mm. At a 5.0 cm distance from the ionization chamber, this can result in an error of  $\pm 1.4\%$  in the measured dose, when using a single catheter. In practice, differences as large as 1.4% were observed when comparing the readings from the three different channels of the phantom. However, the reproducibility of the electrometer reading from all three channels was found to be better than 0.3%, so the overall effect of the radial source positioning error on the electrometer reading is small. The random error in the reading of the barometer and thermometer is estimated to be 0.2%.

Type B uncertainties are determined by the uncertainties in the physical quantities as given in equation 1 and table 1. The largest contribution is expected from the uncertainty of the  $N_k$  value (0.7%) and from the uncertainty in the replacement factor

**Table 4:** Estimated uncertainties, expressed as one standard deviation, resulting from type A (statistical) and type B (systematical) uncertainties for the dose measurements in the cylindrical phantom. For an explanation of the parameters, see table 2.

Parameter	Uncertainty Type A (%)	Parameter	Uncertainty Type B (%)
$M_{\text{uncorr}}$	0.3	$N_k$	0.7
$p_{\text{meas}}$	0.2	$p_r$	1.0
$T_{\text{meas}}$	0.2	$f_{\text{ph}}$	0.3
		$(\mu/\rho)_{\text{air}}^{\text{water}}$	0.3
		$P_{\text{hum}}, p_{\text{ion}}, p_{\text{pol}}, p_{\text{ce}}, k_{\text{st}}, k_{\text{ce}}$	< 0.1
		$f_{\text{cath}}$	0.3
		$f_{\text{tr}}$	0.3

$p_r$  (1.0%, see [22]). The uncertainties in the other parameters are shown in table 4. The estimated combined uncertainty resulting from type A and type B uncertainties for the dose measurements is 1.5%.

## 9.6 Conclusions

The accuracy of the reconstruction method and the dose delivery in HDR, PDR and LDR brachytherapy was determined in 33 institutions in The Netherlands and Belgium.

The accuracy of the reconstruction method was determined using a cubic PMMA phantom containing 25 spheres at well-known positions. The reconstruction accuracy was found to be smaller than 0.5 mm for 36 of 41 localizers. For two localizers, a deviation larger than 1.0 mm was observed, which is most probably caused by an error in the magnification factor applied in the TPS.

The dose delivery accuracy was measured using a cylindrical PMMA phantom containing an NE 2571 ionization chamber and three applicators at 5.0 cm from the ionization chamber. The accuracy of the dose delivery was found to be +0.9% ( $\pm 1.3\%$ , 1 SD) for 21 HDR afterloaders, +1.0% ( $\pm 2.3\%$ , 1 SD) for 12 PDR afterloaders and +1.8% ( $\pm 2.5\%$ , 1 SD) for 15 Selectron LDR afterloaders. For one PDR afterloader, a deviation in dose of +5.0% was measured. The cause for this deviation was a problem with source positioning within the calibration jig. For one Cs LDR afterloader, a deviation in dose of +6.8% was measured. The cause for the deviation is most probably an error in the source strength value on the certificate of the manufacturer.

The results of the measurements showed that an accuracy of physical dose delivery better than 5% was achieved in all but one institution.

## 9.7 References

1. Almeida de CE, Pereira AJ, Marechal MH, et al. Intercomparison of calibration procedures for  $^{192}\text{Ir}$  HDR sources in Brazil. *Phys Med Biol* 1999;44:N31-N38.
2. Baltas D, Geramani K, Ioannidis GT, et al. Comparison of calibration procedures for  $^{192}\text{Ir}$  HDR brachytherapy sources. *Int J Radiat Oncol Biol Phys* 1999;43:653-661.

3. Baltas D. Quality assurance in brachytherapy with special reference to the microSelectron-HDR. Activity (International Selectron Brachytherapy Journal) Special Report No. 2, 1993.
4. DIN (Deutsches Institut für Normung). Klinische Dosimetrie, Brachytherapie mit umschlossenen gammastrahlenden radioaktiven Stoffen, 2. Berlin: Beuth, 1993. p.6809.
5. DIN (Deutsches Institut für Normung). Medizinische ferngesteuerte, automatisch betriebene Afterloading-Anlagen, Konstanzprüfung apparativer Qualitätsmerkmale, 5. Berlin: Beuth, 1992. p.6853.
6. Feroldi P, Galelli M, and Belletti S. A comparison of accuracy of computer treatment planning systems in brachytherapy. *Radiother Oncol* 1992;24:147-154.
7. IEC (International Electrotechnical Commission). Medical electrical equipment, Part 2: particular requirements for the safety of remote-controlled automatically-driven gamma-ray afterloading equipment. Report 601-2-17, 1989.
8. IEC (International Electrotechnical Commission). Medical electrical equipment, Part 2: particular requirements for the safety of remote-controlled automatically-driven gamma-ray afterloading equipment. Report 601-2-17, 1996.
9. Kolkman-Deurloo IKK, Visser AG, Idzes MHM, Levendag PC. Reconstruction accuracy of a dedicated localiser for filmless planning in intra-operative brachytherapy. *Radiother Oncol* 1997;44:73-81.
10. Meertens H. In-phantom calibration of Selectron-LDR sources. *Radiother Oncol* 1990;17:369-378.
11. Nath R, Anderson LL, Luxton G, Weaver KA, Williamson JF, Meigooni AS. Dosimetry of interstitial brachytherapy sources: Recommendations of the AAPM Radiation Therapy Committee Task Group No. 43. *Med Phys* 1995;22:209-234.
12. Nath R, Anderson LL, Meli JA, Olch AJ, Stitt JA, Williamson JF. Code of practice for brachytherapy physics: Report of the AAPM Radiation Therapy Committee Task Group No. 56. *Med Phys* 1997;24:1557-1598.
13. NCS (Netherlands Commission on Radiation Dosimetry). Recommendations for dosimetry and quality control of radioactive sources used in brachytherapy. Synopsis (in English). Report 4, 1991.
14. NCS (Netherlands Commission on Radiation Dosimetry). Recommendations for the calibration of Iridium-192 high dose rate sources. Report 7, 1994.
15. NCS (Netherlands Commission on Radiation Dosimetry). Quality Control of Medical Linear Accelerators. Report 9, 1996.
16. NCS (Netherlands Commission on Radiation Dosimetry). Quality Control (QC) of Simulators and CT scanners and some basic QC methods for Treatment Planning Systems. Report 11, 1997.
17. NCS (Netherlands Commission on Radiation Dosimetry). Quality Control in Brachytherapy. Report 13, 2000.

18. Piermattei A, Azario L. Applications of the Italian protocol for the calibration of brachytherapy sources. *Phys Med Biol* 1997;42:1661-1669.
19. Reynaert N, Verhaegen F, Thierens H. In-water calibration of PDR  $^{192}\text{Ir}$  brachytherapy sources with an NE2571 ionization chamber. *Phys Med Biol* 1998;43:2095-2107.
20. Schaeken B, Vanneste F, Bouiller A, et al.  $^{192}\text{Ir}$  brachytherapy sources in Belgian hospitals. *Nucl Instr Meth Phys Res* 1992;A312:251-256.
21. SFPH (Société Française des Physiciens d'Hôpital). Contrôle de qualité en Curiethérapie par Iridium 192 à haut débit de dose. Rapport No. 11, 1995.
22. Steggerda MJ, Mijnheer BJ. Replacement corrections of a Farmer-type ionization chamber for the calibration of Cs-137 and Ir-192 sources in a solid phantom. *Radiother Oncol* 1994;31:76-84.
23. Venselaar JLM, Brouwer WFM, van Straaten BHM, Aalbers, AHL. Intercomparison of calibration procedures for Ir-192 HDR sources in The Netherlands and Belgium. *Radiother Oncol* 1994;30:155-161.
24. Visser AG. An intercomparison of the accuracy of computer planning systems for brachytherapy. *Radiother Oncol* 1989;15:245-258.
25. Williamson JF, Ezzell GA, Olch AJ, Thomadsen BR. Quality assurance for high dose rate brachytherapy. In: Nag S, editor. *High Dose Rate Brachytherapy: a textbook*, Armonk, NY: Futura, 1994. p.147-212.





## **CHAPTER 10. QUALITY CONTROL OF BRACHYTHERAPY EQUIPMENT IN THE NETHERLANDS AND BELGIUM: CURRENT PRACTICE AND MINIMUM REQUIREMENTS**

RJM Elfrink, IKK Kolkman-Deurloo, HJ van Kleffens, A Rijnders, B Schaeken, AHL Aalbers, WJF Dries, JLM Venselaar

Radiother Oncol 2002; 62; 95-102.

### **10.1 Abstract**

*Background and Purpose:* Brachytherapy is applied in 39 radiotherapy institutions in The Netherlands and Belgium. Each institution has its own quality control (QC) programme to ensure safe and accurate dose delivery to the patient. The main goal of this work is to gain insight into the current practice of QC of brachytherapy in The Netherlands and Belgium and to reduce possible variations in test frequencies and tolerances by formulating a set of minimum QC-requirements.

*Materials and Methods:* An extensive questionnaire about QC of brachytherapy was distributed to and completed by the 39 radiotherapy institutions. A separate smaller questionnaire was sent to nine institutions performing intracoronary brachytherapy. The questions were related to safety systems, physical irradiation parameters and total time spent on QC. The results of the questionnaires were compared with recommendations given in international brachytherapy QC reports.

*Results:* The answers to the questionnaires showed large variations in test frequencies and test methods. Furthermore, large variations in time spent on QC exist, which is mainly due to differences in QC philosophy and differences in the available resources.

*Conclusions:* Based on the results of the questionnaires and the comparison with the international recommendations, a set of minimum requirements for QC of brachytherapy has been formulated. These guidelines will be implemented in the radiotherapy institutions in The Netherlands and Belgium.

## 10.2 Introduction

Brachytherapy is a form of radiation therapy which is mainly used for the treatment of malignant tumours which are accessible for sealed sources. In The Netherlands and Belgium, approximately 3500 patients in 39 radiotherapy institutions are treated annually using High Dose Rate (HDR), Pulsed Dose Rate (PDR) or Low Dose Rate (LDR) remote afterloading brachytherapy.

The accuracy of a brachytherapy dose delivery depends on many physical parameters. In practice, an accuracy of 5-10% in radiation dose delivered to the patient is thought to be achievable [20]. To ensure safe and accurate application of the treatment and to prevent accidental overexposures, a QC programme has to be developed. The goal of the QC programme is to maximize the likelihood that each individual treatment accurately realizes the radiation oncologist's clinical intent and that it is executed with regard to maximum safety of the patient and others who may be exposed to the source during the treatment. In The Netherlands and Belgium, each institution has developed its own QC programme for brachytherapy, following the many guidelines published on this subject [2,4,5,8,10-14,18-23,27,30]. In principle, QC programmes should not vary significantly between different institutions.

Recently, a taskgroup of the Netherlands Commission on Radiation Dosimetry (NCS) studied the QC programmes of medical linear accelerators and other equipment applied in radiotherapy institutions, such as simulators, Computed Tomography (CT) scanners and treatment planning systems (TPSs) [15,24,25]. The investigation of the current QC practice showed that for this equipment large variations in test frequencies, test methods and overall time spent on QC existed, mainly due to differences in philosophy with regard to QC and differences in resources available, such as manpower and QC-equipment. To achieve more consistency among the different QC programmes in the institutions, a set of minimum QC-requirements in the form of two NCS-reports was established, suitable for the situation in The Netherlands and Belgium [24,25].

Until now, no such national guidelines exist for the QC of brachytherapy. A taskgroup on QC of brachytherapy systems of the NCS has been installed with the purpose to gain insight into the current practice of QC of brachytherapy in The Netherlands and Belgium and to reduce variations by formulating a set of minimum QC-requirements, in a similar way as was done before for medical accelerators and simulators and CT-scanners. In addition, the accuracy of implant reconstruction and dose delivery was determined by performing on-site measurements with two

dedicated phantoms in the institutions. The results of these measurements are published elsewhere [6].

In this paper, the current practice of QC of HDR, PDR, LDR and coronary brachytherapy, the comparison of the current QC-practice with international recommendations, and the established set of minimum requirements for QC of brachytherapy will be discussed.

### 10.3 Materials and methods

To gain insight into the current QC-practice, an extensive questionnaire on QC of brachytherapy systems was sent to all 39 radiotherapy institutions in The Netherlands and Belgium. The questionnaire is summarized in table 1. The questions concerned test frequencies, test methods, time required for the tests, action levels of safety systems and irradiation parameters in brachytherapy. In addition, information about the number of patients treated and the brachytherapy equipment (afterloaders, localizers and TPSs) was requested.

Several international reports were studied with respect to the published recommendations on the QC of brachytherapy equipment [2,4,5,8,10-14,18-23,27,30]. The data gathered from the responses to the questionnaire were compared with these recommendations. It was felt necessary to apply a comparable approach to the recently emerged field of intracoronary brachytherapy, mainly because already a large number of approximately 700 patients have been treated in The Netherlands and Belgium and because, apart from a report of the American Association of Physicists in Medicine (AAPM) [21], almost no recommendations have been published until now. Therefore, a small questionnaire consisting of ten questions on installed systems, patient numbers and QC has been sent to all nine centers known to be applying intracoronary brachytherapy (November 1999). Vascular brachytherapy in peripheral arteries is excluded from this small questionnaire because it is always performed with  $^{192}\text{Ir}$  sources in HDR equipment, which is already included in the large questionnaire. From this information, a set of minimum requirements on QC, suitable for the situation in The Netherlands and Belgium, was formulated and published as an NCS-report [26].

**Table 1:** Overview of the questionnaire on QC of brachytherapy which was distributed to all radiotherapy institutions.

Subject	Question
Brachytherapy activities	Which procedure(s) + annual # patients per procedure?
Equipment	
Afterloaders	Which brachytherapy-techniques and -systems in use?
Localization	Which reconstruction systems in use?
Treatment Planning System	Type + version of TPS used?
QC-equipment	Service-contract with manufacturer (Yes/No)?
Afterloaders	
Localization	
Treatment Planning System	
Safety equipment near afterloader	Available (Yes/No)?
Lead screen	
Portable survey meter	
Source handling tools	
Shielded storage container	
Forceps	
Emergency instructions	
Operator's manual	
QC of safety systems	Test Frequency?
Warning lights	Who performs test?
Emergency stop push buttons	Written instruction available?
Interrupt	Time required for test?
Door interlock	
Power loss	
Air pressure loss	
Room radiation monitor	
Emergency procedure	
QC of irradiation parameters	Test frequency, test method, tolerance level?
Irradiation timer	Who performs test?
Source positioning	Written instruction available?
Step size	Time required for test?
Detection of obstructions	
QC of localization procedure	Test frequency, test method, tolerance level?
Implant reconstruction accuracy	Who performs test?
	Written instruction available?
	Time required for test?
QC of sources	Calibration frequency, calibration method, tolerance with source strength certificate, which value in TPS?
Source calibration	Written instruction available?
	Time required for test?
Radiation safety	Test frequency, test method?
Contamination	Who performs test?
Radiation level outside afterloader	Written instruction available?
	Time required for test?

## 10.4 Results

The questionnaire was completed by 37 institutions. The results are presented as test frequency histograms. The following abbreviations are used: HDR for High Dose Rate remote afterloading using  $^{192}\text{Ir}$  sources, PDR for Pulsed Dose Rate remote afterloading using  $^{192}\text{Ir}$  sources, S-LDR for Low Dose Rate remote afterloading with  $^{137}\text{Cs}$  pellets and m-LDR for Low Dose Rate remote afterloading with  $^{192}\text{Ir}$  wires/ribbons or  $^{137}\text{Cs}$  ribbons. In this nomenclature, S-LDR refers to Selectron-LDR, and m-LDR to microSelectron LDR afterloading machines (Nucletron B.V., The Netherlands), which are the most common, although not exclusively used LDR afterloaders in this survey. The abbreviations used for the test frequencies are : P for each patient, D for daily, W for weekly, M for monthly (3M=once every three months), A for annually, SE for each source exchange and Inc for incidentally.

### 10.4.1 Brachytherapy in The Netherlands and Belgium

In 1996, approximately 3500 patients were treated using brachytherapy in The Netherlands and Belgium. The brachytherapy techniques applied in the institutions are summarized in table 2.

**Table 2:** Brachytherapy techniques applied in The Netherlands and Belgium.

Brachytherapy techniques	# Institutions in The Netherlands	# Institutions in Belgium
HDR ( $^{192}\text{Ir}$ )	13	8
PDR ( $^{192}\text{Ir}$ )	6	8
S-LDR ( $^{137}\text{Cs}$ -pellets)	10	9
m-LDR ( $^{192}\text{Ir}$ / $^{137}\text{Cs}$ wires/ribbons)	10	3
Manual ( $^{192}\text{Ir}$ )	12	12
Manual ( $^{137}\text{Cs}$ )	2	3
Manual ( $^{125}\text{I}$ )	3	4
Eye applicator ( $^{90}\text{Sr}$ )	8	2
Eye applicator ( $^{106}\text{Ru}$ )	1	1

### 10.4.2 Time spent on QC activities

The institutions were asked how much time they spend annually on QC activities related to brachytherapy. Figure 1 shows the time spent each year on QC for the different types of remote afterloading equipment in The Netherlands. The average time spent is approximately 8 h for HDR, 14 h for PDR, 6 h for m-LDR and 4 h for S-LDR afterloaders. Most values reported are rough estimates, because it is sometimes hard to distinguish between time spent on preventive maintenance and time spent on QC. Nevertheless, the differences in QC times between the different machines are striking, as well as the inter-institutional differences.

### 10.4.3 QC tests on safety systems

In general, the safety aspects of remote afterloading machines can be subdivided into interlocks, radiation safety and emergency aspects. QC tests on these safety systems should prevent system failure and assure radiation safety for patient and personnel. Often, QC-procedures on safety systems are simple functional tests.

From the inter-institutional survey, it was found that a large variation in test frequency exists. To illustrate this, the test frequency for the emergency stop pushbutton is shown in figure 2. As can be seen from this figure, the test frequency varied

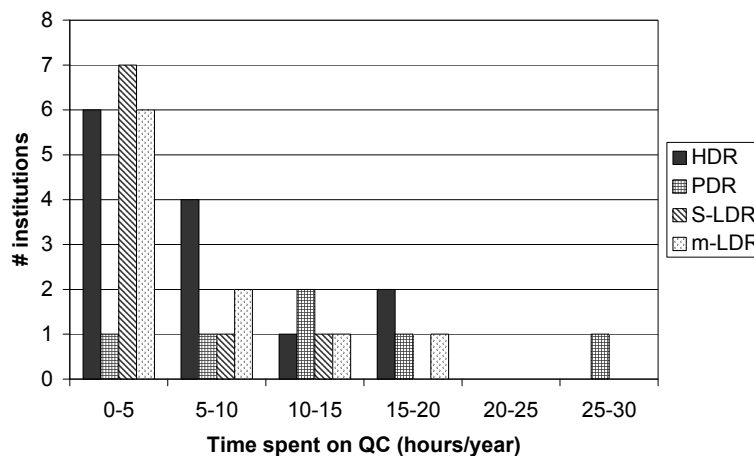


**Figure 1:** Distribution of time spent annually on QC of brachytherapy in The Netherlands.

between each patient and annually. Similar distributions were found for the test of the door interlock, the interrupt button, power loss and the radiation warning lights. Tests on radiation safety, such as radiation level outside the afterloader and a contamination test, are performed regularly in approximately half of the institutions.

Although the likelihood of major emergencies, for example source detachment during treatment, is very low, the dose delivered to patients and staff can be very high. During an emergency, the goal is to keep the dose to patient and personnel as low as possible. Clearly, time is the most important factor in case of an emergency. Therefore, safety equipment should be available during treatments and the emergency procedure should be practised regularly. The QC-inventory showed that the emergency procedure is practised regularly in approximately half of the institutions.

The questionnaire covered many aspects regarding safety systems. A complete description of the results can be found in [26]. A summary of the current median test frequency of the most relevant parameters is given in table 3.

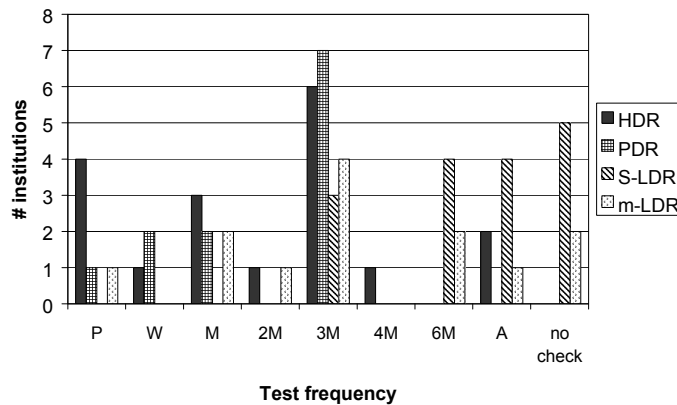


**Figure 2:** Frequency distribution of the test of the emergency stop pushbuttons

**Table 3:** Summary of current QC practice on safety systems and physical parameters in The Netherlands and Belgium. Median test frequencies ( $f_{50\%}$ ) of safety systems are shown for HDR, PDR and LDR brachytherapy. An 'X' in the  $f_{50\%}$  column means that at least 50% of the institutions do not perform this test as part of the QC-programme.

Description	Current median test frequencies ( $f_{50\%}$ )		
	HDR/PDR	S-LDR	m-LDR
<i>Safety systems</i>			
Warning lights	3M	6M	2M
Room monitor	W	3M	P
Emergency pushbuttons	3M	A	3M
Interrupt	3M	6M	3M
Door interlock	3M	6M	3M
Power loss	3M	6M	3M
Air pressure loss	-	6M	6M
Leakage radiation	3M	X	X
Contamination test	4M	X	A
Practising emergency procedure	A	X	X
<i>Physical parameters</i>			
Source calibration	3M	SE	SE
Source position	3M	X	P
Irradiation timer	3M	X	X
Treatment verification	P	P	P

#### 10.4.4 QC tests on physical parameters

The accuracy of a brachytherapy treatment depends on the accuracy of several physical parameters, such as source activity, source position, irradiation time, implant reconstruction and dose calculation algorithm of the TPS.

Because of radioactive decay,  $^{192}\text{Ir}$  HDR and PDR sources are replaced approximately every 3 months. The manufacturer of the sources provides a source strength certificate to indicate the strength of the source delivered to the institution. Recently, several authors compared the source strength of  $^{192}\text{Ir}$  HDR sources provided by the manufacturer with their own measured source strength [1,3,6,28]. Because of the



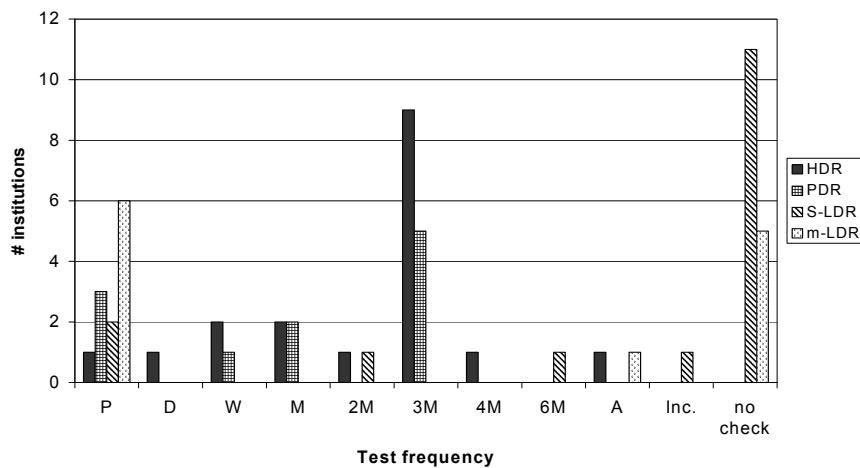


**Figure 3:** Frequency distribution of the test of the source position.

relatively large deviations, the in-house calibration of  $^{192}\text{Ir}$  sources was strongly recommended in those papers. The current source calibration practice in The Netherlands and Belgium is that except for one HDR and two S-LDR afterloaders, in-house calibration of the source(s) is performed in all institutions. In two-third of the institutions applying HDR or PDR brachytherapy, the in-house measured value for the source strength is used in the TPS. For LDR afterloaders, the value on the certificate is used in the TPS in most cases.

Source positioning is another important physical parameter that determines the accuracy of the dose delivered to the patient. Source positioning is usually checked by means of a check ruler or by autoradiography. Figure 3 shows the current test frequencies for QC on source position. As can be seen, the test frequency varies from a test performed during each patient treatment to a test performed only incidentally. The accuracy of source positioning is not checked on a regular basis for more than half of the LDR afterloaders. However, in some afterloaders, the source position is already implicitly checked by the machine. For example, in m-LDR afterloaders, the position of the source-transport cable is checked.

Verification of the temporal accuracy consists of independently measuring the time the source remains at the specified dwell position and comparing this interval with the programmed time setting. Such an independent check of the timer is performed in approximately half of the institutions.

To calculate a dose distribution around radioactive sources, the coordinates of the sources must be determined relative to an arbitrary reference point. The accuracy of the 3D-reconstruction of the implant depends on the accuracy of localization, digitization and the reconstruction algorithm. The results of the questionnaire showed that the accuracy of the reconstruction method by phantom measurements is performed on a regular basis in only four out of 39 institutions. It should, however, be noticed that the reconstruction accuracy is already implicitly checked in some cases, e.g. when using a reconstruction box or when the reconstruction algorithm already implicitly checks the accuracy of the distance between the markers.

Treatment verification concerns the checking of the treatment plan prior to starting the treatment, verification of the delivered dose during the treatment and verification of correct treatment completion after the treatment. It is good clinical practice to evaluate the accuracy of a brachytherapy treatment before treatment commences. To verify that the treatment plan does not contain large errors, a check of the calculated treatment time by an independent method can be performed. However, due to the complexity of the implants and due to source decay, it is often difficult to judge the reliability of a treatment time calculation based on experience. Methods have been proposed for independent verification of the total treatment time for, respectively, one- or two-catheter HDR-procedures [16], planar implants [7,17] or volume implants [29]. We investigated the use of such independent treatment checks in the institutions and found that these are performed in approximately half of the institutions.

Verification of the actual dose delivered during treatment of a patient is difficult. In vivo measurements using thermo luminescence dosimeters (TLD's) or rectal diodes are performed in only four out of 39 institutions. All other institutions check the information on the printout of the treatment console after completion of the treatment. Furthermore, the date, time and source strength in the treatment unit and planning computer are checked before each treatment in most institutions. A summary of the current median test frequencies of the most relevant physical parameters is presented in table 3.

#### *10.4.5 Intracoronary Brachytherapy using beta sources*

Eight out of nine institutions responded to the questionnaire on intracoronary brachytherapy with beta sources. Six different systems were in clinical use, all of

them in manufacturer-sponsored trials (Novoste, Guidant, Boston Scientific, Radiance, Isostent, Mallinckrodt). Therefore, the reported QC measures mainly reflect the trial protocol and not the viewpoint of the institution. However, these viewpoints were taken into consideration for formulating the recommendations.

Six responding institutions performed consistency checks of source strength of at least one of their systems after source exchange; two of these also did absolute measurements of dose rate at 2 mm from the source center, but all used the manufacturer specified dose rates. All participants agreed that due to uncertainties in absolute dose determination of beta-sources, an accuracy level of  $< 15\%$  cannot be achieved at present. Preliminary clinical data indicate that the therapeutical window is large enough to allow these tolerances.

Five institutions also checked source homogeneity with radiochromic film and mentioned that a maximum variation of  $\pm 10\%$  at 2 mm in water is probably difficult to achieve. All participants checked container leakage radiation after source exchange, source leakage after each treatment and catheter integrity before each treatment. Interlock checks and source positioning checks are only performed by some institutions. An emergency procedure (for cases of source retraction malfunction) is available and two institutions have trained this at least once.

The number of publications of QC in intracoronary brachytherapy is very limited [18,21]. The AAPM Task Group 60 [21] gives a list of recommended actions without tolerances and frequencies. Both publications emphasize the provisional character of the recommendations.

## 10.5 Discussion

A brachytherapy QC programme is a planned series of activities that should not vary significantly between different institutions. However, because of differences in guidelines, local conditions, e.g. due to differences in patient workload, and experience, considerable variation among QC programmes occurs. The large variations in time spent on QC per brachytherapy afterloader (figure 1) and variations in test frequency (e.g. figure 2) could not be correlated to the size of the institution. The diversity in protocols is probably mainly due to differences in QC-philosophy and the differences in available resources, including manpower.

**Table 4:** Recommended test frequencies and action levels for HDR-brachytherapy in international reports. The test frequencies and action levels are listed. An ‘-’ means that no recommendation for the test frequency or action level is given in the report.

Test parameter	AAPM [20]	SFPH [27]	IEC [10]	Williamson [30]	DIN [5]
Emergency pushbuttons	-	D	-	D	-
Door interlock	D	D	-	D	-
Power loss	3M	D	-	D	-
Source calibration	3M, $\pm 5\%$	SE, -	-	3M, $\pm 5\%$	3M, -
Source positional accuracy	D, $\pm 1\text{mm}$	M, -	-, $\pm 2\text{mm}$	D, $\pm 1\text{mm}$	M, -
Temporal accuracy	D, $\pm 2\%$	W	-, $\pm 1\%$	D, $\pm 1\%$	W, -

The data gathered from the responses of the questionnaire have been compared with international recommendations on QC [2,4,5,8,10-14,18-23,27,30]. Table 4 shows a few examples of recommended test frequencies and action levels found in the literature for HDR brachytherapy.

Comparing the current QC practice (table 3) with international recommendations (table 4) shows that the current test frequencies are generally lower than international recommendations. This can partly be explained by the fact that the questions in the questionnaire related only to formal checks, i.e. those of which the results are logged. Some checks will be performed more often, however, without logging the results.

It was decided by the task group to formulate the QC recommendations in the form of minimum requirements, which strictly refer to the routine QC tests, and of which execution and results should be documented. No suggestions are given on additional checks after major repair. The suggested test frequencies should therefore be regarded as a minimum and not as an optimum. To establish the minimum requirements for QC, it would be useful to have insight into the probability of a fault occurring, into the probability that if a malfunction occurs, this will not be detected during normal treatment applications, and into the seriousness of the possible consequences of an unnoticed fault. However, data on the probability for a fault to occur are hardly available, except a recent publication of the International Atomic Energy Agency (IAEA) in which accidental overexposures in radiotherapy [9] are described. The minimum requirements are therefore mainly based on experiences in daily practice. Often, in HDR and PDR brachytherapy, QC-checks are performed

during a source exchange. Since source exchange in The Netherlands and Belgium is often on a 3-monthly or 4-monthly basis, a minimum requirement for the test frequency of 4M is often recommended. For LDR brachytherapy, the recommended test frequencies are generally less frequent than for HDR brachytherapy, mainly because the consequences of an error in a safety system are generally less severe for LDR. Table 5 summarizes the minimum requirements for HDR, PDR, LDR and intracoronary brachytherapy.

The implementation of the formulated minimum requirements in the institutions will result in a number of adjustments of the currently applied QC programmes. To investigate the impact of the recommendations, the formulated recommendations have been compared with the current QC practice in each institution (as obtained from the questionnaire). It was found that in order to comply with the recommendation, adjustments of the QC practice (i.e., an increment in test frequency or the introduction of procedures not previously performed) are necessary in all 39 institutions. The average number of adjustments is four for all institutions applying HDR brachytherapy, three for all institutions applying PDR, seven for all institutions applying S-LDR and five for all institutions applying m-LDR brachytherapy. The required adjustments will often hardly increase the total time spent on QC.

We have no reason to believe that the situation observed in the institutions in The Netherlands and Belgium is much different from the situation in other countries, unless a national protocol is adopted. It is expected that variations in QC programmes will decrease as a result of the formulated minimum requirements. It might be useful to study the differences in QC among the various institutions in other countries. The method described in this paper, i.e. the distribution and analysis of an extensive questionnaire, can result in a critical revision of the QC protocols within a country.

## 10.6 Conclusions

QC programmes for brachytherapy were investigated in 39 radiotherapy institutions in The Netherlands and Belgium. The results show a large variation in the applied test frequencies. The frequency of tests on safety systems and physical parameters varies between a test performed each day to a test performed once in a year. The diversity could not be correlated to the size of an institution and is attributed to differences in philosophy with regard to QC, and to differences in available resources.

**Table 5:** Summary of QC-recommendations for HPR/PDR, S-LDR and m-LDR and intracoronary brachytherapy. An ‘-’ means the test or an action level is not applicable.

Description	Test frequency, action level			
	HDR/PDR	S-LDR	m-LDR	Intra-coronary
<i>Safety systems</i>				
Warning lights	4M	4M	4M	-
Room monitor	4M	4M	4M	-
Audio / visual communication system	4M	4M	4M	-
Emergency buttons	4M	6M	6M	-
Interrupt	4M	6M	6M	SE or 4M <sup>1</sup>
Door interlock	4M	6M	6M	-
Power loss	4M	6M	6M	SE or 4M <sup>1</sup>
Air pressure loss	-	6M	6M	-
Unlocked indexer ring	4M	-	-	-
Obstructed applicator	4M	6M	6M	P
Missing applicator	4M	6M	6M	SE or 4M <sup>1</sup>
Leakage radiation	SE	A	A	SE or 4M <sup>1</sup>
Contamination test	SE	A	A	P
Integrity of transfer tubes and applicators	6M	6M	6M	P
Emergency equipment	4M	6M	6M	4M
Emergency source retraction	A	-	-	SE or 4M <sup>1</sup>
Practising emergency procedure	A	A	A	A
<i>Physical parameters</i>				
Source calibration	SE, ± 5 %	SE, Mean ± 5 %	SE, Mean ± 10 %	SE (consistency only)
Source homogeneity	-	-	-	SE
Source position	4M, ± 2 mm	6M, ± 2 mm	P, ± 2 mm	SE
Source length	-	-	P, ± 2 mm	-
Irradiation timer	A, ± 1 %	A, ± 1 %	A, ± 1 %	A
Implant reconstruction	A, 95% < 2 mm	A, 95% < 2 mm	A, 95% < 2 mm	-
Treatment verification	P	P	P	-

<sup>1</sup> whichever is shorter.

The results of the questionnaire, together with international recommendations, were used to develop a set of minimum requirements, suitable for the situation in The Netherlands and Belgium. The recommendations contain approximately 20 test procedures, including test frequencies and action levels.

## 10.7 References

1. Almeida de CE, Pereira AJ, Marechal MH, et al. Intercomparison of calibration procedures for  $^{192}\text{Ir}$  HDR sources in Brazil. *Phys Med Biol* 1999;44:N31-N38.
2. Baltas D. Quality assurance in brachytherapy with special reference to the microSelectron-HDR. Activity (International Selectron Brachytherapy Journal) Special Report No. 2, 1993.
3. Baltas D, Geramani K, Ioannidis GT, et al. Comparison of calibration procedures for  $^{192}\text{Ir}$  HDR brachytherapy sources. *Int J Radiat Oncol Biol Phys* 1999;43:653-661.
4. DIN (Deutsches Institut für Normung). Klinische Dosimetrie, Brachytherapie mit umschlossenen gammastrahlenden radioaktiven Stoffen, 2. Berlin: Beuth, 1993. p. 6809.
5. DIN (Deutsches Institut für Normung). Medizinische ferngesteuerte, automatisch betriebene Afterloading-Anlagen, Konstanzprüfung apparativer Qualitätsmerkmale, 5. Berlin:Beuth, 1992. p. 6853.
6. Elfrink RJM, Kolkman-Deurloo IKK, van Kleffens HJ, et al. Determination of the accuracy of implant reconstruction and dose delivery in brachytherapy in The Netherlands and Belgium. *Radiother Oncol* 2001;59:297-306.
7. Ezzell GA. Quality assurance of treatment plans for optimized high dose rate brachytherapy-planar implants. *Med Phys* 1994;21:659-661.
8. Glasgow G, Bourland JD, Grigsby P, et al. Remote Afterloading Technology: A Report of AAPM Task Group No. 41. American Institute of Physics, New York, 1993.
9. IAEA (International Atomic Energy Agency). Lessons learned from accidental exposures in radiotherapy. Safety reports series No. 17, Vienna, 2000.
10. IEC (International Electrotechnical Commission). Medical electrical equipment, Part 2: particular requirements for the safety of remote-controlled automatically-driven gamma-ray afterloading equipment. Report 601-2-17, 1989.
11. IEC (International Electrotechnical Commission). Medical electrical equipment, Part 2: particular requirements for the safety of remote-controlled automatically-driven gamma-ray afterloading equipment. Report 601-2-17, Amendment 1, 1996.
12. IPEM (Institute of Physics and Engineering in Medicine). Physics aspects of quality control in radiotherapy. Report 81, 1999.

13. Kubo HD, Glasgow GP, Pethel TD, et al. High dose-rate brachytherapy treatment delivery: Report of the AAPM Radiation Therapy Committee Task Group No. 59. *Med. Phys.* 1998;25:375-402.
14. Kutcher GJ, Coia L, Gillin M, et al. Comprehensive QA for radiation oncology: report of the AAPM Radiation Therapy Committee Task Group no. 40. *Med Phys* 1994;21:581-618.
15. Meijer GJ, van Kleffens HJ, Mijnheer BJ. Consistency in quality control programmes for medical electron accelerators in radiotherapy centres. *Radiother Oncol* 1998;48:103-110.
16. Miller AV, Davis MG, and Horton JL. A method for verifying treatment times for simple endobronchial brachytherapy procedures. *Med Phys* 1996;23:1903-1908.
17. Murrer LHP, Kolkman-Deurloo IKK, Manual calculation of treatment time for high dose rate brachytherapy with a flexible intra-operative template (FIT), *Phys Med Biol* 2001;46:1075-1084.
18. Nag S, Cole PE, Crocker I, et al. The American Brachytherapy Society Perspective on Intravascular Brachytherapy. *Cardiovasc Rad Med* 1999;1:8-19.
19. Nath R, Anderson LL, Luxton G, Weaver KA, Williamson JF, Meigooni AS. Dosimetry of interstitial brachytherapy sources: Recommendations of the AAPM Radiation Therapy Committee Task Group No. 43. *Med Phys* 1995;22: 209-234.
20. Nath R, Anderson LL, Meli JA, Olch AJ, Stitt JA, Williamson JF. Code of practice for brachytherapy physics: Report of the AAPM Radiation Therapy Committee Task Group No. 56. *Med Phys* 1997;24:1557-1598.
21. Nath R, Amols H, Coffey C, et al. Intravascular Brachytherapy Physics: Report of the AAPM Radiation Therapy Committee Task Group No. 60. *Med Phys* 1999;26:119-152.
22. NCS (Netherlands Commission on Radiation Dosimetry). Recommendations for dosimetry and quality control of radioactive sources used in brachytherapy. Synopsis (in English). Report 4, 1991.
23. NCS (Netherlands Commission on Radiation Dosimetry). Recommendations for the calibration of Iridium-192 high dose rate sources. Report 7, 1994.
24. NCS (Netherlands Commission on Radiation Dosimetry). Quality Control of Medical Linear Accelerators. Report 9, 1996.
25. NCS (Netherlands Commission on Radiation Dosimetry). Quality Control (QC) of Simulators and CT scanners and some basic QC methods for Treatment Planning Systems. Report 11, 1997.
26. NCS (Netherlands Commission on Radiation Dosimetry). Quality Control in Brachytherapy. Report 13, 2000.
27. SFPH (Société Française des Physiciens d'Hôpital). Contrôle de qualité en Curiethérapie par Iridium 192 à haut débit de dose. Rapport No. 11, 1995.



- 
28. Venselaar JLM, Brouwer WFM, van Straaten BHM, Aalbers AHL. Intercomparison of calibration procedures for Ir-192 HDR sources in The Netherlands and Belgium. *Radiother Oncol* 1994;30:155-161.
  29. Venselaar JLM, Bierhuizen HWJ, and Klop R. A method to check treatment time calculations in Ir-192 high-dose-rate volume implants. *Med Phys* 1995;22:1499-1500.
  30. Williamson JF, Ezzell GA, Olch AJ, Thomadsen BR. Quality assurance for high dose rate brachytherapy. In: Nag S, editor. *High Dose Rate Brachytherapy: a textbook*, Armonk, NY: Futura, 1994. pp. 147-212.



## CHAPTER 11. DETERMINATION OF THE REFERENCE AIR KERMA RATE FOR $^{192}\text{Ir}$ BRACHYTHERAPY SOURCES AND THE RELATED UNCERTAINTY

E van Dijk, IKK Kolkman-Deurloo, PMG Damen

Med Phys 2004; 31(10); 2826-2833.

### 11.1 Abstract

Different methods exist to determine the air kerma calibration factor of an ionization chamber for the spectrum of a  $^{192}\text{Ir}$  high-dose-rate (HDR) or pulsed-dose-rate (PDR) source. An analysis of two methods to obtain such a calibration factor was performed: (i) the method recommended by Goetsch et al. [1] and (ii) the method employed by the Dutch national standards institute NMI [2]. This analysis showed a systematic difference on the order of 1% in the determination of the strength of  $^{192}\text{Ir}$  HDR and PDR sources depending on the method used for determining the air kerma calibration factor. The definitive significance of the difference between these methods can only be addressed after performing an accurate analysis of the associated uncertainties. For an NE 2561 (or equivalent) ionization chamber and an in-air jig, a typical uncertainty budget of 0.94% was found with the NMI-method. The largest contribution in the type B uncertainty is the uncertainty in the air kerma calibration factor for isotope  $i$ ,  $N_k^i$ , as determined by the primary or secondary standards laboratories. This uncertainty is dominated by the uncertainties in the physical constants for the average mass-energy absorption coefficient ratio and the stopping power ratios. This means that it is not foreseeable that the standards laboratories can decrease the uncertainty in the air kerma calibration factors for ionization chambers on a short term. When the results of the determination of the  $^{192}\text{Ir}$  reference air kerma rates in, e.g., different institutes are compared, the uncertainties in the physical constants are the same. To compare the applied techniques, the ratio of the results can be judged by leaving out the uncertainties due to these physical constants. In that case an uncertainty budget of 0.40% (coverage factor = 2) should be taken into account. Due to the differences in approach between the method

used by NMI [2] and the method recommended by Goetsch et al. [1], an extra type B uncertainty of 0.9% ( $k = 1$ ) has to be taken into account when the method of Goetsch et al. [1] is applied. Compared to the uncertainty of 1% ( $k = 2$ ) found for the air calibration of  $^{192}\text{Ir}$ , the difference of 0.9% found is significant.

## 11.2 Introduction

The isotope  $^{192}\text{Ir}$  is frequently used in high dose rate (HDR) and pulsed dose rate (PDR) brachytherapy sources. The source strength has to be determined in terms of the reference air kerma rate ( $\mu\text{Gy}\cdot\text{h}^{-1}$ ) [3,4] or the air kerma strength ( $\mu\text{Gy}\cdot\text{m}^2\cdot\text{h}^{-1}$ ) [5,6] before such a source can be used in clinical practice. This can either be done by an in-air or an in-phantom measurement using an ionization chamber calibrated for  $^{192}\text{Ir}$ , or by a measurement using a well-type ionization chamber [3,7,8]. In the U.S., calibration factors for  $^{192}\text{Ir}$  are only provided for well type ionization chambers.

The problem in deriving an air kerma calibration factor for  $^{192}\text{Ir}$  is that the most important parts of the spectrum of a  $^{192}\text{Ir}$  brachytherapy source fall in an energy gap between the standards for x-rays and the standards for  $\gamma$ -rays established at primary laboratories. It is therefore necessary to determine the air kerma calibration factor using an indirect method. This can be done by approximating the calibration factor for the spectrum of  $^{192}\text{Ir}$  by making use of calibration factors found for other photon energies.

Different methods to determine the source strength for  $^{192}\text{Ir}$  HDR sources are described in the literature [1-3]. The method recommended by the Netherlands Commission on Radiation Dosimetry (NCS) [3], for Accredited Dosimetry Calibration Laboratories (ADCLs) or Secondary Standards Dosimetry Laboratories (SSDLs), is based on a calibrated ionization chamber, an in-air jig and is used for the full uncertainty analysis in this paper. In the U.S., well-type ionization chambers are recommended for the clinical environment, since they are easier to use, and have a much more reproducible geometry that results in greater precision [6,9]. At the University of Wisconsin, a re-entrant ionization chamber for the calibration of  $^{192}\text{Ir}$  HDR sources has been developed, which is commercially available [10]. However, calibration at an ADCL or SSDL of a well-type ionization chamber against a free-in-air calibrated  $^{192}\text{Ir}$  source is necessary.

A calibration method for an ionization chamber for  $^{192}\text{Ir}$  free-in-air was developed by the national standards institute of The Netherlands (NMI) and is based on weighting

the response curve of an ionization chamber over the  $^{192}\text{Ir}$ -spectrum [11]. Another method for the calibration of an ionization chamber was developed by Goetsch et al. [1] and is based on the air kerma calibration factors determined for 250 kVcp x-ray quality and  $^{137}\text{Cs}$   $\gamma$ -rays and on the absorption in the chamber wall for these beam qualities. From the comparison of both methods [11], no clear conclusions could be drawn about significant differences or compliances in the determined air calibration factors for  $^{192}\text{Ir}$ , due to the absence of a thorough analysis of the related uncertainties. To compare the calibration factor determined with the method proposed by the NCS [3] with other methods, the full uncertainty budget of a free-in-air calibration of a  $^{192}\text{Ir}$  HDR or PDR source using a calibrated ionization chamber is analyzed in this paper. The uncertainty budgets follow the guidelines given in the Guide to the Expression of Uncertainty in Measurement (GUM) [12]. The method employed by NMI [2] and the method recommended by Goetsch et al. [1] are described to explain the relevance of the analysis and the difference between both methods.

### 11.3 Materials and methods

#### 11.3.1 Calibration of ionization chambers

In Chapter 13 of Attix [13], the calibration of ionization chambers using x-rays or  $\gamma$ -rays is described. According to Attix [13], the cavity-gas calibration factor ( $N_{\text{gas}}$ ) can be written as:

$$N_{\text{gas}} = \frac{D_{\text{gas}} A_{\text{ion}}}{I} \quad (1)$$

where  $D_{\text{gas}}$  is the mean absorbed dose in the cavity gas,  $A_{\text{ion}}$  is the ion-collection efficiency, assumed to be equal to unity, and  $I$  is the measured current.

When the ionization chamber is filled with air, Eq. (1) can be rewritten for the calibration factor for air kerma ( $N_k$ ) of the ionization chamber as:

$$N_k = \frac{\dot{K}_{\text{air}}}{I} \quad (2)$$

where  $\dot{K}_{air}$  is the kerma rate at a reference point in air in a photon beam when the ionization chamber is absent, and  $I$  is the ionization current produced in the ionization chamber when placed at the same reference point in the photon beam.

An ionization chamber with sufficient build-up material to provide charged particle equilibrium can be considered as a Bragg-Gray cavity. It has been shown in the literature [14] that the Bragg-Gray cavity theory is also valid for the photon energies of the  $^{192}\text{Ir}$  spectrum, as dealt with in this article. The measured ionization current can then be transformed into an air kerma rate ( $\dot{K}_{air}$ ) according to [13]:

$$\dot{K}_{air} = \frac{I}{V \cdot \rho} \cdot \frac{W}{e} \cdot \frac{1}{1 - \bar{g}} \cdot \left( \frac{\bar{S}}{\rho} \right)_{wall}^{air} \cdot \left( \frac{\bar{\mu}_{en}}{\rho} \right)_{air}^{wall} \cdot k_{att} \quad (3)$$

where  $I$  is the measured ionization current,  $V$  is the volume of the ionization chamber,  $\rho$  is the mass density of dry air,  $W$  is the mean energy to produce a pair of ions in dry air by an electron with charge  $e$ ,  $\bar{g}$  is the fraction of energy lost by

bremsstrahlung (assumed to be negligible),  $\left( \frac{\bar{S}}{\rho} \right)_{wall}^{air}$  is the restricted stopping power

ratio of the effective wall material and air, and  $\left( \frac{\bar{\mu}_{en}}{\rho} \right)_{air}^{wall}$  is the ratio of the mass

energy absorption coefficients of the effective wall material and air. Finally,  $k_{att}$  ( $= A_w^{-1}$ ) is the attenuation factor of the photons by the effective wall material.

When Eq. (2) and Eq. (3) are combined, and  $\bar{g}$  is set to zero, the air kerma calibration factor can be expressed as:

$$N_k = \frac{\dot{K}_{air}}{I} = \frac{1}{V \cdot \rho} \cdot \frac{W}{e} \cdot \left( \frac{\bar{S}}{\rho} \right)_{wall}^{air} \cdot \left( \frac{\bar{\mu}_{en}}{\rho} \right)_{air}^{wall} \cdot k_{att} \quad (4)$$

### 11.3.2 The method of Goetsch

Presently, the method as described by Goetsch et al. [1] is generally accepted and used [8,15]. In the article from Goetsch et al. [1] it is shown that the average energy of the  $^{192}\text{Ir}$ -spectrum (i.e. 397 keV) falls about halfway between the  $^{137}\text{Cs}$   $\gamma$ -ray

energy (662 keV) and the average energy of 250 kVcp x-rays (146 keV). For this reason, Goetsch et al. [1] suggest that a simple averaging of the air kerma calibration factors obtained for an ionization chamber at these two energies is a rational basis for deriving a calibration factor for  $^{192}\text{Ir}$ . However, for the interpolation of calibration factors the wall attenuation should be taken into account. According to Goetsch et al. [1], the air kerma calibration factor for  $^{192}\text{Ir}$  can be approximated as follows:

$$A_w^{192\text{Ir}} \cdot N_k^{192\text{Ir}} = \frac{1}{2} \left[ A_w^{250\text{kV}} \cdot N_k^{250\text{kV}} + A_w^{137\text{Cs}} \cdot N_k^{137\text{Cs}} \right] \quad (5)$$

The wall attenuation for photon spectrum  $i$ ,  $A_w^i$ , is the ratio of the ionization current with the wall present and the ionization current with a wall thickness of  $0 \text{ g}\cdot\text{cm}^{-2}$ . The ionization current at a thickness of  $0 \text{ g}\cdot\text{cm}^{-2}$  has been determined by measuring this current for different wall thicknesses and linearly extrapolating the measured values to a wall thickness of  $0 \text{ g}\cdot\text{cm}^{-2}$ .

Goetsch et al. [1] have measured values for  $A_w$  for 250 kVcp x-rays,  $^{137}\text{Cs}$   $\gamma$ -rays and the  $^{192}\text{Ir}$  spectrum. From the measured wall attenuation factors for 250 kVcp x-rays ( $A_w^{250\text{kV}}$ ),  $^{137}\text{Cs}$   $\gamma$ -rays ( $A_w^{137\text{Cs}}$ ) and the  $^{192}\text{Ir}$  spectrum ( $A_w^{192\text{Ir}}$ ), and assuming that  $N_k^{250\text{kV}}$  does not differ more than 10% from  $N_k^{137\text{Cs}}$ , Eq. (5) can be rearranged as:

$$N_k^{192\text{Ir}} = \frac{(1+x)}{2} \left[ N_k^{250\text{kV}} + N_k^{137\text{Cs}} \right] \quad (6)$$

where  $x = 0.0037 (t/9.3 \times 10^{22})$  for a wall thickness of  $t$  electrons $\cdot\text{cm}^{-2}$ .

When Eq. (4) is inserted into Eq. (5), it can be seen that Goetsch et al. [1] make the following assumption:

$$\left( \left( \frac{\bar{S}}{\rho} \right)_{\text{wall}}^{\text{air}} \cdot \left( \frac{\bar{\mu}_{\text{en}}}{\rho} \right)_{\text{air}}^{\text{wall}} \right)_{192\text{Ir}} = \frac{1}{2} \cdot \left[ \left( \left( \frac{\bar{S}}{\rho} \right)_{\text{wall}}^{\text{air}} \cdot \left( \frac{\bar{\mu}_{\text{en}}}{\rho} \right)_{\text{air}}^{\text{wall}} \right)_{\text{x-ray}} + \left( \left( \frac{\bar{S}}{\rho} \right)_{\text{wall}}^{\text{air}} \cdot \left( \frac{\bar{\mu}_{\text{en}}}{\rho} \right)_{\text{air}}^{\text{wall}} \right)_{137\text{Cs}} \right] \quad (7)$$

In figure 1, data for the product of  $\left( \frac{\bar{S}}{\rho} \right)_{\text{wall}}^{\text{air}} \cdot \left( \frac{\bar{\mu}_{\text{en}}}{\rho} \right)_{\text{air}}^{\text{wall}}$  are shown. The open circles have been calculated from the data as found in the appendices of Attix [13], where carbon was used as the wall material. The solid squares are the data for 250 kVcp x-rays (146 keV) and  $^{137}\text{Cs}$   $\gamma$ -rays, as calculated by linear interpolation between the open circle data. The open triangle shows the value for the averaged  $^{192}\text{Ir}$  spectrum at

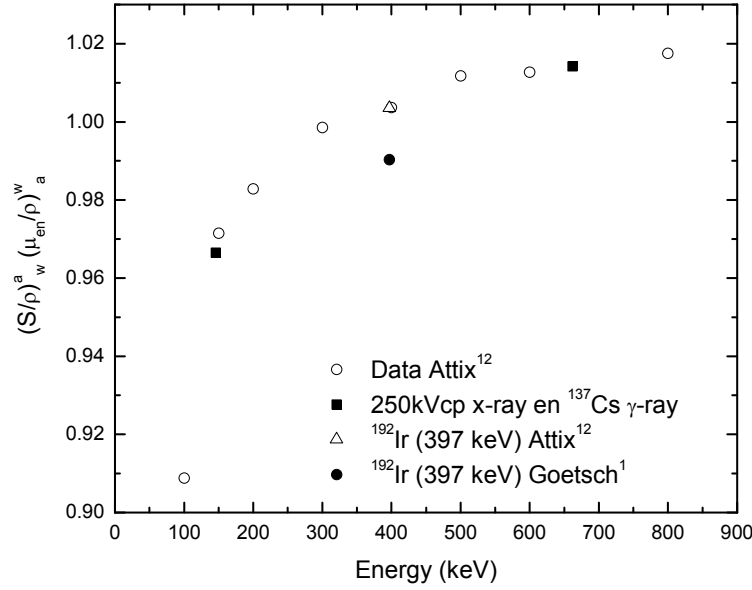


**Figure 1:** Values for  $\left(\frac{\bar{S}}{\rho}\right)_{wall}^{air} \cdot \left(\frac{\bar{\mu}_{en}}{\rho}\right)_{air}^{wall}$  determined with different methods.

397 keV, calculated from the two nearest-neighbor points as found in Attix [13]. Finally, the solid circle shows the number as calculated from Eq. (7), according to the Goetsch-method [1]. It can be seen that the difference in the data calculated with Eq. (7) according to the method of Goetsch et al. [1], compared to the energy dependent data presented in Attix [13], is about 1.3% for 397 keV mono-energetic photons. From figure 1 it can be seen that interpolation over smaller energy ranges will decrease the deviation between theory [13] and the practical approach of Goetsch et al. [1].

The wall attenuation coefficient  $A_w (= k_{att}^{-1})$  is energy dependent. The wall attenuation only depends on the photon mass attenuation coefficient ( $\mu_{att}$ ) and on scatter processes in the wall, and is not dependent on either stopping power ratios or mass energy attenuation coefficient ratios.



**Table 1:** The relevant data of the NE 2561 ionization chamber.

Wall material ionization thimble	Carbon (C)
Carbon density ( $\rho$ )	$1.80 \text{ g}\cdot\text{cm}^{-3}$
Chamber volume (V)	$0.325 \text{ cm}^3$
Chamber shape	Cylindrical with round top
Wall thickness ionization thimble	0.5 mm
Electron density carbon ( $\eta_e$ )	$5.415 \times 10^{23} \text{ electrons}\cdot\text{cm}^{-3}$
Material build-up cap	Delrin ( $\text{CH}_2\text{O}$ )
Thickness build-up cap	$600 \text{ mg}\cdot\text{cm}^{-2}$
Aerial density Delrin	$1.425 \text{ g}\cdot\text{cm}^{-2}$
Electron density Delrin ( $\eta_e$ )	$3.841 \times 10^{23} \text{ electrons}\cdot\text{cm}^{-3}$

Furthermore it is discussed extensively in the literature that the extrapolation method to determine the wall attenuation factor  $A_w$  is not linear, but will become curved for smaller wall thicknesses [16,17].

### 11.3.3 The method used at NMI

The results presented by Goetsch et al. [1] were determined both for a Farmer type ionization chamber and an Exradin A3 chamber. To be able to compare the methods used at NMI [2] and the method recommended by Goetsch et al. [1], the ionization chamber used in this investigation was an NE 2561-chamber, serial number 051. The build-up cap was placed on the ionization thimble not only during the calibration measurements with  $^{137}\text{Cs}$  and  $^{60}\text{Co}$ , but also during the measurements with x-rays. The relevant data of the NE 2561 are summarized in table 1. To be able to determine the air kerma calibration factor for  $^{192}\text{Ir}$  ( $N_k^{192\text{Ir}}$ ) it is necessary to determine the calibration factors of the ionization chamber at mean photon energies [2,11] that cover the photon energy range of the  $^{192}\text{Ir}$ -spectrum. The inverse value of the calibration factors plotted against the corresponding mean photon energy (the response curve) and the most significant  $^{192}\text{Ir}$  spectrum lines are given in figure 2.

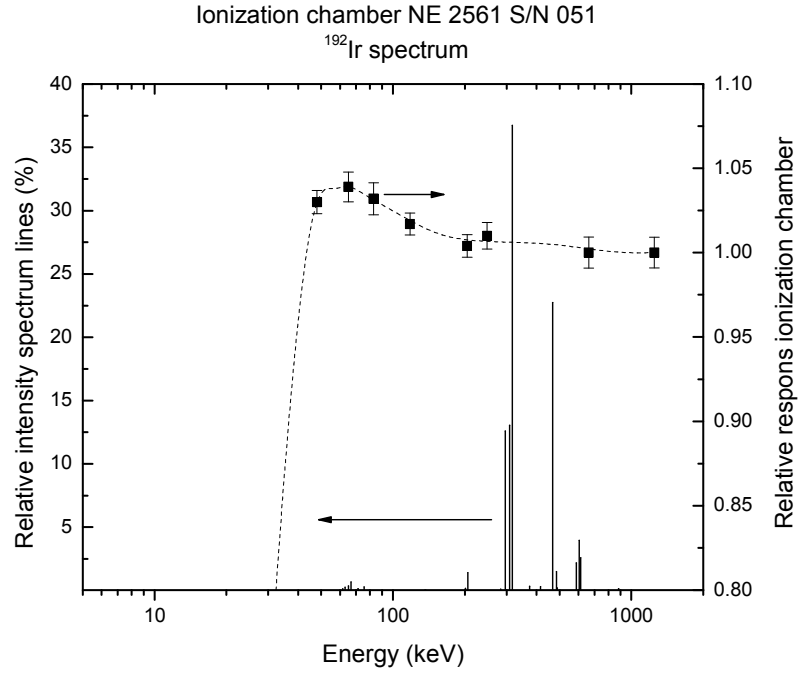


**Figure 2:** The response curve of the ionization chamber NE 2561 in relation to the relative intensity of the spectrum lines of a <sup>192</sup>Ir HDR source.

#### 11.3.3.1 Theory and background

The method used at NMi [2] is based on a different relationship between the air kerma calibration factors. In Eq. (4), the expression for the air kerma calibration factor was given. The only part in this equation that is independent of the photon spectrum is  $\frac{1}{V \cdot \rho} \cdot \frac{W}{e}$ . Since the energy response of an ionization chamber depends

on the mean mass-energy ratio  $\left(\frac{\bar{\mu}_{en}}{\rho}\right)_{wall}^{air}$  and the stopping-power ratio  $\left(\frac{\bar{S}}{\rho}\right)_{air}^{wall}$  of the wall material and air, it is expected that for a specific energy  $E$ , the product

$$N_k^E \cdot A_w^E \cdot \left( \left( \frac{\bar{S}}{\rho} \right)_{air}^{wall} \cdot \left( \frac{\bar{\mu}_{en}}{\rho} \right)_{wall}^{air} \right)^{-1} \text{ is a constant and equals } \frac{1}{V \cdot \rho} \cdot \frac{W}{e}.$$

This means that the contributions to the air kerma calibration factor for the different photon energies of the  $^{192}\text{Ir}$  spectrum have to be weighted over the energy response of the ionization chamber. The method used at NMI is to determine the calibration factors for the ionization chamber at eight different photon energies (ISO narrow-spectrum series [2]) ranging from 48 keV to 1250 keV. These eight selected energies, shown as closed squares in figure 2, cover the complete energy range of the  $^{192}\text{Ir}$  spectrum. The energy response curve is the inverse value of the calibration factors. This function is plotted as a function of the photon energy in figure 2. The relative kerma in air spectrum for the most important peaks of  $^{192}\text{Ir}$  is shown in the figure as well. This spectrum is emitted by a capsulated HDR or PDR  $^{192}\text{Ir}$  source as used in brachytherapy. The spectrum has been calculated at NMI with a Monte Carlo code to correct for the absorption in the capsule [18]. A good approximation of the calibration factor for each of the  $^{192}\text{Ir}$  energy peaks can be made by determining the ratio of the energy dependent component in Eq. (4) for each energy peak of the  $^{192}\text{Ir}$  photon spectrum, with respect to the determined air kerma calibration factor.

The calibration procedure used at NMI for the  $^{192}\text{Ir}$ -photon spectrum is to weigh the sum of the calibration factors for the individual energy peaks with respect to their peak heights.

#### 11.3.3.2 NMI calibration procedure for $^{192}\text{Ir}$

The  $^{192}\text{Ir}$  air kerma calibration factor of the ionization chamber under consideration ( $N_k^{192\text{Ir}}$ ) was determined by weighting the response ( $R = N_k^{-1}$ ) according to the kerma spectrum using the expression [18]:

$$N_k^{192\text{Ir}} = \frac{\sum_{i=1}^n \dot{K}_{air}^i}{\sum_{i=1}^n \dot{K}_{air}^i R_i} \quad (8)$$

where  $i$  is the spectrum line index of the  $^{192}\text{Ir}$  spectrum with energy  $E_i$ ,  $n$  is the number of  $^{192}\text{Ir}$ -spectrum lines taken into account ( $n = 22$ , the spectrum lines at 9 and 9.4 keV are completely attenuated by the source encapsulation),  $\dot{K}_{air}^i$  is the air kerma contribution of the  $i$ th spectrum line, and  $R_i$  is the response for a mean energy of  $E_i$  of the ionization chamber under consideration.

### 11.3.3.3 Determination of the air kerma rate $\dot{K}_{air}^i$

The air kerma spectrum contribution of the  $i$ th spectrum line at 1 meter from the  $^{192}\text{Ir}$  source was obtained by multiplying the relative intensity of each spectrum line ( $f_i$ ) with the energy ( $E_i$ ), the mass energy absorption coefficient  $\left(\frac{\bar{\mu}_{en}}{\rho}\right)_i$  and the correction for photon attenuation in air [18,19]:

$$\dot{K}_{air}^i = f_i E_i \left(\frac{\bar{\mu}_{en}}{\rho}\right)_i e^{-\mu_{att}^i \cdot r} \quad (9)$$

where  $\mu_{att}^i$  is the attenuation coefficient for photons of energy  $E_i$  in air and  $r$  is the distance between the source and the detector (1 m).

### 11.3.3.4 Determination of the response $R_i$

The response  $R_i$  is defined as the inverse of  $N_k^i$ . The latter is determined by a linear interpolation between the air kerma calibration factors, measured by NMi for the set of ISO quality x-rays and the nuclides  $^{137}\text{Cs}$  en  $^{60}\text{Co}$  [2], according to:

$$R_i^{-1} = N_k^i = N_k^A + \frac{(E_i - E_A)}{(E_B - E_A)} (N_k^B - N_k^A) \quad (10)$$

where  $N_k^A$  is the air calibration factor determined by the calibration laboratory, with the lower closest mean x-ray energy  $E_A$  to  $E_i$ , and  $N_k^B$  is the air calibration factor determined by the calibration laboratory, with the higher closest mean x-ray energy  $E_B$  to  $E_i$ . It can be seen in figure 2 that a linear interpolation is allowed, as the response of the ionization chamber does not change much over the energy range of interest.

### 11.3.3.5 The statistical uncertainty in the air kerma calibration factor ( $N_k$ ) in the NMI-method

To determine the uncertainty in the air kerma calibration factor for  $^{192}\text{Ir}$  ( $u_{N_k^{192\text{Ir}}}$ ), all sources of uncertainty have to be taken into account [12]. The uncertainties are divided into type A and type B, where type A are the statistical uncertainties and type B are the non-statistical uncertainties. The type B uncertainties are covered by the type B uncertainties determined during the calibration of the ionization chamber at the calibration laboratory. The type A uncertainty in Eq. (8) can be described as:

$$u_{N_k^{192\text{Ir}}} = \sqrt{\left(\sum_{i=1}^n G_{\dot{K}_i} \cdot u_{\dot{K}_i}\right)^2 + \left(\sum_{i=1}^n G_{N_k^i} \cdot u_{N_k^i}\right)^2} \quad (11)$$

where  $u_{\dot{K}_i}$  is the statistical uncertainty in the air kerma contribution of the  $i$ th spectrum line,  $G_{\dot{K}_i}$  is the sensitivity coefficient for the individual peak height in the  $^{192}\text{Ir}$  kerma spectrum which is the derivative from  $u_{N_k^{192\text{Ir}}}$  to the individually  $\dot{K}_i$ ,  $u_{N_k^i}$  is the statistical uncertainty in the air kerma calibration factor for a mean energy of  $E_i$  of the ionization chamber under test and  $G_{N_k^i}$  is the sensitivity coefficient for the individual calibration which is the derivative from  $u_{N_k^{192\text{Ir}}}$  to each  $N_k^i$ .

### 11.3.3.6 The uncertainty in the air kerma rate $\dot{K}_{air}^i$

The uncertainty  $u_{\dot{K}_{air}^i}$  is composed of the uncertainties in  $f_i$ ,  $E_i$ ,  $\left(\frac{\mu_{en}}{\rho}\right)_i$ ,  $\mu_{att}^i$  and  $r_i$  (see Eq. (9)) and can be determined according to:

$$u_{\dot{K}_{air}^i} = \sqrt{\left(G_{E_i} u_{E_i}\right)^2 + \left(G_{f_i} u_{f_i}\right)^2 + \left(G\left(\frac{\mu_{en}}{\rho}\right)_i u\left(\frac{\mu_{en}}{\rho}\right)_i\right)^2 + \left(G_{\mu_{att}^i} u_{\mu_{att}^i}\right)^2} \quad (12)$$

The individual uncertainties in Eq. (12) are given in table 2.

**Table 2:** The assumed uncertainties in the quantities used to derive  $\dot{K}_{air}^i$ . The results for peak energy and peak height have been calculated with a Monte Carlo code.

Quantity	Symbol	Uncertainty
Peak energy	$u_{E_i}$	0.010 keV
Peak height	$u_{f_i}$	0.4%
Average mass-energy ratio	$u\left(\frac{\mu_{en}}{\rho}\right)_i$	0.2%
Air absorption	$u_{\mu_{att}^i}$	0.2%

The distance  $r$  is only used in the calculation for the air absorption and is considered to be a constant. The values for  $\left(\frac{\mu_{en}}{\rho}\right)_i$  and the air absorption ( $\mu_{att}^i$ ) have been determined by interpolating between the tabulated values for the two nearest known energies. For this reason, a small type A uncertainty is introduced in addition to the type B uncertainty of the tabulated values. Only the type A uncertainty (the statistical component) is taken into account in Eq. (12). The type B uncertainty is taken into account in the uncertainty budget of the calibration factor  $N_k$  of the ionization chamber, given by the SSDL.

#### 11.3.3.7 The statistical uncertainty in $N_k^i$

The statistical uncertainty in  $N_k^i$  can be determined from Eq. (10) according to:

$$u_{N_k^i} = \sqrt{\left(G_{N_k^A} u_{N_k^A}\right)^2 + \left(G_{N_k^B} u_{N_k^B}\right)^2 + \left(G_{E_i} u_{E_i}\right)^2 + \left(G_{E_A} u_{E_A}\right)^2 + \left(G_{E_B} u_{E_B}\right)^2} \quad (13)$$

The individual uncertainties in the quantities in Eq. (13) are given in table 3.

**Table 3:** The assumed uncertainties in the quantities used to derive  $N_k^i$ .

Quantity	Symbol	Uncertainty
Calibration factor	$u_{N_k^A}$	0.21% statistical uncertainty (type A)
	$u_{N_k^B}$	
The x-ray photon energies	$u_{E_A}$	1 keV effective photon energy of the x-ray spectrum during calibration
	$u_{E_B}$	
	$u_{E_i}$	

## 11.4 Results

### 11.4.1 Differences between the method of Goetsch and the NMi method

In the previous sections, the methods of Goetsch et al. [1] and the NMi method have been described. Two major differences can be distinguished between the two methods.

First, Goetsch et al. [1] assume that the average energy of the  $^{192}\text{Ir}$  spectrum (neglecting the two low-energy peaks at 9 and 9.44 keV) is 397 keV. At NMi, however, Monte Carlo calculations have been performed in which the actual photon spectrum coming from an encapsulated  $^{192}\text{Ir}$  HDR source was calculated. This gives an average energy of the photon spectrum of 370 keV [18].

Second, the method of interpolation is completely different for the method of Goetsch et al. [1] and the NMi-method. The method of Goetsch et al. [1] uses a two-point interpolation over the air kerma calibration factors and the wall attenuation. By doing so, a significant difference, as can be seen in figure 1, is introduced by using an

$$\text{approximated value of } \left( \frac{\bar{S}}{\rho} \right)_{\text{wall}}^{\text{air}} \cdot \left( \frac{\bar{\mu}_{\text{en}}}{\rho} \right)_{\text{air}}^{\text{wall}}.$$

The NMi method uses the response function of the ionization chamber. In addition, the NMi method treats each  $^{192}\text{Ir}$  spectrum line individually, and corrects the kerma in air for each spectrum line for the detector response at the energy of interest. In this way, the energy dependence of the  $^{192}\text{Ir}$  spectrum is implemented correctly.

**Table 4:** The assumed uncertainties in the quantities used to derive  $N_k^{192\text{Ir}}$ .

Quantity	Symbol	Value	Distribution	Sensitivity	Uncertainty
$^{192}\text{Ir}$ peak energy	$u_{E_i}$	0.010 keV	Normal	0.5 %/keV	0.005%
$^{192}\text{Ir}$ peak height	$u_{f_i}$	0.4%	Normal	0.02	0.008%
Average mass-energy ratio	$u\left(\frac{\mu_{en}}{\rho}\right)$	0.2%	Normal	0.02	0.004%
Air absorption	$u_{\mu_{att}}$	0.2%	Normal	0.0001	0.000%
Air kerma calibration factor (type A)	$u_{N_k}$	0.21%	Normal	1.0	0.21%
Effective photon energy	$u_{E_k}$	1.0 keV	Normal	0.03 %/keV	0.03%

#### 11.4.2 Results of uncertainties in $N_k^{192\text{Ir}}$ from NMi

The air kerma calibration factor of the ionization chamber NE 2561 for  $^{192}\text{Ir}$  as found with the method used at NMi was 0.6% lower than the air kerma calibration factor for  $^{137}\text{Cs}$ . The uncertainty budget is given in table 4.

The total of the type A uncertainty is 0.21% and the type B uncertainty in the air kerma calibration factor  $N_k^i$  is 0.37%. The type B uncertainty is based on the type B uncertainties of 248 keV effective energy x-rays and  $^{137}\text{Cs}$   $\gamma$ -rays. This gives a total uncertainty of type A combined with type B of 0.43%. Including a coverage factor 2, this gives a total uncertainty of 0.9%.



### 11.4.3 Comparison of $N_k^{192\text{Ir}}$ determined by NMI and Goetsch

When using the method of Goetsch et al. [1], the approximated air kerma calibration factor of the ionization chamber NE 2561 for  $^{192}\text{Ir}$  is 0.3% higher than the NMI [2] air kerma calibration factor for  $^{137}\text{Cs}$ , while the air kerma calibration factor for  $^{192}\text{Ir}$  with the NMI method is 0.6% lower than the air kerma calibration factor for  $^{137}\text{Cs}$ , which gives a total difference of 0.9% in  $N_k^{192\text{Ir}}$  compared to Goetsch et al. [1]. There are not enough data available to determine the uncertainty in the calibration factor as determined with the method of Goetsch et al. [1], e.g., due to the uncertainties in the determination of the wall correction factors  $A_w$ . The total uncertainty in the air kerma calibration factor derived by NMI is 1.0% ( $k = 2$ ).

## 11.5 Discussion

### 11.5.1 General discussion

When an ionization chamber is used in practice, the uncertainty in the calibration factor is a direct measure of the reliability and the traceability of the measurements performed with that ionization chamber. This uncertainty is given by the calibration authorities and has to be used as the non-statistical (type B) uncertainty in the evaluation of the uncertainties in the determination of air kerma rates in practice.

The largest contribution in the type B uncertainty is the uncertainty in the air kerma calibration factor  $N_k^i$  as determined by the national standards laboratory. This uncertainty is dominated by the uncertainties in the physical constants for the average mass-energy absorption coefficient ratio and the stopping power ratios. This means that it is not foreseeable that the Primary Standards Dosimetry Laboratories (PSDLs) are able to decrease the uncertainty in the in-air calibration factors for ionization chambers on a short term.

Because of the deviation of 0.9% in the air kerma calibration factor as found with the method of Goetsch et al. [1] compared to the NMI method, we are of the opinion that the type B uncertainty found for the method recommended by Goetsch et al. [1] should be raised by at least 1.0%. This means that for a typical  $^{192}\text{Ir}$  calibration by an SSDL [15], the uncertainty should be raised from 2.15% to 2.8% ( $k=2$ ).

### 11.5.2 Consequences in $^{192}\text{Ir}$ HDR source calibrations and the related uncertainties

In the case of an in-air determination of the air kerma rate of a brachytherapy HDR or PDR source, different techniques are used, giving more or less similar results. To perform the uncertainty analysis, as an example, we have used the NCS protocol nr. 7 of 1994 [3]. This protocol is based on an in-air calibration jig. The jig has to be stable and rigid, allowing a reproducible repositioning of an ionization chamber and the source catheter. The distance between the ionization chamber and the massive parts of the jig should be at least 200 mm in order to minimize the contribution of radiation scatter from the surroundings. A double-catheter system, where each catheter is placed at the same distance on either side of the chamber, is preferred. The measuring distance is defined as the distance between the center of the thimble of the ionization chamber and the center of the  $^{192}\text{Ir}$  source. The recommended measuring distance is 100 mm. The measurements to determine the reference air kerma rate  $\dot{K}_{ref}$  ( $\mu\text{Gy}\cdot\text{h}^{-1}$ ) should be performed with an ionization chamber, having an air kerma calibration factor ( $\mu\text{Gy}$  per unit reading) in combination with build-up cap and electrometer, determined traceable to a National Standards Laboratory.

To ensure full traceability of the calibration of the HDR or PDR source, not only the reference air kerma rate, but also the related uncertainty in the measured reference air kerma rate has to be determined, taking into account all sources of uncertainty present in the calibration procedure.

When an HDR or PDR brachytherapy source is calibrated using this protocol, the following relation is obtained:

$$\dot{K}_{ref} = \frac{M \cdot N_k \cdot f_{tr} \cdot f_{rs} \cdot d^2}{t} \quad (14)$$

where

$$M = M_{uncor} \cdot p_t \cdot p_p \cdot p_{hum} \cdot p_{ion} \cdot p_{pol} \cdot p_{nu} \quad (15)$$

In Eq. (15),  $M$  is the corrected instrument reading, integrated over the total exposure time  $t$  of the measurement with the source at its position in each of the two catheters,  $M_{uncor}$  is the uncorrected instrument reading,  $p_t$  is the air temperature correction factor to standard air temperature,  $p_p$  is the air pressure correction factor to standard air pressure,  $p_{hum}$  is the air humidity correction factor,  $p_{ion}$  is the ion recombination

correction factor,  $p_{pol}$  is the correction for polarity effects,  $p_{nu}$  is the correction for the dose non-uniformity over the chamber wall, calculated by the theory of Kondo and Randolph [20], published in 1960 and corrected to the work of Tölle et al. [21],  $N_k$  is the air kerma calibration factor for the ionization chamber for the  $^{192}\text{Ir}$  gamma-ray spectrum (in  $\mu\text{Gy}$  per unit reading),  $f_{tr}$  is the correction factor for source transport time,  $f_{rs}$  is the correction factor for room scatter for a wall to chamber distance of 0.5

**Table 5:** The assumed type A uncertainties (coverage factor = 1) in the quantities used to derive  $\dot{K}_{ref}$ .

Quantity	Symbol	Typical value	Value of uncertainty	Distribution	Sensitivity	Uncertainty contribution
Instrument reading	$M_{uncor}$	1.000	0.05%	Normal	1	0.05%
Air temperature	$p_t$	22°C	0.2 °C	Normal	0.34%.°C <sup>-1</sup>	0.07%
Air pressure	$p_p$	101 kPa	0.1 kPa	Normal	1.0%.kPa <sup>-1</sup>	0.10%
Air humidity	$p_{hum}$	50 %	20%	Normal	0	0.00%
Ion recombination	$p_{ion}$	1.000	0.05/ $\sqrt{3}$ %	Rectang.	1	0.03%
Polarity	$p_{pol}$	1.000	0.05/ $\sqrt{3}$ %	Rectang.	1	0.03%
Dose non-uniformity*	$p_{nu}$	1.001	0.1/ $\sqrt{3}$ %	Rectang.	1	0.07%
Source transport time (t > 600 s)	$f_{tr}$	1.000	0.05/ $\sqrt{3}$ %	Rectang.	1	0.03%
Room scatter	$f_{rs}$	0.999	0.05/ $\sqrt{3}$ %	Rectang.	1	0.03%
Distance between the two source positions	$2 \times d$	200 mm	0.2/ $\sqrt{3}$ mm	Rectang.	1.0%.mm <sup>-1</sup>	0.12%
Central position ionization chamber	$d$	100 mm	0.2/ $\sqrt{3}$ mm	Rectang.	0.01%.mm <sup>-1</sup>	0.002%
Total exposure time	$t$	> 600 s	0.02%	Normal	1	0.02%

\* The dose nonuniformity correction has been adjusted according to the work of Tölle et al. [21].

m or more,  $d$  is the source-to-chamber axis distance for the jig, relative to the reference distance of 1 m.

All the variables and their uncertainties given in the previous sections have to be taken into account to determine the overall uncertainty in the calibration of the reference air kerma rate of an HDR or PDR source. The uncertainty due to the calibration of the ionization chamber is the total uncertainty of type A combined with type B and is considered to be a type B uncertainty in this section. The values and the uncertainty budget for the calibration of an HDR or PDR source are given in table 5. The uncertainties stated for the individual uncertainty sources are estimated for a practical procedure.

The total of the type A uncertainty is 0.20% and the type B uncertainty in the air kerma calibration factor  $N_k^{192\text{Ir}}$  is 0.42%. This gives a total uncertainty of type A combined with type B of 0.47%. Including a coverage factor 2, gives a total uncertainty of 1.0%.

### 11.5.3 The use of well-type ionization chambers in clinical practice

In the U.S., well-type ionization chambers are recommended for the clinical environment, since they are mechanically and electrically stable instruments, they are easy to use, and give reproducible results [10]. However, for the calibration of  $^{192}\text{Ir}$  sources, the well-type ionization chamber is a tertiary level instrument. The well-type ionization chamber must be calibrated for the  $^{192}\text{Ir}$  spectrum by a PSDL or SSDL that uses a reference  $^{192}\text{Ir}$  source, in terms of kerma strength in air.

The uncertainty in the calibration of the reference  $^{192}\text{Ir}$  source is a major contributor to the uncertainty in the calibration factor of the well-type ionization chamber determined by the PSDL or SSDL. When the reference source has been calibrated according to the method of Goetsch et al. [1], the final type B uncertainty in the well-type calibration factor should be raised by at least 1% ( $k = 1$ ) compared to reference sources calibrated with the method described in this paper.

## 11.6 Conclusions

The measured source strength for an HDR or PDR source found with a NE 2561 (or equivalent) ionization chamber and an in-air jig has a typical uncertainty of 1.0% ( $k$

= 1). This uncertainty level is state of the art at this moment for standard laboratories. The largest contribution in the type B uncertainty is the uncertainty in the air kerma calibration factor  $N_k^i$  as determined by the national standards laboratory. Parts of the uncertainty budgets of the PSDLs are the uncertainties assigned to the physical constants used.

When measurements are made to compare the results of the determination of the  $^{192}\text{Ir}$  reference air kerma rates between, for instance, different institutes, the uncertainties in the physical constants are the same. To compare the techniques used and the measurements performed, the ratio of the results can be judged leaving out the uncertainties due to these physical constants. In this case an uncertainty of 0.40% (coverage factor = 2) should be taken into account.

Due to the differences in approach between the method used by NMi [2] and the method recommended by Goetsch et al. [1], an extra type B uncertainty of 0.9% ( $k = 1$ ) has to be taken into account when the method of Goetsch et al. [1] is applied. Compared to the uncertainty of 1% ( $k = 2$ ) found for the air calibration of  $^{192}\text{Ir}$ , as described in this work, the difference of 0.9% found is significant.

## 11.7 References

1. S.J. Goetsch, F.H. Attix, D.W. Pearson, and B.R. Thomadsen, "Calibration of  $^{192}\text{Ir}$  high-dose-rate afterloading system", *Med. Phys.* **18**, 462-467 (1991).
2. J.J. Petersen, E. van Dijk, and A.H.L. Aalbers, "Comparison of methods for derivation of  $^{192}\text{Ir}$  calibration factors for NE 2561 & 2571 ionization Chambers", Report S-EI-94.01, NMi Van Swinden Laboratorium (NMi, Delft, The Netherlands, 1994).
3. Netherlands Commission on Radiation Dosimetry (NCS), "Recommendations for the Calibration of Iridium-192 High Dose Rate Sources", NCS Report No 7 (NCS, Delft, The Netherlands, 1994).
4. Netherlands Commission on Radiation Dosimetry (NCS), "Quality Control in Brachytherapy, Current practice and minimum requirements", NCS Report No 13 (NCS, Delft, The Netherlands, 2000).
5. R. Nath, L.L. Anderson, G. Luxton, K.A. Weaver, J.F. Williamson, and A.S. Meigooni, "Dosimetry of interstitial brachytherapy sources: Recommendations of the AAPM Radiation Therapy Committee Task Group No. 43", *Med. Phys.* **22**, 209-234, (1995).
6. R. Nath, L.L. Anderson, J.A. Meli, A.J. Olch, J.A. Stitt, and J.F. Williamson, "Code of practice for brachytherapy physics: Report of the AAPM Radiation Therapy Committee Task Group No. 56", *Med. Phys.* **24**, 1557-1598, (1997).

7. L.A. deWerd, "Brachytherapy Dosimetric Assessment: Source Calibration", in "Categorical Course in Brachytherapy Physics Syllabus", Bruce Thomadsen editor, pp. 143-153, RSNA publications, Oak Brook, IL, (1997).
8. IAEA, "Calibration of photon and beta ray sources used in brachytherapy", Technical Document 1274 (2002).
9. M.H. Maréchal, C.E. de Almeida, I.H. Ferreira, and C.H. Sibata, "Experimental derivation of wall correction factors for ionization chambers used in high dose rate  $^{192}\text{Ir}$  source calibration", *Med. Phys.* **29**, 1-5, (2002).
10. S.J. Goetsch, F.H. Attix, L.A. deWerd, and B.R. Thomadsen, "A new re-entrant ionization chamber for the calibration of iridium-192 high dose rate sources", *Int. J. Radiation Oncology Biol. Phys.* **24**, 167-170, (1992).
11. E. van Dijk, "Comparison of two different methods to determine the air kerma rate calibration factor,  $N_k$ , for  $^{192}\text{Ir}$ " In: Proceedings of the "International Symposium on Standards and Codes of Practice in Medical Radiation Physics", (IAEA-CN-9675, Vienna, Austria, 2002).
12. International Organization for Standardization, "Guide to the Expression of Uncertainty in Measurement", First edition, ISBN 92-67-10188-9 (ISO, place, 1993).
13. F.H. Attix, "Introduction to radiological physics and radiation dosimetry", John Wiley & Sons, 1996, ISBN 0-471-01146-0.
14. J. Borg, I. Kawrakow, D.W.O. Rogers and J.P. Seuntjes, "Monte Carlo Study of Correction Factors for Spencer-Attix Cavity Theory at Photon Energies at or above 100 keV", *Med. Phys.* **27**, 1804-1813 (2000).
15. K.E. Stump, L.A. DeWerd, J.A. Micka and D.R. Anderson, "Calibration of new high dose rate  $^{192}\text{Ir}$  sources", *Med. Phys.* **29**, 1483-1488, (2002).
16. D.W.O. Rogers and A.F. Bielajew, "Wall attenuation and scatter corrections for ion chambers: measurements versus calculations", *Phys. Med. Biol.* **35**, 1065-1078 (1990).
17. A.F. Bielajew, "On the technique of extrapolation to obtain wall correction factors for ion chambers irradiated by photon beams", *Med. Phys.* **17**, 583-587 (1990).
18. F. Verhaegen, E. van Dijk, H. Thierens, A. Aalbers, and J. Seuntjes, "Calibration of low activity  $^{192}\text{Ir}$  brachytherapy sources in terms of reference air kerma rate with large volume spherical ionization chambers", *Phys. Med. Biol.* **37**, 2071-2082 (1992).
19. J.H. Hubbel, "Photon Mass Attenuation and Energy-absorption Coefficients from 1 keV to 20 MeV", *Int. J. Appl. Radiat. Isot.* **33**, 1269-1290 (1982).
20. S. Kondo and M.L. Randolph, "Effect of finite size of ionization chambers on measurements of small photon sources", *Rad. Research* **13**, 37-60, (1960).
21. H. Tölli, A.F. Bielajew, O. Mattsson, G. Sernbo, and K.A. Johansson, "Fluence non-uniformity effects in air kerma determination around brachytherapy sources", *Phys. Med. Biol.* **42**, 1301-1318 (1997).

## CHAPTER 12. SUMMARY, GENERAL CONCLUSIONS AND FUTURE PERSPECTIVES

### 12.1 Summary and general conclusions

The current practice of intraoperative brachytherapy (IOBT) is based on the use of an HDR afterloader containing a single stepping Iridium-192 source located in an Integrated Brachytherapy Unit (Nucletron B.V., The Netherlands), enabling integration of the entire procedure (implantation, implant reconstruction, dose planning and irradiation) in a single session. This thesis discusses:

- Techniques and results of fractionated HDR and PDR brachytherapy in head and neck cancer (*chapter 2*);
- Optimization of the dose distribution through dwell time optimization (*chapters 3 and 4*);
- (On-line) implant reconstruction in the IBU with the dedicated brachytherapy localiser (*chapters 5 and 6*);
- The technique and results of IOBT for patients with locally advanced or recurrent rectal cancer (*chapters 7 and 8*);
- Quality control in (intraoperative) brachytherapy (*chapters 9, 10 and 11*).

#### 12.1.1 Dose optimization

In *chapter 3* it was shown that, in contrast to a regular two-plane volume implant, in which geometric optimization resulted in a 28% increase of the treated volume, the treated volume of an example of an ‘irregular’ base of tongue (BOT) implant did not increase after geometric optimization. However, a reduction of the overdosed volume was seen, accompanied by an increase in the uniformity index UI and a decrease of the dose nonuniformity ratio DNR. Therefore, the method for dose specification should be kept unchanged after geometric optimization in case of the BOT implant, while 90-95% of the mean central dose should be chosen as a reference dose or the range of active dwell positions should be shortened in case of the regular volume

implant in order to keep the treated volume comparable with the non-optimized dose distribution. In *chapter 4* it was concluded that the current implementation of anatomy based inverse planning, as implemented in PLATO BPS, resulted in a too low target coverage when used in HDR prostate implants and that graphical optimization was needed for fine tuning of the dose distribution. Graphical optimization was shown to be a powerful tool resulting in a significantly higher target coverage in combination with maximum normal tissue sparing. As graphical optimization is a rather time consuming procedure other techniques for anatomy based inverse treatment planning should be considered for routine use in intraoperative brachytherapy [3,6,8-13,16].

### *12.1.2 (On-line) implant reconstruction*

In *chapter 5* it is shown that accurate implant reconstruction is possible with the dedicated IBU localiser. The average reconstruction error due to the accuracy of the read-out of the localiser settings is less than 0.24 mm. Using filmless reconstruction and limiting the use to implants located near the isocenter the average reconstruction error remains below 0.65 mm, with the increase due to the finite pixel size and geometric distortions. When applying a dedicated image distortion correction algorithm, separating the geometric distortion and the magnetic distortion, it is proven that accurate on-line (filmless) implant reconstruction is possible without limitations regarding the usable range of the field of view of the image intensifier (*chapter 6*). The reconstruction error with eccentric positioning of the QA phantom remains limited to 0.1 mm. However, due to the method used, the C-arm angle is limited to those angles for which the magnetic distortion has been calibrated.

### *12.1.3 IOBT for rectal cancer*

Intraoperative brachytherapy (IOBT) using a 5 mm thick Flexible Intraoperative Template (FIT) was introduced in the Erasmus MC – Daniel Den Hoed Cancer Center for treatment of rectal cancer, head and neck cancer and pancoast tumors. To reduce the procedure time, treatment planning is performed using standard plans, that neglect the curvature of the FIT. In *chapter 7*, the individual treatment plans of 32 patients with rectal cancer, treated this way, were evaluated. A mean treatment dose of  $9.55 \pm 0.21$  Gy was found for the individual plan, instead of the prescribed 10 Gy.



In 63% of the clips, the dose was larger than 15.0 Gy, indicating a gap between the FIT and the target smaller than 5 mm. In 18% of the clips, the dose was smaller than 13.0 Gy indicating that locally the gap was larger than 5 mm. *Chapter 8* reports the local failure rate, site of local recurrence and survival rate of 37 patients with locally advanced or recurrent rectal cancer, treated with external beam radiotherapy, surgery and IOBT. With a median follow up of surviving patients of three years, 12 patients (32%) experienced a local recurrence, of which five (15%) were IOBT in-field. The local failure rate was significantly different for primary disease versus recurrent. The overall survival was significantly different for primary versus recurrent tumors and according to stage and grade.

#### 12.1.4 Brachytherapy QA

A taskgroup on QA of brachytherapy systems of the Netherlands Commission on Radiation Dosimetry (NCS) investigated the accuracy of brachytherapy treatments and the practice of brachytherapy QA in The Netherlands and Belgium. In *chapter 9* the accuracy of implant reconstruction and dose delivery was determined in 33 radiotherapy institutions. The average reconstruction accuracy was  $-0.07$  mm ( $\pm 0.4$  mm, 1 SD) for 41 localizers. The average deviation of the measured dose from the prescribed dose was  $+0.9\%$  ( $\pm 1.3\%$ , 1 SD) for 21 HDR afterloading systems,  $+1.0\%$  ( $\pm 2.3\%$ , 1 SD) for 12 PDR afterloaders, and  $+1.8\%$  ( $\pm 2.5\%$ , 1 SD) for 15 LDR afterloaders. It was concluded that a very good accuracy of brachytherapy implant reconstruction and dose delivery is achieved in The Netherlands and Belgium. In *chapter 10* the practice of brachytherapy QA was evaluated by distributing an extensive questionnaire to all institutions. The answers to the questionnaires showed large variations in test frequencies and test methods. Furthermore, large variations in time spent on QC exist, which is mainly due to differences in QC philosophy and differences in the available resources. Based on the results of the questionnaires and a comparison with international recommendations, a set of minimum requirements for QC of brachytherapy has been formulated [17]. These guidelines are being implemented in the radiotherapy institutions in The Netherlands and Belgium. The two methods in use to obtain the air kerma calibration factor of an ionization chamber for the spectrum of Iridium-192 sources are analysed in *chapter 11*. This analysis revealed a systematic difference on the order of 1% in the determination of the reference air kerma rate of HDR and PDR sources, depending on the method

used. This difference is significant in relation to the overall uncertainty in the calibration of an HDR or PDR source.

## 12.2 Future developments

Despite the developments in EBRT, (IO)BT still remains to have an important role to play in radiation oncology, e.g. with regard to target motion. For example, a recent study in our institute has shown that tumors of the tonsil, soft palate and base of tongue move up to 3 mm due to normal respiration, requiring PTV margins in EBRT. In (IO)BT this margin is not needed as the dose distribution moves with the catheters (and thus the target) and because one can expect target fixation due to catheter insertion.

Future developments in IOBT should focus on:

- Introduction of image guided therapy by integrating anatomical information from 3D-imaging, preferably MRI, in IOBT treatment planning and providing on-line the (biologic) summation of the dose distributions from previous (EBRT) irradiation and IOBT during the IOBT procedure;
- Optimization of the IBU design and introduction of multichannel afterloaders, shortening overall procedure times;
- Development of new low-energy isotopes, reducing the required shielding of the brachytherapy room.

### 12.2.1 Image guided therapy

In the current set-up, imaging based on 2D images acquired with the dedicated IBU localiser is used. The next step is to proceed to image guided therapy, i.e. to integrate 3D anatomical information in the planning process of all applications, as is customary in EBRT. Preferably, this should be MRI with its favourable soft tissue contrast. Guidelines for the use of MRI in brachytherapy of various anatomical sites are being developed [3,5,7,18,20,22]. With the availability of 3D anatomical information it becomes possible to evaluate the IOBT plan in relation to previous irradiation, e.g. EBRT. Ideally, on-line (biologic) summation of IOBT and previous irradiation should be available, enabling optimization of IOBT in the context of optimization of the entire treatment. In order to do so, further research should be done on image

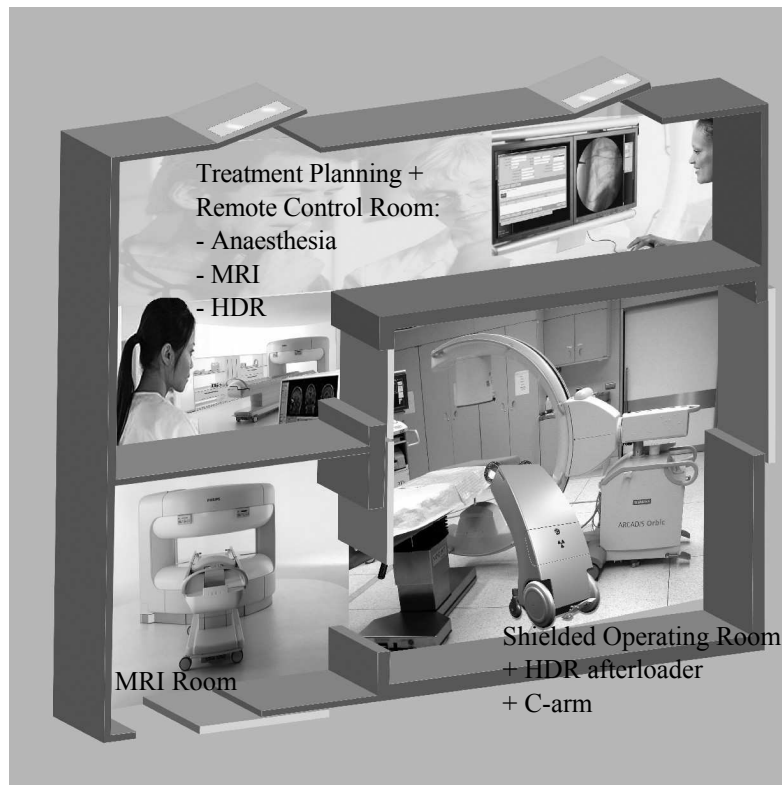


**Figure 1:** Proposed set-up for an improved brachytherapy department consisting of an MRI-based intraoperative brachytherapy unit.

registration, compensating anatomy deformation due to previous treatments and/or implantation of the BT applicators or catheters, as demonstrated by Christensen et al. [2].

#### 12.2.2 Optimization of the IBU design

The current design of the IBU with the afterloader and imaging in a shielded OR was developed as the ideal environment for IOBT. However, by integrating both the afterloader and the imaging equipment in the OR, it turned out that the capacity cannot be used optimally, especially during long lasting surgery preceeding IOBT. Therefore, in future, the imaging equipment, e.g. an (open) MRI, should be located in a separate room directly accessible from the brachytherapy OR (see figure 1). This way, the imaging equipment remains available to other procedures during the

surgical phase and the irradiation of the IOBT procedure. The OR could be equipped with a (mobile) C-arm for visualization or, in case a separate room with an MRI is not feasible, with an isocentric C-arm with cone beam CT facilities. A second BT room, e.g. at the radiotherapy department, should be available, either equipped with its own afterloader or using a transportable afterloader, for fractionated treatments and relatively simple applications, e.g. intraluminal treatments.

### *12.2.3 New developments in multichannel afterloaders*

Overall procedure times can be shortened by the introduction of multichannel afterloaders using multiple sources concurrently and performing the irradiation concurrently with the necessary check cable runs, as recently proposed by Isodose Control B.V., The Netherlands ([www.flexitron.net](http://www.flexitron.net)). The afterloader manufactured by Isodose Control, the Flexitron, is very suitable for the presented future design of an HDR-IOBT unit. It features full flexibility as it can be configured as an LDR, MDR, PDR or HDR afterloader. Applicability in separate treatment rooms is enabled by its transportability. It is configured with up to 40 channels in combination with reduced treatment times by using two source drives and a separate dummy drive which can operate simultaneously. For HDR-IOBT these two source drives can contain several combinations of sources, e.g. two new Iridium-192 HDR sources (strongly reducing treatment times), a new Iridium-192 HDR source in combination with a decayed Iridium-192 HDR source (reducing treatment times and costs or enabling PDR treatment), a combination of a new Iridium-192 HDR source and a low-energy-source or two low-energy-sources.

### *12.2.4 New (low-energy) isotopes*

The costs of the proposed future design of an IOBT unit can be reduced and the implementation of an IOBT program simplified when using new low-energy isotopes, e.g. Ytterbium-169 [15] or Thulium-170, requiring less shielding of the room [4]. Ytterbium-169 was introduced as a promising isotope for use in intravascular brachytherapy [19], but it has recently been proposed for use in HDR prostate brachytherapy too [14]. In order to obtain accurate dose calculations for these low-energy isotopes new dose calculation algorithms should be developed, separating the primary and scatter components [21]. This is especially important when considering

inhomogeneities and shielding, as demonstrated by Carlsson-Tedgren and Ahnesjö [1].

### 12.3 References

1. Carlsson-Tedgren ÅK, Ahnesjö A. Accounting for high Z shields in brachytherapy using collapsed cone superposition for scatter dose calculation. *Med Phys* 2003; 30:2206-2217.
2. Christensen GE, Carlson B, Chao KSC, et al. Image-based dose planning of intracavitary brachytherapy: registration of serial-imaging studies using deformable anatomic templates. *Int J Radiat Oncol Biol Phys* 2001; 51:227-243.
3. Citrin D, Ning H, Guion P, et al. Inverse treatment planning based on MRI for HDR prostate brachytherapy. *Int J Radiat Oncol Biol Phys* 2005; 61:1267-1275.
4. Granero D, Pérez-Calatayud J, Ballester F, Bos AJJ, Venselaar J. Broad-beam transmission data of new brachytherapy sources, Tm-170 and Yb-169. *Radiat Prot Dosimetry* 2005 (advance access published July 19).
5. Haie-Meder C, Pötter R, van Limbergen E, et al. Recommendations from gynaecological (GYN) Gec-Estro Working Group (1): concepts and terms in 3D image based 3D treatment planning in cervix cancer brachytherapy with emphasis on MRI assessment of GTV and CTV. *Radiother Oncol* 2005; 74:235-245.
6. Hsu ICJ, Lessard E, Weinberg V, Pouliot. Comparison of inverse planning simulated annealing and geometrical optimization for prostate high-dose-rate brachytherapy. *Brachytherapy* 2004; 3:147-152.
7. Kirisits C, Pötter R, Lang S, Dimopoulos J, Wachter-Gerstner N, Georg D. Dose and volume parameters for MRI-based treatment planning in intracavitary brachytherapy for cervical cancer. *Int J Radiat Oncol Biol Phys* 2005; 62:901-911.
8. Lachance B, Béliveau-Nadeau D, Lessard E, et al. Early clinical experience with anatomy based inverse planning dose optimization for high dose rate boost of the prostate. *Int J Radiat Oncol Biol Phys* 2002; 54:1:86-100.
9. Lahanas M, Baltas D, Zamboglou N. Anatomy-based three-dimensional dose optimization in brachytherapy using multiobjective genetic algorithms. *Med Phys* 1999; 26:9:1904-1918.
10. Lahanas M, Baltas D, Zamboglou N. A hybrid evolutionary algorithm for multi-objective anatomy-based dose optimization in high-dose-rate brachytherapy. *Phys Med Biol* 2003; 48:399-415.
11. Lahanas M, Baltas D, Giannouli S. Global convergence analysis of fast multi-objective gradient-based dose optimization algorithms for high-dose-rate brachytherapy. *Phys Med Biol* 2003; 48:599-617.

12. Lessard E, Pouliot J. Inverse planning anatomy based dose optimization for HDR brachytherapy of the prostate using fast simulated annealing algorithm and dedicated objective function. *Med Phys* 2001; 28:5:773-779.
13. Lessard E, Hsu IC, Pouliot J. Inverse planning for interstitial gynaecologic template brachytherapy: truly anatomy based planning. *Int J Radiat Oncol Biol Phys* 2002; 54:4:1243-1251.
14. Lymperopoulou G, Papagiannis P, Sakelliou L, Milickovic N, Giannouli S, Baltas D. A dosimetric comparison of  $^{169}\text{Yb}$  versus  $^{192}\text{Ir}$  for HDR prostate brachytherapy. *Med Phys* 2005; 32:3832-3842.
15. Medich DC, Tries MA, Munro JJ 3<sup>rd</sup>. Monte Carlo characterization of an Ytterbium-169 high dose rate brachytherapy source with analysis of statistical uncertainty. *Med Phys* 2006; 33:163-172.
16. Milickovic N, Lahanas M, Papagiannopoulou M, Zamboglou N, Baltas D. Multi-objective anatomy-based dose optimization for HDR-brachytherapy with constraint free deterministic algorithms. *Phys Med Biol* 2002; 47:2263-2280.
17. NCS (Netherlands Commission on Radiation Dosimetry). Quality control in brachytherapy. Report 13, 2000.
18. Nag S, Cardenes H, Chang S, et al. Proposed guidelines for image-based intracavitary brachytherapy for cervical carcinoma: report from image-guided brachytherapy working group. *Int J Radiat Oncol Biol Phys* 2004; 60:1160-1172.
19. Patel N, Fan P, Chiu-Tsao ST, et al. Ytterbium-169: a promising new radionuclide for intravascular brachytherapy. *Cardiovasc Radiat Med* 2001; 2:173-180.
20. Pötter R, Haie-Meder C, van Limbergen E, et al. Recommendations from gynaecological (GYN) Gec-Estro Working Group (2): concepts and terms in 3D image-based treatment planning in cervix cancer brachytherapy – 3D dose volume parameters and aspects of 3D image-based anatomy, radiation physics, radiobiology. *Radiother Oncol* 2006; 78:67-77.
21. Russell KR, Carlsson Tedgren ÅK, Ahnesjö A. Brachytherapy source characterization for improved dose calculations using primary and scatter dose separation. *Med Phys* 2005; 32:2739-2752.
22. Schultze J, Schneider R, Kimmig B, Kovacs G. Interstitial brachytherapy in the head and neck region: when has imaging for treatment planning to be performed ? *Röntgenpraxis* 2002; 54:232-237.

## SAMENVATTING

Brachytherapie is een behandeling waarbij tumoren bestraald worden door radioactieve bronnen vlakbij of in de tumor te plaatsen m.b.v. tijdelijk geïmplanteerde applicatoren of afterloading catheters/naalden. Tegenwoordig wordt voor intra-operatieve brachytherapie (IOBT) gebruik gemaakt van een hoog-dosistempo (HDR) afterloader, die een stappende Iridium-192 puntbron bevat. Deze afterloader bevindt zich in een geïntegreerde brachytherapie unit (IBU), waardoor het mogelijk is de gehele behandelprocedure (implantatie, reconstructie, dosisplanning en bestraling) in één sessie te concentreren. Dit proefschrift beschrijft de volgende onderwerpen die betrekking hebben op (IO)BT:

- Toepassing van HDR/PDR brachytherapie bij hoofd hals tumoren;
- Optimalisatie van de dosisverdeling;
- Reconstructie van het implantaat m.b.v. de brachytherapie lokalisator;
- Techniek en resultaten van IOBT bij patienten met een rectum tumor;
- Kwaliteitscontrole in (IO)BT.

In *hoofdstuk 2* worden de protocollen voor HDR/PDR brachytherapie bij hoofd hals tumoren beschreven.

Omdat HDR/PDR afterloaders gebruik maken van een stappende Iridium-192 puntbron is het mogelijk de dosisverdeling te optimaliseren door de verblijftijden van de bron op alle posities in het implantaat te optimaliseren. In *hoofdstuk 3* worden de effecten van geometrische optimalisatie in interstitiële volume implantaten beschreven ten aanzien van het bestraalde volume, de dosishomogeniteit en de keuze van de referentie isodose. Hieruit bleek het bestraalde volume met 28% toe te nemen na optimalisatie in geval van een regelmatig tweevlaks implantaat terwijl het bestraalde volume in een voorbeeld van een onregelmatig implantaat (van de tongbasis) onveranderd bleef in combinatie met een toename van de dosishomogeniteit. In *hoofdstuk 4* wordt aangetoond dat de implementatie van inverse optimalisatie in Plato BPS resulteert in een te lage target coverage in het geval van HDR prostaatimplantaties en dat grafische optimalisatie leidt tot aanzienlijk betere resultaten.

Voor de IBU is een speciale brachytherapie lokalisator ontwikkeld. In *hoofdstuk 5* wordt de reconstructienauwkeurigheid van deze lokalisator bepaald d.m.v. simulaties en metingen. De reconstructienauwkeurigheid t.g.v. de uitlezing van de lokalisatorinstellingen is beter dan 0.24 mm. Reconstructie van doorlichtbeelden, met het implantaat dichtbij het isocentrum van de lokalisator, resulteert in een grotere reconstructiefout ( $\leq 0.65$  mm), dankzij de pixelgrootte en beeldverstoreningen. Wanneer gebruik gemaakt wordt van correctie-algorithmes die de geometrische en de magnetische beeldverstorening separaat corrigeren blijkt het mogelijk een nauwkeurige reconstructie te verkrijgen (reconstructiefout  $\leq 0.1$  mm) zonder restricties m.b.t. de positie van het implantaat. Echter, de C-arm hoek is beperkt tot die hoeken waarvoor de magnetische beeldverstorening gecalculeerd is (*hoofdstuk 6*).

IOBT m.b.v. een 5 mm dik flexibel intraoperatief template (FIT) wordt in het Erasmus MC – Daniel Den Hoed Oncologisch Centrum gebruikt bij de behandeling van patiënten met een rectum-, hoofd-hals- of pancoasttumor. Om de totaal benodigde tijd te reduceren wordt gebruik gemaakt van standaardplanningen die de werkelijke kromming van het FIT verwaarlozen. In *hoofdstuk 7* worden de individuele behandelplannen van 32 patiënten met een rectumtumor, die met deze techniek behandeld zijn, geëvalueerd. Een gemiddelde afgegeven dosis van  $9.55 \pm 0.21$  Gy wordt gevonden in plaats van de voorgeschreven 10 Gy. In 63% van de clips wordt een dosis  $\geq 15.0$  Gy gevonden, hetgeen aangeeft dat de aansluiting tussen het FIT en het doelvolumen beter is dan 5 mm. In 18% van de clips is de dosis  $\leq 13.0$  Gy, hetgeen duidt op een aansluiting slechter dan 5 mm. In *hoofdstuk 8* worden de klinische resultaten van 37 patiënten met een primaire, gevorderde of lokaal recidief rectumtumor, die behandeld zijn met externe radiotherapie, chirurgie en IOBT, gerapporteerd. Bij een gemiddelde follow-up van drie jaar hadden 12 patiënten (32%) een lokaal recidief, waarvan vijf (12%) zich bevonden in het IOBT bestralingveld. Er was een significant verschil tussen patiënten met een primaire tumor en patiënten met een lokaal recidief m.b.t. lokaal falen en overleving.

Een werkgroep “QA van brachytherapie systemen” van de Nederlandse Commissie voor Stralingsdosimetrie (NCS) heeft de nauwkeurigheid van brachytherapie behandelingen en de status van de brachytherapie kwaliteitscontroles onderzocht in Nederland en België. In *hoofdstuk 9* is de nauwkeurigheid van de reconstructie en de dosisafgifte onderzocht in 33 radiotherapie afdelingen. De gemiddelde reconstructienauwkeurigheid was  $-0.07$  mm ( $\pm 0.4$  mm, 1 SD) voor 41 lokalisatoren. De gemiddelde afwijking tussen de gemeten dosis en de voorgeschreven dosis was  $+0.9\%$  ( $\pm 1.3\%$ , 1 SD) voor 21 HDR afterloaders,  $+1.0\%$  ( $\pm 2.3\%$ , 1 SD) voor 12



PDR afterloaders, en  $+1.8\%$  ( $\pm 2.5\%$ , 1 SD) voor 15 LDR afterloaders. In *hoofdstuk 10* is de status van de brachytherapie kwaliteitscontroles onderzocht d.m.v. een enquête. De antwoorden op deze enquête laten een grote variatie in frequenties, methodieken en tijdsbelasting van de kwaliteitscontroles zien. De resultaten van deze enquête en de vergelijking met internationale richtlijnen hebben geleid tot een set van richtlijnen m.b.t. brachytherapie kwaliteitscontroles dat gepubliceerd is als NCS rapport 13. In *hoofdstuk 11* worden de twee beschikbare methodes voor de bepaling van de air-kerma kalibratiefactor voor een ionisatiekamer voor het spectrum van een Iridium-192 bron geanalyseerd. Hieruit blijkt een systematisch verschil van ongeveer 1% in de bepaling van HDR en PDR bronsterktes, afhankelijk van de gebruikte methode.

In *hoofdstuk 12* worden de toekomstige ontwikkelingen in IOBT beschreven. Deze richten zich op de introductie van beeldgestuurde therapie (b.v. gebruik makend van MRI), optimalisatie van het IBU concept, introductie van nieuwe meerkanaals afterloaders leidend tot verkorting van de totale tijd benodigd voor IOBT en de introductie van nieuwe laag-energetische bronnen die het mogelijk maken de benodigde afscherming van een behandelkamer te verminderen.



## DANKWOORD

Dit proefschrift is een weerspiegeling van jarenlange activiteiten op het gebied van de brachytherapie binnen een grote groep enthousiastelingen. Een ieder persoonlijk bedanken voor zijn/haar bijdrage binnen dit geheel is ondoenlijk en heeft ook nog eens het risico in zich iemand te vergeten. Toch wil ik er een aantal uitlichten:

- Allereerst mijn ouders voor de enorme stimulansen om door te leren en de geboden mogelijkheden datgene te doen wat ik graag wilde.
- Prof.dr. P.C. Levendag voor zijn jarenlange vertrouwen dat dit boekje er ooit eens zou komen.
- Prof.dr. B.J.M. Heijmen voor het laatste zetje, dat uiteindelijk geleid heeft tot de afronding, in een voor mij moeilijke tijd.
- Prof.dr. R.J. Baatenburg de Jong en prof.dr.ir. J.J.W. Lagendijk voor hun kritische beoordeling van dit proefschrift.
- De (ex-)medewerkers van de KFI en radiotherapie in het ErasmusMC voor de jarenlange samenwerking met niet alleen ruimte voor het vakinhoudelijke maar ook volop belangstelling voor een ieder persoonlijk.
- De leden van de NCS subcommissie ‘QA van brachytherapie systemen’ voor de fijne samenwerking tijdens de voorbereiding van NCS rapport 13 en de daaruit volgende artikelen.
- De AudioVisuele Dienst voor de vele plaatjes, dia’s en posters door de jaren heen.
- Mijn paranimfen: Joost voor de inspirerende discussies op basis van jouw klinische en mijn fysieke ervaring, die geleid hebben tot twee hoofdstukken in zowel jouw als mijn boekje; en Jack voor de altijd weer positieve stimulansen voor een breed kader aan activiteiten.
- Kirsten en Hanny voor het goede voorbeeld, de gezelligheid en de roddels: Kunnen wij het maken ? ... Nou en of !
- Tenslotte mijn allerbeste maatjes Han, Thomas en Stijn; ondanks de vooruitzichten hoop ik dat we nog lang samen kunnen blijven genieten !



## LIST OF PUBLICATIONS

### Journal publications

IKK Deurloo, AG Visser, M Morawska, CAJF van Geel, GC van Rhoon, PC Levendag. Application of a capacitive-coupling interstitial hyperthermia system at 27 MHz: study of different applicator configurations. *Phys Med Biol* 1991; 36:119-132.

IKK Kolkman-Deurloo, AG Visser, CGJH Niël, N Driver, PC Levendag. Optimization of interstitial volume implants. *Radiother Oncol* 1994; 31:229-239.

IKK Kolkman-Deurloo, AG Visser, PC Levendag. Filmless planning: a new concept in brachytherapy. *Activity* 1995; Special Report 6:63-69.

IKK Kolkman-Deurloo, AG Visser, MHM Idzes, PC Levendag. Reconstruction accuracy of a dedicated localiser for filmless planning in intra-operative brachytherapy. *Radiother Oncol* 1997; 44:73-81.

IKK Kolkman-Deurloo, JJ Nuytens, PEJ Hanssens, PC Levendag. Intraoperative HDR brachytherapy for rectal cancer using a flexible intraoperative template: standard plans versus individual planning. *Radiother Oncol* 2004; 70:75-79.

IKK Kolkman-Deurloo, XGJ Deleye, PP Jansen, PCM Koper. Anatomy based inverse planning in HDR prostate brachytherapy. *Radiother Oncol* 2004; 73:73-77.

IKK Kolkman-Deurloo, WJM de Kruijf, PC Levendag. On-line implant reconstruction in HDR brachytherapy. *Radiother Oncol* 2006; 78:53-59.

AG Visser, IKK Deurloo, PC Levendag, ACC Ruifrok, B Cornet, GC van Rhoon. An interstitial hyperthermia system at 27 MHz. *Int J Hyperthermia* 1989; 5:265-276.

AG Visser, IKK Deurloo, CAJF van Geel, GC van Rhoon, PC Levendag. Evaluation of a capacitive-coupling interstitial hyperthermia system. *Activity* 1991; 5:114-119.

LHP Murrer, IKK Kolkman-Deurloo. Manual calculation of treatment time for high dose rate brachytherapy with a flexible intraoperative template (FIT). *Phys Med Biol* 2001; 46:1075-1084.

RJM Elfrink, IKK Kolkman-Deurloo, HJ van Kleffens, A Rijnders, B Schaeken, AHL Aalbers, WJF Dries, JLM Venselaar. Determination of the accuracy of implant reconstruction and dose delivery in brachytherapy in The Netherlands and Belgium. *Radiother Oncol* 2001; 59:297-306.

RJM Elfrink, IKK Kolkman-Deurloo, HJ van Kleffens, A Rijnders, B Schaeken, AHL Aalbers, WJF Dries, JLM Venselaar. Quality control of brachytherapy equipment in The Netherlands and Belgium: current practice and minimum requirements. *Radiother Oncol* 2002; 62:95-102.

JJ Nuytens, IKK Kolkman-Deurloo, M Vermaas, FT Ferenschild, WJ Graveland, JH de Wilt, PEJ Hanssens, PC Levendag. High dose rate intraoperative radiotherapy for close or positive margins in patients with locally advanced or recurrent rectal cancer. *Int J Radiat Oncol Biol Phys* 2004; 58:106-112.

E van Dijk, IKK Kolkman-Deurloo, PMG Damen. Determination of the reference air kerma rate for  $^{192}\text{Ir}$  brachytherapy sources and the related uncertainty. *Med Phys* 2004; 31:2826-2833.

RJM Elfrink, HJ van Kleffens, IKK Kolkman-Deurloo, AHL Aalbers, WJF Dries, A Rijnders, B Schaeken, JLM Venselaar. Quality control in brachytherapy. Current practice and minimum requirements. Report 13 of the Netherlands Commission on Radiation Dosimetry (NCS), 2000.

ACC Ruifrok, PC Levendag, RF Lakeman, IKK Deurloo, AG Visser. Dose-effect relation of interstitial low-dose-rate radiation ( $\text{Ir}^{192}$ ) in an animal tumor model. *Int J Radiat Oncol Biol Phys* 1990; 18:31-36.

ACC Ruifrok, PC Levendag, RF Lakeman, IKK Deurloo, AG Visser. Combined treatment with interstitial hyperthermia and interstitial radiotherapy in an animal tumor model. *Int J Radiat Oncol Biol Phys* 1991; 20:1281-1286.

LAM Pop, PC Levendag, CAJF van Geel, IKK Deurloo, AG Visser. Lack of therapeutic gain when low dose rate interstitial radiotherapy is combined with cisplatin in an animal tumour model. *Eur J Cancer* 1992; 28a:1471-1474.

CAJF van Geel, AG Visser, CMC van Hooije, GJM van den Aardweg, IKK Kolkman-Deurloo, RSJP Kaatee, PC Levendag. Interstitial hyperthermia and interstitial radiotherapy of a rat rhabdomyosarcoma; effects of sequential treatment and consequences for clonogenic repopulation. *Int J Hyperthermia* 1994; 10:835-844.

G Kovács, R Pötter, T Loch, J Hammer, IKK Kolkman-Deurloo, JMCH de la Rosette, H Bertermann. GEC/ESTRO-EAU recommendations on temporary brachytherapy using stepping sources for localised prostate cancer. *Radiother Oncol* 2005; 74:137-148.

PC Levendag, PIM Schmitz, PP Jansen, WMH Eijkenboom, AG Visser, IKK Kolkman-Deurloo, D Sipkema, LL Visch, S Senan. Fractionated high-dose-rate brachytherapy in primary carcinoma of the nasopharynx. *J Clin Oncol* 1998; 16:2213-2220.

PC Levendag, PIM Schmitz, PP Jansen, S Senan, WMH Eijkenboom, CA Meeuwis, IKK Kolkman-Deurloo, AG Visser. Fractionated high-dose-rate and pulsed-dose-rate brachytherapy: first clinical experience in squamous cell carcinoma of the tonsillar fossa and soft palate. *Int J Radiat Oncol Biol Phys* 1997; 38:497-506.

### Book chapters

IKK Deurloo, AG Visser, ACC Ruifrok, RF Lakeman, GC van Rhoon, PC Levendag. An interstitial hyperthermia system at 27 MHz. In: *Brachytherapy 2, Proceedings of the 5<sup>th</sup> International Brachytherapy Working Conference* 1988. Ed. RF Mould, Nucletron International BV, Leersum 1989; 564-571.

IKK Deurloo, AG Visser, ACC Ruifrok, RF Lakeman, GC van Rhoon, PC Levendag. An interstitial hyperthermia system at 27 MHz. In: Hyperthermic Oncology, Proceedings of the 5<sup>th</sup> International Symposium on Hyperthermic Oncology. Eds. Tsutomu Sugahara and Masao Saito, Taylor and Francis 1989; 874-875.

BR Thomadsen, IKK Kolkman-Deurloo, F Goodin, RR Kuske. New frontiers in high dose-rate brachytherapy. In: General practice of radiation oncology physics in the next century; AAPM 2000 summer school proceedings. Ed. A Shiu, D Mellenberg, Medical Physics Publishing, Madison WI, 2000; 293-325.

PC Levendag, AG Visser, IKK Kolkman-Deurloo, WMH Eijkenboom, CA Meeuwis. HDR brachytherapy with special reference to nasopharyngeal cancer. In: Brachytherapy from Radium to Optimization, Eds. RF Mould, JJ Battermann, AA Martinez, BL Speiser, Nucletron International BV, Veenendaal 1994; 121-131.

PC Levendag, AG Visser, IKK Kolkman-Deurloo, WMH Eijkenboom, CA Meeuwis. HDR & PDR brachytherapy with special reference to base of tongue cancer. In: Brachytherapy from Radium to Optimization, Eds. RF Mould, JJ Battermann, AA Martinez, BL Speiser, Nucletron International BV, Veenendaal 1994; 132-148.

PC Levendag, RSJP Kaatee, AG Visser, IKK Kolkman-Deurloo, GC van Rhoon, CA Meeuwis, CAJF van Geel, CMC van Hooije. Interstitial radiation and/or interstitial hyperthermia for advanced and/or recurrent cancers in the head and neck: a pilot study. In: Medical radiology: Interstitial and intracavitary thermoradiotherapy. Eds. MH Seegenschmiedt, R Sauer, Springer Verlag 1993; 233-239.

BR Thomadsen, PV Houdek, G Edmundson, R van der Laarse, IKK Kolkman-Deurloo, AG Visser. Treatment planning and optimization. In: High Dose Rate (HDR) Brachytherapy: A textbook. Ed. S Nag, Futura Publishing Company, Amonk NY 1994; 79-145.

PC Levendag, C de Pan, D Sipkema, AG Visser, IKK Kolkman-Deurloo, PP Jansen. High-dose-rate interstitial and endocavitary brachytherapy in cancer of the head and neck. In: Principles and practice of brachytherapy (using afterloading systems). Eds. Joslin, Hall, Flynn, Arnold Publishers, London 2001; 296-316.





## CURRICULUM VITAE

Inger-Karine Deurloo werd geboren op 10 juni 1964 te Lørenskog, Noorwegen. Na het behalen van het Europees Baccalaureaat aan de Europese School te Bergen in 1982, begon zij met de studie Technische Natuurkunde aan de Universiteit Twente te Enschede. Na afronding van de ingenieursopleiding in 1987 is zij gaan werken als projektmedewerker bij de afdeling Radiotherapie – Klinische Fysica van de Dr. Daniel Den Hoed Kliniek in Rotterdam. In 1994 rondde zij de opleiding tot klinisch fysicus radiotherapie af en sindsdien is zij werkzaam als klinisch fysicus radiotherapie bij het huidige Erasmus MC – Daniel Den Hoed Oncologisch Centrum.

In 1991 trouwde zij met Han Kolkman. Zij zijn de trotse ouders van Thomas (1998) en Stijn (2000).

